HYDRODYNAMICS OF FLUVIAL STRATA WITHIN THE WILLIAMS FORK FORMATION
BY

BENJAMIN PAUL CAMPANARO

Submitted to the graduate degree program in Geology and the Graduate Faculty of the University of Kansas in partial fulfillment of the requirements for the degree of Master of Science.

_____
Chairperson Diane Kamola

_____
Michael Blum

_____
Andreas Möller

Date Defended: July 3, 2017

The Thesis Committee for BENJAMIN PAUL CAMPANARO
certifies that this is the approved version of the following thesis:

HYDRODYNAMICS OF FLUVIAL STRATA WITHIN THE WILLIAMS FORK FORMATION

_____

Chairperson Diane Kamola

Date approved: July 3, 2017

HYDRODYNAMICS OF FLUVIAL STRATA WITHIN THE WILLIAMS FORK FORMATION

ABSTRACT

Fluvial sandstones within the middle part of the Late Cretaceous Williams Fork Formation were interpreted to gain insights to hydrodynamics of the ancient fluvial system. Emphasis is placed on a thick (~75 m), laterally extensive (up to 10 km) amalgamated fluvial sandstone. An empirical approach is used to allow comparison of interpreted data with data from modern systems collected from the literature. Hydrodynamic data is then applied to interpretations of the Williams Fork Formation fluvial systems to determine planform morphologies (e.g. braided vs. meandering), morphological styles (e.g. contributive vs. distributive), size (flow depth and drainage area) and characteristics (slope). Individual channel-belts within an amalgamated sandstone are interpreted to represent a ~7 m bankfull flow depth, low gradient (~10^{-4}) and low sinuosity fluvial system with an average grain size of medium lower sand. By comparison to modern fluvial systems within a compiled database (n>430), planform morphology is interpreted as either irregularly sinuous, irregularly sinuous with meandering floodplain topography or split with bars. These findings challenge previous interpretations of fluvial planform morphology in the Williams Fork Formation. Interpretations from this study based on a paleo-hydrodynamic approach favor deposition from fluvial systems in a low gradient coastal plain that had more meandering-like qualities than braided. Fluvial scaling relationships of modern systems assist in development of improved analogs for the stratigraphic record. Features such as channel depth are used to propose slope, and in turn, interpretations of fluvial planform morphology. Based on the analysis of the compiled modern fluvial database, planform morphologies of rivers are characterized by certain values and ranges of bankfull flow depth, slope and average bed sediment grain size. Detrital zircon U-Pb dating of the Williams Fork Formation provides maximum depositional ages for the top and bottom of the formation, 70.1 ± 1.8 Ma and 74.09 ± 0.48 Ma, respectively.

Keywords: Fluvial, amalgamated, hydrodynamics, planform, detrital zircon

Table of Contents

INTRODUCTION

Sheet sandstones form an important component of the upper Cretaceous Williams Fork Formation exposed in western Colorado. These fluvial sandstones form the lowest unit of repetitive stratal packages which occur throughout the middle and upper section of this formation (Fig. 1). Sandstones were studied through detailed fieldwork, supplemented with data acquired for paleo-hydrodynamic analysis. Data was collected to develop a comprehensive analysis of the fluvial systems that compose the sheet sandstones.

Quantitative analysis of fluvial strata can give insights to characteristics such as flow depth, drainage area and discharge (Bhattacharya and Tye, 2004; Davidson and North, 2009; Sømme et al., 2009; Holbrook and Wanas, 2014). Quantification of how fluvial systems change vertically in a stratigraphic section can be used to interpret fluvial architecture. These analyses can assist in determining more accurate modern analogs for interpreting fluvial systems in the stratigraphic record.

Fluvial sandstones within the middle part of the Williams Fork Formation are often multistory, and are vertically and laterally amalgamated to form sheet sandstones. Fluvial strata in one well-exposed sheet sandstone are interpreted to help quantify paleo-hydrodynamics (i.e. flow depth, slope) and planform morphology (i.e. meandering vs. braided; contributive vs. distributive). These interpreted results are compared with a database of fluvial characteristics from modern systems compiled from the literature (n>430). This database assists in displaying relationships between bankfull flow depth, slope and average bed sediment grain size. These are compared with modern planform morphologies and used to interpret planform morphologies of the studied interval.

Because the age of this formation is not well constrained, detrital zircons were analyzed from the top and base of the formation to determine a maximum depositional age. In addition, detrital zircons were used for provenance and drainage area reconstruction.

GEOLOGIC SETTING

The study area is located in the Piceance Basin, to the east of Grand Junction, Colorado and is exposed along the drainage of the Colorado River, see Figure 2. Excellent exposures and

abundant subsurface data is available along the Colorado River. Exposures studied are along Route 65 in Plateau Creek Canyon, one of the drainages to the Colorado River. Outcrops are vertical cliffs separated by small reentrants, which produce exposures that are oriented both parallel and perpendicular to paleo-flow direction.

Deposition of the Williams Fork Formation occurred within the foredeep of the Sevier Foreland Basin, approximately 200 km east of the leading edge of the Sevier Fold and Thrust Belt (DeCelles and Coogan, 2006). During this time the foredeep was dominated by fluvial deposits. Time-equivalent marine strata of this formation are not preserved in the foreland basin, however, two thin marine sandstones in northwestern Colorado are proposed to correlate to the upper part of the Williams Fork Formation (Hancock and Eby, 1930; Zapp and Cobban, 1960; Murray, 1966; Roehler, 1990; Brownfield et al., 2000). The Williams Fork Formation contains the deposits of eastward draining fluvial systems, which carried sediment from the thrust belt (Johnson, 1987). In general, the Williams Fork Formation in the study area shows little structural deformation. It was deposited during a global highstand in sea-level (Cooper, 1977; Miller et al., 2005). The paleo-climate was warm and humid, with the average temperature estimated at 19˚C (Sellwood and Valdes, 2006; Dennis et al., 2013; Upchurch et al., 2015).

The Williams Fork Formation overlies marginal marine and shoreface strata of the Iles Formation (Mt. Garfield Formation) and is overlain by the fluvial and lacustrine strata of the Wasatch Formation, see Figure 1. The Williams Fork Formation is known as the Hunter Canyon Formation in outcrop expression in the Book Cliffs region of the Piceance Basin and is dominantly composed of fluvial and overbank deposits (Hettinger and Kirschbaum, 2002). The age of the uppermost Williams Fork Formation is contested. In general, ages from palynologic and ammonite zones based on biostratigraphy and/or calibration by volcaniclastics suggest a Maastrichtian age of deposition, however, ages proposed for the youngest deposits range from Maastrichtian to upper Paleocene (Johnson and May, 1980; Patterson et al., 2003; Laskowski et al., 2013).

The lower third of the Williams Fork Formation is composed mainly of floodplain deposits

with discontinuous fluvial sandstones (e.g. Cole and Cumella, 2003, 2005; Pranter et al., 2007). The middle and upper intervals of the Williams Fork Formation contain significantly less overbank deposits than the lower interval of this formation. Stratal packages of fluvial deposits are defined in the middle and upper intervals and are expressed as repetitive vertical successions (Ost, 2010). In general, a stratal package shows an upward vertical trend from high to low net-to-gross fluvial strata, see Figure 1. The pattern is tripartite and discussed in detail by Ost (2010). At the base, it begins with vertically and laterally amalgamated fluvial sheet sandstones, which are typically 8-20 m thick. The amalgamated fluvial sandstones are overlain by an interval with thick (~8 m) laterally-amalgamated fluvial sandstones encased in overbank mudstones and siltstones. This interval is overlain by a mud/siltstone dominated interval (overbank deposits) with isolated, thin (~1 m thick) channelized sandstones. The stratal pattern is significant because it dominates the stratigraphic expression of the middle and upper section of the formation (Ost, 2010). The stratal pattern repeats sixteen times in the middle section of the formation, and three times in the upper section. This study will focus on the intervals of amalgamated fluvial sandstones that occur at the base of the stratal package.

STUDY AREA AND METHODOLOGY

The study area was chosen because of quality and lateral extent of the outcrop. The field area is the location of previous research projects: a Light Detection and Ranging (LiDAR) study (German, 2006), and an outcrop study paired with subsurface data from a well in Parachute Field, see Figure 2 (Keeton, 2012, 2015). Data from these studies are used to cross-check flow depth calculations or determine width to thickness ratios of fluvial systems in the Williams Fork Formation. The sandstone of interest is one of the sheet sandstones, which forms the basal unit in one of the stratal packages defined by Ost (2010), and has been the focus of previous studies. It has been informally named the upper Williams Fork Formation Sandstone (Leibovitz, 2010), a sandstone within the upper Williams Fork Formation (German, 2006), a sandstone within the middle Williams Fork Formation (Keeton, 2015), the middle Williams Fork Formation 2 (Foster, 2010) and the Big Kahuna sandstone (informally named by Rex Cole at Mesa State University e.g. Foster, 2010). For simplicity and ease of discussion, the amalgamated sandstone of this

study will be informally referred to as the Big Kahuna sandstone.

Two sections, on outcrops number two and three, see Figure 3a,b, were measured in detail at the decimeter scale for facies descriptions, using a Jacob Staff and Brunton compass. Data was collected using Miall's (1996) facies classification, but are presented here in a descriptive manner. In addition, dimensions of channel-fills, channel-belts, lateral accretion deposits and scour surfaces were collected on multiple vertical outcrop exposures. Data from vertical cliff exposures were collected using a laser range finder (TruPulse® 200X) and transferred to photomosaics of the outcrops (Fig. 3a,b and 4 and Appendix Fig. A1-A15). Stratigraphic sections and their locations are in Appendix Figures A1-A15. Based on completeness of exposure and accessibility, the data used in hydrodynamic calculations is limited to and collected from eight of ten successions interpreted as amalgamated channel-fills and channel-belts. Channel-belt is used here as the deposit which records the path that a channel migrates over time, similar to the term channel bodies of Gibling (2006). This is in contrast to channel-fill, which is defined as a fill of a channel form (Gibling, 2006). The amalgamated sandstone of this study, the Big Kahuna sandstone, is characterized by a maximum thickness of ~75 m in the study area, has a maximum lateral extent of 10 km in outcrop expression as traced by Ost (2010) and contains many internal scour surfaces. In general, the Big Kahuna sandstone forms massive cliff exposures. Lateral accretion deposits are observed, but are uncommon features within the Big Kahuna sandstone. Thin, isolated intervals of interbedded sandstone, siltstone and mudstone occur twice in the studied interval, within the upper 15 m of the Big Kahuna sandstone seen in Figure 3a,b and 4. Descriptions of these interbedded intervals are limited to these exposures. These intervals are laterally discontinuous and transition into scour surfaces within 900 m.

FACIES DESCRIPTIONS OF THE BIG KAHUNA SANDSTONE

Description: Cross-bedded facies

Cross-bedded sandstone facies have two end members: wedge and festoon cross-bedded sandstone, and planar tabular cross-bedded sandstone, see Figure 5a,b. Wedge and festoon cross-bedded sandstones are the dominant facie in the study area and comprise approximately 85% of the measured sections (Appendix Fig. A3 and A4). Cross-bed thickness ranges from 10 to

55 cm and the average cross-bed thickness is 29 cm (n=87). In general, cross-bed extent is less than 5 m and cross beds are observed to stack vertically. In general, no vertical trend in cross-bed thickness is observed, however, in places, a vertical decrease in cross-bed thickness or grain size is noted. Sandstones are light brown and are moderately sorted with fine to medium grain-size sand. Foresets are inclined at 5-25˚ with an average apparent dip of 17˚, n=72 (Appendix Fig. A3 and A4). Cross-bedded sandstones commonly contain rip-up clasts, which are concentrated on the tangential base or along foreset surfaces, and soft sediment deformation is rare. These sandstones are equivalent to Miall's (1996) St facies. For simplicity, in the remainder of the text the term St facies is used for wedge and festoon cross-bedded sandstone.

Planar tabular cross-bedded sandstone comprises approximately 5% of the measured sections (Appendix Fig. A3 and A4) and range from 45 to 140 cm in thickness with an average of 76 cm (n=23). Planar tabular cross-stratified beds typically overlie low-relief scour surfaces. In general, cross-bed extent is greater than 5 m and cross-beds are not observed to stack vertically. Sandstones are light brown and are poorly to moderately sorted with fine to medium grain size sand. Foresets are inclined at 15-25˚ with an average apparent dip of 21˚, n=8 (Appendix Fig. A3 and A4). Low angle dips are interpreted as apparent dips from oblique exposures. Cross-bedded sandstones commonly contain rip-up clasts of siltstone and mudstone, which are concentrated on the tangential base. Casts of wood are found within the planar tabular cross-beds and range from 20-40 cm in diameter. These sandstones are equivalent to Miall's (1996) Sp facies. For simplicity, in the remainder of the text the term Sp facies is used for planar tabular cross-bedded sandstone.

Interpretation: Cross-bedded facies

The majority of cross-beds in the St facies are interpreted as deposits of sinuous crested (3-D) dunes, formed from unidirectional currents in a river. Most dunes in the St facies are interpreted to have formed in equilibrium with bankfull flow. This is supported by a unimodal distribution in cross-strata thickness, see Figure 6, and the lack of unit bar features in the majority of the cross-beds (Smith, 1978; Bridge, 2003). In modern studies of rivers in bankfull stage, dune height, and therefore cross-bed thickness, have a unimodal distribution when

deposited from a single event during bankfull flow (Levey, 1978; Bridge, 2003). Because these cross-beds are interpreted to be in equilibrium with bankfull conditions, they are used in hydrodynamic calculations.

Some cross-beds of the St facies are interpreted as unit bars (Fig. 6). Smith (1978) and Sambrook-Smith et al. (2006) define a unit bar as a simple form with large-scale inclined strata that is unmodified from migration. These typically contain a slip-face near the angle of repose and are not superimposed onto other bar forms. The dimensions of a unit bar scale to flow width and height (Kelly, 2006). In this study, isolated cross-beds measuring over 40 cm in thickness which contain foresets that are near the angle of repose are interpreted as unit bars. This cross-bed thickness is significantly larger than the average thickness (29 cm) of the St facies cross-beds. Rip-up clasts and imprints from large wooden debris (logs) are associated with cross-beds interpreted as unit bars. In modern fluvial systems, large wooden debris is often found in bar deposits (Gurnell et al., 2001; Lassettre et al., 2007).

When unit bars amalgamate, they form compound bars (Bridge, 2003). Compound bars form from several erosional and depositional events to produce a more complicated internal stratigraphy. Compound bars are not recognized in the study area. This suggests that the unit bars were buried quickly by 3-D dunes of the St facies, preventing compound bars from forming. Cross-beds interpreted as unit bar deposits were not included in hydrodynamic calculations because bars scale differently to flow depth and sufficient information was not collected to determine flow depth. In general, bars are used to predict channel width (e.g. Lunt et al., 2004), which was not calculated in this study.

Planar tabular cross-beds of the Sp facies are interpreted as relatively straight crested (2-D) unit bars accreting dominantly in the downstream direction, and migrating across the floor of a channel, over a basal lag. Because all cross-bed thicknesses exceed 40 cm and do not stack vertically, these are interpreted as unit bars, see Figure 6. Similar deposits have been labeled as deposits of cross-bar channels (Bridge, 2003; Lunt et al., 2004). These deposits are interpreted to be a progradational feature that is not in equilibrium with bankfull flow. All cross-beds interpreted as unit bar deposits were not used in hydrodynamic calculations.

Description: Interbedded sandstone, siltstone and mudstone facies

Interbedded deposits of very fine-grained sandstone, siltstone, and mudstone comprise approximately 10% of the measured sections (Appendix Fig. A3 and A4). Fine-grained facies are limited in extent and exposed in only a few locations because of their susceptibility to weathering and erosion. Interbedded interval thickness range from 1.6-4.7 m, can contain up to 55% sandstone and typically overlie the St facies. In localized areas, the interbedded deposits show soft sediment deformation when overlain by either the Sp or St facies. Sandstones are current-rippled or contain climbing ripple cross-beds, and individual bed thicknesses range from 2-6 cm. The maximum bedset thickness is 60 cm. Sandstones are typically separated by 20 cm of siltstone or mudstone. Sandstones are light brown and are moderately sorted with very fine to fine grain-size sand.

Burrowing is observed sparsely in sandstones of the interbedded facies, see Figure 5c, but when present, can homogenize the contact between the strata. Although most burrowing is nondescript, *Planolites* and *Naktodemasis bowni* are identified. *Planolites* burrows are 1-3 cm in diameter and have an active backfill of mudstone and very fine sandstone. These burrows are unbranched, cylindrical and oblique to bedding. *Naktodemasis bowni* are 2-3 cm in diameter, oblique to bedding, and actively filled with a meniscate backfill of very fine sandstone. *Naktodemasis bowni* is found in continental settings and has been interpreted to occur in well-drained floodplains (Smith et al., 2008).

Massive and bioturbated siltstones to mudstones have individual bed thickness ranging from 5 to 35 cm. They are either teal/grey or maroon, composed of angular to subangular blocky peds and commonly contain orthogonal slickenside surfaces. In the fine-grained beds, passively-filled structures ranging from 1-16 cm in diameter with a downward taper are identified as rhizoliths. Orientations are vertical to horizontal in sandstone, and oblique to horizontal in mudstone/siltstone and in places show bark-like textures. Thicker rhizoliths, ranging up to 16 cm in thickness and up to 40 cm long, extend vertically from these facies through underlying beds.

Interpretation: Interbedded sandstone, siltstone and mudstone facies

In this study, interbedded sandstones, siltstones and mudstones are interpreted to have been deposited from overbank flooding. The sandstone and siltstone deposits are interpreted to represent stacked and sometimes vertically amalgamated crevasse splay deposits. Interbedded deposits with sedimentary structures associated with rapid deposition rates (climbing ripples) or massive texture are characteristic of deposition from overbank flow. Farrell (1987) and Smith et al., (1989) have interpreted similar interbedded fine sands and muds as overbank facies. Although individual burrows are not recognized in the mudstone and siltstones in this study, the massive texture may be due to bioturbation. The interbedded strata is equivalent to Miall's (1996) Fsm facies. For simplicity, in the remainder of the text, the term Fsm facies is used for interbedded sandstone, massive siltstone and mudstone facies.

Mudstone features with subangular blocky peds and slickenslide surfaces are also described in soil horizons of the Willwood Formation (Kraus and Brown, 1988). The teal/gray color of the mudstones and siltstones can be formed in a reducing environment and the maroon color can be formed in an oxidizing environment (Wright, 1992). Alternations of colors are attributed to variations in water saturation in the floodplain (Lehman, 1989; Wright, 1992).

VERTICAL SUCCESSIONS AND ARCHITECTURAL ELEMENTS OF THE BIG KAHUNA SANDSTONE

Three vertical successions of facies arrangements are observed in the two measured sections: (1) Sp-St, (2) St-Stand (3) Sp-Fsm. Figure 7 displays schematic profiles of these successions in the study area. The first succession consists of Sp facies overlain by St facies. The Sp-St vertical succession has a thickness range of 1.1-3.8 m. At the base, planar tabular cross-beds of the Sp facies overlie a sharp, low relief, erosional surface with large lateral extent that is traced across the outcrop. The Sp facies in this vertical succession are overlain by St facies and in some places the St facies vertically decrease in cross-bed thickness and grain size. The top of the Sp-St vertical succession is overlain by an erosional surface.

The second vertical succession, the St-St succession, has a thickness range of 0.9-4.5 m. The St-St succession is identified where cross-beds of successive St facies are separated by a major

scour surface. The erosional surface typically expresses more relief than the erosional surface that underlies the Sp-St succession. There is up to 6 m of relief along the basal scour surface, which is in many places accentuated by rip-up clasts. In general, there are few vertical trends in cross-bed thickness or grain size in the St-St succession.

The least common facies succession, the Sp-Fsm succession, is an upward fining succession, see Figure 5d. This succession is only observed in one locality (38.9 m on Appendix Fig. A3 and A6). It has limited exposure with a maximum thickness of 2.6 m, and only ~20 m of lateral extent before it is truncated by an overlying surface. The vertical succession begins with an Sp facie overlain by St facies that have a medium lower grain-size. Overlying the St facies are beds of very fine sandstone. The very fine sandstone nodular beds are elongated in the horizontal direction, however, internal laminations are not observed due to weathering. The very fine sandstone vertically becomes light brown to grey with the incorporation of fine-grained sediment. There is also a vertical transition in texture from platy to blocky peds. The very fine sandstone interval is sharply overlain by a 15 cm thick massive mudstone. This results in an overall upward fining succession of sandstone vertically into mudstone. There are no trace fossils observed in this facies.

The facies of the upward fining succession from sandstone to mudstone, Sp-Fsm, is interpreted as channel abandonment followed by a passive fill. The contact between the medium lower and very fine sandstone is interpreted to represent the time of abandonment due to the shift in deposition and preservation of finer-grained sediments. Abandonment could have been caused by avulsion or a meander cut-off. This would allow an increase in mud deposition and preservation due to a lower energy setting. Farrell (1987) and Bridge (2006) have described and interpreted similar deposits of fluvial successions with fine-grained sediment overlying coarser-grained bar deposits as passive channel-fills. Channel-fill thickness can be used as a proxy for paleo-flow depth (Mohrig et al., 2000). The interpreted channel-fill is not fully exposed; therefore, the thickness represents a minimum value.

Sp-St and St-St arrangements are separated by scour surfaces or less commonly, the Fsm facies. Neither the Sp-St or St-St vertical successions contain surfaces of subaerial exposure or

rooted horizons. The vertical successions of (1) Sp-St facies and (2) St-St facies are interpreted as partially preserved bar deposits. Both successions are observed to stack vertically. The St-St succession is the most common in occurrence. The Sp-St facies are interpreted to represent thalweg, basal bar and unit bar deposits. The St-St facies are interpreted to represent components of compound bar deposits. The interpreted depositional process that would result in these two successions would be produced by migrating bars and channels. Erosion by overlying Sp-St or St-St successions are interpreted to cause the partial preservation. The successions' erosional surface likely represents the scour that occurs with channel reoccupation. Both Sp-St and St-St represent portions of channel-fill deposits. McLauren and Steel (2007) interpret a similar process for the fluvial sheet sandstones within the upper Cretaceous Castlegate Formation of Utah. Upward fining successions within these vertical arrangements are interpreted to represent the complete preservation of migrating bars. The lack of subaerial exposure surfaces or bioturbated horizons suggest that the fluvial system was not ephemeral, or these features were not preserved due to erosion from migrating bars and channels.

Paleo-current data was not collected in this study, but was obtained from previous studies by German (2006) and Keeton (2015). Published data was collected from the field area of this study, from the Big Kahuna sandstone in adjacent outcrops nearby and from subsurface borehole images from Parachute Field (German, 2006; Keeton, 2015). Measurements from cross-beds indicate east to northeast flow directions, see Figure 8. A sinuosity of 1.1 was calculated from cross-beds using borehole imagery from Keeton's (2012, 2015) study of the middle Williams Fork Formation, which includes the Big Kahuna sandstone. This is interpreted to represent a low sinuosity fluvial system.

Major erosional and depositional surfaces within the Big Kahuna sandstone

A hierarchy of bedding surfaces is observed within the study area, which are subdivided by extent and/or relief: (1) surfaces with large extent with low relief, (2) surfaces with small extent with high relief and (3) surfaces with small extent that show a consistent orientation. Surfaces with large lateral extent are the most prominent feature within the Big Kahuna sandstone in

the study area. These surfaces have low relief and typically occur at 8-13 m intervals when observed where the sections were measured, however, along the inaccessible cliff exposures, surface relief ranges from 4.5-25 m. These are distinct surfaces that typically extend across the entire outcrop expression and are labeled as type 1 surfaces in Figure 3a. Some segments of the outcrop are highly weathered, and are cavernous in expression (with numerous tafoni features). Bed surfaces cannot be correlated across this weathering pattern. A few of these surfaces extend short distances across the outcrop and are truncated by another surface. These surfaces are interpreted as a common surface of channel-belt migration. The stratigraphic sections bracketed by these intervals are used in hydrodynamic analysis of the outcrops (Fig. 3). The second type of surface (type 2 surface) shows higher relief (≤6 m), but has significantly less lateral extent than the first surface type (expression is less than outcrop length). The more limited lateral extent is due to truncation by another surface or loss of expression from weathering where outcrop exposures contain a tafoni or massive texture. Surfaces cannot be correlated or identified in outcrops with these textures. These type 2 surfaces are not as prominent as the first type of surface and are not as easily distinguished in outcrop. Type 2 surfaces are interpreted as internal scours, but some could be poorly or partially expressed type 1 surfaces.

The third surface type has limited extent and occurs as clusters of surfaces that display a consistent orientation. These surfaces (type 3 surfaces) are bounded by the type 1 surfaces. The surface clusters are usually truncated by the overlying surfaces (type 1 surface) and in places have a tangential base and display downlap with respect to the underlying surfaces. Vertical relief of the surfaces ranges from 4.5 – 10.6 m with an average of 6.7 m (n=10). Erosion by an overlying surface results in the wide range of relief observed for these surfaces. Surfaces that occur in clusters are characterized by a dip of 5-10˚. As seen in Figure 4, the type 3 surfaces (shown in green) have a consistent dip, vertical relief and orientation. When the outcrop face changes orientation, the angle of dip is observed to decrease as seen in Figure 4. A laser range finder was used to measure vertical relief on these inaccessible cliff exposures. Therefore, if thickness between type 1 surfaces are representative of paleo-flow depth then all measured

values are likely minimum values. The deposits bracketed by the collection of surfaces are interpreted to be sandstone dominated. Type 3 surfaces display a consistent orientation and are interpreted as lateral accretion surfaces. Lateral accretion surfaces are formed as a result of channel migration, which deposits sediment on the inner bank of a bend. Observations in this study are similar to the descriptions of lateral accretion of Miall (1985) and point-bar deposits of Pranter et al. (2007). Lateral accretion surfaces are most prevalent in outcrop number 5 and outcrop number 4. Lateral accretion surfaces are relatively less common within the outcrops to the west, outcrop number 1 and 2, where cliff exposures contain less fine grained deposits. The thickest intervals between type 1 surfaces occur in the western, sand-dominated outcrops. These exposures are weathered and have a massive texture, which is non-conducive for interpretation of internal deposits and surfaces.

Lateral accretion surfaces are commonly used for determining paleo-flow depth in the stratigraphic record (Mohrig et al., 2000; Pranter et al., 2007; Wu et al., 2015). In the study area, vertical relief of lateral accretion surfaces do not represent the complete channel depth because of truncation from overlying erosional surfaces. Ethridge and Schumm (1977) determined an empirical relationship for flow depth between the straight and curved sections of a channel from experimental and modern fluvial systems. They determined that the depth of the straight reach of a channel is approximately equal to 0.585 multiplied by the depth of the meandering reach of a channel. If the 10.6 m relief of the lateral accretion surface represents the entire depth of the meandering section, then the minimum depth of the equivalent straight reach would be 6.2 m.

Interpretation of channel-belts

Type 1 surfaces (low-relief erosional surfaces with large lateral extent) are the most prominent features within the Big Kahuna sandstone and are interpreted to be a common surface feature of channel-belt migration. The thickness of a channel belt is the distance between the deepest scour to the uppermost deposits of the highest bankfull flow conditions, provided the entire section is preserved (Salter, 1993). Sandstone thicknesses between consecutive low-relief surfaces range from 4.5-25 m. This thickness would represent paleo-flow

depth, if the interpreted interval is the deposit of one channel-belt. However, these intervals are not interpreted to represent paleo-flow depth, because it is interpreted that the large range in interval thicknesses is caused by erosion from overlying channels. This results in an interval thickness that is less than paleo-flow depth. Weathering of cliff exposures masks type 1 surfaces, which could result in the overestimation of channel-belt thickness. This could then result in an interpreted interval thickness that is much larger than paleo-flow depth. These compiled observations indicate that the thicknesses between low-relief surfaces are not an accurate reflection of paleo-flow depth, although this thickness may be a proxy for a minimum value of paleo-flow depth.

The type 1 surfaces (intervals between the large, low-relief erosional surfaces) are interpreted as vertically and laterally amalgamated channel-belt and channel-fill deposits due to the complexity or absence of internal surfaces. For further discussion and calculations, the sections between the type 1 surfaces are referred to as intervals. Intervals are coded differently on outcrops due to difficulty correlating from one outcrop face to the next. Outcrop number 2 is numerically (1-6) coded and outcrop number 3 is alphabetically (A-D) coded for the measured sections, see Figure 3a, b. Different codes were applied to each outcrop due to loss of type 1 surfaces between outcrop expressions. Because the intervals may represent amalgamated channel-belts and channel-fills, the gross thickness does not necessarily represent the thickness of a single channel-belt or channel-fill. Amalgamation of channel-belt and channel-fill deposits in an interval would result in a complicated, stacked fluvial architecture that consists of multistory sandbodies.

HYDRODYNAMICS OF THE BIG KAHUNA SANDSTONE

Paleo-flow depth

Fluvial scaling relationships are predictive in that most features (e.g. depth, slope, drainage area) are dependent on grain size and discharge (i.e. grain size is directly related to slope and discharge is directly related to flow depth and drainage area). A scaling relationship is when measurements of a river's feature is comparable to the same feature of other rivers, regardless of the order of magnitude. Through scaling relationships, parameters such as flow depth,

discharge and drainage area can be compared between fluvial systems and therefore are predictive (Lee and Julien, 2006; Blum et al., 2013). Flow depth is important because it can be used to gain estimations of slope and backwater length in the stratigraphic record.

There are three major approaches in the literature for determining paleo-flow depth: measuring channel-fill height, measuring point-bar height, and empirical relations with cross-bed thickness (Fig. 9a) (Mohrig et al., 2000; Leclair and Bridge, 2001; McLaurin and Steel, 2007; Pranter et al., 2007). Cross-bed thickness is used to determine paleo-flow depth in this study because of incomplete or poor preservation of channel-fill deposits. Point bar thickness is not used as a flow depth indicator because lateral accretion deposits are not commonly observed in the study area. Cross-bed thickness is used to determine paleo-flow depth in this study because of excellent preservation in outcrop exposures. Leclair and Bridge (2001) experimentally determined that dune height and cross-bed thickness are directly related to the flow depth that formed them. Dune height and flow depth are calculated from cross-bed thicknesses via the methods of Leclair and Bridge (2001) and are discussed in full in Appendix 2bi. Based on this model, paleo-flow depth estimations from the stratigraphic record encompass a range of possible values because velocity cannot be directly measured from the rock record. This range is also calculated because bedform stability occurs over a range of velocities. It is unknown if the studied cross-beds formed from dunes near the edge or center of its stability field, which could affect dune height. The methods used in this study account for any dune within the stability field, therefore, they provide a range of plausible flow depths.

The method of using cross-beds to determine flow depth has been tested in several modern rivers (Gabel, 1993; Leclair and Bridge, 2001; Lunt et al., 2004). Studies of the stratigraphic record have calculated similar paleo-flow depths from cross-beds to depths estimated from channel-fill thicknesses (Adams and Bhattacharya, 2005; Holbrook et al., 2006; McLaurin and Steel, 2007). These studies further validate the use of empirical relations of cross-bed thickness to determine paleo-flow depth. Use of this method has been gaining momentum in the literature (e.g. Li et al., 2010; Chen et al., 2014; Ielpi et al., 2014; Bhattacharya et al., 2016). Compaction of the subarkose sandstone in the field area is interpreted to have negligible

effects on cross-bed thickness.

Leclair and Bridge's (2001) model used data from their experimental findings and published data on modern fluvial systems. Paleo-flow depth calculated from cross-bed thickness contains uncertainties due to assumptions within the model. There are two assumptions within Leclair and Bridge's (2001) model. The first assumption is that variation in cross-bed thickness is mostly attributed to variations in dune height. The second assumption is that the dunes of interest did not change drastically over time or space. Scatter in the model results can be attributed to incorrect collection of data from modern systems. A possible source of error leading to data scatter is that dune height and flow conditions (e.g. velocity) collected from modern fluvial systems may not have been in equilibrium at the time of data collection. This could potentially produce incorrect results from using two unrelated features. There are also potential errors with the application of Leclair and Bridge's (2001) model. Collection of cross-bed thicknesses is limited to fluvial channel bar deposits. Other unidirectional processes that form dunes were not incorporated into the model. Another source of error in the application of the model could be from the number of measured cross-beds. If the collected dataset is too small to define a probability density function (pdf) then a constant (beta, related to variations in trough scour depth) in the model is estimated from data collected by Leclair and Bridge (2001).

Paleo-flow depth is calculated from cross-beds interpreted as dune deposits. Based on 87 field measurements, the average thickness of cross-beds interpreted as dunes is 29 cm. Thickness was plotted against count to display the range and distribution of all cross-bed deposits, see Figure 6. Cross-beds interpreted as either dunes (blue) or unit bars (yellow) show a bimodal distribution in thickness and are easy to distinguish from each other in outcrop expression. Unit bar cross-beds are distinguished from dunes by having a simple form with steep foreset angles that does not stack vertically (Smith, 1978; Sambrook-Smith et al., 2006). Unit bars in this study commonly occur with rip-up clasts, wooden debris and large, low-relief scour surfaces. Bimodal distributions of dunes and unit bars are also seen in data from modern fluvial systems (Levey, 1978). Bar dimensions relate to channel width and are not included in hydrodynamic calculations. The unimodal peak in thickness of cross-beds interpreted as dune

deposits can reflect preservation of similar flow conditions. This study interprets that dune deposits were formed in bankfull conditions. Bankfull flow depth will have the largest dunes due to the deepest flow depth. The largest dunes have the deepest scour depth, therefore, the largest dunes will be preferentially preserved relative to smaller dunes that formed during shallower baseflow flow depths (Leclair et al., 1997).

Dune height and cross-bed thickness are directly related to flow depth (Leclair and Bridge, 2001). As a simplification, channel forms are concave up, and dune deposits are interpreted to record multiple flow depths, with the thickest cross-beds corresponding to bankfull flow. Because there is a distribution of flow depths recorded by dune deposits, the 90th percentile (P90) is interpreted to be a close approximation to bankfull flow depth. The P90 is interpreted to incorporate the range of cross-beds observed and allows for fluctuation in the maximum and minimum flow depth. Fluctuations in the maximum flow depth are likely to be related to deep scours that are spatially discontinuous and do not reflect bankfull depth. The P50 of calculated flow depths would represent a depth between day to day and bankfull flow. Bankfull flow depth is important because channels form during bankfull flow stages (Williams, 1978; Church, 2006).

A flow depth for the fluvial system was estimated from the P90 of each interval (Table 1). P90 flow depths from seven intervals are in close agreement, and data from eight intervals are used to calculate flow depth. Two intervals (4 & 6) are in disagreement with the other intervals, it is interpreted that the data is reflecting poor exposures or outcrop inaccessibility. Data from those outlier intervals were not included when calculating flow depth. Table 1 contains the calculated interval P90 flow depth and the corresponding grain sizes (minimum, maximum and average). The bankfull paleo-flow depth for the median P90 ranges from 4.0 - 7.2 m. Cross-bed thicknesses and calculated flow depths used in this study are in Appendix 2bii, iii. Figure 9b is a histogram of all calculated flow depths. The P90 of all interpreted dunes is 6.9 m. Previous studies of the Big Kahuna sandstone have estimated similar flow depths. Flow depths determined from Keeton's (2012) average calculated dune height in the middle Williams Fork Formation provide a depth of 5.1 m. This is within the median P90 range calculated from

deposits grouped by interval (table 1) of this study and is similar to the P50 flow depth of all dune cross-beds (4.9 m). The P90 of this study is also in close agreement with the average thickness (7.8 m) of channel-belts and channel-fills measured with LiDAR (German, 2006). Based on the P90 of this study, the calculated bankfull paleo-flow depth of individual channels within the Big Kahuna sandstone was approximately 7 m. Differences between flow depth calculated from cross-bed thickness and thickness between type 1 surfaces (interval thickness) could be due to a bias from the location of the measurements. Cross-bed thickness was collected at weathered reentrants while measurements using a laser range finder are from vertical cliffs. Differences in weathering could be related to grain size, therefore, it could represent differences in the depositional process or different fluvial systems.

Width-thickness ratio of channel-belt deposits

Fluvial systems go through downstream transformations after entering the backwater zone. The backwater zone is defined by the distance between the river mouth and the location upstream where the channel base is the same elevation as base-level (Paola and Mohrig, 1996). Within the backwater zone, channel forms are narrower, deeper and migrate less compared to the channels upstream of this zone (Hudson and Kesel, 2000; Nittrouer et al., 2012). Changes in channel migration inside the backwater zone cause width to thickness ratios of channel-belt deposits to be distinctly different from the upstream ratio (Blum et al., 2013). Because width to thickness ratios of channel-belts change predictively downstream, they can be used as a locational tool for gross depositional environment for studies in the stratigraphic record.

Using LiDAR, German (2006) measured width and thickness dimensions of 113 fluvial sandbodies, which are reinterpreted in this study as channel-belt and channel-fill sandstones. Data was collected from six outcrops of the Big Kahuna Sandstone in Plateau Creek Canyon, including the one from this study (see inset map of Figure 10). German (2006) used width to thickness ratios (W:T), defined by Friend et al. (1979), to identify ribbon (W:T < 15:1) or sheet (W:T > 15:1) sandstone geometries. German's (2006) W:T ratios are used in this study to determine the backwater influence in the study area. Backwater influence can be determined by W:T ratios of channel-belt deposits (Blum et al., 2013). Ranges of W:T ratios from within and

outside the backwater reach were collected from the stratigraphic record and modern systems (Gibling, 2006; Blum et al., 2013) and plotted in Figure 10. W:T ratios of 30-70:1 are representative of channel-belts within the backwater reach, and highlighted in light green in Figure 10. Ratios of 70-300:1 are representative of channel-belts upstream of the backwater effects, and highlighted in dark green in Figure 10. The average W:T ratio of channel-belts upstream of the backwater effects is approximately 200:1. Ratios of 6-30:1 are representative of channel-fills, as opposed to channel-belt deposits, and will not be used to determine the backwater zone. This study uses Gibling's (2006) definition of channel-belts, which are the deposits that record the migration of a channel over time, as opposed to channel-fill, which records the fill of an individual channel form.

Width to thickness ratios from German (2006) are grouped by orientation: perpendicular (prp) and oblique (obl) to paleo-flow on Figure 10. Exposures that were interpreted as parallel to paleo-flow were not used to determine backwater effect because they do not provide a representative width of the fluvial deposits. They do, however, help establish channel thickness, and so are included in Figure 10. Deposits within the channel-belt domain that are perpendicular (prp), oblique (obl) and perpendicular to oblique (prp/obl) have an average W:T ratio of 46:1 (n=41) (Fig. 10). Symbol color used in Figure 10 represents W:T ratios plotted by orientation to paleo-flow. Symbol shape represents W:T ratios plotted by complete versus incomplete (e.g. truncated) exposure. Ranges of ratios are highlighted according to the definitions of Gibling (2006) and Blum et al. (2013). The schematic map, upper right, displays by color, where these processes occur in map view. The calculated W:T ratio of 46:1 from the Big Kahuna sandstone, is interpreted to represent deposition within the backwater zone.

Width to thickness ratios of the channel-belt sandstones plot within the backwater effects. Width to thickness ratios from German (2006) are interpreted here as a minimum value because the maximum outcrop exposure is approximately 900 m. Widths of complete exposures of channel-fills and channel-belts are well within the extent of the outcrop and complete exposures of channel-belts are clustered around 39-55:1. These observations indicate that the W:T of 46:1 is likely close to its actual value. Modern channel-belts within the

backwater effects are approaching the end of the fluvial system and typically fall within the coastal plain environment.

Paleo-slope

Slope is a unitless measure of elevation gain or loss over distance. It is related to river morphology such as braided and meandering (e.g. Leopold and Wolman, 1957; Schumm and Khan, 1972). Application of slope estimations in the stratigraphic record is important for insights in supporting an interpretation on river morphology.

There are two primary methods to estimate slope from the stratigraphic record. Slope is most commonly estimated by multiplying grain size by constants and dividing by flow depth. The constants are Shields number and submerged specific gravity of the sediment. These constants have been adjusted in different investigations for various grain sizes or compositions (e.g. Paola and Mohrig, 1996; Holbrook and Wanas, 2014; Lynds et al., 2014). This is considered a simplistic approach and a rough estimate because Shields number is held constant.

Another method of slope calculation allows Shields number to change with grain size. By setting two equations with two unknown variables (slope and Shields number) equal to each other, the common variable (Shields number) can be left unknown and the second variable (slope) can be determined. This method involves using a modified river slope equation from Parker (1978) and an equation that relates the minimum threshold of incipient suspension to Shields number from Wilkerson and Parker (2011). This approach was developed by Lynds et al. (2014) and is discussed in further detail in Appendix 2c. This study calculates slope using this method with application of the Julien assessment. The Julien assessment holds the minimum threshold of incipient suspension (u^*_{sf}/w_s) constant so that it does not change with grain size. As discussed in Lynds et al. (2014), this modification was justified from experimental studies, when several grain sizes reached a constant value of incipient suspension (Laursen, 1958; Niño et al., 2003).

The Lynds et al. (2014) Method Number Two was established for fluvial systems composed of very fine- to medium-grained size sand. This method was selected because the average grain size of the Big Kahuna sandstone is lower medium, and because it allows for fluctuations in

Shields number and has a known error range (factor of 2) from testing on modern fluvial data (n>1200).

All combinations of calculated P90 flow depths (lower limit, upper limit, and median) and measured average grain sizes were used to calculate the full range of possible paleo-slope, (see table 1). The average paleo-slope calculated for all of the intervals is $7.6*10^{-5}$ with an uncertainty range of $3.8*10^{-5}$ to $1.5*10^{-4}$. The calculated minimum and maximum paleo-slope is $4.7*10^{-5}$ – $1.3*10^{-4}$, respectively, with an uncertainty of $2.4*10^{-5}$ to $2.6*10^{-4}$. All paleo-slope calculations are located in table 2. Paleo-slope calculations indicate a low gradient river (~10^{-4}). Higher gradient rivers (>10^{-3}) are not within the uncertainty of the paleo-slope calculations.

Backwater length

The backwater length is the distance from the shoreline to a point upstream where the river is affected by base-level (Blum et al., 2013). Backwater length can be used as a predictive measure to help estimate distance from a paleo-shoreline and to estimate total dimensions of delta plain environments (Blum et al., 2013; Bhattacharya et al., 2016). Backwater length is defined by flow depth divided by slope; in this study, a range is estimated using the array of calculated values for flow depth and slope for each interval (Paola and Mohrig, 1996). Values estimated for the backwater length are a first order approximation due to the propagated error of the large ranges of flow depths and slopes. Calculations are most sensitive to changes in slope (the denominator) because it is several orders of magnitude smaller than flow depth (the numerator). This is further complicated in application to the stratigraphic record when paleo-slope is estimated by paleo-flow depth which is also empirically derived.

First order estimates of the backwater length for the study area are approximately 100 km (see table 3). This would indicate that a paleo-shoreline should be located within approximately 100 km of the study area. There are no known coeval marine deposits to the Big Kahuna sandstone in Colorado. There are limited exposures of time equivalent marine strata within a 100 km radius of the study area. The Big Kahuna sandstone has been correlated approximately 60 km from the study area in the subsurface (Leibovitz, 2010; Keeton, 2012). The location of potential paleo-shorelines are further explored in the discussion section.

COMPARISON TO MODERN FLUVIAL SYSTEMS

Slope of modern rivers

Quantitative studies of fluvial systems in the stratigraphic record are significant because they allow for direct comparison of these systems with modern systems, which assists in determining the best modern analog. The range of calculated paleo-slopes from the intervals within the Big Kahuna sandstone were compared to elevation profiles of modern rivers. Elevation profiles of eleven modern rivers were collected from Digital Elevation Models (DEM). These eleven rivers were chosen because they discharge into a large body of water and therefore have a theoretical backwater length. Rivers selected have a range of slopes, climatic conditions, planform morphologies and occur considered by some in various tectonic settings. Data used from these rivers is limited to 100 km from the mouth to compare their slopes to the estimates of the Williams Fork Formation.

DEMs are collected from the United States Geological Survey (USGS) and the literature. Both Shuttle Radar Topography Mission (SRTM) and Advanced Spaceborne Thermal Emission and Reflection Radiometer (ASTER) data is used with 1/3 to 1 arc second resolution. ASTER Global Digital Elevation Map (GDEM) data is used and is a product of The Ministry of Economy, Trade, and Industry (METI) and the National Aeronautics and Space Administration (NASA). DEMs of Italy are collected from the literature (Tarquini et al., 2007, 2012). Environmental Systems Research Institute (ESRI) mapping software, ArcMap 10.2, is used to trace channels and extract elevation data.

Figure 11 displays river elevation profiles and illustrates the relationship between slope and planform morphology. The x and y axis are in distance, while the top and right sides of the graph indicate points of constant slope. River elevation profiles are shown in different patterns which represent planform morphology: braided rivers are dashed lines, transitional rivers are dashed-dotted lines and meandering rivers are solid lines. Williams Fork Formation paleo-slope estimates are shown by shaded regions: green represents the average slope, red is the associated uncertainty (factor of 2) and yellow represents the uncertainty of the calculated range of slope estimates. Fading of slope estimations in the down dip direction is to emphasize

that the backwater length calculations are approximately, but not limited to, 100 km from the river mouth. The faded range of slope estimates are shown because the actual distance from the paleo-shoreline to the study area is unknown due to the limited outcrop exposure and preserved rock record.

Slope estimates of the studied interval (~10^{-4}) plot closest to the modern Adgie, Ili and Trinity Rivers (Fig. 11). These rivers have meandering and transitional (transitional to braided) planform morphologies. Elevation profiles of braided rivers have slopes greater than 10^{-3}. Maximum uncertainty of slope calculations would be similar to slope of the Trinity River and the Adige River. The metrics of paleo-slope estimations place the deposits of study outside of the slopes of modern braided rivers.

Parameter space of fluvial planform morphologies

The transition from meandering to braided planform morphologies have been quantified through empirical relationships involving flow depth, grain size, discharge and flow width (e.g. Leopold and Wolman, 1957; Parker, 1976; Kleinhans and Van den Berg, 2011). The majority of these studies involve comparing two or more of the above variables, and are based on modern fluvial systems. Discharge can be measured in modern fluvial systems, but is difficult to determine from the rock record. Flow depth, however, as discussed earlier, is more easily estimated, although there are uncertainties in estimating this value as well.

This study presents a semi-quantitative relationship between slope, bankfull flow depth and average bed sediment grain size with planform morphology. This study uses the term parameter space because these variables occur in certain ranges for planform morphologies. These three variables can be used to better interpret planform morphology from the stratigraphic record.

Data of modern fluvial systems was compiled from the literature (Schumm, 1968; Osterkamp et al., 1982; Church and Rood, 1983; Trampush, 2014). Values of river slope, bankfull flow depth and average bed sediment grain size of modern rivers are cross-plotted and are then compared to their planform morphology. Flow depth used refers to bankfull flow depth or channel dimensions of the two-year flood or the five-year flood. Grain size refers to

the average or 50th percentile grain size of the bed sediment and slope refers to river channel slope. See Appendix 3 for all data (over 430 points) on rivers mostly in North America.

Terminology of planform morphology used in this study is modified and paraphrased from Church and Rood (1983), see Table 4. Most definitions from Church and Rood (1983) remain unchanged, but the data has been reinterpreted due to modification of definitions and addition of definitions. Church and Rood (1983) have defined categories for anastomosed and braided/anastomosed planform morphologies. Upon evaluation of their raw database, systems that were originally classified with anastomosed are reclassified as braided or split with bars because anastomosed morphologies were not recognized (Makaske, 2001). The category of irregularly sinuous has been expanded into three categories: irregularly sinuous, irregular sinuous with meandering topography in floodplain and irregular sinuous with rapids. Due to strict criteria of classification, many rivers within the categories of irregularly sinuous and irregular sinuous with meandering topography in floodplain would be considered as a meandering planform morphology to most geologists. This classification was kept from Church and Rood (1983) to illustrate the differences in endmember planform morphologies (braided and meandering).

Cross-plots of slope, grain size and flow depth colored by planform morphology, are shown in Figure 12. Figures 12a,b display the gravel-sand transition by the gap in grain size data. Rivers tend to be gravel or sand dominated because granule gravel (2-4 mm) rivers are typically not observed (Parker and Cui, 1998; Cui and Parker, 1998). This gap is also a transition of slope, flow depth and planform morphology in the database. The modern Allt Dubhaig River contains a gravel-sand transition which is also a transition in slope and planform morphology (Ferguson and Ashworth, 1991). Figure 12a shows that increase in slope associates with an increase in grain size which has been previously established by the work of Schumm (1981). Figure 12c displays that an increase in slope relates to a decrease in flow depth. It is known that flow depth has a direct relationship with discharge and drainage area (Blum et al., 2013). It is also known that slope is indirectly related to discharge and drainage area (Wolman, 1955; Flint, 1974). Figure 12d shows the direct relationship between flow depth and drainage area. The

relationship is similar to previously published results (Blum et al., 2013).

Figure 13 is a 3D scatter plot of slope, average bed sediment grain size and bankfull flow depth. The colors represent the same planform morphologies as Figure 12 with the addition of grey shadows used strictly to illustrate data position. These graphs further display that certain planform morphologies are observed in ranges of slope, grain size and flow depth, see Figures 12a,b,c and 13. The results of this analysis are as follows.

1) Braided rivers typically have slopes greater than 10^{-3}. Braided rivers with slopes less than 10^{-3} in this database have glaciated headlands.

2) Fluvial systems characterized by chute channels and other minor secondary channels are dominantly observed in sediment >10 mm and slopes above 10^{-3}.

3) Rivers in the categories of meandering and irregular sinuous with meandering floodplain topography are dominantly observed in slopes less than 10^{-3}.

4) Rivers split with bars are typically observed with grain sizes >10 mm and in slopes >$3.0x10^{-4}$.

5) Rivers classified as irregular sinuous with rapids are observed in flow depths less than 1 m, steep slopes around 10^{-2} and grain sizes above 10 mm.

6) Rivers classified as irregularly sinuous are seen across all ranges of slope, grain size and flow depth. This wide spectrum illustrates that either this definition is too broad and requires further quantification of channel features for classification, or this is an easily obtainable equilibrium state for rivers in all types of systems. This wide range would raise the notion that this planform morphology is the most common type of river; not perfectly symmetrical in sinuosity and containing few to no sub-aerially exposed detached bars.

The trends discussed above are recorded in Table 5 and contains the range and 50^{th} percentile for a planform morphology's slope, grain size and flow depth organized by grain sizes less than and greater than 2 mm. Modern rivers with approximately 7 m flow depth, 10^{-4} slope and an average grain size of medium sand are typically irregularly sinuous, irregular sinuous with meandering floodplain topography or split with bars in planform morphology. Rivers with braided morphologies close to these calculated characteristics have glaciated headlands. End

member planform morphologies, such as braided, meandering and minor secondary channels, are observed in certain ranges of slope, grain size and flow depth. This is significant because all three of these parameters can be measured or estimated in the stratigraphic record. Slope, grain size and flow depth can provide quantitative guidance in stratigraphic interpretations of fluvial planform morphology through direct comparison to modern systems.

GEOCHRONOLOGY

Depositional ages of the non-marine Williams Fork Formation are hard to constrain because of the absence of ash beds and index fossils. Proposed ages involve correlations across substantial distances and biozones that allow for interpretation. Pollen stratigraphy analyses place the depositional age of the lowermost part of the formation near the Campanian-Maastrichtian boundary (Johnson and May, 1980; Patterson et al., 2003). However, there is little agreement on the age of the uppermost deposits of the formation using pollen stratigraphy and detrital zircon analyses (Johnson and May, 1980; Patterson et al., 2003; Laskowski et al., 2013). To improve age constraints detrital zircons were collected near the lower and upper contacts, (Fig. 2). A maximum depositional age (MDA) can be estimated from the youngest population of detrital zircon grains in a sample, and may not represent the absolute age of the formation.

Pollen stratigraphy analyses of mudstones from the Williams Fork Formation yield conflicting ages for this formation, with a 5-10 Ma difference on the age of the upper contact. Based on palynologic samples collected from the southwestern Piceance Basin, Johnson and May (1980) propose that deposition of the Williams Fork Formation began in the late Campanian to early Maastrichtian and ended at the Maastrichtian – Paleocene boundary. Patterson et al. (2003) used palynologic samples from well cuttings from the north central part of the Piceance Basin, and interpreted the upper formation boundary of the Williams Fork to occur in the middle to upper Paleocene. Their samples, however, contained both Cretaceous and Paleocene palynomorphs, and the Cretaceous palynomorphs were interpreted as reworked (Patterson et al., 2003).

Ammonite zones have been used to date strata underlying the Williams Fork Formation.

Marine strata of the Pierre Shale underlying the Trout Creek Sandstone Member of the Iles Formation, in Kremmling, CO, contain the ammonite zone *Didymoceras cheyennense* (Izett et al., 1971). The Trout Creek Sandstone Member is time equivalent to the Rollins Sandstone Member (Iles Fm.), which underlies the Williams Fork Formation in the study area (Fisher et al., 1960; Johnson and May 1980; Madden, 1989). The ammonite zone *D. cheyennense* yields Ar-Ar dates from sanidine of 73.8 ± 0.1 Ma (Izett et al., 1998).

Ammonite zones are dated using volcaniclastic beds from marine strata equivalent to the Twentymile and Lion Canyon Sandstone Members of the Williams Fork Formation, which are exposed in the northeast Piceance and southern Sand Wash Basins, (Fig. 14) (Roehler, 1990; Franczyk et al., 1992; Brownfield et al., 2000). These two marine sandstones are the only marine sandstones within the Williams Fork Formation. Zapp and Cobban (1960) and Roehler (1990) correlated the Twentymile sandstone to the middle Williams Fork Formation in the northeast Piceance and southern Sand Wash Basin, based on ammonite biozones. The Twentymile Sandstone Member contains the ammonite zone *Baculites reesidei*, and yields Ar-Ar dates from sanidine of 72.94 ± 0.45 Ma (Baadsgaard, 1993; Cobban et al., 2006). The Lion Canyon Sandstone Member is stratigraphically beneath the Price Coal, above the Goff Coal and is approximately equivalent to the middle to upper Williams Fork Formation in the Danforth Hills Coal Field, (Fig. 14) (Hancock and Eby, 1930; Murray, 1966; Brownfield et al., 2000; Leibovitz, 2010). Several studies have correlated the Lion Canyon Sandstone Member to intervals outside of the Piceance Basin; it is proposed to be equivalent to the Fox Hills Sandstone and/or an isolated marine sandstone within the Lewis Shale in the Sand Wash and Washakie Basins, in Colorado and Wyoming, based on marker beds (Zapp and Cobban, 1960; Brownfield et al., 2000). The Lewis Shale overlies the Williams Fork Formation in the Sand Wash Basin (Roehler, 1990). The Lion Canyon Sandstone Member contains the ammonite zone *Baculites clinolobatus* (Franczyk et al., 1992), which is associated with a bentonite dated at 69.59 ± 0.36 Ma, using Ar-Ar of sanidine (Obradovich, 1993; Cobban et al., 2006). In the northeast Piceance Basin, both sandstone members have been interpreted to have a depositional strike of northwest to southeast (Zapp and Cobban, 1960; Franczyk et al., 1992;

Leibovitz, 2010).

An altered ash deposit near Craig, CO, known as the Yampa Bed, is located within the C-D coal bed of the Williams Fork Formation, (Fig. 14), and is proposed to be equivalent to the Fairfield Coal Group, which includes the Cameo Coal Seam, at the base of the Williams Fork Formation (Brownfield and Johnson, 1986; Johnson and Brownfield, 1988; Brownfield et al., 2000; Johnson et al., 2000). The altered ash bed is dated at 72.5 ± 5.1 Ma, using K-Ar dating of andesine (Brownfield and Johnson, 2008).

Detrital zircon samples of the Williams Fork Formation were collected by Laskowski et al. (2013) from drill cuttings and core from the middle and upper portion of the Williams Fork Formation from wells in the Piceance Creek and Love Ranch fields. Laskowski et al. (2013) interpreted maximum depositional ages from the middle and upper sections of the formation to be Maastrichtian to Selandian in age. The youngest grain ages used for maximum depositional ages in the middle section yielded 71.7 ± 2.0 Ma, 64.7 ± 0.4 Ma and 61.6 ± 0.8 Ma. The youngest grain ages used for maximum depositional ages in the upper section yielded 67.3 ± 5.9 Ma and 63.9 ± 3.8 Ma.

In this study, samples were collected for detrital zircon analysis from fluvial sandstones at the base and top of the Williams Fork Formation, from outcrops near the study area in Coal Canyon and near Mesa, CO (see Fig. 2). The sample from the base of the formation (sample WF-04) is from a current-rippled, fine-grained sandstone, interpreted as a fluvial channel-fill sandstone. The fluvial sandstone is within the Cameo Coal seam located in Coal Canyon, and sampled at ~5 m above the Rollins Sandstone Member – Williams Fork Formation contact. The sample from the top of the formation (sample WF-01) was taken from a wedge-shaped cross-bedded medium-grained sandstone, interpreted as part of an amalgamated channel-belt sandstone. The outcrop is approximately 10 m below the Williams Fork Formation – Wasatch Formation contact and located near Mesa, CO.

Methods for zircon extraction are paraphrased from Lippert (2014). U-Pb analyses of detrital zircon grains from the two samples collected were obtained by laser ablation inductively coupled mass spectrometry (LA-ICP-MS). Zircon grains were separated using

standard mineral separation techniques. At least 300 grains per sample were handpicked under a binocular microscope and mounted in an epoxy disc that was polished to expose the grains' internal structures. Appendix 4a lists the complete methods of mineral separation and sample preparation.

Two samples (WF-01 & WF-04) were analyzed at the IGL (Isotope Geochemistry Lab), Department of Geology, The University of Kansas, using a Thermo Scientific Element2 ICP-MS, attached to a Photon Machines Analyte.G2 193 nm ArF excimer laser ablation system (Appendix 4b). Circular spots of 20 µm diameter were ablated with the laser at 2.0 J cm^{-2} fluency and 10 Hz repetition rate. A carrier gas of He transported the ablated material to the ICP. Elemental fractionation, downhole fractionation and calibration drift were corrected by bracketing measurements of unknowns with GJ1 zircon reference material (Jackson et al., 2004) and data reduction using the VizualAge data reduction scheme (Petrus and Kamber, 2012) for the IOLITE software package (Paton et al., 2010; 2011). Results for the zircon reference material GJ1 and secondary zircon reference material Plešovice and Fish Canyon Tuff are shown in Appendix 4c.

Concordia plots, concordia ages and weighted mean U-Pb ages were prepared and calculated using the ISOPLOT software (Ludwig, 2008). The results of the U-Pb analyses are shown in Appendix 4d for the detrital zircons. Grains determined to be in the youngest populations are in bold font and shaded rows. The youngest population of grains is determined by the mean age of a group of at least 3 grains whose ages overlap within 2 standard deviations (σ) following the rationale of Dickinson and Gehrels (2009).

Zircons analyses were inspected for reliability. They were not used for calculations or plots if they were more than 5% discordant, less than 8 seconds in duration, or had abnormally high uncertainties. Discordance criteria for exclusion from calculations were uncertainty weighted age differences greater than 1.2 for $^{206}Pb/^{238}U$ grains younger than 1000 Ma, or the $^{207}Pb/^{235}U$ versus $^{206}Pb/^{238}U$ discordance greater than 5% for $^{207}Pb/^{206}Pb$ dates of grains older than 1000 Ma.

LA-ICP-MS yielded 507 acceptable detrital zircon analyses. Figure 15 are Tera-Wasserburg concordia diagrams of the youngest detrital zircon populations. The plotted line is the

calculated age in millions of years. The interpreted youngest zircon results for each sample are plotted in black for the error ellipses of single grain measurements (2σ), the error ellipses for the estimated MDA are shown in blue (2σ).

The MDA for the base of the formation (WF-04) yielded 74.09 ± 0.48 Ma (n=9; MSWD=1.14; probability=0.31). Therefore, the base of the formation is likely to not be older than this age. The sample from near the top of the formation (WF-01) yielded a MDA of 70.1 ± 1.8 Ma (n=3; MSWD=1.11; probability=0.35). Consequently, the top of the formation is likely to not be older than this age. Detrital zircon analyses are within the same range of the previous palynomorphic dates, Campanian-Maastrichtian to late Maastrichtian-Paleocene (Johnson and May, 1980; Patterson et al., 2003). This reinforces previously published palynomorph ages based on biozone stratigraphy.

Detrital zircons were also used for provenance analysis by plotting age versus normalized frequency for the entire samples in a kernel density plot, see Figure 16. Highlighted regions are typical sources for detrital zircons in North America based on age and peak height correlates to abundance. Major peaks are observed around 73 and 165 Ma, which are interpreted to be western Cordilleran signals. Another major peak is observed around 1640 and 1700 Ma, which is interpreted to be a Yavapai/Mazatzal signal. It is interpreted that detrital zircons were derived from the Sevier Fold and Thrust Belt, and the youngest zircons were sourced from Cretaceous arc magmatism of the Cordillera. These findings are in agreement with a larger study using detrital zircons from the Colorado Plateau and Wyoming (Laskowski et al., 2013).

Potential source terrains for sediment within the Williams Fork Formation were determined by comparison of detrital zircon ages to igneous deposits of similar age and close proximity. Locations and ages of igneous bodies were collected from the western North American Volcanic and intrusive rock Database (NAVDAT). Values used were within the range of the youngest detrital zircon population samples collected in this study. Potential source areas were limited to 1,000 km of the study area. Figure 17a shows the location of intermediate to felsic volcanic rocks that have been radiometrically dated to between 75-69 Ma. This range represents the oldest and youngest ages in the youngest detrital zircon populations of the two

samples from this study, shown in Figure 17b. The closest potential source areas are near the Nevada – Utah border and in central Nevada. In the middle to early Cenozoic, basin and range extension increased the area of Nevada and western Utah. Palinspastic reconstruction of that region by McQuarrie and Wernicke (2005), place dated igneous bodies at the time of deposition of the Williams Fork Formation near the Nevada-Utah border or inside western Utah (Fig. 17a).

It is possible to reconstruct the drainage area by knowing the source terrain and hydrodynamics of the ancient fluvial system. Bankfull flow depths of 7 m calculated in this study suggest that the fluvial system was comparable in size to modern fluvial systems with drainage areas on the order of 10,000's of km^2, likely around 60,000 km^2. This is calculated from the regression of modern river data in Figure 12d. This regression is similar to other published relationships relating flow depth or discharge to drainage area (Syvitski and Milliman, 2007; Sømme et al., 2009; Blum et al., 2013). A potential paleo-drainage reconstruction for the Williams Fork Formation is shown in Figure 17a.

DISCUSSION

Fluvial deposits within the amalgamated sandstone have the following characteristics: average grain size of medium lower sand, interpreted bankfull flow depth of ~7 m, average channel-belt W:T ratios within the backwater reach (46:1), interpreted low gradient system (~10^{-4}), interpreted backwater length on the order of 100 km and an interpreted drainage area approximately 60,000 km^2. Based on these estimates individual channel-belts within the Big Kahuna sandstone would represent a low sinuosity and low gradient fluvial system within the backwater zone. Modern fluvial systems with similar grain size, flow depth and slope have planform morphologies that are irregularly sinuous, irregular sinuous with meandering floodplain topography or split with bars (terminology of Table 4). Analysis of the modern fluvial dataset shows that slope and grain size have the most influence on determining the type of planform morphology. This hydrodynamic analysis contrasts with previous interpretations of the Big Kahuna sandstone as deposits of a high gradient system with a braided planform morphology (Cole and Cumella, 2005; German, 2006; Foster, 2010; Ost, 2010; Keeton, 2015).

Based on facies models, previous studies have labeled the Big Kahuna sandstone as a result

of braided planform morphology. Evidence is based on physical observations such as lateral continuous extent of the sandstone, discontinuous and rare mudstone intervals, many internal scours, wedge and planar tabular cross-bed dominated sandstones, low sinuosity calculations from cross-beds and low abundance of lateral accretion deposits. These features are the standard for braided river deposits in facies models (e.g. Rust, 1977; Walker and Cant, 1984). Meandering fluvial deposits, based on facies models, have nearly opposite physical observations relative to braided systems. Evidence includes ribbon (W:T < 15) type sandstones, abundance of mudstone intervals, high sinuosity calculations from cross-beds and abundance of lateral accretion deposits (e.g. Bernard et al., 1962; Allen, 1963; Ore, 1964; Walker and Cant, 1984; Collinson, 2009). Physical observations of the Big Kahuna sandstone fit the facies model for braided planform morphologies. The features listed for the two facies models are considered by some to be non-unique to individual fluvial planform morphologies (Bluck, 1971; Jackson, 1976, 1978; Collinson, 1978; Harvey et al., 1985; Miall, 1985; Bristow, 1987; Shukla et al., 1999; Bridge, 2006; Ruben et al., 2006; Paola et al., 2009; Ethridge, 2010; Hartley et al., 2015). These features (i.e. sandstone geometry, abundance of mudstone intervals, sinuosity) are critical to understanding the fluvial systems' autogenic signals and response to allogenic forcings. These features, however, do not provide information on drivers that determine the size of the system. Grain size and discharge determine many features in fluvial systems such as flow depth and slope, and therefore also planform morphology (e.g. Leopold and Wolman, 1957; Parker, 1976; Williams, 1978; Schumm, 1981; Osterkamp et al., 1983; Church, 2006; Kleinhans and Van den Berg, 2011; Blum et al., 2013; Trampush et al., 2014).

Hydrodynamic calculations of the Big Kahuna sandstone calculated in this study are similar to flow depths estimated in previous studies (German, 2006; Keeton, 2012). A reproducible flow depth makes predictions of dependent features more reliable, such as slope or drainage area. As discussed earlier, calculations of paleo-flow depth include a range of values and all uncertainties included in the model of calculating flow depth are further propagated in dependent calculations (e.g. slope and backwater). Paleo-slope was estimated within a factor of 2 from published empirical relations involving grain size and flow depth. Estimates of grain size,

flow depth and slope in the stratigraphic record allow a direct comparison with over 430 modern rivers. Provided the paleo-hydrodynamic calculations are correct, they suggest that the outcrops in the study area represent a fluvial system that had more meandering-like qualities than braided in planform morphology.

Channel-belt width to thickness ratios and sinuosity calculations indicate that there was limited lateral migration of the channels. Reduction of channel-belt migration is observed within the backwater reach of modern fluvial systems, which is independent of planform morphology. Within the channels, bars migrated by both downstream and lateral accretion. The presence of isolated unit bars and lack of compound bars indicates a system with high deposition rates with a lack of multiple erosional and depositional events. This led to a simpler stratigraphic pattern where unit bars were quickly buried from the migration of smaller bed forms. Channel-belts with limited lateral migration seem juxtaposed with the observation of the large sheet sandstone. It is interpreted that low rates of accommodation encouraged cannibalization of older deposits, which over time amalgamated the channel-belt sandstones.

Channel-belt width to thickness ratios indicate that the fluvial system at the study area was within the backwater reach. Backwater length calculations provide a first order estimate of 100 km during the time of fluvial deposition. Time equivalent shorelines for the Big Kahuna sandstone have not been identified to the east of the study area. The only marine sandstones proposed as equivalent to the Williams Fork Formation occur in the northeast Piceance Basin and southern Sand Wash Basin of northwest Colorado: The Twentymile and Lion Canyon Sandstone Members of the Williams Fork Formation. The Twentymile Sandstone Member is ~140 km from the study area (Roehler, 1990; Brownfield and Johnson, 2008) and the Lion Canyon Sandstone is ~85 km from the study area (Leibovitz, 2010).

A basinwide subsurface study of the Williams Fork Formation in the Piceance Basin identified a large linear northeast trending sandstone, up to 120 m in thickness and ~30 km in width (Leibovitz, 2010). Determined from previous outcrop and paired outcrop and subsurface studies, this sandstone is in a similar stratigraphic position to the Big Kahuna sandstone (Ost, 2010; Keeton, 2015) and has been informally named the Upper Williams Fork (UWF) Sandstone

(Leibovitz, 2010). The UWF sandstone is approximately 340 m above the base of the formation in the southern Piceance Basin. The UWF sandstone is similar to the Big Kahuna sandstone; a thick laterally continuous sandstone trending northeast, containing few upward fining successions (Leibovitz, 2010).

If the trend of the UWF sandstone is projected approximately 6 km to the southeast, the study area would fall within its path and the observed outcrop thickness (~75 m) would be similar to the subsurface thickness, see Figure 18. The subsurface isopach by Leibovitz (2010) is a map of the same sandstone discussed in this study. Previous studies interpreted that the abnormal thickness and large lateral extent of the Big Kahuna sandstone was initiated from a large drop in base-level (Leibovitz, 2010; Ost, 2010). The Big Kahuna sandstone is interpreted to be part of the deposits of an incised valley fill with the gross dimensions of approximately 120 m thickness and 30 km width (Leibovitz, 2010).

Modern fluvial systems within the backwater zone are typically distributive in planform morphology. The Big Kahuna sandstone was deposited within the backwater reach in the study area, however, the planform morphology would likely be contributive because it was contained by a valley. A subsurface study by Foster (2010) noted a sharp down-dip change in net-to-gross (N:G) ratio of sandstone and fluvial architecture of the Big Kahuna sandstone. In the Parachute Field (location on Fig. 2), the high N:G linear sandstone, as shown by Leibovitz (2010), becomes less defined in its lateral extent and the N:G ratio drops. Foster (2010) interpreted this change in fluvial deposition to a normal fault, with a hanging wall that hada shallower slope causing the fluvial morphology to become distributive. While a fault could have changed the style of fluvial deposition, this study interprets that the change to a distributive morphology reflects that the fluvial system became unconfined within the backwater zone. The Nile, Orinoco and Rhone Rivers are modern examples of fluvial systems within their backwater reach that become distributive in planform morphology after leaving confinement of a valley (Hartley et al., 2017). The Big Kahuna sandstone within the valley was likely contributive in planform morphology and after leaving the confinement of the valley, in Parachute Field, the fluvial system became distributive in planform morphology.

Subsurface studies have shown that the Big Kahuna sandstone, near the study area, is characterized by discrete lithological boundaries that have high erosional relief and large lateral extent (Foster, 2010; Leibovitz, 2010). Previous studies have interpreted the Big Kahuna sandstone as the fill of an incised valley (Leibovitz, 2010; Ost, 2010). Incised valleys form by a lowering of base-level, resulting in fluvial incision and valley widening (Shanley and McCabe, 1994). During valley widening, older fluvial deposits within the valley are reworked and removed (Posamentier and Vail, 1988; Van Wagoner et al., 1990; Strong and Paola, 2006). Although the majority of fluvial incision occurs during the base-level fall, valley widening continues to occur during the subsequent rise with continued removal of older deposits and deposition of younger deposits within the valley. The incisional relief and erosional surface are the sole record of the incisional phase of valley development. Younger deposits from the base-level rise, including the Big Kahuna sandstone, compose the valley fill and overprint older deposits within the valley.

Subsequent base-level rise is often episodic, resulting in a multistorey valley fill fluvial sandstone (Shanley and McCabe, 1994; Amorosi et al., 2008). Rivers preferentially occupy low lying topography in valleys and reoccupy older channel-belt positions (Posamentier and Vail, 1988; Shanley and McCabe, 1994; Hajek et al., 2010). Channel-belt migration results in reworking of valley fill deposits during each base-level position. Experimental studies of fluvial systems in rapidly subsiding valleys show that channel-belt position shifts laterally because of the relief of previous deposits. Repetition of shifting channel-belt position produces a sheet-like architecture (Sheets et al., 2002; Martin et al., 2011).

This sheet-forming process repeats with each base-level rise, which records the beginning of each stratal package identified by Ost (2010). Within Ost's (2010) unit 2 of the Williams Fork Formation, sheet sandstones (Ost's subunit 2a) occur repeatedly in the identified stratal pattern (Fig. 1). Ost (2010) interpreted that the erosion associated with the base of each subunit 2a was not significant enough to completely remove underlying stratal packages. Ost (2010) interpreted the deposition of the Big Kahuna sandstone to represent the amalgamation of two stratal packages. The base-level fall associated with the uppermost subunit 2a within the Big

Kahuna sandstone exhibits a greater amount of downcutting than typically associated with the basal erosion surface of subunit 2a. This is interpreted to result from a significantly larger magnitude of base-level fall, one which removed the underlying subunits 2b and 2c and resulting in the amalgamation of two subunits 2a. Leibovitz (2010) also interpreted the incised valley fill in his study area as forming from a two-stage event.

If the Big Kahuna sandstone represents an incised valley fill resulting from base-level rise, then the basal surface represents all that remains of the base-level fall. Fluvial deposits within the valley fill correspond to a relative rise in base-level, and it is for this stage of valley fill that backwater length is possible to be calculated. The backwater length estimated at 100 km represents the approximate distance to the paleo-shoreline during the late lowstand to early transgression. The lowstand shoreline associated with the erosional phase of valley development was significantly further basinward of the transgressive paleo-shoreline. The backwater length for this stage is indeterminable. The backwater length for the erosional phase of incised valley development is indeterminable because all strata deposited during that time were replaced by deposits during the subsequent base-level rise (Strong and Paola, 2006). There is no stratigraphic record of the lowstand phase in the study area to calculate the backwater length. Any estimate of backwater length for the lowstand phase of valley development is therefore limited to a position relative to the transgressive shoreline, basinward of the 100 km distance calculated in this study.

During the erosional stage of incised valley development, a significant amount of sediment was transported basinward to the lowstand paleo-shoreline. Given the size of the incised valley fill, the lowstand deposit should be substantial. Ost (2010) proposed approximately 19 episodes of base-level fall within the middle and upper Williams Fork Formation. Each base-level fall should have an associated lowstand shoreline. Ost (2010) identified 19 amalgamated sandstones (subunit 2a) at the base of each of the 19 stratal packages. Each subunit 2a should have a time equivalent marine lowstand deposit. The lowstand deposits should result in a thick clastic succession basinward of the study area. These lowstand marine deposits have not been identified. While lowstand shorelines should be well developed, typically, transgressive

shoreline sandstones are poorly preserved in the clastic system because most of the sand in the transgressive stage is stored updip in the continental realm. Transgressive shorelines are typically sediment-starved and often preserved only by a ravinement surface (Posamentier and Vail, 1988; Boyd et al., 1992; Cattaneo and Steel, 2003). Modern transgressive shorelines are dominated by the rollover process and beach sand is constantly reworked as the shoreline moves landward.

The Twentymile and the Lion Canyon Sandstone Members represent deposits of transgressive shorelines of the Williams Fork Formation (Roehler, 1990; Franczyk et al., 1992; Leibovitz, 2010). The Lion Canyon Sandstone Member falls within the estimated backwater length for this study, but the coeval non-marine section for the Lion Canyon Sandstone is unknown. The Lion Canyon Sandstone Member has been correlated to be approximately time equivalent to the middle to upper section of the Williams Fork Formation (Brownfield et al., 2000; Leibovitz, 2010). The Lion Canyon Sandstone Member has not been proposed to be time equivalent to the Big Kahuna sandstone.

The Big Kahuna sandstone is overlain by an interval of fluvial sandstones encased in overbank deposits. Fluvial sandstones within this overlying interval (Ost's subunit 2b) are characterized by a sharp base, contain upward fining grain size trends and have thicknesses ranging from 8 – 16 m (Ost, 2010), see Figure 1. Fluvial sandstones within this interval are laterally amalgamated, but show relatively less vertical amalgamation than the underlying sandstone interval (Ost's subunit 2a). Subunit 2c, overlying subunit 2b, composes thin (≤1 m) lenticular sandstones encased in mudstone. Subunit 2c is dominated by overbank deposits and is the final subunit of the stratal package defined by Ost (2010) which shows an overall vertical decrease in net to gross sandstone.

Compared to the amalgamated sandstone of subunit 2a, the overlying strata (subunit 2b) have greater preservation of overbank deposits. In subunit 2a, channel-belt migration is proposed to be constrained to a valley that caused reworking of floodplain deposits by numerous avulsion events, resulting in a lateral and vertical amalgamation of fluvial sandstones. Deposits vertically amalgamated due to low rates of accommodation. During

deposition of subunit 2b, it is interpreted that the channel-belts were no longer restricted to a valley, and the frequency of avulsions relatively decreased in the observed area. This process paired with relatively larger rates of accommodation in subunit 2b resulted in less reworking of overbank deposits and greater preservation of floodplain sediments. Avulsion paired with vertical accommodation resulted in the vertical alternation of fluvial sands and overbank fines which produced the multistorey architecture of subunit 2b. Chamberlin and Hajek (2015) interpret a similar process to form comparable multistorey sandstones within the lower Williams Fork Formation. Avulsions can cause channel-belt clustering, which can be coeval with allogenic processes such as relative sea-level rise (Hajek et al., 2010; Chamberlin and Hajek, 2015; Heller et al., 2015; Hampson, 2016). Greater vertical accumulation of overbank deposits within subunit 2b and 2c suggests a higher accommodation setting than subunit 2a. A trend is defined whereby accommodation generally increases within the stratal packages identified by Ost (2010). Higher accommodation is likely caused by increased tectonic subsidence or relative sea-level rise. It is plausible that both factors were present in the foreland basin setting.

The fluvial architecture of the Williams Fork Formation is similar to the Late Quaternary deposits of the Po River of the Po-Adriatic Basin, northeastern Italy. Fluvial deposits of the Po River contain several records of base-level change and have been described in detail by Amorosi et al. (2008). The following is paraphrased from their work.

The Po River incised multiple times during the Late Quaternary, and each incision event was associated with a eustatic fall. Each incision event produced an incised valley, which was later filled by amalgamated fluvial sandstones. Incised valleys are separated by organic-rich overbank deposits with thin lenticular fluvial sandbodies. Base-level changes are recorded by alternating deposits of amalgamated fluvial sandstones (base-level fall) and strata dominated by organic-rich overbank deposits (base-level rise).

Amorosi et al. (2008) proposed that the amalgamated sandstones were deposited during sea-level lowstand to early transgression and that the overbank dominated intervals were deposited during times of transgression and sea-level highstand. This produced a vertical succession of alternating amalgamated sandstones and overbank dominated strata, similar to

what has been described in the middle part of the Williams Fork Formation.

CONCLUSIONS

In this paper, a 75 m thick, amalgamated, medium-lower grain-sized fluvial sandstone from the Williams Fork Formation is described from outcrop. Facies descriptions and measurements of internal geometries allow for a paleo-hydrodynamic analysis. This sandstone is within the middle part of the Williams Fork Formation and is informally called the Big Kahuna sandstone. Facies descriptions and paleo-hydrodynamics calculations from this study combined with modern fluvial data allow a direct comparison between the stratigraphic record and modern fluvial systems. Hydrodynamic calculations were applied to sandstone deposits within interpreted channel-belts. Using paleo-flow depth and paleo-slope, values derived from grain size and cross-bed thickness, a planform morphology was interpreted by comparison to data of modern river's flow depth, slope and grain size. The channel-belts of study are interpreted to represent low sinuosity systems, that in planform morphology had no consistent meander wavelength and few to no subaerially exposed bars. From this study, the channel-belts' planform morphology is classified as either irregularly sinuous, irregular sinuous with meandering floodplain topography or split with bars. The amalgamated sandstone occurs at the base of a previously recognized stratal package within this formation and its analyses provides a better understanding of the stratal pattern. The amalgamated sandstone is underlain by a surface that represents base-level fall and forms a sheet geometry that fills an incised valley. The amalgamated sandstone records deposition during base-level rise associated with late lowstand to early transgressive events.

This study also provides data illustrating modern fluvial scaling relationships and how different planform morphologies occur with certain ranges of grain size, slope and flow depth. Geologists can use modern fluvial relationships to better interpret the stratigraphic record. Important characteristics of modern systems, such as average bed sediment grain size and bankfull flow depth can also be determined in the stratigraphic record, which aids in the direct comparison of modern and ancient fluvial systems. Furthermore, grain size and flow depth are related to most features within fluvial systems (i.e. channel slope), which allows further

quantitative comparison and prediction. It is proposed that these variables (grain size, channel slope and flow depth) can be used as a semi-quantitative method to predict planform morphology in the stratigraphic record. The most important step in applying these relations to the rock record is the ability to accurately identify paleo-flow depth and paleo-slope because most fluvial features are closely related to flow depth.

REFERNECES:

ADAMS, M.M., AND BHATTACHARYA, J.P., 2005, No change in fluvial style across a sequence boundary, Cretaceous Blackhawk and Castlegate Formations of central Utah, USA: Journal of Sedimentary Research, v. 75, p. 1038-1051.

ALLEN, J.R.L., 1963, Henry Clifton Sorby and the sedimentary structures of sands and sandstones in relation to flow conditions: Sedimentology, v. 42, p. 223-228.

AMOROSI, A., PAVESI, M., LUCCHI, M.R., SARTI, G., AND PICCIN, A., 2008, Climatic signature of cyclic fluvial architecture from the Quaternary of the central Po Plain, Italy: Sedimentary Geology, v. 209, p. 58-68.

ASCHOFF, J., AND STEEL, R., 2011, Anomalous clastic wedge development during the Sevier-Laramide transition, North American Cordilleran foreland basin, USA: Geological Society of America, Bulletin, v. 123, p. 1822-1835.

BAADSGAARD, H., LERBEKMO, J.F., WIJBRANS, J.R., SWISHER III, C.C., AND FANNING, M., 1993, Multimethod radiometric age for a bentonite near the top of the Baculites reesidei Zone of southwestern Saskatchewan (Campanian-Maastrichtian stage boundary?): Canadian Journal of Earth Sciences, v. 30, p. 769-775.

BERNARD, H.A., LEBLANC, R.J., AND MAJOR, C.J., 1962, Recent and Pleistocene geology of southeast Texas, *in* Rainwater, E.H., and Zingula, R.P., eds., Geology of the Gulf Coast and centeral Texas: Geological Society of America, Guidebook for 1962 Annual Meeting, p. 175-224.

BHATTACHARYA, J.P., COPELAND, P., LAWTON, T.F., AND HOLBROOK, J., 2016, Estimation of source area, river paleo-discharge, paleoslope, and sediment budgets of linked deep-time depositional systems and implications for hydrocarbon potential: Earth-Science Reviews, v. 153, p. 77-110.

BHATTACHARYA, J.P., AND TYE, R.S., 2004, Searching for modern Ferron analogs and application to subsurface interpretation: Regional to wellbore analog for fluvial-deltaic reservoir modeling: The Ferron Sandstone of Utah: American Association of Petroleum Geologists, Studies in Geology, v. 50, p. 39-57.

BLUCK, B.J., 1971, Sedimentation in the meandering River Endrick: Scottish Journal of Geology, v. 7, p. 93-138.

BLUM, M.D., MARTIN, J., MILLIKEN, K., AND GARVIN, M., 2013, Paleovalley systems: insights from Quaternary analogs and experiments: Earth-Science Reviews, v. 116, p. 128-169.

BOYD, R., DALRYMPLE, R., AND ZAITLIN, B.A., 1992, Classification of clastic coastal depositional environments: Sedimentary Geology, v. 80, p. 139-150.

BRIDGE, J.S., 2003, Rivers and floodplains: forms, processes, and sedimentary record: Oxford, Blackwell Scientific Publishing, 491 p.

BRIDGE, J.S., 2006, Fluvial facies models: recent developments: *in* Posamentier, H.W., Walker, R.G., eds., Facies Models Revisited: SEPM, Special Publication, v. 84, p. 85-170.

BRISTOW, C.S., 1987, Brahmaputra River: channel migration and deposition, *in* Ethridge, F.G., Flores, R.M. and Harvey, M.D., eds., Recent Developments in Fluvial Sedimentology: Contributions from the Third International Fluvial Sedimentology Conference: SEPM, Special Publication, v. 39, p. 63-74.

BROWNFIELD, M.E., AND JOHNSON, E.A., 1986, A regionally extensive altered air-fall ash for use in

correlation of lithofacies in the Upper Cretaceous Williams Fork Formation, northeastern Piceance Creek and southern Sand Wash basins, Colorado: *in* Stone, D.S., ed., New interpretations of northwest Colorado geology: Rocky Mountain Association of Geologists 1986 symposium, p. 293-295.

BROWNFIELD, M.E., AND JOHNSON, E.A., 2008, The Yampa Bed - a regionally extensive tonstein in the Williams Fork Formation, Northwestern Piceance Creek and Southern Sand Wash Basins, Colorado: U.S. Geological Survey, Scientific Investigations, Report 2008-5033, 32 p.

BROWNFIELD, M.E., ROBERTS, L.N.R., JOHNSON, E.A., AND MERCIER, T.J., 2000, Assessment of the distribution and resources of coal in the Fairfield Group of the Williams Fork Formation, Danforth Hills coal field, northwest Colorado: Geologic Assessment of Coal in the Colorado Plateau: Arizona, Colorado, New Mexico, and Utah, Chapter M, U.S. Geological Survey, Professional Paper 1625-B, p. 1-19.

CATTANEO, A., AND STEEL, R.J., 2003, Transgressive deposits: a review of their variability: Earth-Science Reviews, v. 62, p. 187-228.

CHAMBERLIN, E.P., AND HAJEK, E.A., 2015, Interpreting paleo-avulsion dynamics from multistory sand bodies: Journal of Sedimentary Research, v. 85, p. 82-94.

CHEN, S., STEEL, R.J., DIXON, J.F., AND OSMAN, A., 2014, Facies and architecture of a tide-dominated segment of the Late Pliocene Orinoco Delta (Morne L'Enfer Formation) SW Trinidad: Marine and Petroleum Geology, v. 57, p. 208-232.

CHURCH, M., AND ROOD, K., 1983, Catalogue of alluvial river channel regime data. Department of Geography, University of British Columbia, Vancouver, Canada, 99 p.

COBBAN, W.A., WALASZCZYK, I., OBRADOVICH, J.D., AND MCKINNEY, K.C., 2006, A USGS zonal table for the Upper Cretaceous middle Cenomanian-Maastrichtian of the Western Interior of the United States based on ammonites, inoceramids, and radiometric ages: U.S. Geological Survey, Open-File Report 2006–1250, 46 p.

COLE, R.D., AND CUMELLA, S.P., 2003, Stratigraphic architecture and reservoir characteristics of the Mesaverde Group, southern Piceance Basin, Colorado: *in* Peterson, K.M., Olson, T.M., and Anderson, D.S., eds., Piceance Basin 2003 Guidebook: Denver, Colorado, Rocky Mountain Association of Geologists, p. 385-442.

COLE, R.D., AND CUMELLA, S.P., 2005, Sand-body architecture in the lower Williams Fork Formation (Upper Cretaceous), Coal Canyon, Colorado, with comparison to the Piceance Basin subsurface, Cretaceous sand body geometries in the Piceance Basin area of northwest Colorado: The Mountain Geologist, v. 42, p. 85-107.

COLLINSON, J.D., 1978, Vertical sequence and sand body shape in alluvial sequences, *in* Miall, A.D. ed., Fluvial Sedimentology: Canadian Society of Petroleum Geologists Memoir, v. 5, p. 577-586.

COLLINSON, J.D., 2009, Alluvial Sediments, *in* Reading, H.G., ed., Sedimentary environments: processes, facies and stratigraphy, John Wiley & Sons.

COOPER, M.R., 1977, Eustacy during the Cretaceous: its implications and importance: Palaeogeography, Palaeoclimatology, Palaeoecology, v. 22, p. 1-60.

CUI, Y., AND PARKER, G., 1998, The arrested gravel front: stable gravel-sand transitions in rivers,

Part 2: General numerical solution: Journal of Hydraulic Research, v. 36, p. 159-182.
DAVIDSON, S.K., AND NORTH, C.P., 2009, Geomorphological regional curves for prediction of drainage area and screening modern analogues for rivers in the rock record: Journal of Sedimentary Research, v. 79, p. 773-792.
DECELLES, P.G., AND COOGAN, J.C., 2006, Regional structure and kinematic history of the Sevier fold-and-thrust belt, central Utah: Geological Society of America, Bulletin, v. 118, p. 841-864.
DENNIS, K.J., COCHRAN, J.K., LANDMAN, N.H., AND SCHRAG, D.P., 2013, The climate of the Late Cretaceous: new insights from the application of the carbonate clumped isotope thermometer to Western Interior Seaway macrofossil: Earth and Planetary Science Letters, v. 362, p. 51-65.
DICKINSON, W.R., AND GEHRELS, G.E., 2009, Use of U–Pb ages of detrital zircons to infer maximum depositional ages of strata: a test against a Colorado Plateau Mesozoic database: Earth and Planetary Science Letters, v. 288, p. 115-125.
ETHRIDGE, F.G., 2010, Interpretation of ancient fluvial channel deposits: review and recommendations: *in* Stephanie, K., Davidson, S.K., Leleu, S., North, C.P., eds., From River to Rock Record: SEPM, Special Publication, v. 97, p. 9-35.
ETHRIDGE, F.G., AND SCHUMM, S.A., 1977, Reconstructing paleochannel morphologic and flow characteristics: methodology, limitations, and assessment: *in* Miall, A.D., ed., Fluvial Sedimentology: Canadian Society of Petroleum Geologists Memoir, v. 5, p. 703-721.
FARRELL, K.M., 1987, Sedimentology and facies architecture of overbank deposits of the Mississippi River, False River region, Louisiana: *in* Ethridge, F.G., Flores, R.M., and Harvey, M.D., eds., Recent Developments in Fluvial Sedimentology: SEPM, Special Publication, v. 39, p. 111-120.
FERGUSON, R., AND ASHWORTH, P., 1991, Slope-induced changes in channel character along a gravel-bed stream: The Allt Dubhaig, Scotland: Earth Surface Processes and Landforms, v. 16, p. 65-82.
FISHER, D.J., ERDMANN, C.E., AND REESIDE JR., J.B., 1960, Cretaceous and Tertiary formations of the Book Cliffs, Carbon, Emery, and Grand Counties, Utah, and Garfield and Mesa Counties, Colorado, U.S. Geological Survey, Professional Paper 332, 80 p.
FLINT, J.J., 1974, Stream gradient as a function of order, magnitude, and discharge: Water Resources Research, v. 10, p. 969-973.
FOSTER, R.M., 2010, Sequence Stratigraphy of the upper Cretaceous middle Williams Fork Formation, Piceance Basin, Northwestern Colorado: implications for reservoir sandstones: [Unpublished M.S. thesis]: University of Colorado at Boulder, 207 p.
FRANCZYK, K.J., FOUCH, T.D., JOHNSON, R.C., MULENAAR, C.M., AND COBBAN, W.A., 1992, Cretaceous and Tertiary paleogeographic reconstructions for the Uinta-Piceance Basin study area, Colorado and Utah: U.S. Geological Survey, Bulletin 1787-Q, 37 p.
FRIEND, P.F., SLATER, M.J., AND WILLIAMS, R.C., 1979, Vertical and lateral building of river sandstone bodies, Ebro Basin, Spain: Journal of the Geological Society of London, v. 136, p. 39-46.
GABEL, S.L., 1993, Geometry and kinematics of dunes during steady and unsteady flows in the Calamus River, Nebraska, USA: Sedimentology, v. 40, p. 237-269.

GERMAN, Q.A., 2006, Analysis of fluvial sandstone-body characteristics and architecture in a high net-to-gross system: Upper Williams Fork Formation, Plateau Creek Canyon, Piceance Basin, Colorado: [Unpublished M.S. thesis]: University of Colorado, Boulder, Colorado, 141 p.

GIBLING, M.R., 2006, Width and thickness of fluvial channel bodies and valley fills in the geological record: a literature compilation and classification: Journal of Sedimentary Research, v. 76, p. 731-770.

GURNELL, A.M., PETTS, G.E., HANNAH, D.M., SMITH, B.P.G., EDWARDS, P.J., KOLLMANN, J., WARD, J.V., AND TOCKNER, K., 2001, Riparian vegetation and island formation along the gravel-bed Fiume Tagliamento, Italy: Earth Surface Processes and Landforms, v. 26, p. 31-62.

HAJEK, E.A., HELLER, P.L., AND SHEETS, B.A., 2010, Significance of channel-belt clustering in alluvial basins: Geology, v. 38, p. 535-538.

HAMPSON, G.J., 2016, Towards a sequence stratigraphic solution set for autogenic processes and allogenic controls: Upper Cretaceous strata, Book Cliffs, Utah, USA: Journal of the Geological Society, v. 173, p. 817-836.

HANCOCK, E.T., AND EBY, J.B., 1930, Geology and Coal Resources of the Meeker Quadrangle, Moffat and Rio Blanco Counties, Colorado: U.S. Geological Survey, Bulletin 812, p. 191-242.

HARTLEY, A.J., OWEN, A., SWAN, A., WEISSMANN, G.S., HOLZWEBER, B.I., HOWELL, J., NICHOLS, G., AND SCUDERI, L., 2015, Recognition and importance of amalgamated sandy meander belts in the continental rock record: Geology, v. 43, p. 679-682.

HARTLEY, A.J., WEISSMANN, G.S., AND SCUDERI, L., 2017, Controls on the apex location of large deltas: Journal of the Geological Society, v. 174, p. 10-13.

HARVEY, M.D., CREWS, S., PITLICK, J., AND BLAIR, T., 1985, Holocene braided rivers of eastern Colorado and the sedimentologic effects of Lawn Lake dam failure in the Rocky Mountain National Park, *in* Flores, R.M., and Harvey, M., eds., Field Guidebook to Modern and Ancient Fluvial Systems in the United States: Fort Collins, Colorado, Third International Fluvial Sedimentology Conference, p. 87-105.

HELLER, P.L., PAOLA, C., HWANG, I., JOHN, B., AND STEEL, R., 2001, Geomorphology and sequence stratigraphy due to slow and rapid base-level changes in an experimental subsiding basin (XES 96-1): American Association of Petroleum Geologists, Bulletin, v. 85, p. 0817-0838.

HELLER, P.L., RATIGAN, D., TRAMPUSH, S., NODA, A., MCELROY, B., DREVER, J., AND HUZURBAZAR, S., 2015, Origins of bimodal stratigraphy in fluvial deposits: An example from the Morrison Formation (Upper Jurassic), western USA: Journal of Sedimentary Research, v. 85, p. 1466-1477.

HETTINGER, R.D., AND KIRSCHBAUM, M.A., 2002, Stratigraphy of the Upper Cretaceous Mancos Shale (upper part) and Mesaverde Group in the southern part of the Uinta and Piceance basins, Utah and Colorado: U.S. Geological Survey, Investigations Series I-2764, 21 p.

HOLBROOK, J., SCOTT, R.W., AND OBOH-IKUENOBE, F.E., 2006, Base-level buffers and buttresses: a model for upstream versus downstream control on fluvial geometry and architecture within sequences: Journal of Sedimentary Research, v. 76, p. 162-174.

HOLBROOK, J., AND WANAS, H., 2014, A fulcrum approach to assessing source-to-sink mass balance using channel paleohydrologic paramaters derivable from common fluvial data sets with an example from the Cretaceous of Egypt: Journal of Sedimentary Research, v. 84, p. 349-372.

HUDSON, P.F., AND KESEL, R.H., 2000, Channel migration and meander-bend curvature in the lower Mississippi River prior to major human modification: Geology, v. 28, p. 531-534.

IELPI, A., GIBLING, M.R., BASHFORTH, A.R., LALLY, C., RYGEL, M.C., AND AL-SILWADI, S., 2014, Role of vegetation in shaping Early Pennsylvanian braided rivers: architecture of the Boss Point Formation, Atlantic Canada: Sedimentology, v. 61, p. 1659-1700.

IZETT, G.A., COBBAN, W.A., DALRYMPLE, G.B., AND OBRADOVICH, J.D., 1998, 40Ar/39Ar age of the Manson impact structure, Iowa, and correlative impact ejecta in the Crow Creek Member of the Pierre Shale (Upper Cretaceous), South Dakota and Nebraska: Geological Society of America, Bulletin, v. 110, p. 361-376.

IZETT, G.A., COBBAN, W.A., AND GILL, J.R., 1971, The Pierre Shale near Kremmling, Colorado, and its correlation to the east and the west, U.S. Geological Survey, Professional Paper 684-A, 19 p.

JACKSON II, R.G., 1976, Depositional model of point bars in the lower Wabash River: Journal of Sedimentary Petrology, v. 48, p. 579-594.

JACKSON II, R.G., 1978, Preliminary evaluation of lithofacies models for meandering alluvial streams, *in* Miall, A.D. ed., Fluvial Sedimentology, Canadian Society of Petroleum Geologists Memoir, v. 5, p. 543-576.

JACKSON, S.E., PEARSON, N.J., GRIFFIN, W.L., AND BELOUSOVA, E.A., 2004, The application of laser ablation-inductively coupled plasma-mass spectrometry to in situ U–Pb zircon geochronology: Chemical Geology, v. 211, p. 47-69.

JOHNSON, E.A., AND BROWNFIELD, M.E., 1988, Regional correlation of the middle coal group of the Upper Cretaceous Mesaverde Group, Yampa coal field, Moffat and Routt counties, Colorado: U.S. Geological Survey, Coal Series Map C.

JOHNSON, E.A., ROBERTS, L.N.R., BROWNFIELD, M.E., AND MERCIER, T.J., 2000, Geology and resource assessment of the middle and upper coal groups in the Yampa coal field, northwestern Colorado, Chapter P: Geologic assessment of coal in the Colorado Plateau: Arizona, Colorado, New Mexico, and Utah: U.S. Geological Survey, Professional Paper 1625-B, CD-ROM, 81 p.

JOHNSON, R.C., 1987, Geologic history and hydrocarbon potential of late Cretaceous-age, low-permeability reservoirs, Piceance Basin, western Colorado: Final Report, U.S. Geological Survey, Bulletin 1787-E.

JOHNSON, R.C., AND MAY, F., 1980, A study of the Cretaceous-Tertiary unconformity in the Piceance Creek basin, Colorado: The underlying Ohio Creek Formation (Upper Cretaceous) redefined as a member of the Hunter Canyon or Mesaverde Formation: U.S. Geological Survey, Bulletin 1482-B, 27 p.

KEETON, G.I., 2012, Sedimentological and stratigraphic characteristics of fluvial sandstones based on outcrop spectral-gamma-ray data and borehole images, Williams Fork Formation, Piceance Basin, Colorado: [Unpublished Ph.D. thesis]: University of Colorado at Boulder,

70 p.
KEETON, G.I., PRANTER, M.J., COLE, R.D., AND EDMUND, R., 2015, Stratigraphic architecture of fluvial deposits from borehole images, spectral-gamma-ray response, and outcrop analogs, Piceance Basin, Colorado: American Association of Petroleum Geologists, Bulletin, v. 99, p. 1929-1956.
KELLY, S., 2006, Scaling and hierarchy in braided rivers and their deposits: examples and implications for reservoir modelling: *in* Sambrook Smith, G.H., Best, J.L., Bristow, C.S., and Petts, G.E., eds., Braided Rivers; Process, Deposits, Ecology and Management, International Association of Sedimentologists, Special Publication, v. 36, p. 75-106.
KIRSCHBAUM, M.A., AND HETTINGER, R.D., 2004, Facies analysis and sequence stratigraphic framework of Upper Campanian strata (Neslen and Mount Garfield Formations, Bluecastle Tongue of the Castlegate Sandstone, and Mancos Shale), eastern Book Cliffs, Colorado and Utah: U.S. Geological Survey, Digital Data Report DDS-69-G.
KLEINHANS, M.G., AND VAN DEN BERG, J.H., 2011, River channel and bar patterns explained and predicted by an empirical and a physics-based method: Earth Surface Processes and Landforms, v. 36, p. 721-738.
KRAUS, M.J., AND BROWN, T.M., 1988, Pedofacies analysis; a new approach to reconstructing ancient fluvial sequences: Geological Society of America, Special Paper, v. 216, p. 143-152.
LASKOWSKI, A.K., DECELLES, P.G., AND GEHRELS, G.E., 2013, Detrital zircon geochronology of Cordilleran retroarc foreland basin strata, western North America: Tectonics, v. 32, p. 1027-1048.
LASSETTRE, N.S., PIÉGAY, H., DUFOUR, S., AND ROLLET, A.J., 2007, Decadal changes in distribution and frequency of wood in a free meandering river, the Ain River, France: Earth Surface Processes and Landforms, v. 33, p. 1098-1112.
LAURSEN, E.M., 1958, The total sediment load of streams: American Society of Civil Engineers, Journal of the Hydraulics Division, Proceedings, v. 84, p. 1-36.
LECLAIR, S.F., AND BRIDGE, J.S., 2001, Quantitative interpretation of sedimentary structures formed by river dunes: Journal of Sedimentary Research, v. 71, p. 713-716.
LECLAIR, S.F., BRIDGE, J.S., AND WANG, F., 1997, Preservation of cross-strata due to migration of subaqueous dunes over aggrading and non-aggrading beds: comparison of experimental data with theory: Geoscience Canada, v. 24, p. 55-66.
LEE, J., AND JULIEN, P.Y., 2006, Downstream hydraulic geometry of alluvial channels: Journal of Hydraulic Engineering, v. 132, p. 1347-1352.
LEHMAN, T.M., 1989, Upper Cretaceous (Maastrichtian) paleosols in trans-Pecos Texas: Geological Society of America, Bulletin, v. 101, p. 188-203.
LEIBOVITZ, M.B., 2010, Sequence stratigraphy of the upper cretaceous upper Williams Fork Formation, Piceance Basin, northwest Colorado, and its contribution to the basin-centered gas accumulation: [Unpublished M.S. thesis]: University of Colorado at Boulder, 155 p.
LEOPOLD, L.B., AND WOLMAN, M.G., 1957, River channel patterns - braided, meandering, and straight: U.S. Geological Survey, Professional Paper 282B, p. 39-85.

LEVEY, R.A., 1978, Bed-form distribution and internal stratification of coarse-grained point bars, Upper Congaree River, South Carolina: *in* Miall, A.D., ed., Fluvial Sedimentology, Canadian Society of Petroleum Geologists, Memoir, v. 5, p. 105-127.

LI, W., BHATTACHARYA, J.P., AND CAMPBELL, C., 2010, Temporal evolution of fluvial style in a compound incised-valley fill, Ferron "Notom Delta", Henry Mountains Region, Utah (USA): Journal of Sedimentary Research, v. 80, p. 529-549.

LIPPERT, P.G., 2014, Detrital U-Pb geochronology provenance analyses: case studies in the Greater Green River Basin, Wyoming, and the Book Cliffs, Utah: University of Kansas, 154 p.

LUDWIG, K.R., 2008, User's Manual for Isoplot 3.70: a geochronological toolkit for Microsoft Excel: Berkeley Geochronology Center Special Publication, 76 p.

LUNT, I.A., BRIDGE, J.S., AND TYE, R.S., 2004, A quantitative, three-dimensional depositional model of gravelly braided rivers: Sedimentology, v. 51, p. 377-414.

LYNDS, R.M., MOHRIG, D., HAJEK, E.A., AND HELLER, P.L., 2014, Paleoslope reconstruction in sandy suspended-load-dominant rivers: Journal of Sedimentary Research, v. 84, p. 825-836.

MADDEN, D.J., 1989, Stratigraphy, depositional environments, and paleogeography of coal-bearing strata in the Upper Cretaceous Mesaverde Group, central Grand Hogback, Garfield County, Colorado: U.S. Geological Survey, Bulletin 1483, 45 p.

MAKASKE, B., 2001, Anastomosing rivers: a review of their classification, origin and sedimentary products: Earth-Science Reviews, v. 53, p. 149-196.

MARTIN, J., CANTELLI, A., PAOLA, C., BLUM, M., AND WOLINSKY, M., 2011, Quantitative modeling of the evolution and geometry of incised valleys: Journal of Sedimentary Research, v. 81, p. 64-79.

MCLAURIN, B.T., AND STEEL, R.J., 2007, Architecture and origin of an amalgamated fluvial sheet sand, lower Castlegate Formation, Book Cliffs, Utah: Sedimentary Geology, v. 197, p. 291-311.

MCQUARRIE, N., AND WERNICKE, B.P., 2005, An animated tectonic reconstruction of southwestern North America since 36 Ma: Geosphere, v. 1, p. 147-172.

MIALL, A.D., 1985, Architectural-element analysis: a new method of facies analysis applied to fluvial deposits: Earth-Science Reviews, v. 22, p. 261-308.

MIALL, A.D., 1996, The geology of fluvial deposits: sedimentary facies, basin analysis, and petroleum geology Heidelberg, Springer-Verlag, Inc., 582 p.

MILLER, K.G., KOMINZ, M.A., BROWNING, J.V., WRIGHT, J.D., MOUNTAIN, G.S., KATZ, M.E., SUGARMAN, P.J., CRAMER, B.S., CHRISTIE-BLICK, N., AND PEKAR, S.F., 2005, The Phanerozoic record of global sea-level change: Science, v. 310, p. 1293-1298.

MOHRIG, D., HELLER, P.L., PAOLA, C., AND LYONS, W.J., 2000, Interpreting avulsion process from ancient alluvial sequences: Guadalope-Matarranya system (northern Spain) and Wasatch Formation (western Colorado): Geological Society of America, Bulletin, v. 112, p. 1787-1803.

MURRAY, F.N., 1966, Stratigraphy and structural geology of the Grand Hogback monocline, Colorado: University of Colorado: Ph.D. thesis.

NIÑO, Y., FABIAN, L., AND MARCELO, G., 2003, Threshold for particle entrainment into suspension:

Sedimentology, v. 50, p. 247-263.
NITTROUER, J.A., SHAW, J., LAMB, M.P., AND MOHRIG, D., 2012, Spatial and temporal trends for water-flow velocity and bed-material sediment transport in the lower Mississippi River: Geological Society of America, Bulletin, v. 124, p. 400-414.
OBRADOVICH, J.D., 1993, A Cretaceous time scale, *in* Caldwell, W.G.E. and Kauffman, E.G., eds., Evolution of the Western Interior Basin: Geological Association of Canada, Special Paper, v. 39, p. 379-396.
ORE, H.T., 1964, Some criteria for recognition of braided stream deposits: Contributions to Geology, v. 3, p. 1-14.
OST, R.C., 2010, Stratal patterns of the Williams Fork (Hunter Canyon) Formation, Piceance Basin, Colorado [Unpublished M.S. thesis]: University of Kansas, 99 p.
OSTERKAMP, W.R., FOSTER, G.R., AND LANE, L.J., 1983, An analytical treatment of channel-morphology relations: U.S. Geological Survey, Professional Paper 1288, US Government Printing Office, 21 p.
OSTERKAMP, W.R., HEDMAN, E.R., AND WISEMAN, A.G., 1982, Geometry, basin-characteristics, discharge, and particle-size data from gaged stream-channel sites, Western United States, U.S. Geological Survey, Open File Report 82-93, p. 56.
PAOLA, C., AND MOHRIG, D., 1996, Palaeohydraulics revisited: palaeoslope estimation in coarse-grained braided rivers: Basin Research, v. 8, p. 243-254.
PAOLA, C., STRAUB, K., MOHRIG, D., AND REINHARDT, L., 2009, The "unreasonable effectiveness" of stratigraphic and geomorphic experiments: Earth-Science Reviews, v. 97, p. 1-43.
PARKER, G., 1976, On the cause and characteristic scales of meandering and braiding in rivers: Journal of Fluid Mechanics, v. 76, p. 457-480.
PARKER, G., 1978, Self-formed straight rivers with equilibrium banks and mobile bed, Part 1. The sand-silt river: Journal of Fluid Mechanics, v. 89, p. 109-125.
PARKER, G., AND CUI, Y., 1998, The arrested gravel front: stable gravel-sand transitions in rivers, Part 1: Simplified analytical solution: Journal of Hydraulic Research, v. 36, p. 75-100.
PATON, C., HELLSTROM, J., BENCE, P., WOODHEAD, J., AND HERGT, J., 2011, Iolite: Freeware for the visualisation and processing of mass spectrometric data: Journal of Analytical Atomic Spectrometry, v. 26, p. 2508-2518.
PATON, C., WOODHEAD, J.D., HELLSTROM, J.C., HERGT, J.M., GREIG, A., AND MAAS, R., 2010, Improved laser ablation U-Pb zircon geochronology through robust downhole fractionation correction: Geochemistry, Geophysics, Geosystems, v. 11, p. 36.
PATTERSON, P.E., KRONMUELLER, K., AND DAVIES, T.D., 2003, Sequence stratigraphy of the Mesaverde Group and Ohio Creek conglomerate, northern Piceance Basin, Colorado: *in* Peterson, K.M., Olson, T.M., and Anderson, D.S., eds., Piceance Basin 2003 Guidebook: Denver, Colorado, Rocky Mountain Association of Geologists, p. 115–129.
PETRUS, J.A., AND KAMBER, B.S., 2012, VizualAge: a novel approach to Laser Ablation ICP-MS U-Pb geochronology data reduction: Geostandards and Geoanalytical Research, v. 36, p. 247-270.
POSAMENTIER, H.W., AND VAIL, P.R., 1988, Eustatic controls on clastic deposition II—sequence and systems tract models: *in* Wilgus, C.K., Hastings, B.S., Kendall, C.G.St.C., Posamentier,

H.W., Ross, C.A., Van Wagoner, J.C., eds., Sea Level Changes – An Integrated Approach. SEPM, Special Publication, v. 42, p. 125-154.

PRANTER, M.J., ELLISON, A.I., COLE, R.D., AND PATTERSON, P.E., 2007, Analysis and modeling of intermediate-scale reservoir heterogeneity based on a fluvial point-bar outcrop analog, Williams Fork Formation, Piceance Basin, Colorado: American Association of Petroleum Geologists, Bulletin, v. 91, p. 1025-1051.

ROEHLER, H.W., 1990, Stratigraphy of the Mesaverde Group in the central and eastern greater Green River Basin, Wyoming, Colorado, and Utah: U.S. Geological Survey, Professional Paper 1508, 52 p.

RUBIN, Y., LUNT, I.A., AND BRIDGE, J.S., 2006, Spatial variability in river sediments and its link with river channel geometry: Water resources research, v. 42, p. 12.

RUST, B.R., 1977, Depositional models for braided alluvium: *in* Miall, A.D., ed., Fluvial sedimentology: Canadian Society of Petroleum Geologists, Memoir, v. 5, p. 605-625.

SALTER, T., 1993, Fluvial scour and incision: models for their influence on the development of realistic reservoir geometries: *in* North, C.P., Prosser, D.J., eds., Characterization of Fluvial and Aeolian Reservoirs: Geological Society of London, Special Publication, v. 73, p. 33-51.

SAMBROOK-SMITH, G.H., ASHWORTH, P.J., BEST, J.L., WOODWARD, J., AND SIMPSON, C.J., 2006, The sedimentology and alluvial architecture of the sandy braided South Saskatchewan River, Canada: Sedimentology, v. 53, p. 413-434.

SCHUMM, S.A., 1968, River adjustment to altered hydrologic regimen-Murrumbidgee River and paleochannels, Australia, U.S. Geological Survey Professional Paper 598.

SCHUMM, S.A., 1981, Evolution and response of the fluvial system, sedimentologic implications: SEPM, Special Publication, v. 31, p. 19-29.

SCHUMM, S.A., AND KHAN, H.R., 1972, Experimental study of channel patterns: Geological Society of America, Bulletin, v. 83, p. 1755-1770.

SELLWOOD, B.W., AND VALDES, P.J., 2006, Mesozoic climates: General circulation models and the rock record: Sedimentary Geology, v. 190, p. 269-287.

SHANLEY, K.W., AND MCCABE, P.J., 1994, Perspectives on the sequence stratigraphy of continental strata: American Association of Petroleum Geologists, Bulletin, v. 78, p. 544-568.

SHEETS, B.A., HICKSON, T.A., AND PAOLA, C., 2002, Assembling the stratigraphic record: depositional patterns and time-scales in an experimental alluvial basin: Basin Research, v. 14, p. 287-301.

SHUKLA, U.K., SINGH, I.B., SRIVASTAVA, P., AND SINGH, D.S., 1999, Paleocurrent patterns in braid-bar and point-bar deposits: Examples from the Ganga River, India: Journal of Sedimentary Research, v. 69, p. 992-1002.

SMITH, J.J., HASIOTIS, S.T., KRAUS, M.J., AND WOODY, D.T., 2008, *Naktodemasis bowni*: new ichnogenus and ichnospecies for adhesive meniscate burrows (AMB), and paleoenvironmental implications, Paleogene Willwood Formation, Bighorn Basin, Wyoming: Journal of Paleontology, v. 82, p. 267-278.

SMITH, N.D., 1978, Some comments on terminology for bars in shallow rivers: *in* Miall A.D., ed., Fluvial Sedimentology, Canadian Society of Petroleum Geologists, Memoir, v. 5, p. 85-

88.
SMITH, N.D., CROSS, T.A., DUFFICY, J.P., AND CLOUGH, S.R., 1989, Anatomy of an avulsion: Sedimentology, v. 36, p. 1-23.
SØMME, T.O., HELLAND-HANSEN, W., MARTINSEN, O.J., AND THURMOND, J.B., 2009, Relationships between morphological and sedimentological parameters in source-to-sink systems: a basis for predicting semi-quantitative characteristics in subsurface systems: Basin Research, v. 21, p. 361-387.
STRONG, N., AND PAOLA, C., 2006, Fluvial landscapes and stratigraphy in a flume: The Sedimentary Record, v. 4, p. 4-7.
SYVITSKI, J.P., AND MILLIMAN, J.D., 2007, Geology, geography, and humans battle for dominance over the delivery of fluvial sediment to the coastal ocean: The Journal of Geology, v. 115, p. 1-19.
TARQUINI, S., ISOLA, I., FAVALLI, M., MAZZARINI, F., BISSON, M., PARESCHI, M.T., AND BOSCHI, E., 2007, TINITALY/01: a new triangular irregular network of Italy: Annals of Geophysics, v. 50, p. 407-425.
TARQUINI, S., VINCI, S., FAVALLI, M., DOUMAZ, F., FORNACIAI, A., AND NANNIPIERI, L., 2012, Release of a 10-m-resolution DEM for the Italian territory: Comparison with global-coverage DEMs and anaglyph-mode exploration via the web: Computers & Geosciences, v. 38, p. 168-170.
TRAMPUSH, S.M., HUZURBAZAR, S., AND MCELROY, B., 2014, Empirical assessment of theory for bankfull characteristics of alluvial channels: Water Resources Research, v. 50, p. 9211-9220.
UPCHURCH, G.R., KIEHL, J., SHIELDS, C., SCHERER, J., AND SCOTESE, C., 2015, Latitudinal temperature gradients and high-latitude temperatures during the latest Cretaceous: Congruence of geologic data and climate models: Geology, v. 43, p. 683-686.
VAN WAGONER, J.C., MITCHUM, R.M., CAMPION, K.M., AND RAHMANIAN, V.D., 1990, Siliciclastic sequence stratigraphy in well logs, cores, and outcrops: concepts for high-resolution correlation of time and facies: American Association of Petroleum Geologists, Methods in Exploration 7.
VERMEESCH, P., 2012, On the visualisation of detrital age distributions: Chemical Geology, v. 312, p. 190-194.
WALKER, R.G., AND CANT, D.J., 1984, Sandy fluvial systems, *in* Walker, R.G., ed., Facies Models, 2nd edition, Reprint Geoscience Cananda, p. 71-89.
WILKERSON, G.V., AND PARKER, G., 2011, Physical basis for quasi-universal relationships describing bankfull hydraulic geometry of sand-bed rivers: Journal of Hydraulic Engineering, v. 137, p. 739-753.
WOLMAN, M.G., 1955, The natural channel of Brandywine creek, Pennsylvania, U.S. Geological Survey, Professional Paper 271, p. 56.
WRIGHT, V.P., 1992, Paleosol recognition: a guide to early diagenesis in terrestrial settings, *in* Wolf, K.H., and Chilingarian, G.V., eds., Diagenesis, III, Chapter 12 Developments in Sedimentology: Amsterdam, Elsevier, p. 591-619.
WU, C., BHATTACHARYA, J.P., AND ULLAH, M.S., 2015, Paleohydrology and 3D facies architecture of

ancient point bars, Ferron Sandstone, Notom Delta, south-central Utah, USA: Journal of Sedimentary Research, v. 85, p. 399-418.

ZAPP, A.D., AND COBBAN, W.A., 1960, Some Late Cretaceous strand lines in northwestern Colorado and northeastern Utah: U.S. Geological Survey, Professional Paper, v. 400, p. B246-B249.

Table 1: 90th percentile flow depth calculations

	Grain Size [mm]			
Interval	Average	Smallest grain size	Largest grain size	Flow depth P90 [m]
6	0.363	0.250	0.500	
5	0.268	0.177	0.350	6.5 ± 1.4
4	0.300	0.250	0.350	
3	0.242	0.177	0.350	5.6 ± 1.1
2	0.257	0.177	0.350	6.9 ± 1.5
1	0.278	0.177	0.500	6 ± 1.2
D	0.300	0.250	0.350	7.2 ± 1.5
C	0.254	0.177	0.350	7.1 ± 1.5
B	0.273	0.177	0.350	6.8 ± 1.4
A	0.257	0.177	0.350	4 ± 0.8
Avg 1,2,3,5	0.273	0.177	0.500	6.3 ± 1.3
Avg A-D	0.265	0.177	0.350	7 ± 1.4
Avg 1,2,3,5 & A-D	0.270	0.177	0.500	6.9 ± 1.4

Note: Grain size average represents the average value within the interpreted interval. Minimum and maximum grain sizes refer to the range of the sand classification. Avg = average, P90 = 90th percentile

Table 2: Paleo-slope calculations

	Slope calculated using		
Interval	P90 flow depth	Lower limit P90 flow depth	Upper limit P90 flow depth
6			
5	7.0E-05	8.8E-05	5.8E-05
4			
3	6.1E-05	7.7E-05	5.1E-05
2	5.9E-05	7.4E-05	4.9E-05
1	8.4E-05	1.1E-04	7.0E-05
D	8.6E-05	1.1E-04	7.2E-05
C	5.6E-05	7.0E-05	4.7E-05
B	7.1E-05	8.9E-05	5.9E-05
A	1.0E-04	1.3E-04	8.4E-05
Avg 1,2,3,5	7.6E-05	9.6E-05	6.4E-05
Avg A-D	6.3E-05	8.0E-05	5.3E-05
Avg 1,2,3,5 & A-D	6.7E-05	8.4E-05	5.6E-05

Note: Slope was calculated using Lynds et al. (2014) method #2 with the Julien assumption. Avg = average, P90 = 90^{th} percentile

Table 3: Backwater length estimations

	Backwater length [km] calculated using		
Interval	P90 flow depth	Lower limit P90 flow depth	Upper limit P90 flow depth
6			
5	93	58	133
4			
3	91	57	132
2	117	73	168
1	72	45	103
D	84	53	121
C	127	80	182
B	97	61	139
A	40	25	57
Avg 1,2,3,5	93	59	134
Avg A-D	87	55	125
Avg 1,2,3,5 & A-D	90	57	129

Note: Avg = average, P90 = 90th percentile

Table 4: Planform morphology definitions

Database Code	Planform morphology	Definition	Examples
1	Irregularly sinuous	Recognition criteria for this single thread channel is from well-defined banks and an inconsistent meander wavelength. Sinuous pattern of the channel is varied and does not have an obvious single meander wavelength. Due to strict terms of classification, most would refer to channels within this category as meandering. Straight channels are included in this category whether it be natural or from human modification. In addition, channels that have no recognizable banks or bars are included due to dense vegetation.	Rosebud River near Carstairs Creek, AB; Arrow River near Titley, UK
2	Meandering	Single thread channels of this group have a repetitions sine curve geometry that contain a similar meander wavelength. This definition includes meanders that are confined to valley walls and that are entrenched. The number of rivers in this classification is purposefully small to emphasize the groups distribution.	Beaver River near Cold Lake Reserve, AB; McClintock River near Whitehorse, YT
3	Minor secondary channels	Recognition criteria of this channel type are the notable occurrence of crevasse splays, chute channels or detached diagonal bars. The secondary channels here are smaller than the main channel and are typically occupied during flood stages and dry during day to day flow.	Elk River near Clark, CO; Jumping Pound Creek near Jumping Pound, AB
4	Split with bars	Classification of channels is determined by substantial flow around both sides of bars or islands. An island can be an alluvial or non-alluvial feature that is at the elevation of the floodplain or higher and contains normal floodplain vegetation. Islands are not overlapping or a continuous feature in the channel (planform is not heavily braided). Only a small portion of the channel is split from the island (channel is not anastomosed). Channels that contain elements of both category 3 and 4 are classified as a 4.	Red Deer River near Jenner Ferry, AB; Peace River near Taylor, BC

Database Code	Planform morphology	Definition	Examples
5	Braided	This group comprises rivers which flow in individual channels divided by channel bars at moderate to low flow and at high flow the bars are typically submerged. Therefore, the sediment is mobile on the bars and the intervening channels are not stable.	Sisquoc River near Garey, CA; Elbo River at Fullerton Ranch and at Bragg Creek, AB
6	Irregularly sinuous, meandering floodplain	This has the same definition as irregularly sinuous, category 1, in that these single thread channels do not have a consistent meander wavelength. This category is separated from the previous by the abundance of scroll bar topography and meander cut-offs in the adjacent floodplain. Most would refer to this group as meandering.	Blacks Fork River near Little America, WY; Salcha River near Salchaket, AK
7	Irregularly sinuous, rapids	This category is a sub-set of irregularly sinuous, category 1. These single-thread channels banks are defined/limited by valley walls. The dominant expression of the water surface is white crests observed from satellite imagery. These are interpreted to be rapids where the water is at supercritical flow.	Jemez River near Jemez, NM; Big Boulder Creek, ID

Table 5: Charateristics of modern rivers

	Code	1	2	3	4	5	6	7	2 & 6
	Planform morphology	Irregularly sinuous	Meandering	Minor 2nd channels	Split with bars	Braided	Irregularly sinuous w/ meandering floodplain	Irregularly sinuous w/ rapids	
Bankfull depth (m)									
Grain size <2 mm	Count	35	3	0	23	15	21	0	24
	Minimum	0.5	2.5	-	0.4	0.7	1.4	-	1.4
	Maximum	13.9	2.9	-	11.2	3.7	9.4	-	9.4
	P50	2.1	2.7	-	3.0	1.5	2.7	-	2.7
Grain Size >2 mm	Count	126	2	57	110	21	14	9	16
	Minimum	0.2	0.5	0.3	0.6	0.5	1.0	0.3	0.5
	Maximum	11.2	1.6	4.9	8.8	4.6	5.0	0.9	5.0
	P50	1.0	1.1	1.1	1.7	1.2	1.9	0.5	1.8

	Code	1	2	3	4	5	6	7	2 & 6
	Planform morphology	Irregularly sinuous	Meandering	Minor 2nd channels	Split with bars	Braided	Irregularly sinuous w/ meandering floodplain	Irregularly sinuous w/ rapids	
Grain size (mm)									
Grain size <2 mm	Count	35	3	0	23	15	21	0	24
	Minimum	0.04	0.4	-	0.1	0.1	0.1	-	0.1
	Maximum	1.4	0.6	-	1.2	1.9	1.3	-	1.3
	P50	0.3	0.6	-	0.3	0.5	0.3	-	0.4
Grain Size >2 mm	Count	126	2	57	110	21	14	9	16
	Minimum	3.4	23.0	14.0	2.7	2.3	5.0	15.0	5.0
	Maximum	190.0	45.0	117.0	145.0	200.0	86.0	120.0	86.0
	P50	45.0	34.0	51.0	48.5	15.4	19.0	31.0	19.0
Slope									
Grain size <2 mm	Count	35	3	0	23	15	21	0	24
	Minimum	7.0E-5	2.1E-4	-	4.0E-5	1.2E-3	1.1E-4	-	1.1E-4
	Maximum	7.0E-3	5.3E-4	-	1.5E-2	9.0E-3	1.2E-3	-	1.2E-3
	P50	5.1E-4	2.1E-4	-	3.0E-4	3.8E-3	1.9E-4	-	2.1E-4
Grain Size >2 mm	Count	126	2	57	110	21	14	9	16
	Minimum	2.2E-4	2.0E-3	8.0E-4	2.6E-4	4.0E-4	5.9E-4	7.4E-3	5.9E-4
	Maximum	7.6E-2	2.3E-3	2.1E-2	1.9E-2	6.7E-2	2.0E-3	5.0E-2	2.3E-3
	P50	2.9E-3	2.2E-3	3.2E-3	1.9E-3	7.7E-3	1.1E-3	3.5E-2	1.2E-3

Figure captions

Figure 1: Stratigraphic column of the Williams Fork Formation and bounding formations. The expanded schematic of the Williams Fork Formation emphasizes the stratal pattern identified by Ost (2010). The middle and upper section of the formation are composed of stacked stratal packages of high-to-low net-to-gross fluvial deposits. Modified from Ost (2010).

Figure 2: Location map of the Piceance Basin and generalized outcrop belt of the Mesaverde Group, which contains the Williams Fork Formation. The study area is located in the Plateau Creek Canyon, which is in the southwestern part of the Piceance Basin. Outcrops are outlined in black. Outcrops from previous studies are 1, 2, 4 and 5. Hydrodynamic calculations of this study are from outcrops two and three. Modified from Pranter et al. (2007).

Figure 3: Interpreted and non-interpreted outcrop photomosaics of outcrop two (A) and outcrop three (B). Outcrop two is oblique to the viewer so a parallax is introduced which complicates the interpretation. Black dotted lines show the location of a vertical section (sections MK-01, MK-02, MK-03 and IC-02) measured with a Laser Range Finder. Black bars below vertical sections serve as scales and are approximately 5x5 meters. Note the large, low-relief scour surfaces (type 1 surface, yellow), surfaces that show greater relief (type 2 surface, black), surfaces with similar dip and orientation (type 3 surface, green) and cross-beds (red).

Figure 4: Interpreted and non-interpreted photomosaic of outcrop 5. Outcrop is arcuate in shape and turns toward the viewer on the right-hand side of the photo. Black dotted lines are locations of vertical sections measured (sections LK-01, LK-02 and LK-03) with a Laser Range Finder. Black bars below vertical sections serve as scales and are approximately 5x5 meters.

Note the large, low-relief scour surfaces (type 1 surface, yellow) and surfaces that show internal scours and changes in lithology (type 2 surface, black). Between the low-relief surfaces, surfaces with the same dip, orientation and relief are highlighted in green (type 3 surface). Green surfaces with a tangential base and alternating lithologies are interpreted as lateral accretion deposits. Red surfaces represent cross-beds.

Figure 5: Sedimentary features within outcrop numbers 2 and 3: A) wedge-shaped cross-bedded sandstone (cross-beds highlighted in white), B) planar tabular and wedge-shaped cross-bedded sandstone (cross-beds highlighted in white), C) interval of burrowed sandstone within interbedded lithofacies containing *Planolites* and *Naktodemasis bowni* burrows, D) very fine sandstone fining upward to mudstone.

Figure 6: Histogram of cross-bed thickness from two measured sections of the amalgamated sandstone in outcrop numbers 2 and 3. Blue bars are interpreted as dune deposits and yellow bars are interpreted as unit bar deposits. Cross-beds less than 60 cm thick are in the St facies and above 60 cm are in the Sp facies. Cross-beds interpreted as dune deposits display a unimodal distribution and are used for hydrodynamic calculations. Cross-beds interpreted as unit bar deposits have steep foresets, large lateral extent (>5 m) and do not stack vertically. Plotted data is from measured sections (intervals 1,2,3,5 and A-D, see Appendix 2bii,iii).

Figure 7: Schematic profiles of three vertical successions in outcrop numbers 2 and 3. Profiles display generalized grain size trends and sedimentary structures associations. Two letter codes refer to lithofacies classification of Miall (1996). The abbreviations are as follows: St is sand size

grains and wedge and festoon cross-bedded, Sp is sand size grains and planar tabular cross-bedded, Fsm is fine grained (silt to mud) and is massive in texture.

Figure 8: Paleo-flow direction rose diagrams from the amalgamated sandstone of interest collected from cross-bed orientation. The left diagram (orange) was collected by German (2006) from outcrop number 2. Outcrop measurements indicate an average azimuth of 92˚ with a standard deviation of 13.82˚ (n=21). The right diagram (blue) was collected by Keeton (2015) from equivalent strata in Parachute Field using subsurface borehole imaging. Subsurface measurements indicate 63.5˚ vector average with a circular standard deviation of 37.5˚ (n=148). The calculated sinuosity of the subsurface data is 1.1. Modified from German (2006) and Keeton (2015).

Figure 9: A) Simplified cartoon illustrating the general relationship between flow depth and cross-bed thickness. In this study, flow depth was estimated from cross-bed thickness of interpreted dunes. Modified from Ethridge and Schumm (1978). B) Histogram of calculated median flow depths against count of calculated flow depth. The right-hand axis is cumulative percentage. P90 is the 90^{th} percentile. Plotted data are from intervals 1, 2, 3, 5 and A-D, which can be found in Appendix 2bii,iii.

Figure 10: Scatter plot of thickness versus width of channel-belt deposits. Dimensions were collected from German (2006) using aerial LiDAR from the outcrops outlined in black in the study area map. Width to thickness (W:T) ratios from German (2006) are grouped by orientation: perpendicular (prp) and oblique (obl) to paleo-current direction. W:T ratios are also grouped by completeness of exposure: complete versus incomplete (e.g. truncated, covered).

Data is plotted on fields, which are ranges of width to thickness ratios that represent the presence or absence of backwater effects, which is previously defined from measurements made in the stratigraphic record and modern fluvial systems (Gibling, 2006; Blum et al., 2013). Ratio ranges are emphasized by color. Fields defining channel-belt deposits within the backwater reach are defined as 30-70:1 and are color coded light green. Fields defining channel-belts upstream from the backwater effects are defined as 70-300:1 and are color coded dark green. Channel-belts are highlighted in the same color in the schematic map of a fluvial system which shows the extent of the backwater reach. Channel-fills are defined as 6-30:1 and are not used to determine backwater effects. Dimensions of channel-belts and channel-fills within the amalgamated sandstone, taken from German (2006), plot in all three fields. The data plots primarily in the channel-belt field within the 30-70:1 domain. W:T ratios within the channel-belt domain that are perpendicular, oblique and perpendicular to oblique have an average W:T ratio of 46:1 (n=41). The average W:T ratio of channel-belts within the Big Kahuna sandstone are interpreted to represent deposition within the backwater reach.

Figure 11: Modern river elevation profiles are shown by lines. Line pattern associates with planform morphology (braided=dashed; transitional=dash-dot; meandering=solid). The right and upper axes of the graph are labels of constant slope. The slope calculations of the Big Kahuna sandstone are shown by the highlighted area. The fading of the highlighted area represents the uncertainty in the paleo-slope calculations (~100 km from the river mouth to the study area). First order estimations of slope are similar to that of the Adige, Ili and Trinity

Rivers. Digital elevation models were collected from the USGS (SRTM and ASTER data) and Tarquini et al. (2007, 2012).

Figure 12: Over 430 data points of modern rivers displaying relationships of slope, grain size and flow depth with interpreted planform morphology. Figure D contains over 370 data points. As defined in table 4, planform morphologies were categorized with strict criteria to help illustrate any differences between meandering and braided. Many rivers within the category of irregularly sinuous and irregularly sinuous with meandering floodplain topography would be classically labeled as meandering. Data and sources are located in Appendix 3.

Figure 13: Three-dimensional scatter plot of slope, bankfull flow depth, average bed sediment grain size and planform morphology from the same data in figure 12. Point locations are also displayed as a grey shadow on the side axes strictly for illustrative purposes, which are also the 2D graphs of figure 12a,b,c. Data and sources are located in Appendix 3.

Figure 14: Schematic stratigraphic correlation chart from the northern Piceance Basin to the southern Sand Wash Basin in northwestern Colorado. The Twentymile and Lion Canyon Sandstone Members of the Williams Fork Formation are clastic shallow marine deposits which record the last transgressions of the Cretaceous Western Interior Seaway. Modified from Brownfield et al. (2000).

Figure 15: Tera-Wasserburg concordia diagram of the youngest detrital zircon populations for the base and top of the Williams Fork Formation. Single grain analyses are shown by black ellipses (2σ) and the concordia age of the youngest population is shown by blue ellipses (2σ). Maximum depositional ages are interpreted for the base of the formation as 74.09 ± 0.48 Ma

(MSWD: 1.14, Probability: 0.31, n: 9) and the top as 70.1 ± 1.8 Ma (MSWD: 1.11, Probability: 0.35, n: 3). ISOPLOT software was used to determine concordia ages (Ludwig, 2008).

Figure 16: Kernel density plots of the two detrital zircon samples from this study displays normalized frequency of grain abundance against age. Interpreted source signal is labeled on the upper x-axis. Youngest detrital zircons are interpreted to be sourced from cordilleran magmatism. Kernel density plots were created with the application Densityplotter.jar and have a bandwidth of 10 (Vermeesch, 2012).

Figure 17: A) Map of western USA with locations of radiometrically dated volcanic deposits. Data was compiled from the western North American Volcanic and Intrusive Rock Database (NAVDAT). Ages shown are within the range of the youngest and oldest detrital zircons of the two youngest populations. Only data within 1000 km of the study area is shown. Arrows represent approximate position of igneous deposits pre-Cenozoic extension (McQuarrie and Wernicke, 2005). Reconstruction of the Williams Fork Formation paleo-drainage is shown from the dashed line (~65,000 km^2). Paleo-drainage area was estimated from the regression in figure 12d. B) Youngest detrital zircon populations from this study are plotted by stratigraphic position against age. Grey bars represent the two sigma error from the weighted mean age calculated from ISOPLOT (Ludwig, 2008).

Figure 18: Subsurface isopach map interpreted by Leibovitz (2010) of the Upper Williams Fork (UWF) Sandstone. Well distribution has a large influence on predicted isopach thickness. NW and SE sides are interpreted to be the edges of an incised valley fill. Subsurface data is projected to the SW to incorporate the field area of this study. The yellow-green circle is the

location and observed thickness (~75 m) at the outcrop of study. Thickness projections show that the area of study would fall within the incised valley fill and projected valley fill thickness. The grey shading represents the outcrop exposure of the Williams Fork Formation. Modified from Leibovitz (2010).

Figure 1

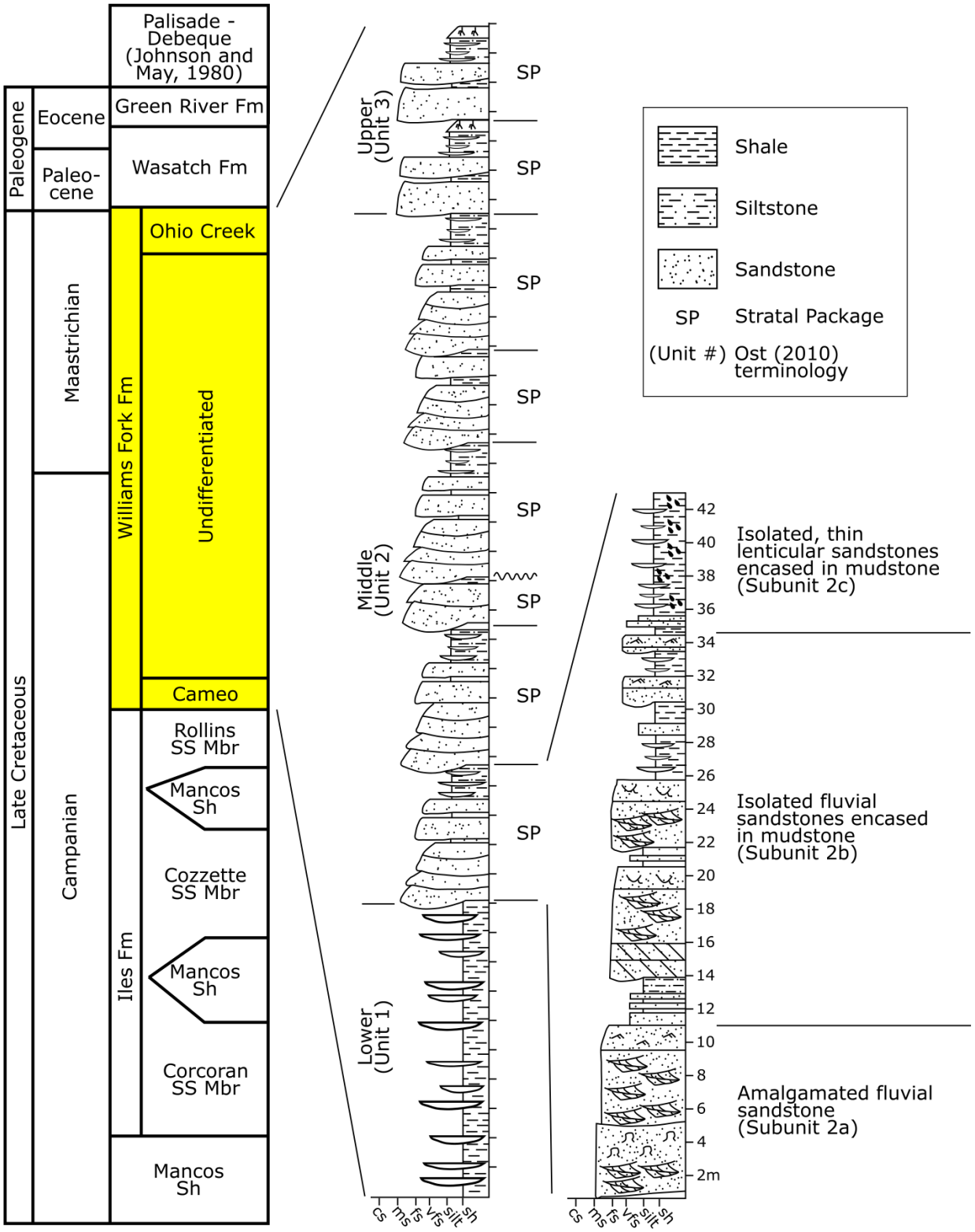
Palisade - Debeque (Johnson and May, 1980)
Paleogene
Eocene
Paleo-cene
Green River Fm
Wasatch Fm
Late Cretaceous
Maastrichian
Campanian
Williams Fork Fm
Ohio Creek
Undifferentiated
Cameo
Rollins SS Mbr
Mancos Sh
Cozzette SS Mbr
Iles Fm
Mancos Sh
Corcoran SS Mbr
Mancos Sh
Upper (Unit 3)
Middle (Unit 2)
Lower (Unit 1)
SP
Shale
Siltstone
Sandstone
Stratal Package
(Unit #) Ost (2010) terminology
Isolated, thin lenticular sandstones encased in mudstone (Subunit 2c)
Isolated fluvial sandstones encased in mudstone (Subunit 2b)
Amalgamated fluvial sandstone (Subunit 2a)
cs
ms
fs
vfs
silt
sh
42
40
38
36
34
32
30
28
26
24
22
20
18
16
14
12
10
8
6
4
2m

Figure 2

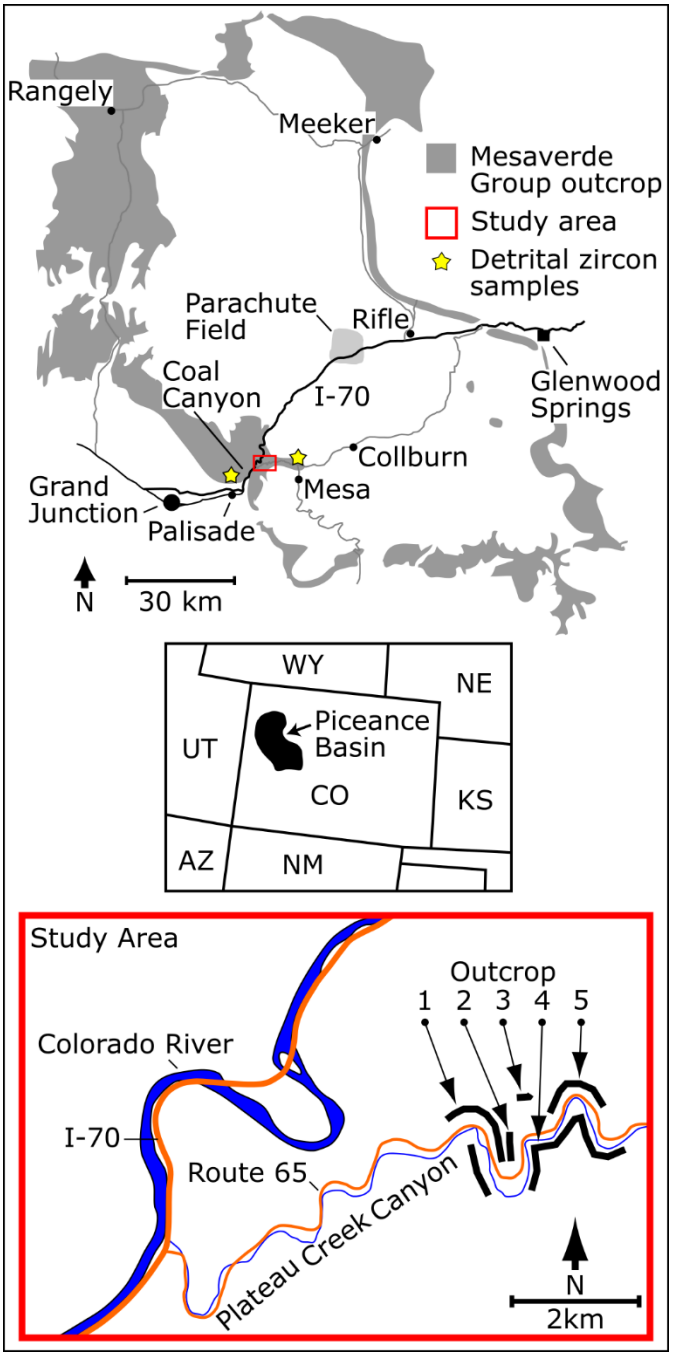
Rangely
Meeker
Mesaverde Group outcrop
Study area
Detrital zircon samples
Parachute Field
Rifle
Coal Canyon
I-70
Glenwood Springs
Collburn
Mesa
Grand Junction
Palisade
N
30 km
WY
NE
Piceance Basin
UT
CO
KS
AZ
NM
Study Area
Outcrop
1 2 3 4 5
Colorado River
I-70
Route 65
Plateau Creek Canyon
N
2km

Figure 3a

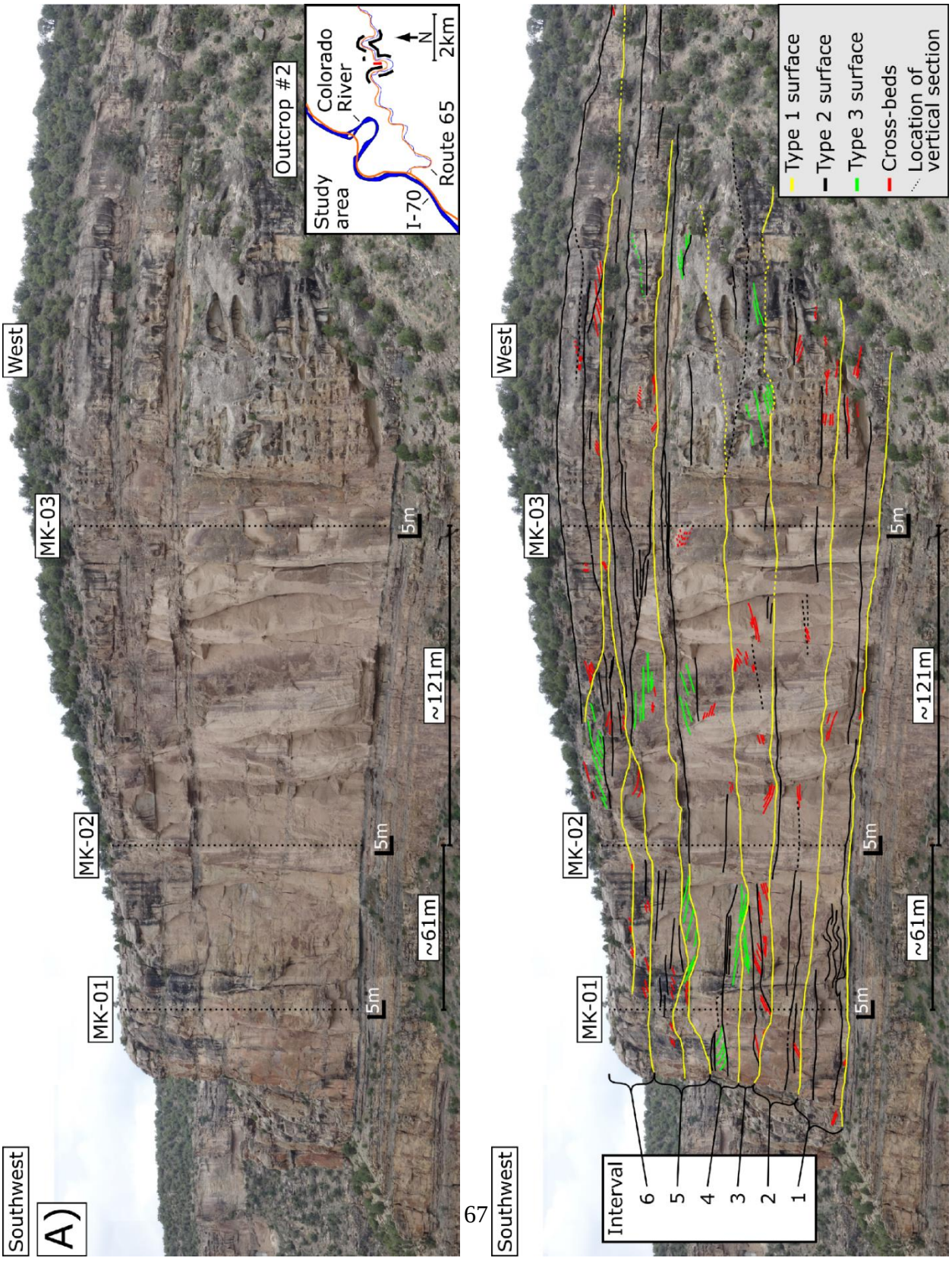
A)
Southwest
West
MK-01
MK-02
MK-03
~61m
~121m
5m
Outcrop #2
Colorado River
Study area
I-70
Route 65
N
2km
Interval
6
5
4
3
2
1
Type 1 surface
Type 2 surface
Type 3 surface
Cross-beds
Location of vertical section

Figure 3b

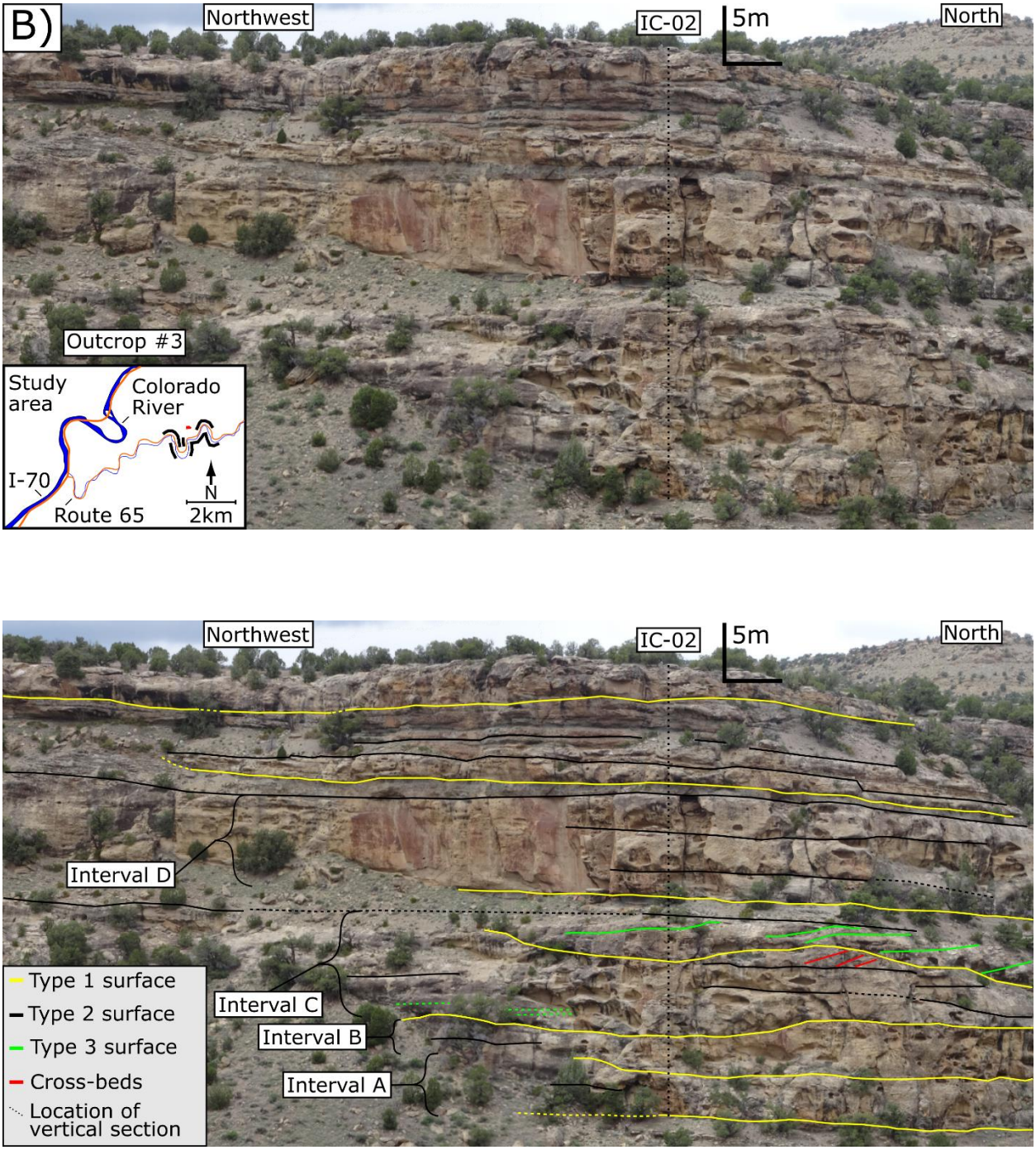
B)
Northwest
IC-02
5m
North
Outcrop #3
Study area
Colorado River
I-70
Route 65
N
2km
Northwest
IC-02
5m
North
Interval D
Interval C
Interval B
Interval A
Type 1 surface
Type 2 surface
Type 3 surface
Cross-beds
Location of vertical section

Figure 4

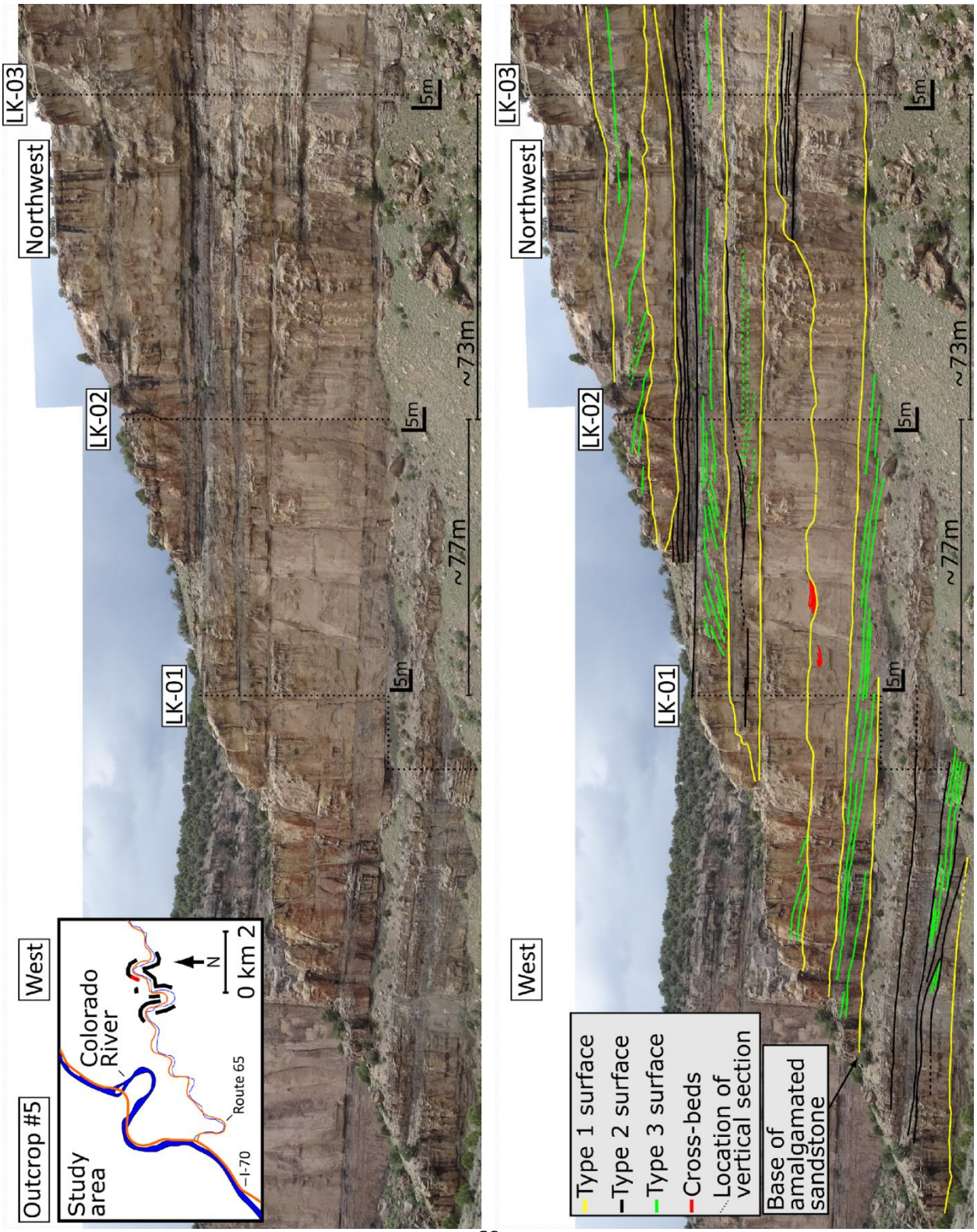
Outcrop #5
West
Study area
Colorado River
I-70
Route 65
N
0 km 2
LK-01
LK-02
LK-03
Northwest
5m
~77m
~73m
Type 1 surface
Type 2 surface
Type 3 surface
Cross-beds
Location of vertical section
Base of amalgamated sandstone

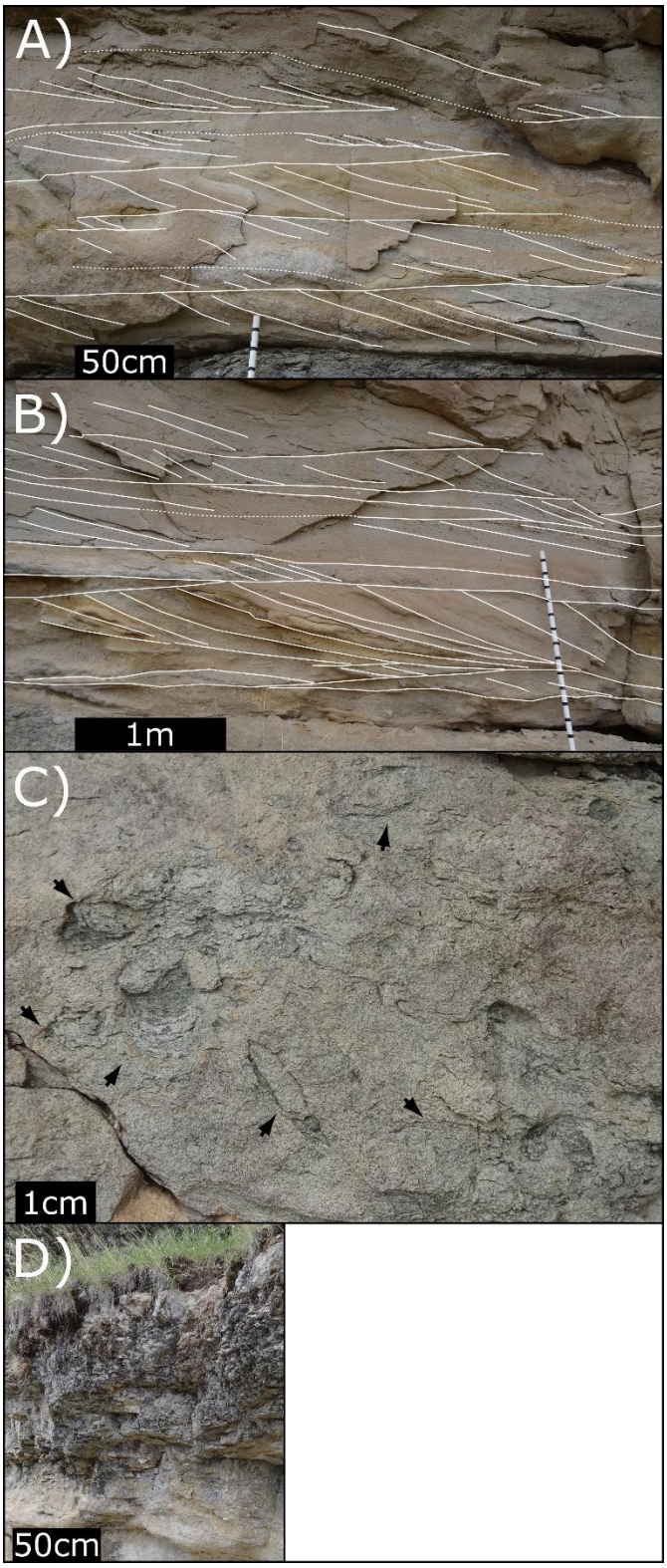

Figure 5

Figure 6

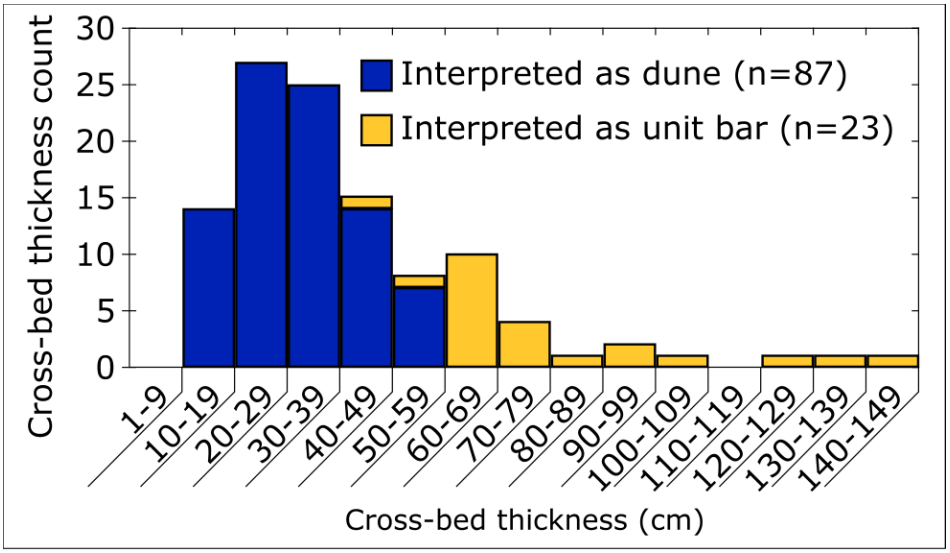

Figure 7

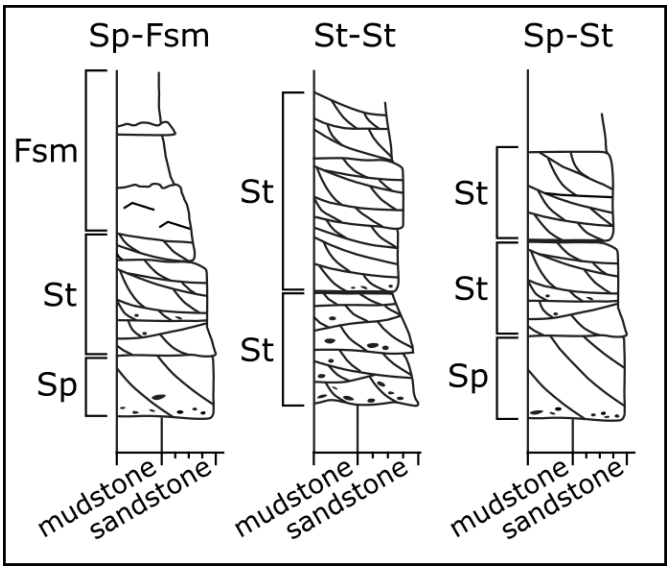

Figure 8

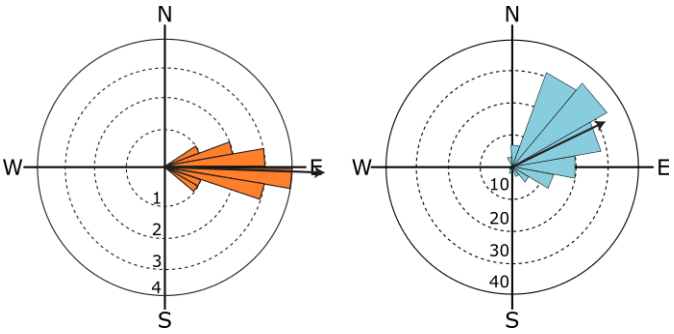

Figure 9

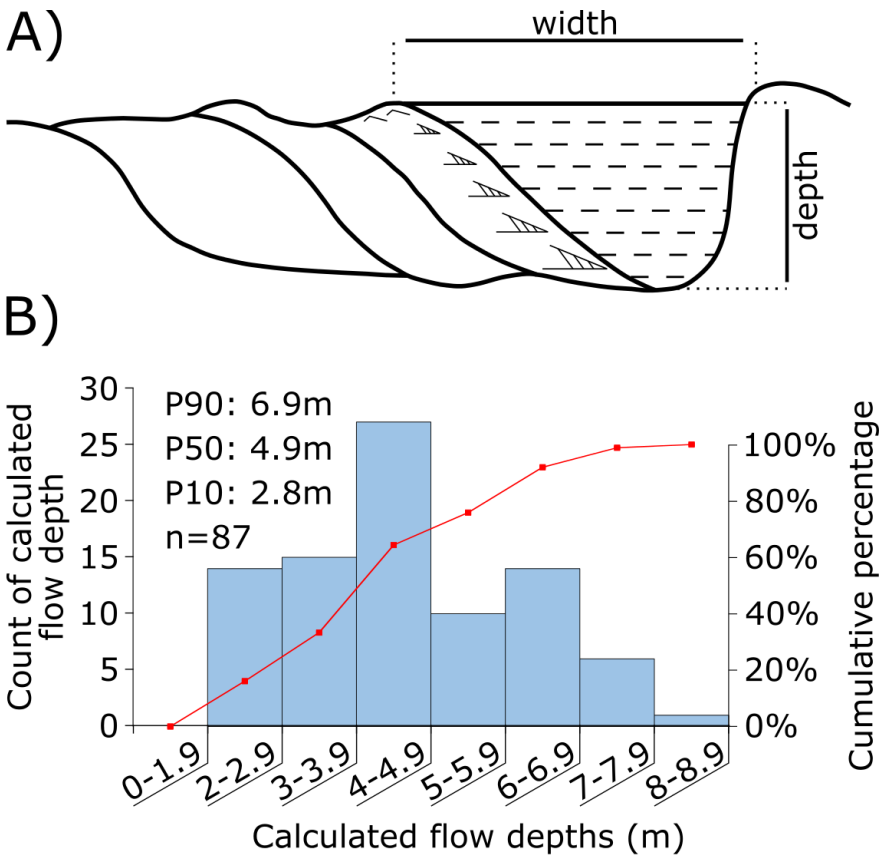

Figure 10

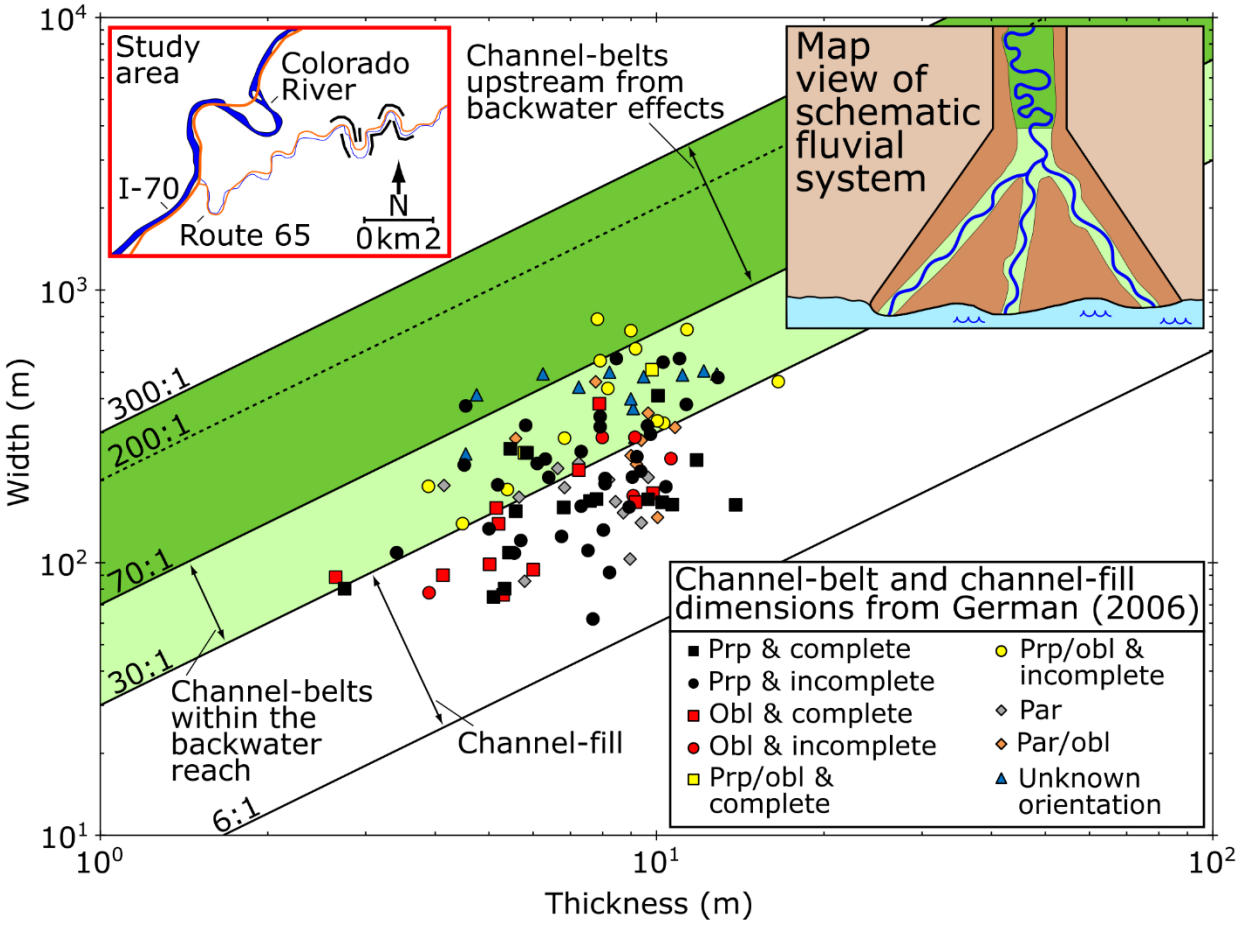
Study area
Colorado River
I-70
Route 65
N
0km2
Channel-belts upstream from backwater effects
Map view of schematic fluvial system
300:1
200:1
70:1
30:1
6:1
Channel-belts within the backwater reach
Channel-fill
Channel-belt and channel-fill dimensions from German (2006)
Prp & complete
Prp & incomplete
Obl & complete
Obl & incomplete
Prp/obl & complete
Prp/obl & incomplete
Par
Par/obl
Unknown orientation
Width (m)
Thickness (m)
10^4
10^3
10^2
10^1
10^0
10^1
10^2

Figure 11

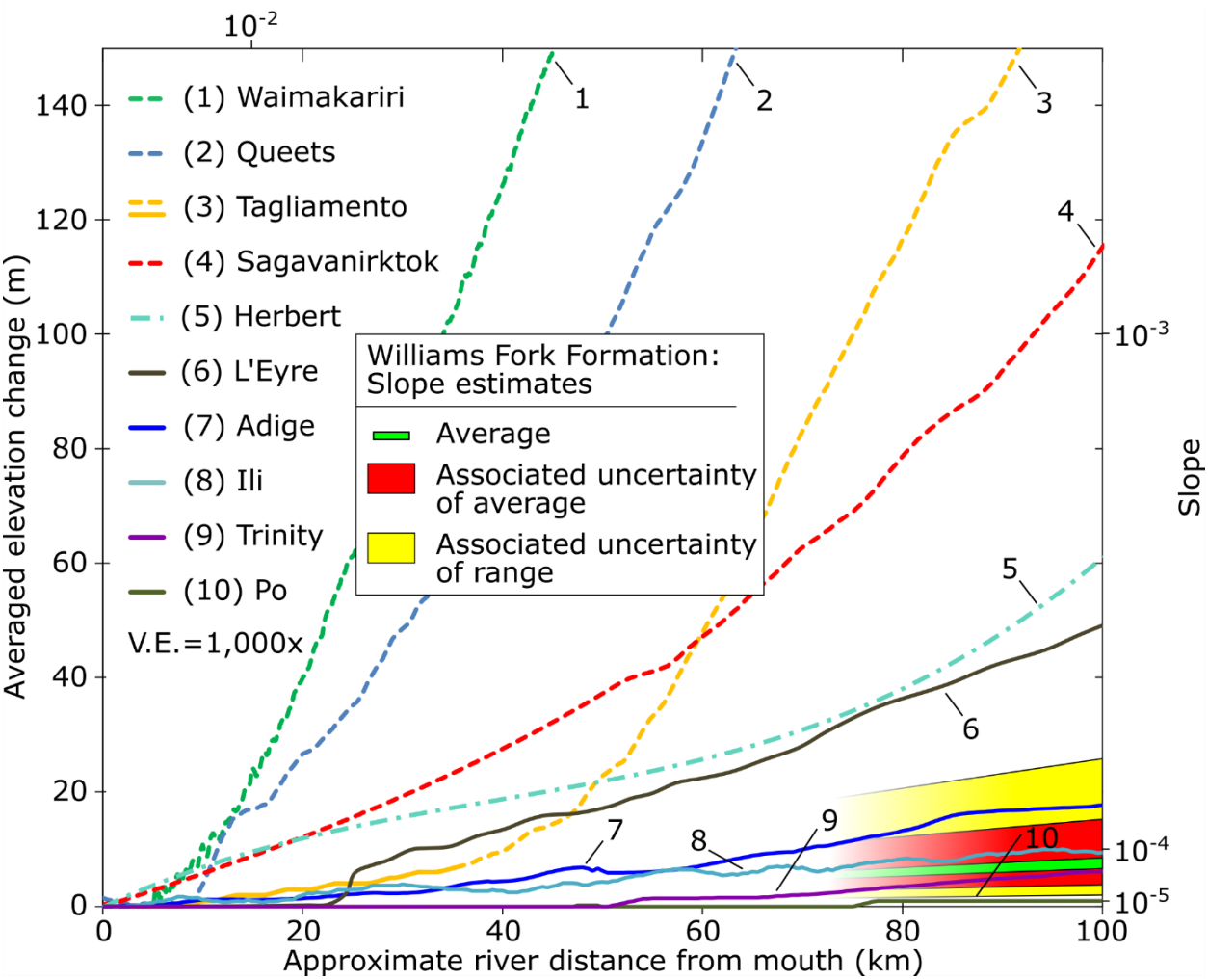
10-2
(1) Waimakariri
(2) Queets
(3) Tagliamento
(4) Sagavanirktok
(5) Herbert
(6) L'Eyre
(7) Adige
(8) Ili
(9) Trinity
(10) Po
V.E.=1,000x
Williams Fork Formation:
Slope estimates
Average
Associated uncertainty of average
Associated uncertainty of range
Averaged elevation change (m)
Slope
Approximate river distance from mouth (km)
0
20
40
60
80
100
120
140
10-3
10-4
10-5

Figure 12

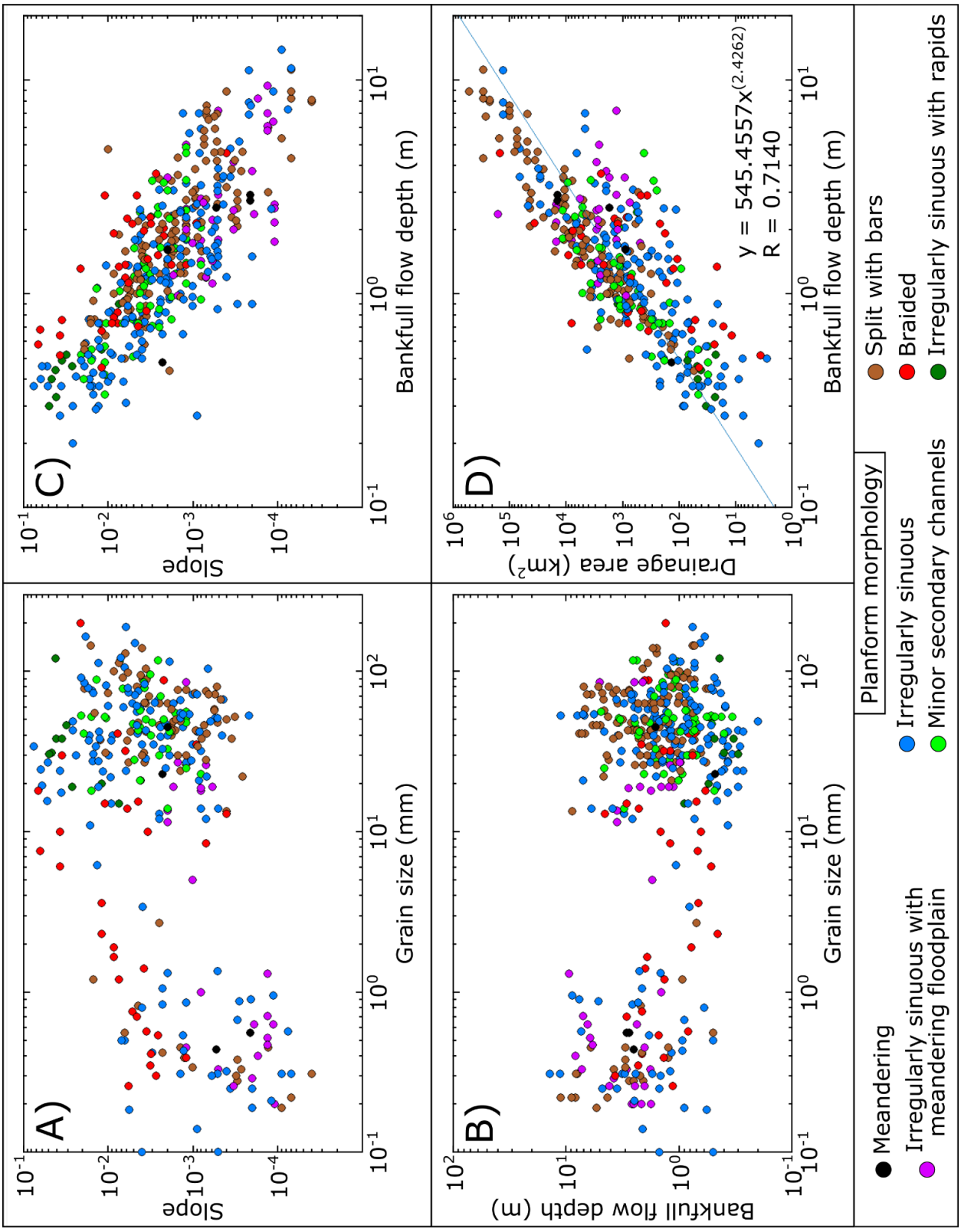
A)
B)
C)
D)
Slope
Grain size (mm)
Bankfull flow depth (m)
Drainage area (km²)
y = 545.4557x^(2.4262)
R = 0.7140
Planform morphology
Meandering
Irregularly sinuous with meandering floodplain
Irregularly sinuous
Minor secondary channels
Split with bars
Braided
Irregularly sinuous with rapids

Figure 13

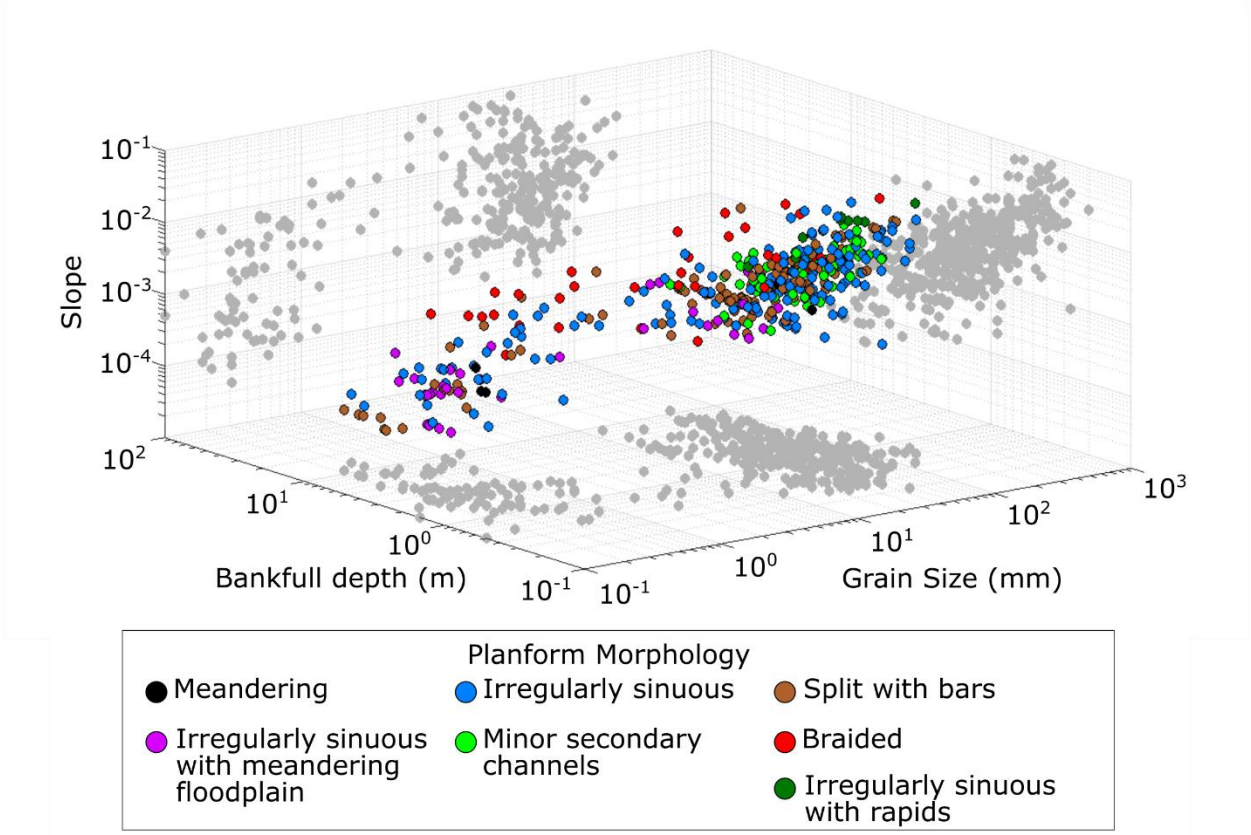
Slope
10^{-1}
10^{-2}
10^{-3}
10^{-4}
10^{2}
10^{1}
10^{0}
10^{-1}
Bankfull depth (m)
10^{-1}
10^{0}
10^{1}
10^{2}
10^{3}
Grain Size (mm)
Planform Morphology
Meandering
Irregularly sinuous
Split with bars
Irregularly sinuous with meandering floodplain
Minor secondary channels
Braided
Irregularly sinuous with rapids

Figure 14

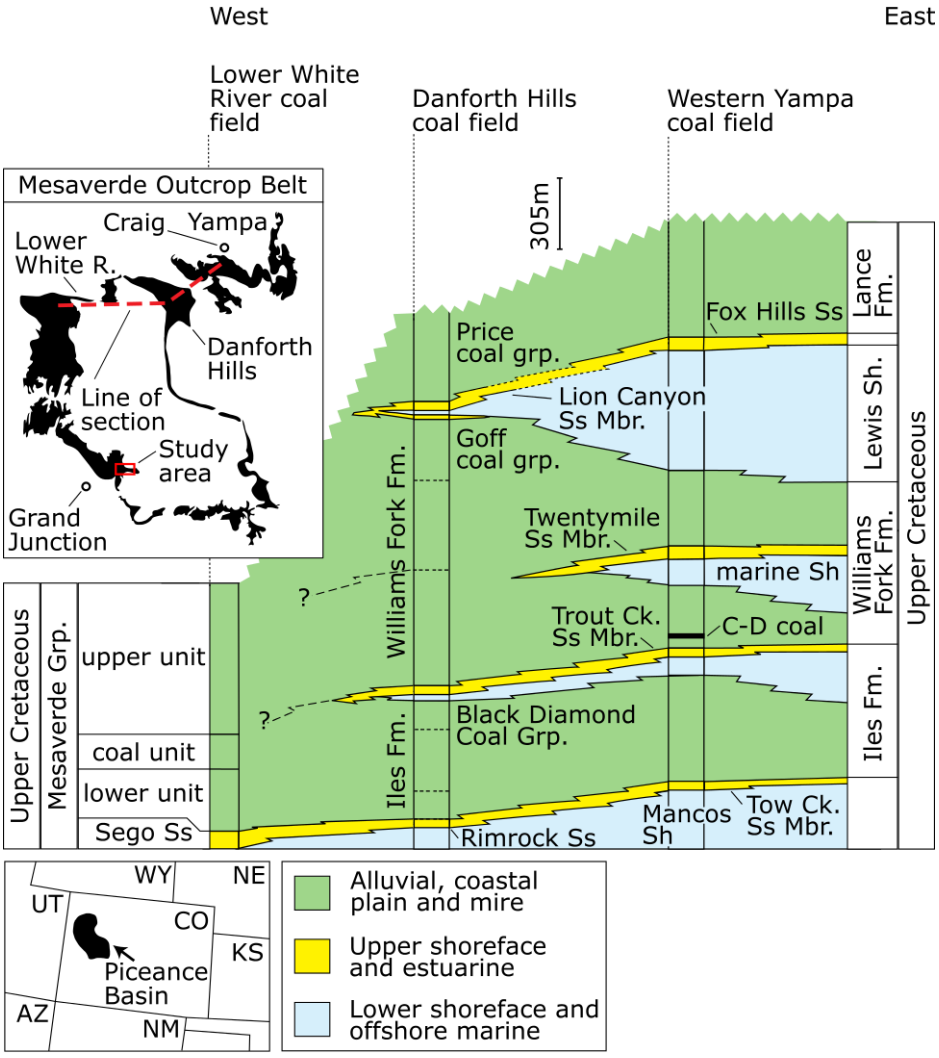
West
East
Lower White River coal field
Danforth Hills coal field
Western Yampa coal field
Mesaverde Outcrop Belt
Craig
Yampa
Lower White R.
Danforth Hills
Line of section
Study area
Grand Junction
305m
Fox Hills Ss
Lance Fm.
Price coal grp.
Lion Canyon Ss Mbr.
Lewis Sh.
Goff coal grp.
Twentymile Ss Mbr.
marine Sh
Williams Fork Fm.
Upper Cretaceous
Trout Ck. Ss Mbr.
C-D coal
Iles Fm.
Black Diamond Coal Grp.
Mancos Sh
Tow Ck. Ss Mbr.
Rimrock Ss
Upper Cretaceous
Mesaverde Grp.
upper unit
coal unit
lower unit
Sego Ss
WY
NE
UT
CO
KS
Piceance Basin
AZ
NM
Alluvial, coastal plain and mire
Upper shoreface and estuarine
Lower shoreface and offshore marine

Figure 15

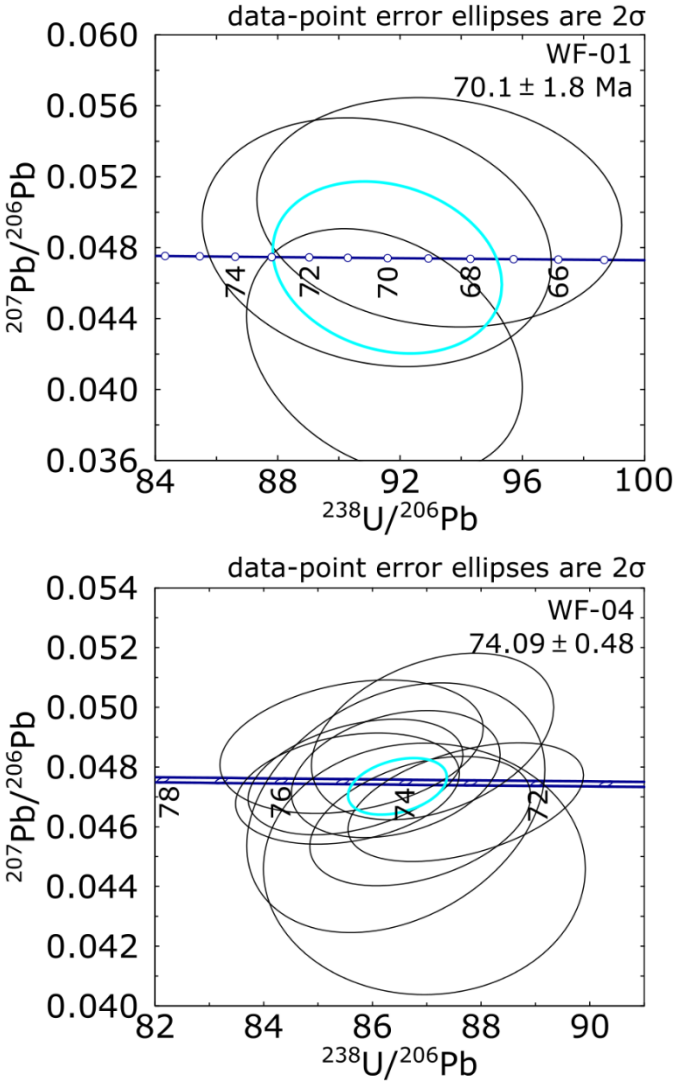
data-point error ellipses are 2σ
WF-01
70.1 ± 1.8 Ma
0.060
0.056
0.052
0.048
0.044
0.040
0.036
84
88
92
96
100
$^{207}Pb/^{206}Pb$
$^{238}U/^{206}Pb$
74
72
70
68
66
data-point error ellipses are 2σ
WF-04
74.09 ± 0.48
0.054
0.052
0.050
0.048
0.046
0.044
0.042
0.040
82
84
86
88
90
$^{207}Pb/^{206}Pb$
$^{238}U/^{206}Pb$
78
76
74
72

Figure 16

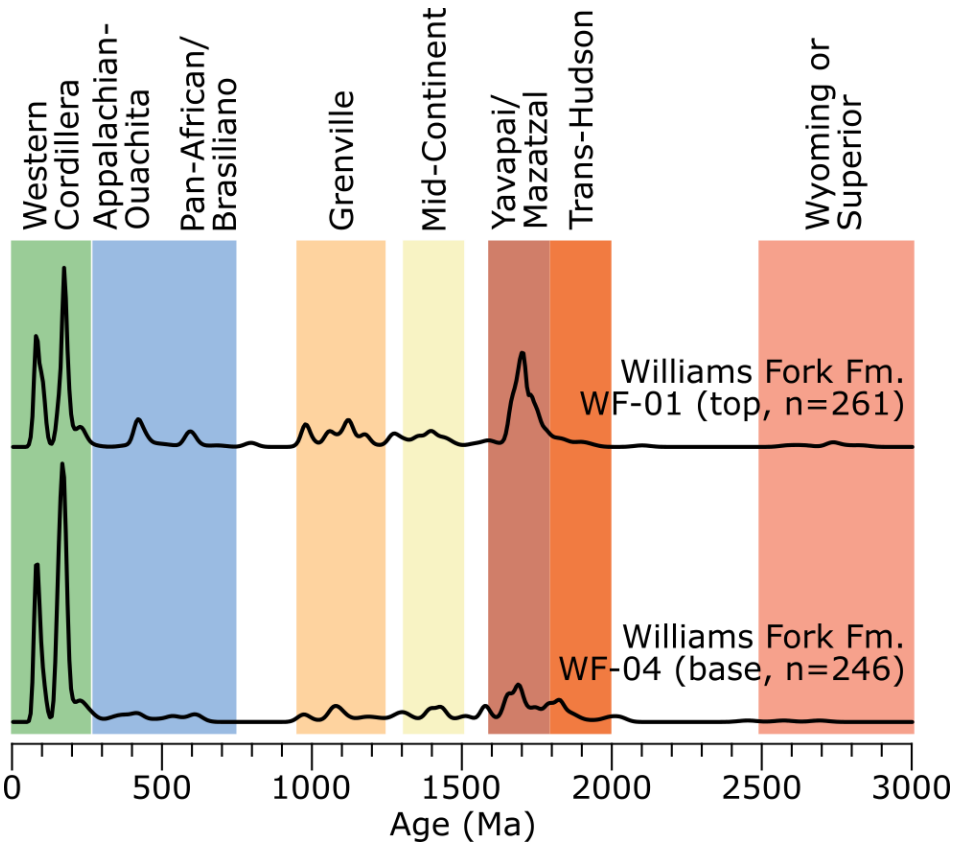
Western Cordillera
Appalachian-Ouachita
Pan-African/Brasiliano
Grenville
Mid-Continent
Yavapai/Mazatzal
Trans-Hudson
Wyoming or Superior
Williams Fork Fm.
WF-01 (top, n=261)
Williams Fork Fm.
WF-04 (base, n=246)
0
500
1000
1500
2000
2500
3000
Age (Ma)

Figure 17

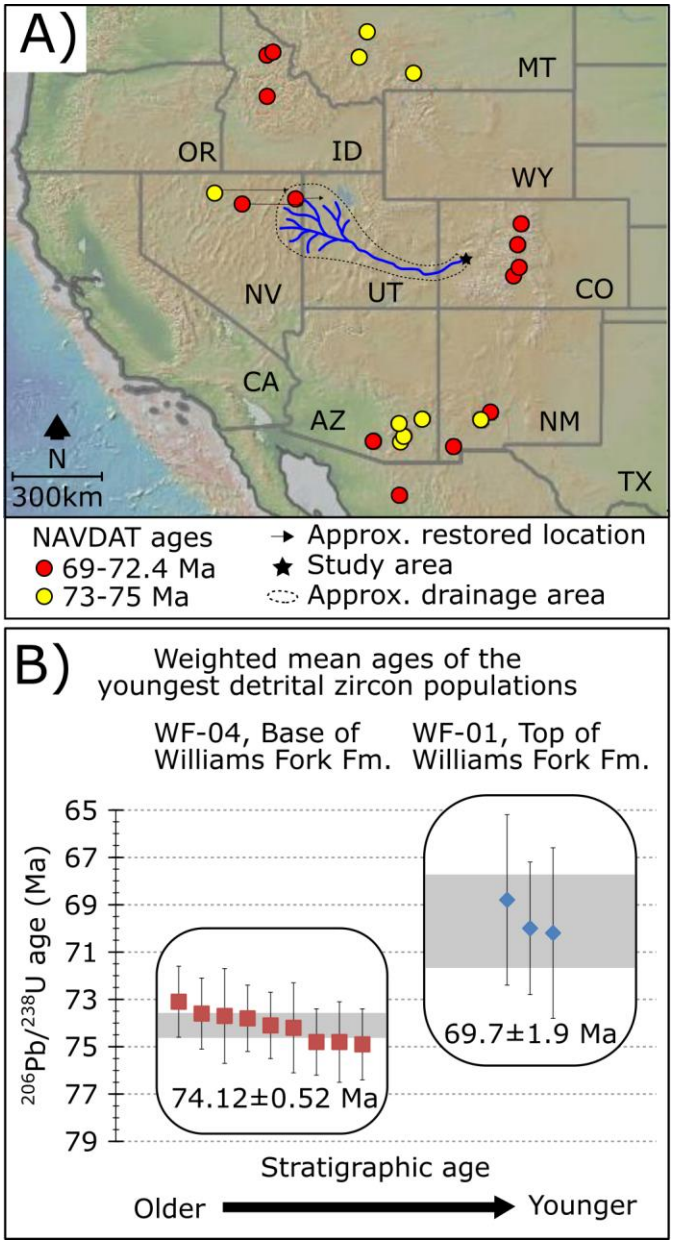
A)
MT
OR
ID
WY
NV
UT
CO
CA
AZ
NM
TX
N
300km
NAVDAT ages
69-72.4 Ma
73-75 Ma
Approx. restored location
Study area
Approx. drainage area
B)
Weighted mean ages of the youngest detrital zircon populations
WF-04, Base of Williams Fork Fm.
WF-01, Top of Williams Fork Fm.
65
67
69
71
73
75
77
79
206Pb/238U age (Ma)
74.12±0.52 Ma
69.7±1.9 Ma
Stratigraphic age
Older
Younger

Figure 18

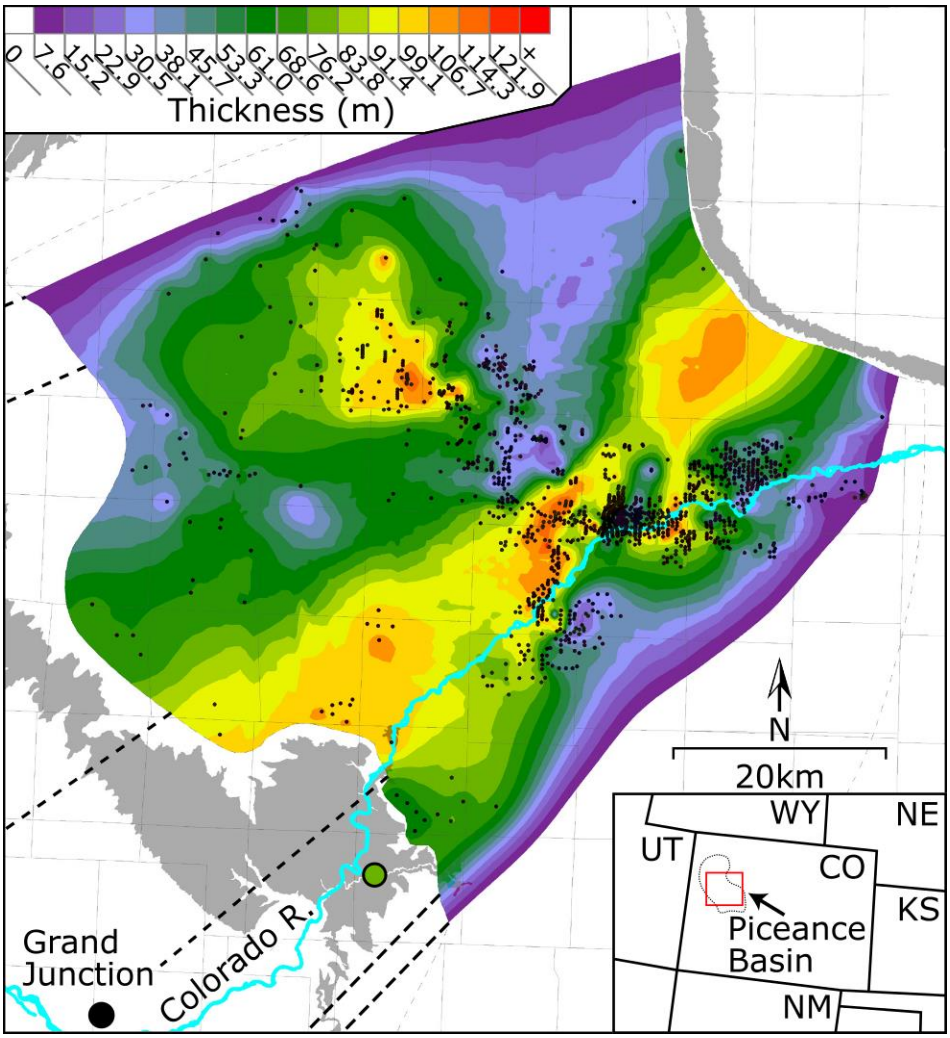
0
7.6
15.2
22.9
30.5
38.1
45.7
53.3
61.0
68.6
76.2
83.8
91.4
99.1
106.7
114.3
121.9
+
Thickness (m)
N
20km
WY
NE
UT
CO
KS
Piceance
Basin
NM
Grand
Junction
Colorado R.

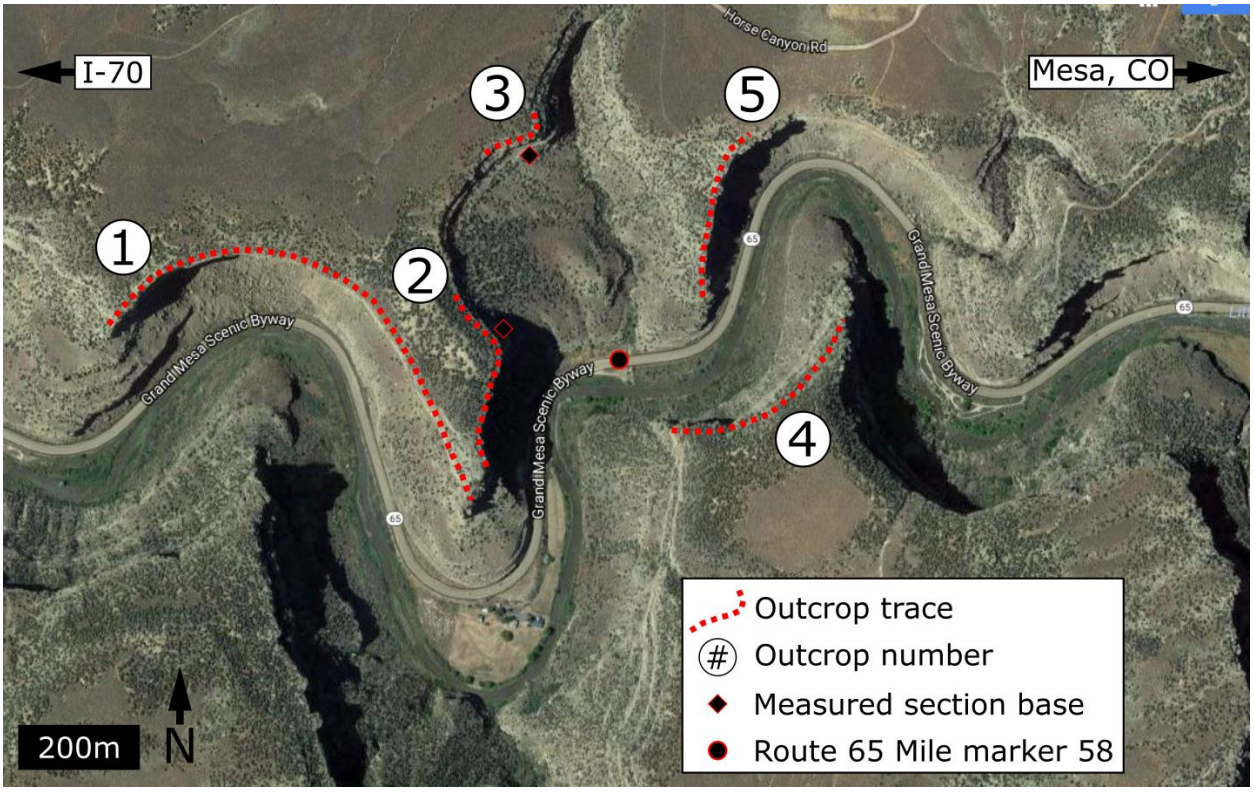

Figure A1) Google Earth imagery displaying outcrop locations within the study area of Plateau Creek Canyon. Outcrops 2 and 3 were the locations of measured sections. Outcrops 1-5 were measured with a laser range finder. Vertical sections from the laser range finder are in appendix 1.2. Vertical sections are labeled with a two letter code followed by a number. The letters refer to

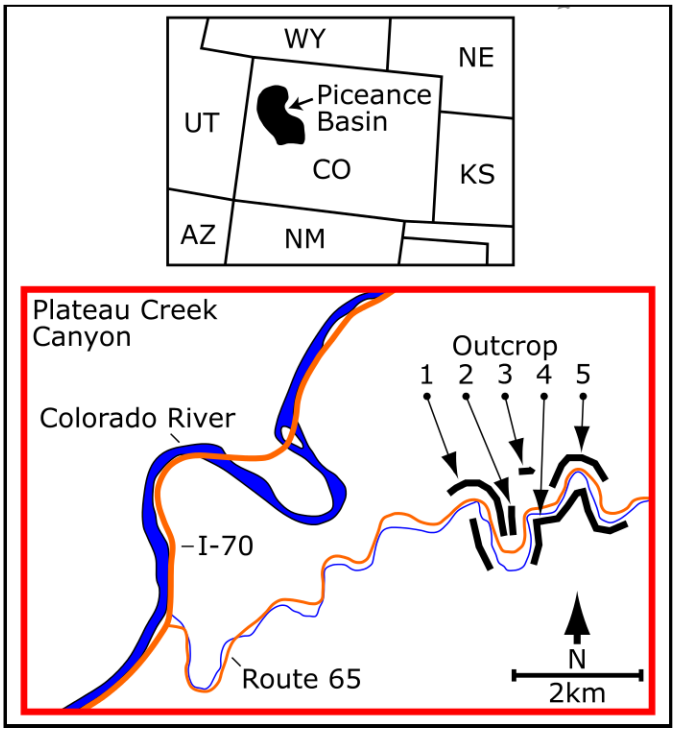

the outcrop and the numbers refer to the section within the outcrop. Two letter codes are as follows:

Outcrop 1 = BK

Outcrop 2 = MK

Outcrop 3 = IC

Outcrop 4 = KR

Outcrop 5 = LK

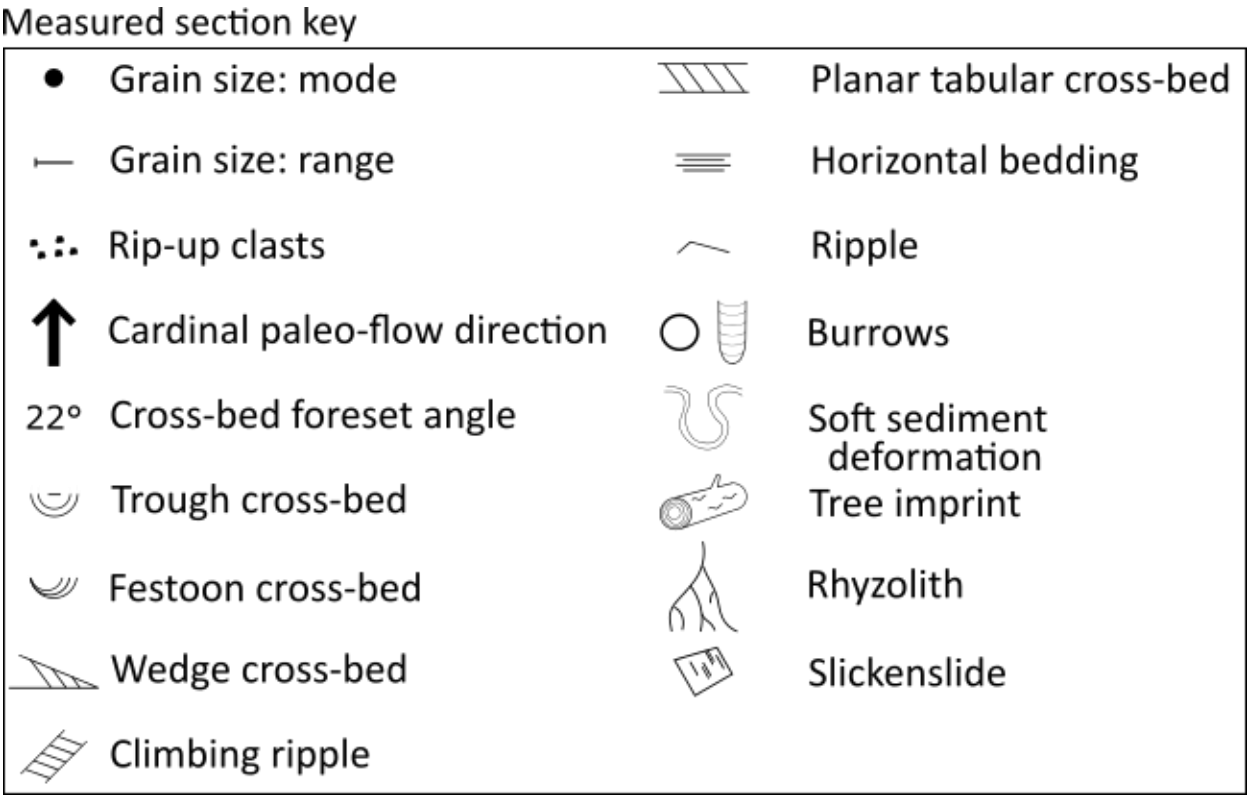

Figure A2) Symbol legend for measured sections

Figure A3) Outcrop 2 (MK) measured section

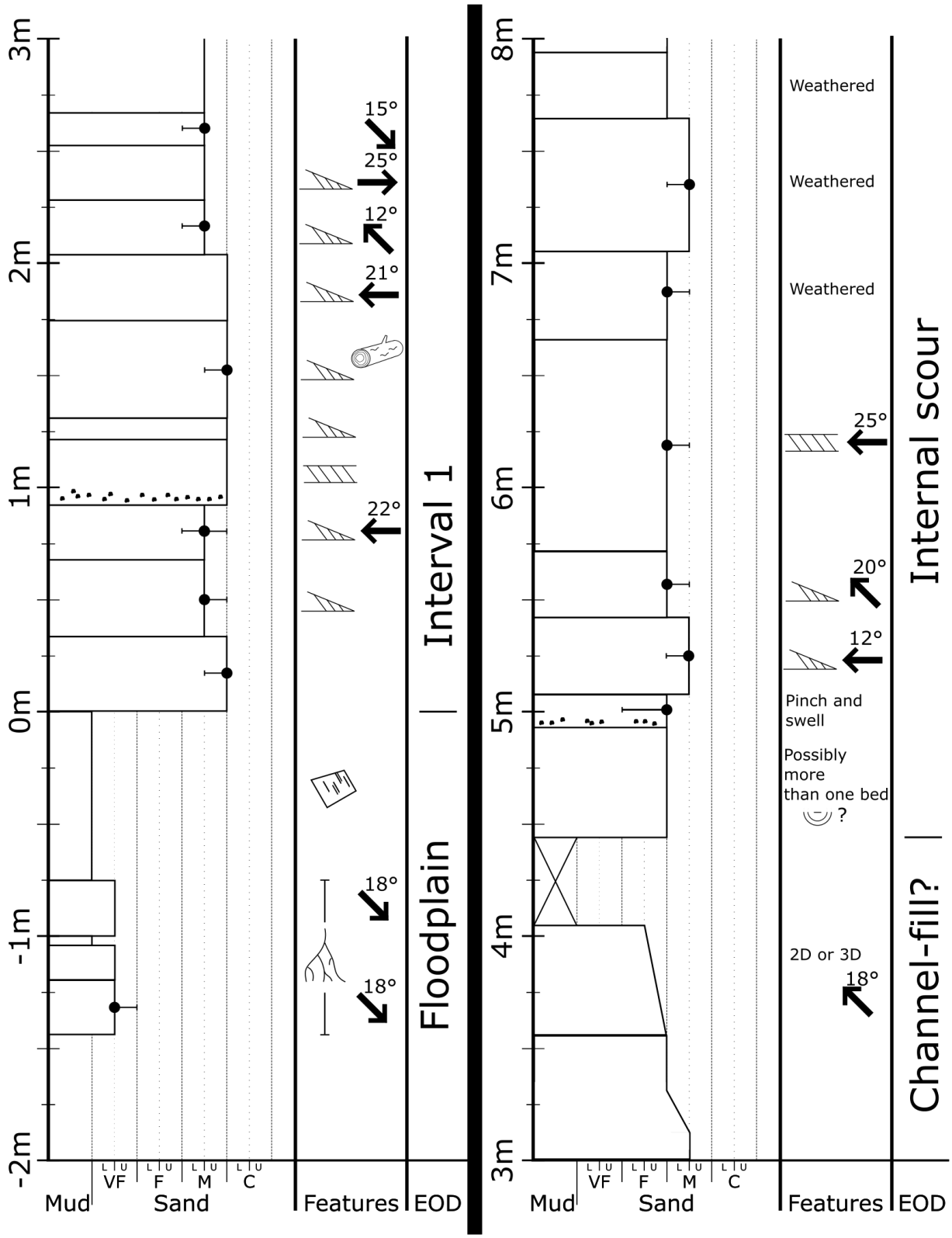
3m
2m
1m
0m
-1m
-2m
Mud
VF
F
M
C
Sand
Features
EOD
15°
25°
12°
21°
22°
18°
18°
Floodplain
Interval 1
8m
7m
6m
5m
4m
3m
Weathered
Weathered
Weathered
25°
20°
12°
Pinch and swell
Possibly more than one bed
?
2D or 3D
18°
Internal scour
Channel-fill?

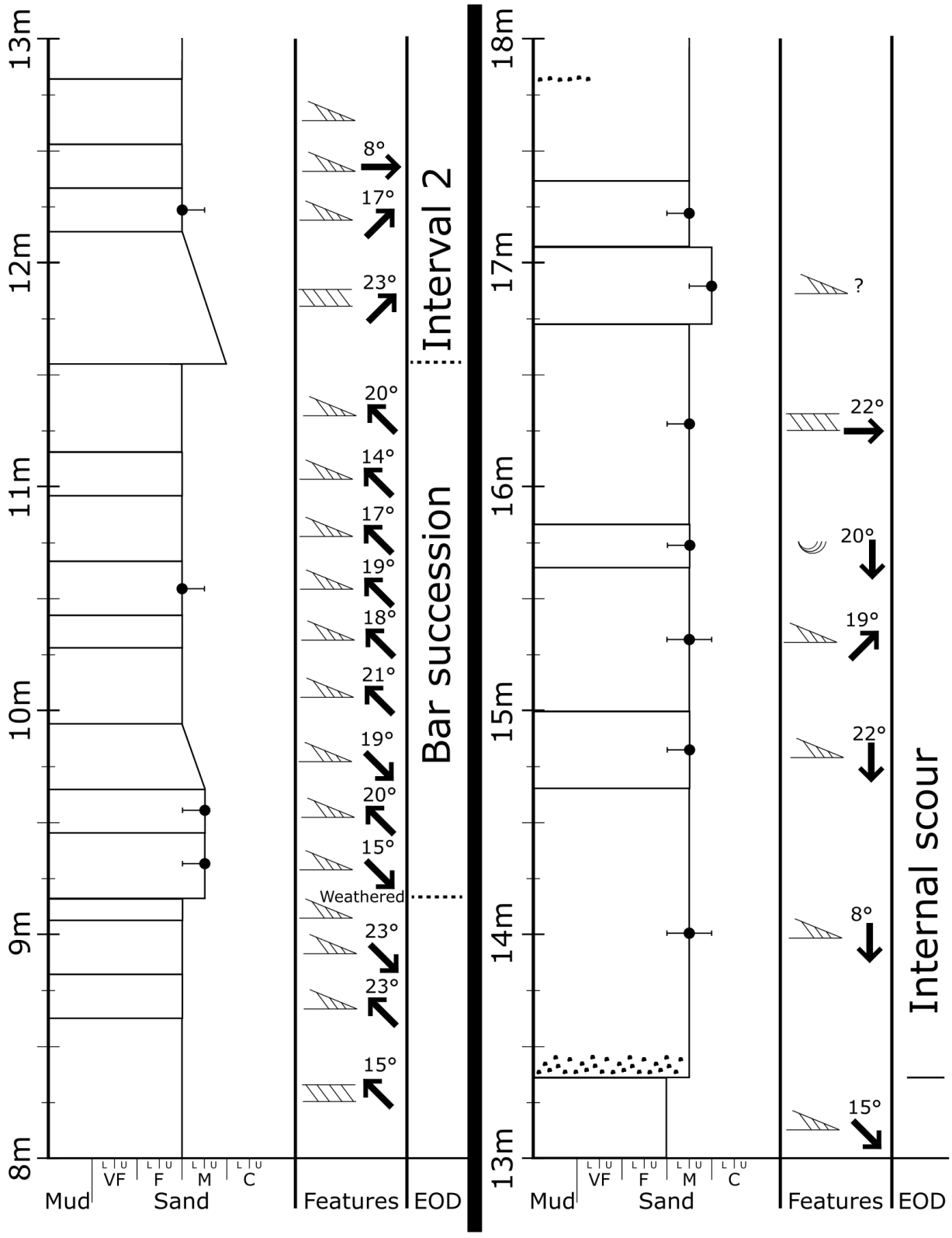
13m
12m
11m
10m
9m
8m
Mud
VF
F
M
C
Sand
Features
EOD
8°
17°
23°
20°
14°
17°
19°
18°
21°
19°
20°
15°
Weathered
23°
23°
15°
Interval 2
Bar succession
18m
17m
16m
15m
14m
13m
?
22°
20°
19°
22°
8°
15°
Internal scour

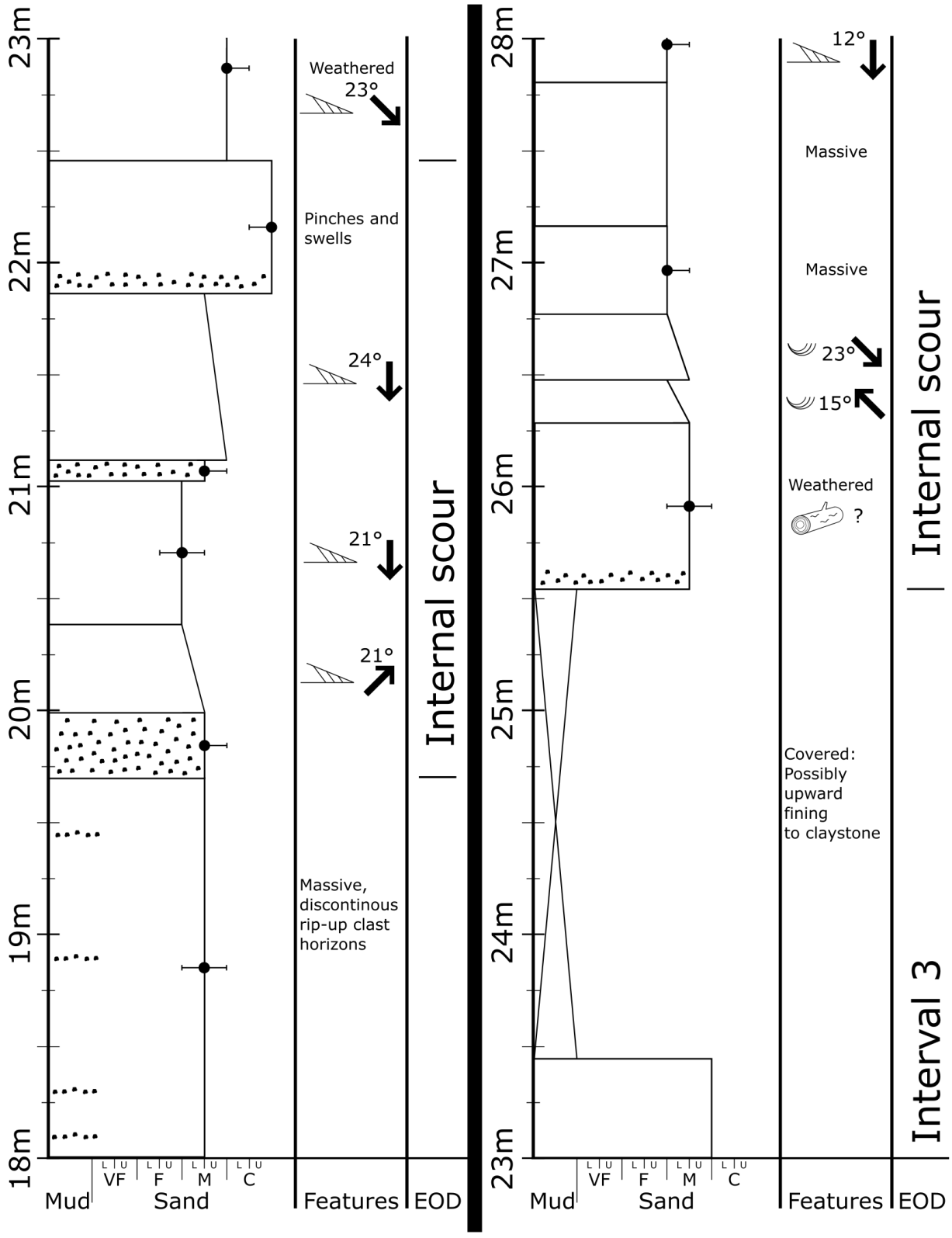
23m
22m
21m
20m
19m
18m
Weathered
23°
Pinches and swells
24°
21°
21°
Massive, discontinous rip-up clast horizons
Internal scour
Mud
VF
F
M
C
Sand
Features
EOD
28m
27m
26m
25m
24m
23m
12°
Massive
Massive
23°
15°
Weathered
?
Covered: Possibly upward fining to claystone
Internal scour
Interval 3

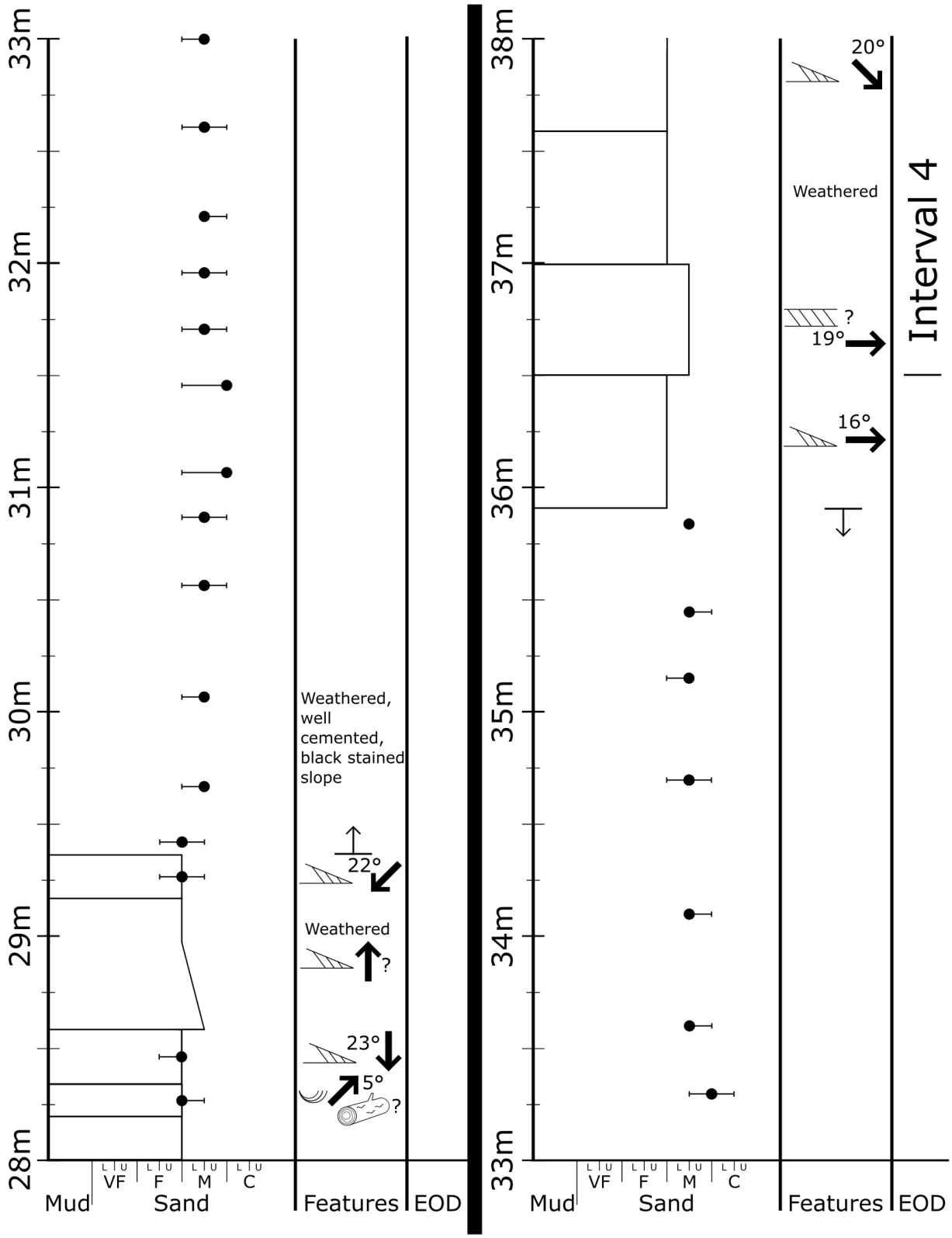
33m
32m
31m
30m
29m
28m
Mud
VF
F
M
C
Sand
Features
EOD
Weathered, well cemented, black stained slope
22°
Weathered
?
23°
5°
?
38m
37m
36m
35m
34m
33m
20°
Weathered
?
19°
16°
Interval 4

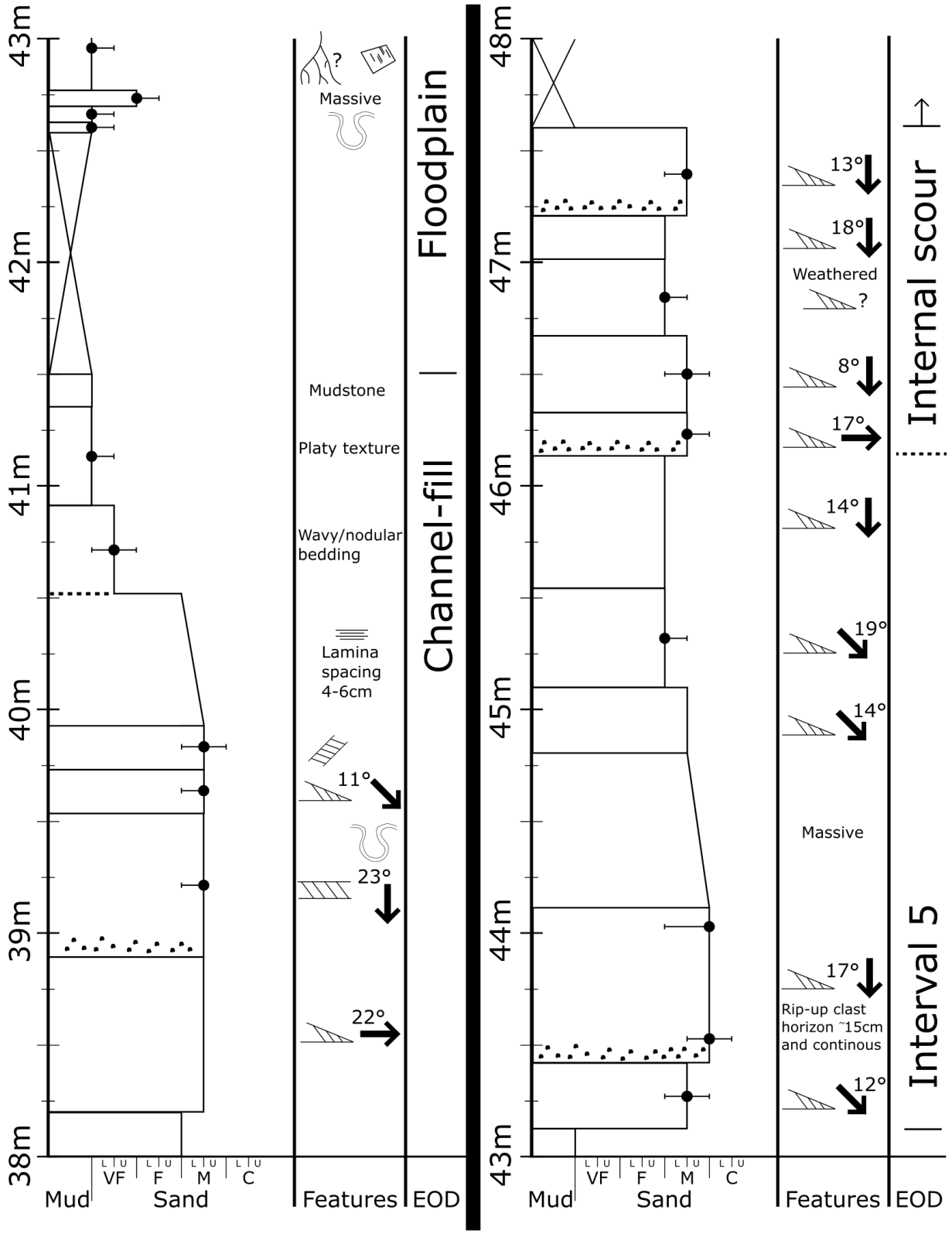
43m
42m
41m
40m
39m
38m
Mud
VF
F
M
C
Sand
Massive
Mudstone
Platy texture
Wavy/nodular bedding
Lamina spacing 4-6cm
11°
23°
22°
Features
EOD
Floodplain
Channel-fill
48m
47m
46m
45m
44m
43m
13°
18°
Weathered
8°
17°
14°
19°
14°
Massive
17°
Rip-up clast horizon ~15cm and continous
12°
Internal scour
Interval 5

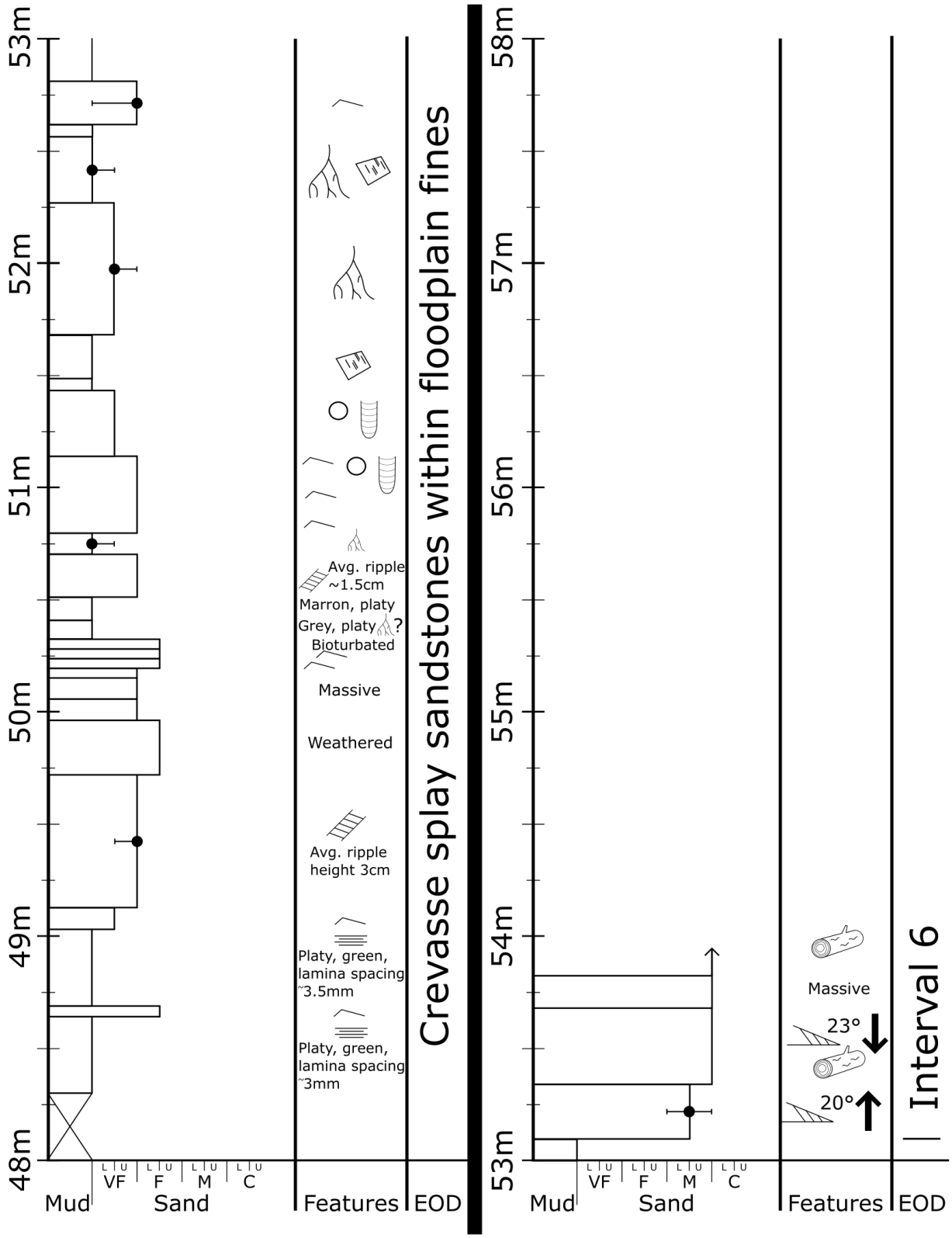
53m
52m
51m
50m
49m
48m
Mud
VF
F
M
C
Sand
Features
EOD
Avg. ripple ~1.5cm
Marron, platy
Grey, platy ?
Bioturbated
Massive
Weathered
Avg. ripple height 3cm
Platy, green, lamina spacing ~3.5mm
Platy, green, lamina spacing ~3mm
Crevasse splay sandstones within floodplain fines
58m
57m
56m
55m
54m
53m
Massive
23°
20°
Interval 6

Figure A4) Outcrop 3 (IC) measured section

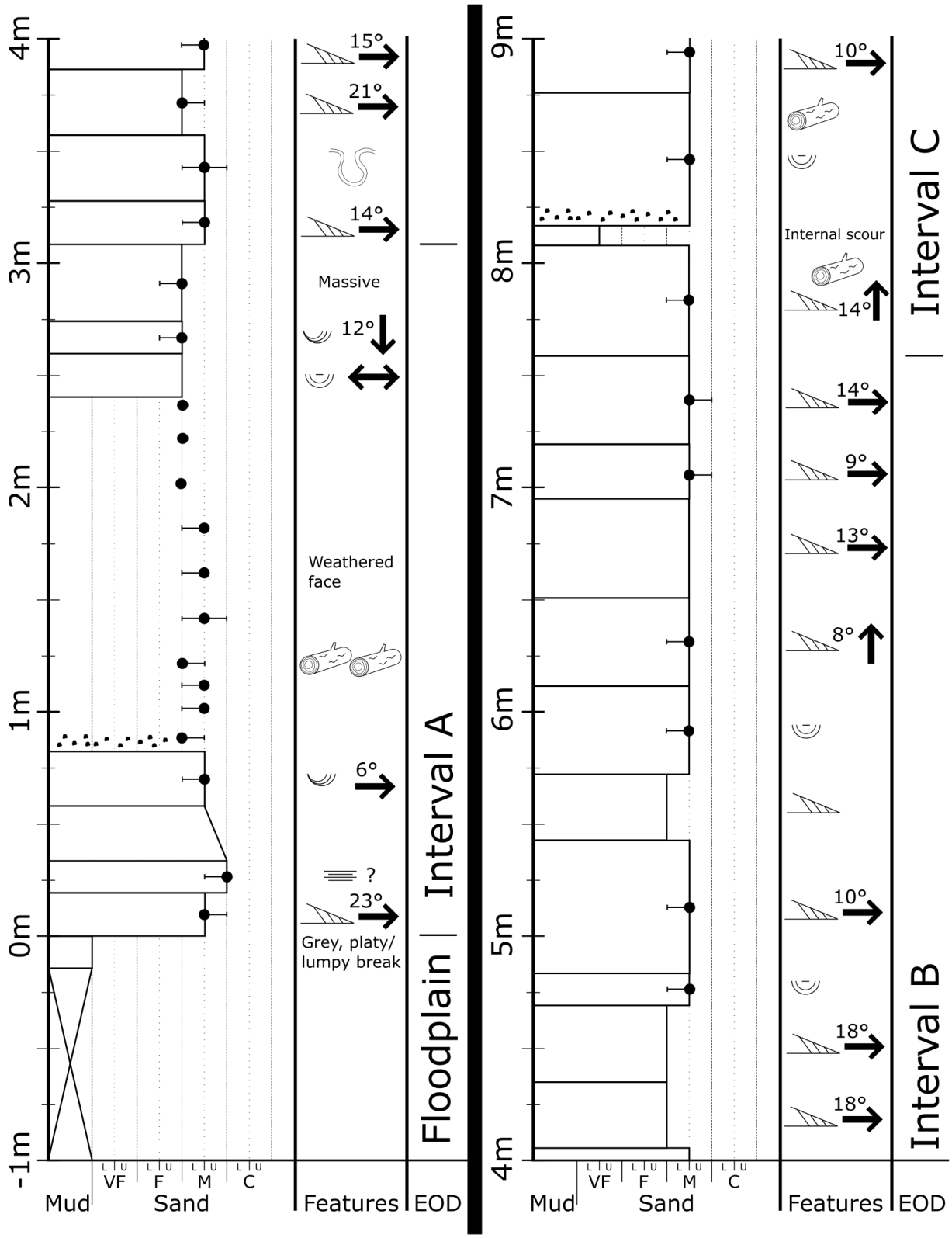
4m
3m
2m
1m
0m
-1m
Mud
VF
F
M
C
Sand
Features
EOD
Floodplain | Interval A
15°
21°
14°
Massive
12°
Weathered face
6°
?
23°
Grey, platy/ lumpy break
9m
8m
7m
6m
5m
4m
Internal scour
10°
14°
14°
9°
13°
8°
10°
18°
18°
Interval B | Interval C

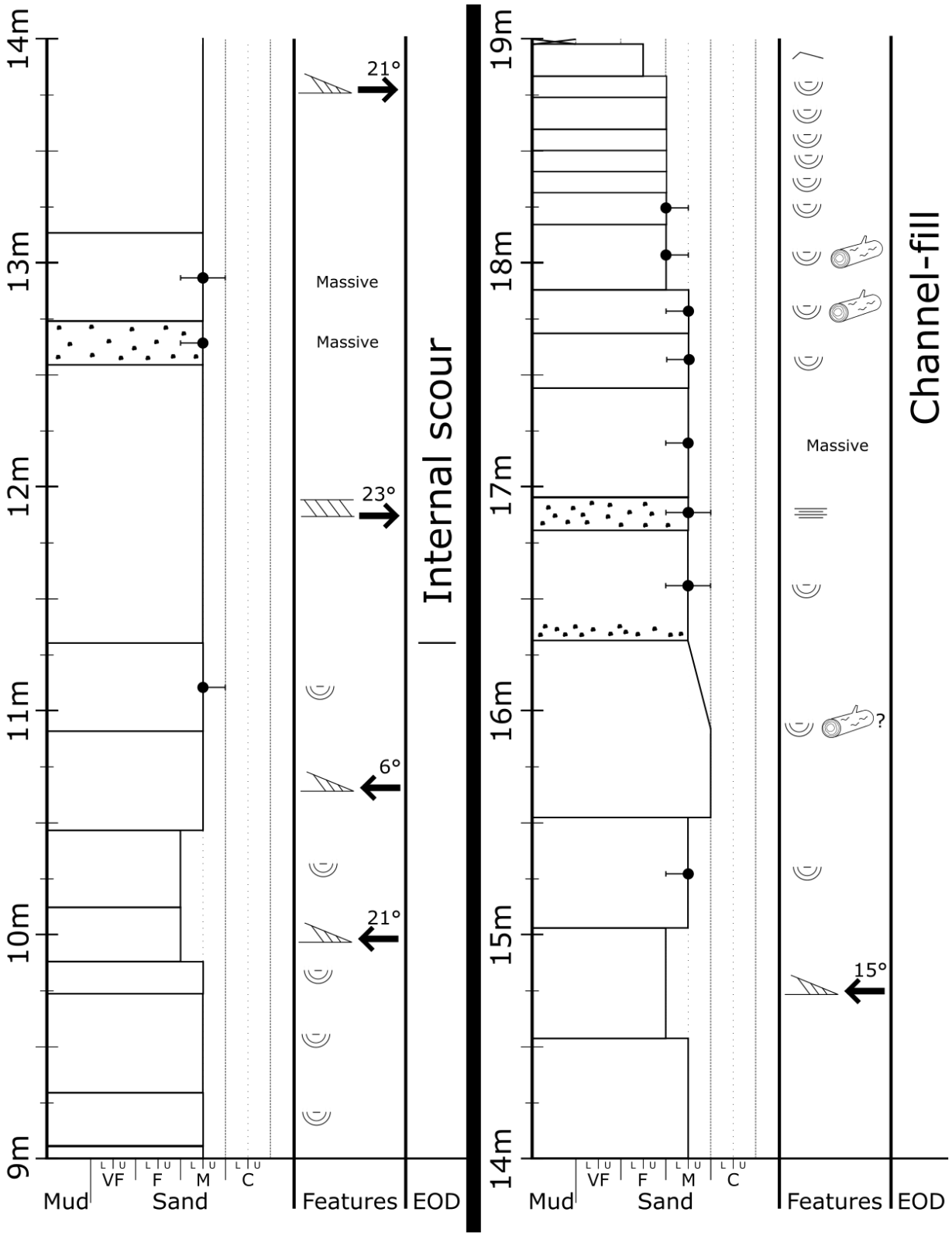
14m
13m
12m
11m
10m
9m
21°
Massive
Massive
23°
6°
21°
Internal scour
19m
18m
17m
16m
15m
14m
Massive
?
15°
Channel-fill
Mud
VF
F
M
C
Sand
Features
EOD
Mud
VF
F
M
C
Sand
Features
EOD

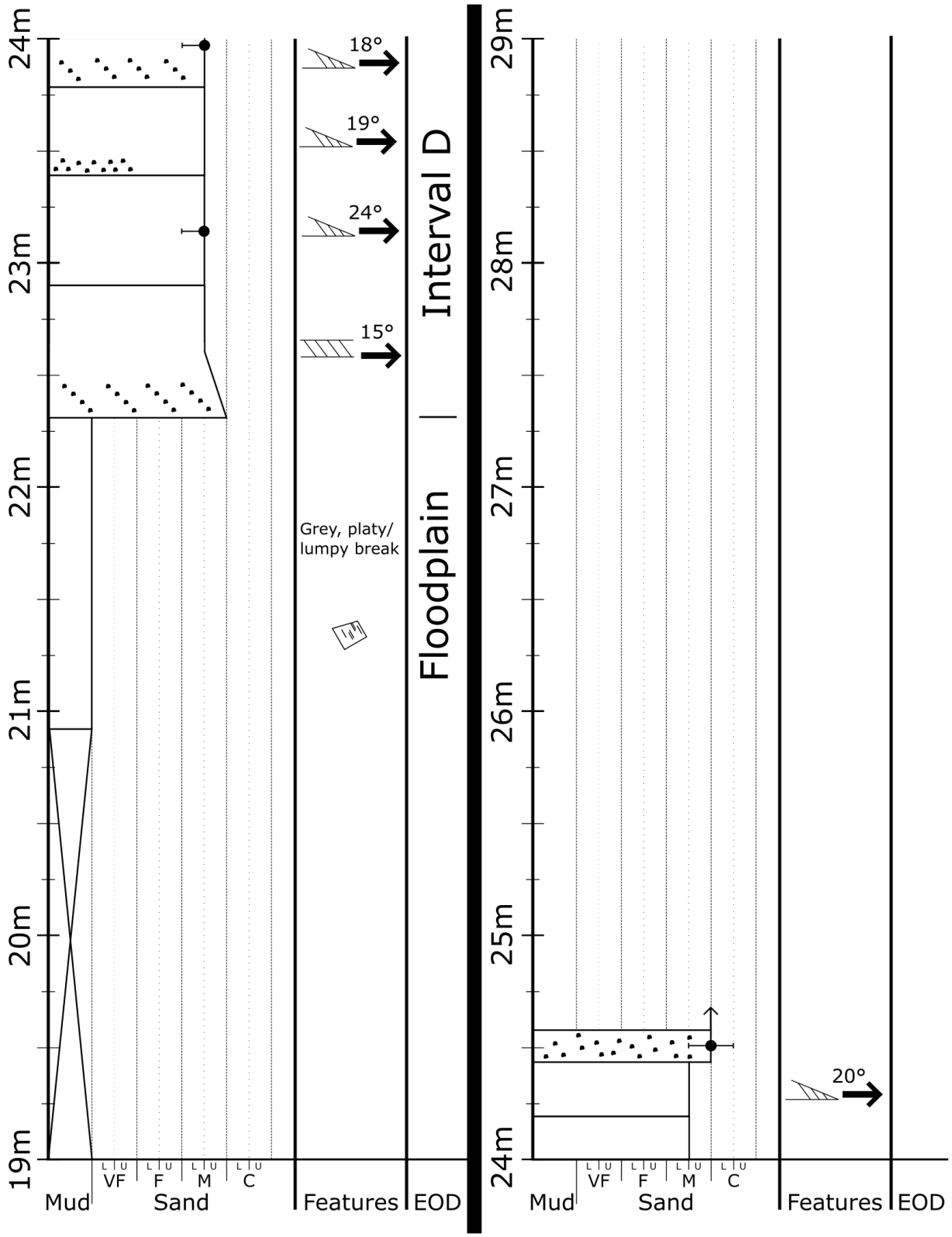
24m
23m
22m
21m
20m
19m
18°
19°
24°
15°
Interval D
Floodplain
Grey, platy/
lumpy break
L U
VF
F
M
C
Mud
Sand
Features
EOD
29m
28m
27m
26m
25m
24m
20°

Appendix 1.2 - Vertical sections

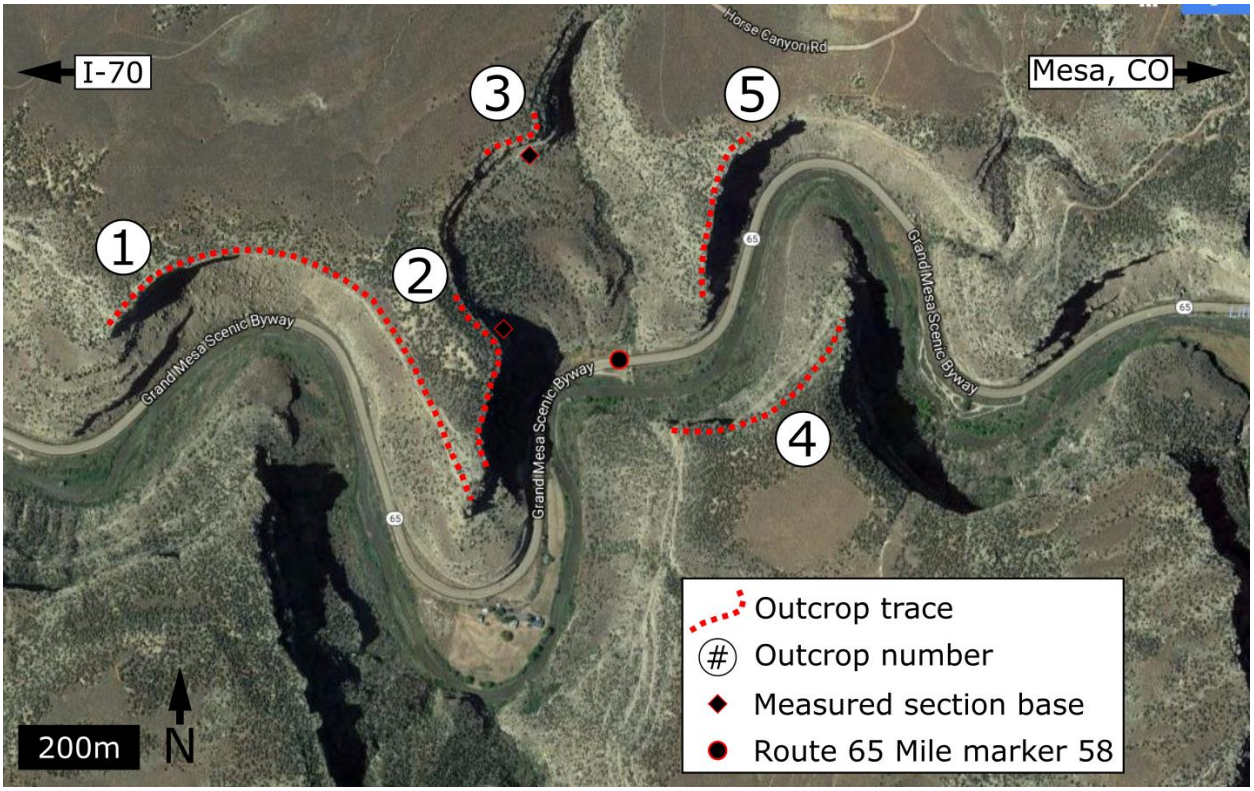

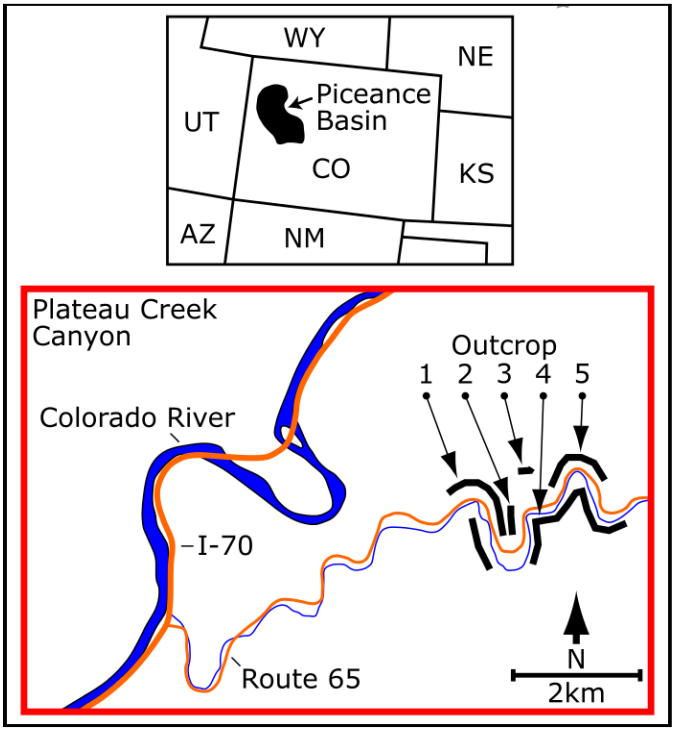

Figure A5) Google Earth imagery displaying outcrop locations within the study area of Plateau Creek Canyon. Outcrops 2 and 3 were the locations of measured sections. Outcrops 1-5 were measured with a laser range finder. Vertical sections from the laser range finder are in appendix 1.2. Vertical sections are labeled with a two letter code followed by a number. The letters refer to the outcrop and the numbers refer to the section within the outcrop. Two letter codes are as follows:

Outcrop 1 = BK

Outcrop 2 = MK

Outcrop 3 = IC

Outcrop 4 = KR

Outcrop 5 = LK

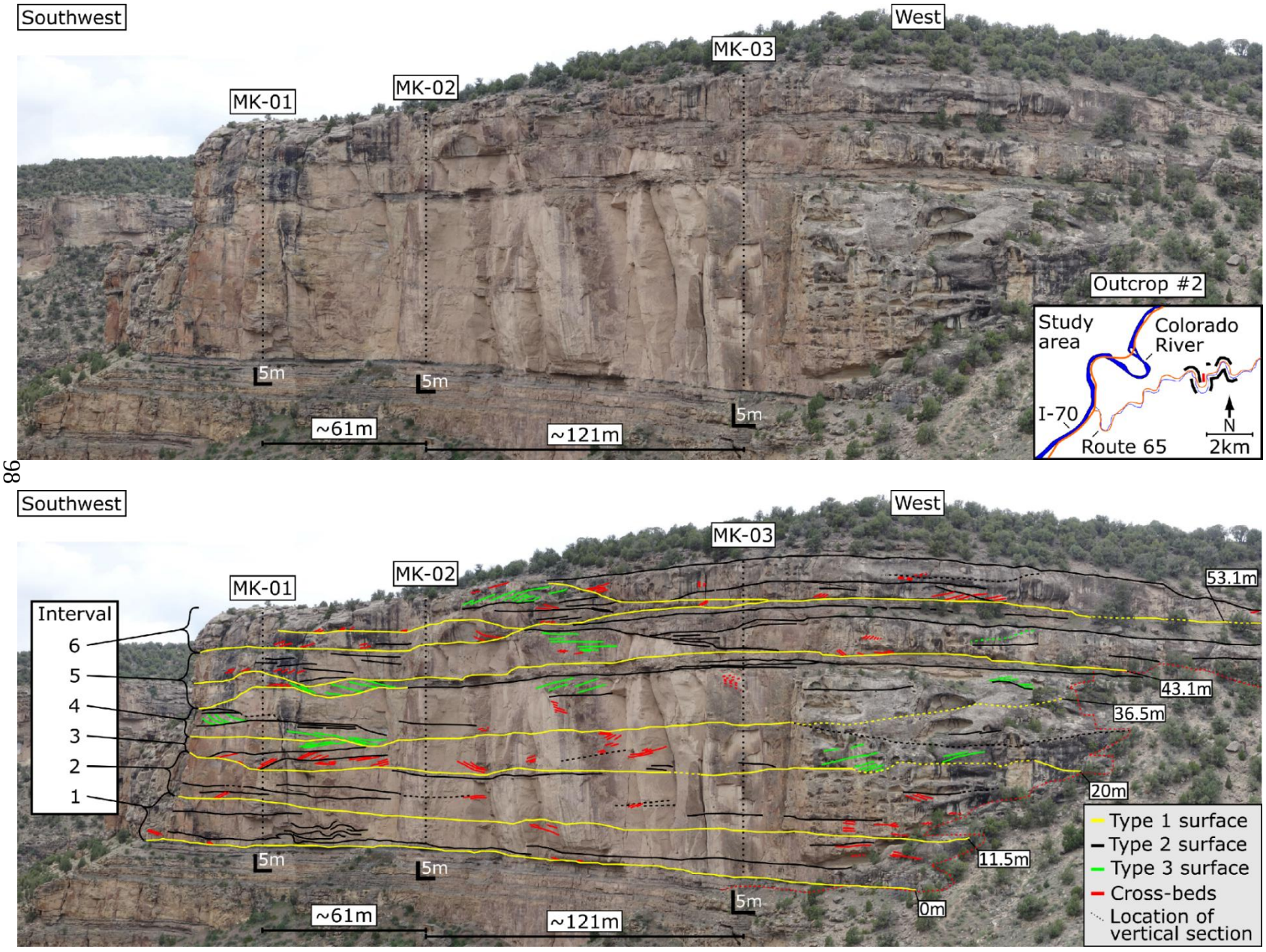
Southwest
West
MK-01
MK-02
MK-03
5m
5m
5m
~61m
~121m
Outcrop #2
Study area
Colorado River
I-70
Route 65
N
2km
Southwest
West
MK-01
MK-02
MK-03
Interval
6
5
4
3
2
1
53.1m
43.1m
36.5m
20m
11.5m
0m
5m
5m
5m
~61m
~121m
Type 1 surface
Type 2 surface
Type 3 surface
Cross-beds
Location of vertical section

Figure A6 (previous page): Photomosaic of outcrop #2 non-interpreted (upper) and interpreted (lower). Field of view is west to the southwest. Vertical dotted lines are the location of the vertical sections completed with the laser range finder. The red dashed line in the lower photomosaic is the path taken in for the measured section. Black bars below vertical sections are 5x5m scale bars. Key surfaces are labeled in meters that correlate to the measured section.

Figure A7 (next page): Vertical sections from outcrop #2

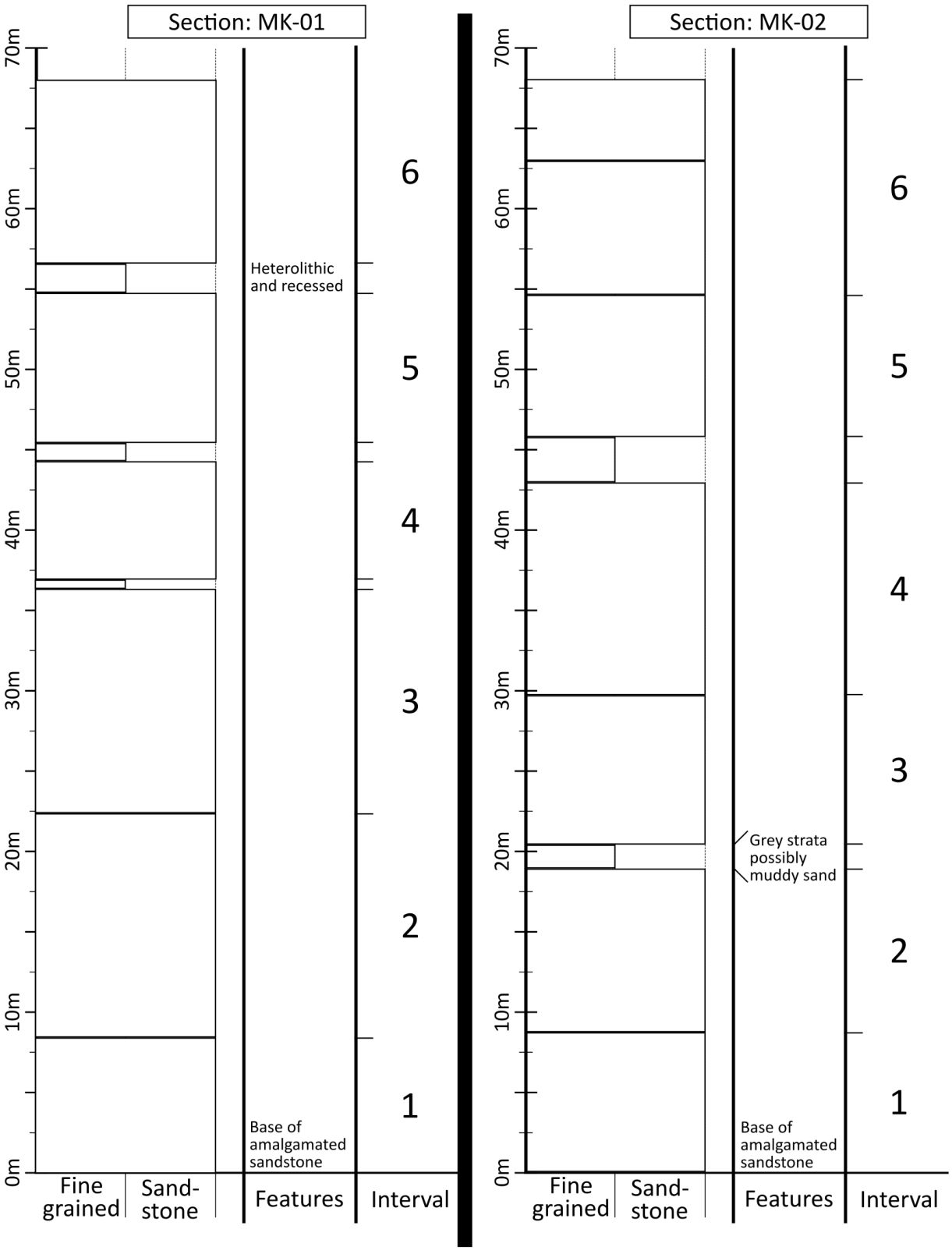
Section: MK-01
70m
60m
50m
40m
30m
20m
10m
0m
Heterolithic and recessed
Base of amalgamated sandstone
6
5
4
3
2
1
Fine grained
Sand-stone
Features
Interval
Section: MK-02
Grey strata possibly muddy sand
Base of amalgamated sandstone

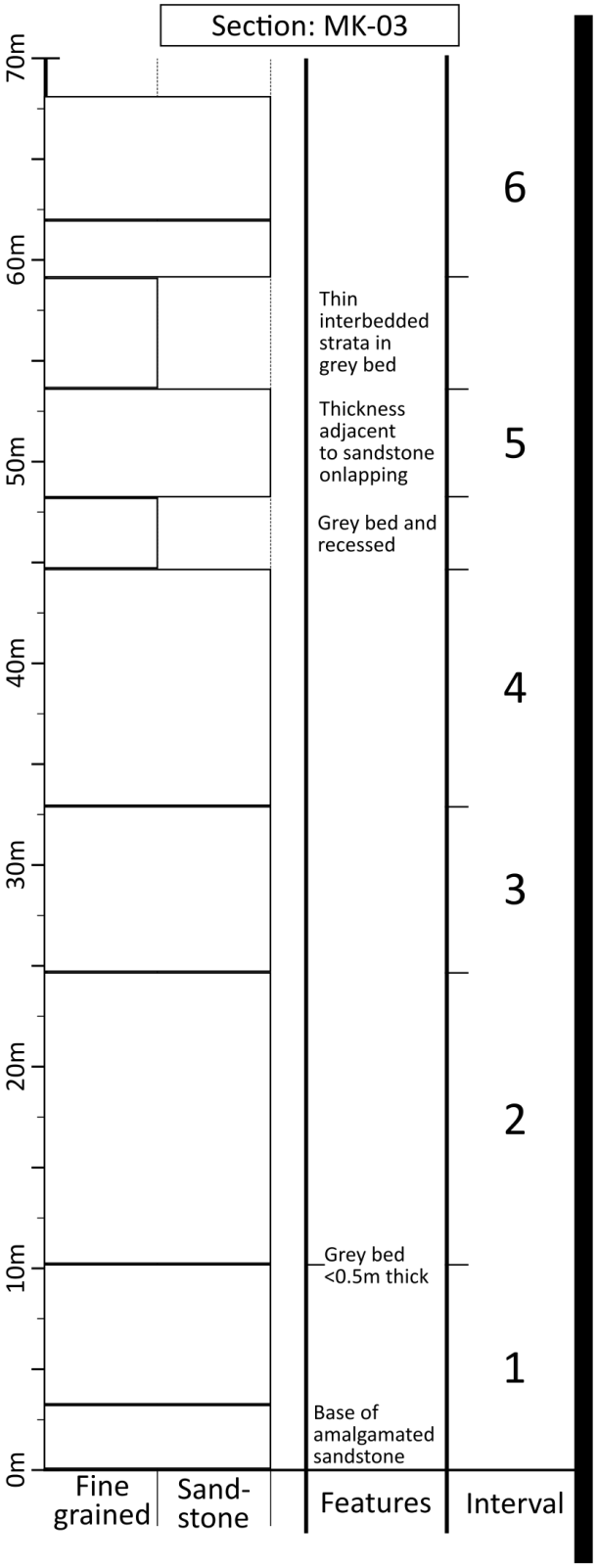
Section: MK-03
70m
60m
50m
40m
30m
20m
10m
0m
Thin interbedded strata in grey bed
Thickness adjacent to sandstone onlapping
Grey bed and recessed
Grey bed <0.5m thick
Base of amalgamated sandstone
6
5
4
3
2
1
Fine grained
Sand-stone
Features
Interval

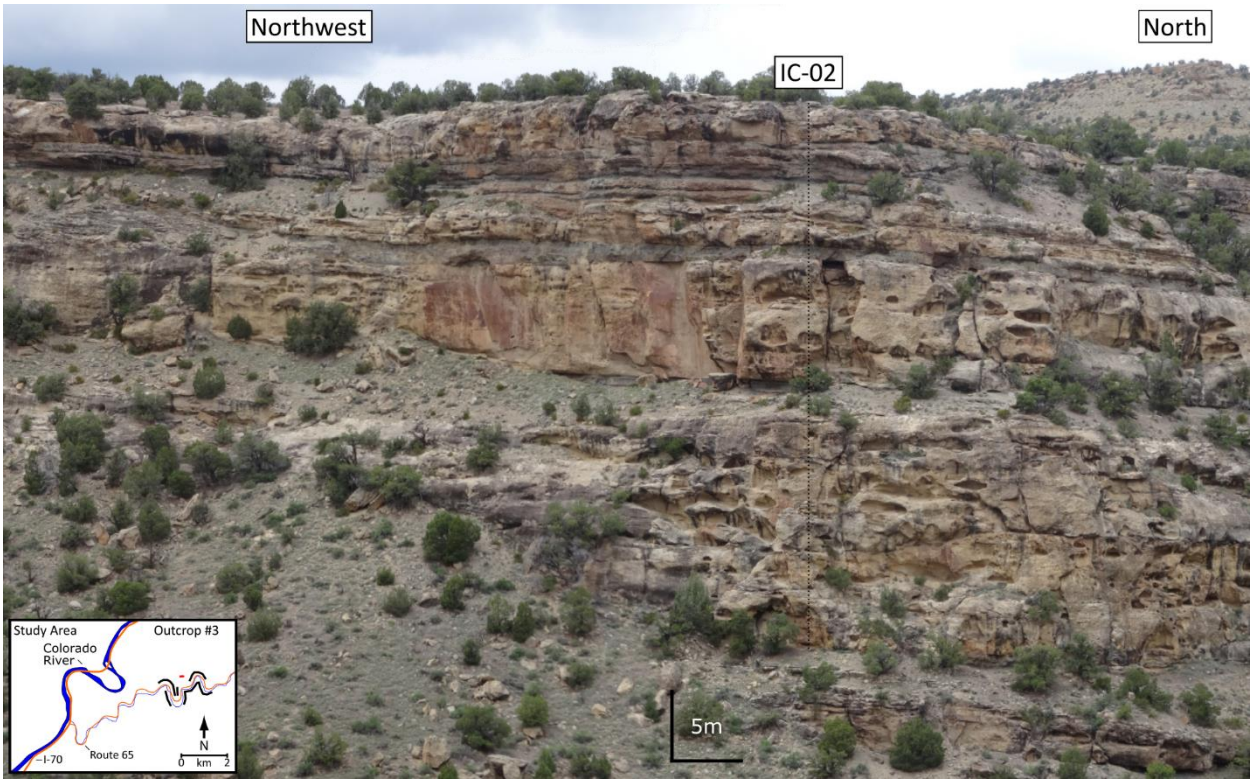
Northwest
North
IC-02
Study Area
Outcrop #3
Colorado River
I-70
Route 65
N
0 km 2
5m

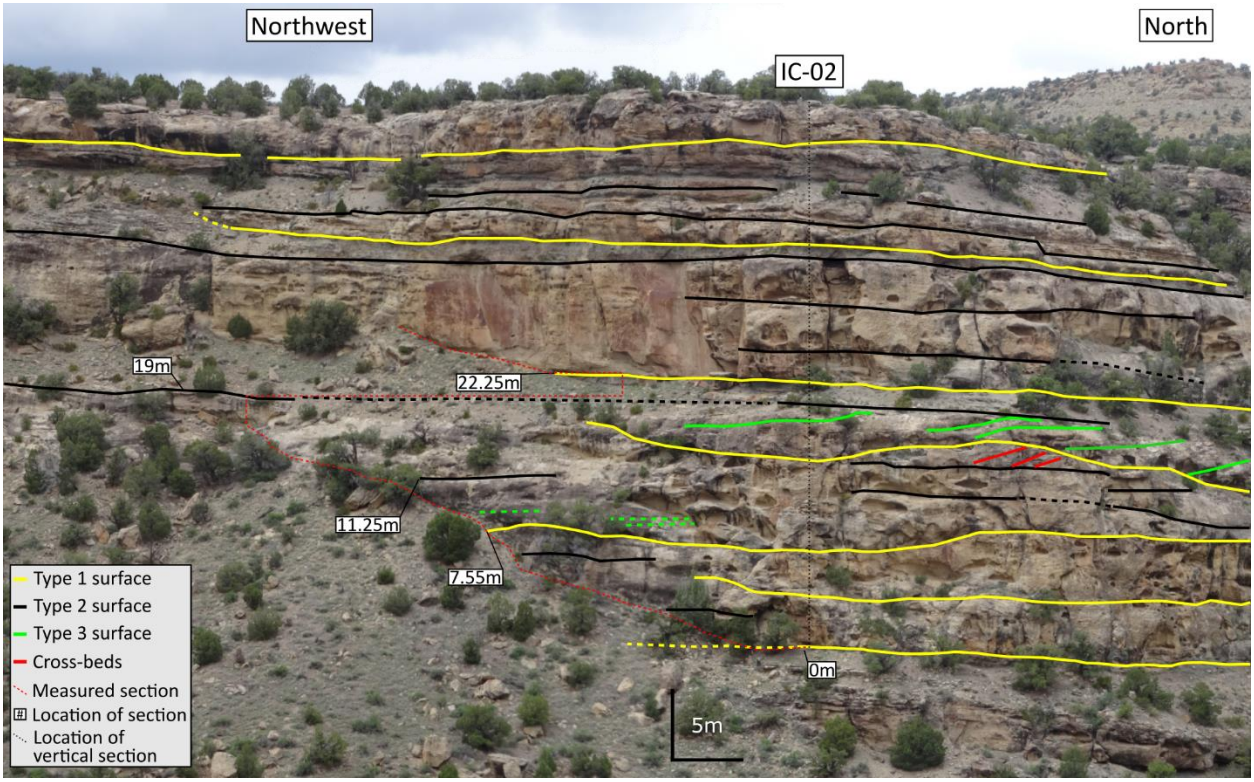
Northwest
North
IC-02
19m
22.25m
11.25m
7.55m
0m
Type 1 surface
Type 2 surface
Type 3 surface
Cross-beds
Measured section
Location of section
Location of vertical section
5m

Figure A7 (previous page): Photomosaic of outcrop #3 non-interpreted (upper) and interpreted (lower). Field of view is north to the northwest. Vertical dotted lines are the location of the vertical sections completed with the laser range finder. Black bars at base of photo are 5x5m scale bars. The red dashed line in the lower photomosaic is the path taken in for the measured section. Key surfaces are labeled in meters that correlate to the measured section.

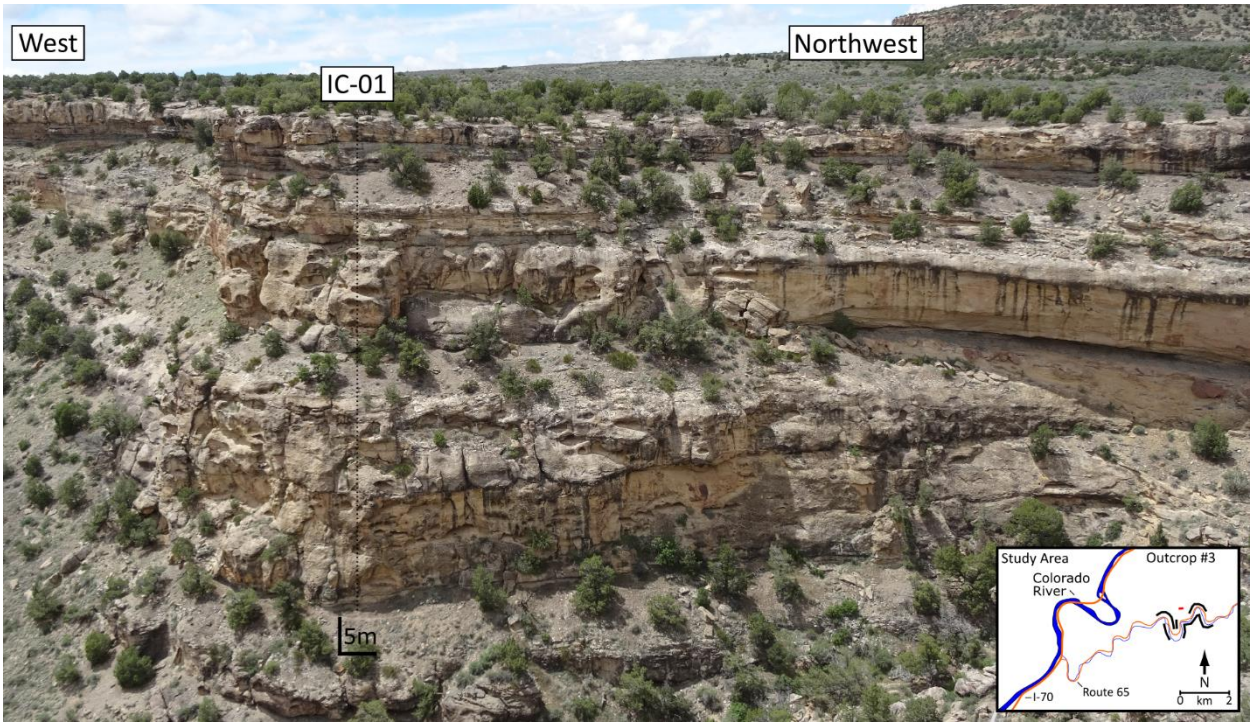
West
Northwest
IC-01
5m
Study Area
Outcrop #3
Colorado River
I-70
Route 65
N
0 km 2

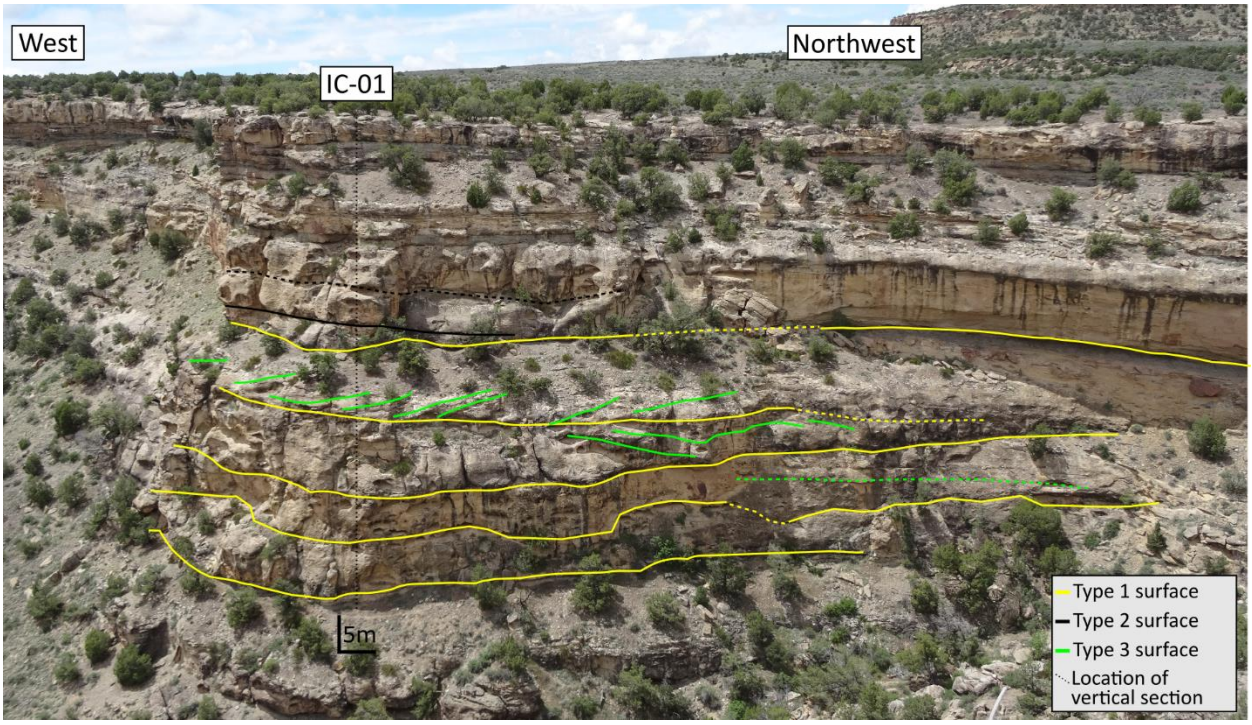
West
Northwest
IC-01
5m
Type 1 surface
Type 2 surface
Type 3 surface
Location of vertical section

Figure A8 (previous page): Photomosaic of the outcrop #3 from the opposite side of the nose, non-interpreted (upper) and interpreted (lower). Field of view is northwest to the west. Vertical dotted lines are the location of the vertical sections completed with the laser range finder. Black bars at base of photo are 5x5m scale bars.

Figure A9 (next page): Vertical sections from outcrop #3

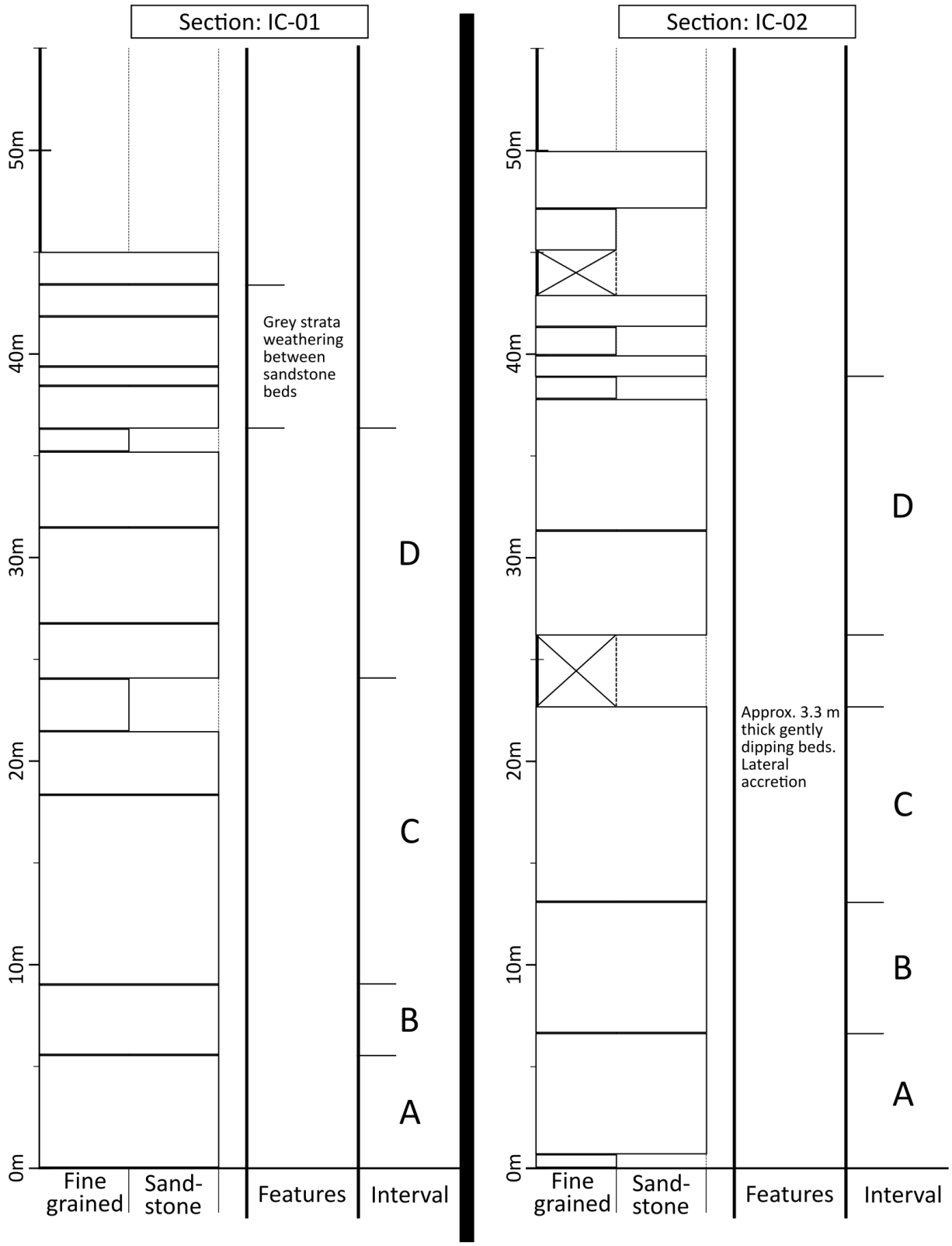
Section: IC-01
Section: IC-02
50m
40m
30m
20m
10m
0m
Grey strata weathering between sandstone beds
Approx. 3.3 m thick gently dipping beds. Lateral accretion
D
C
B
A
Fine grained
Sand-stone
Features
Interval

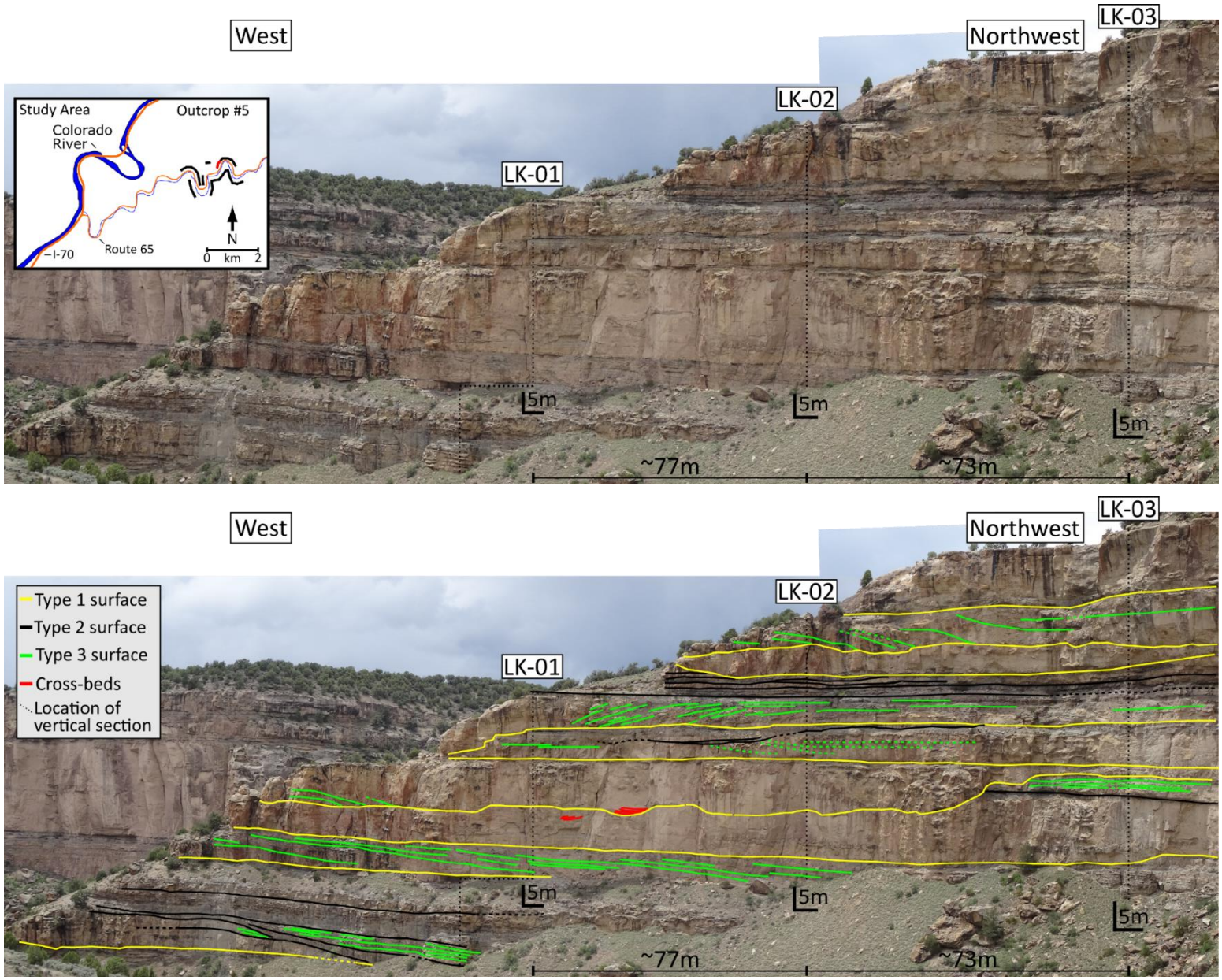
West
Northwest
LK-03
LK-02
LK-01
Study Area
Outcrop #5
Colorado River
I-70
Route 65
N
0 km 2
5m
5m
5m
~77m
~73m
West
Northwest
LK-03
LK-02
LK-01
Type 1 surface
Type 2 surface
Type 3 surface
Cross-beds
Location of vertical section
5m
5m
5m
~77m
~73m

Figure A10 (previous page): Photomosaic of the outcrop #5 non-interpreted (upper) and interpreted (lower). Field of view is northwest to west. Vertical dotted lines are the location of the vertical sections completed with the laser range finder. Key surfaces are labeled in meters that correlate to the measured section. Black bars below each vertical section are 5x5 m scale for those sections of the mosaics. Changes in scale size are due to change in outcrop distance from observer.

Figure A11 (next page): Vertical sections from outcrop #5

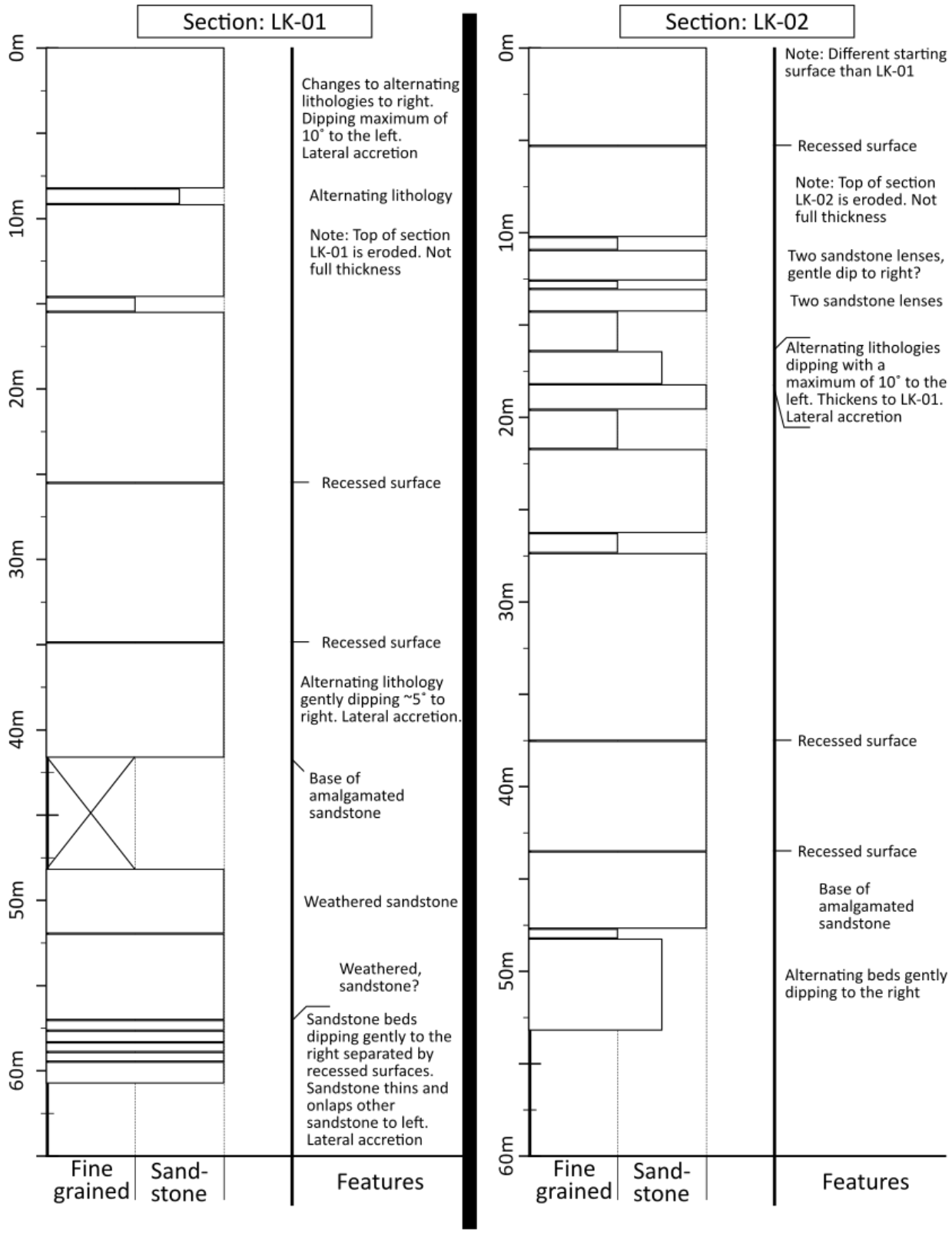
Section: LK-01
0m
10m
20m
30m
40m
50m
60m
Changes to alternating lithologies to right. Dipping maximum of 10˚ to the left. Lateral accretion
Alternating lithology
Note: Top of section LK-01 is eroded. Not full thickness
Recessed surface
Recessed surface
Alternating lithology gently dipping ~5˚ to right. Lateral accretion.
Base of amalgamated sandstone
Weathered sandstone
Weathered, sandstone?
Sandstone beds dipping gently to the right separated by recessed surfaces. Sandstone thins and onlaps other sandstone to left. Lateral accretion
Fine grained
Sand-stone
Features
Section: LK-02
0m
10m
20m
30m
40m
50m
60m
Note: Different starting surface than LK-01
Recessed surface
Note: Top of section LK-02 is eroded. Not full thickness
Two sandstone lenses, gentle dip to right?
Two sandstone lenses
Alternating lithologies dipping with a maximum of 10˚ to the left. Thickens to LK-01. Lateral accretion
Recessed surface
Recessed surface
Base of amalgamated sandstone
Alternating beds gently dipping to the right
Fine grained
Sand-stone
Features

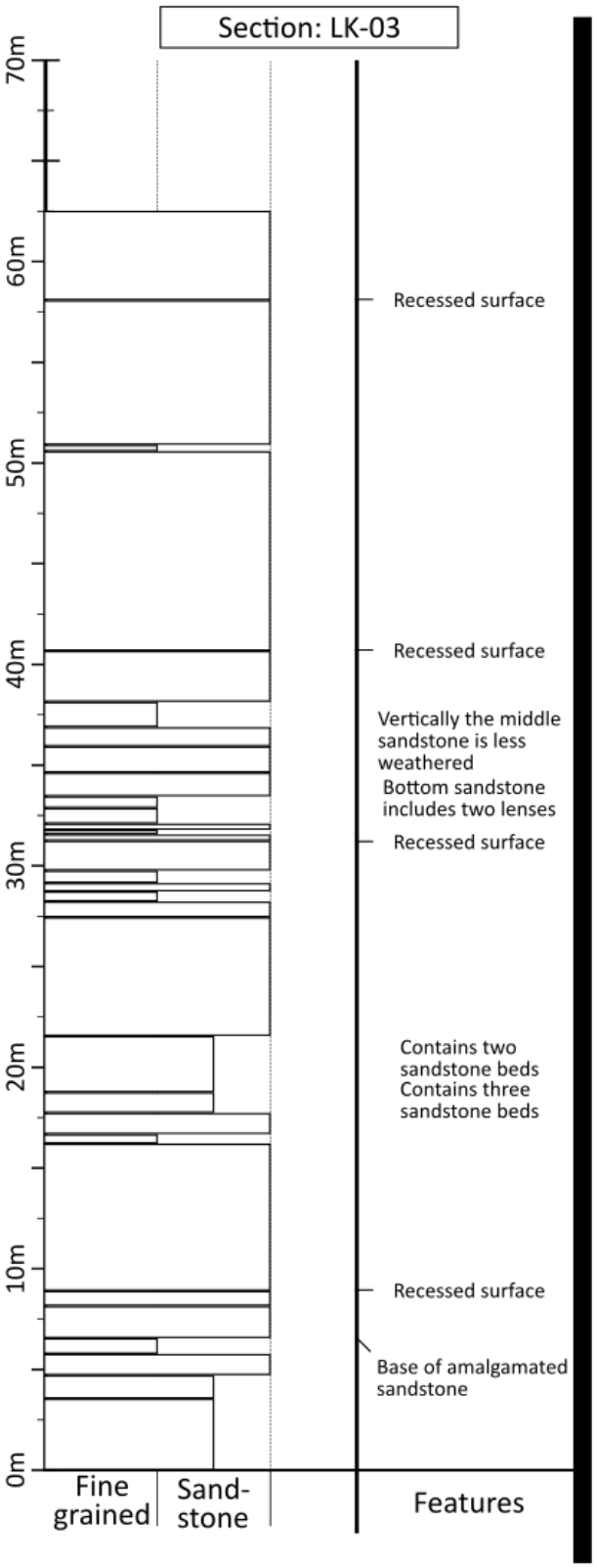
Section: LK-03
70m
60m
50m
40m
30m
20m
10m
0m
Recessed surface
Recessed surface
Vertically the middle sandstone is less weathered
Bottom sandstone includes two lenses
Recessed surface
Contains two sandstone beds
Contains three sandstone beds
Recessed surface
Base of amalgamated sandstone
Fine grained
Sand-stone
Features

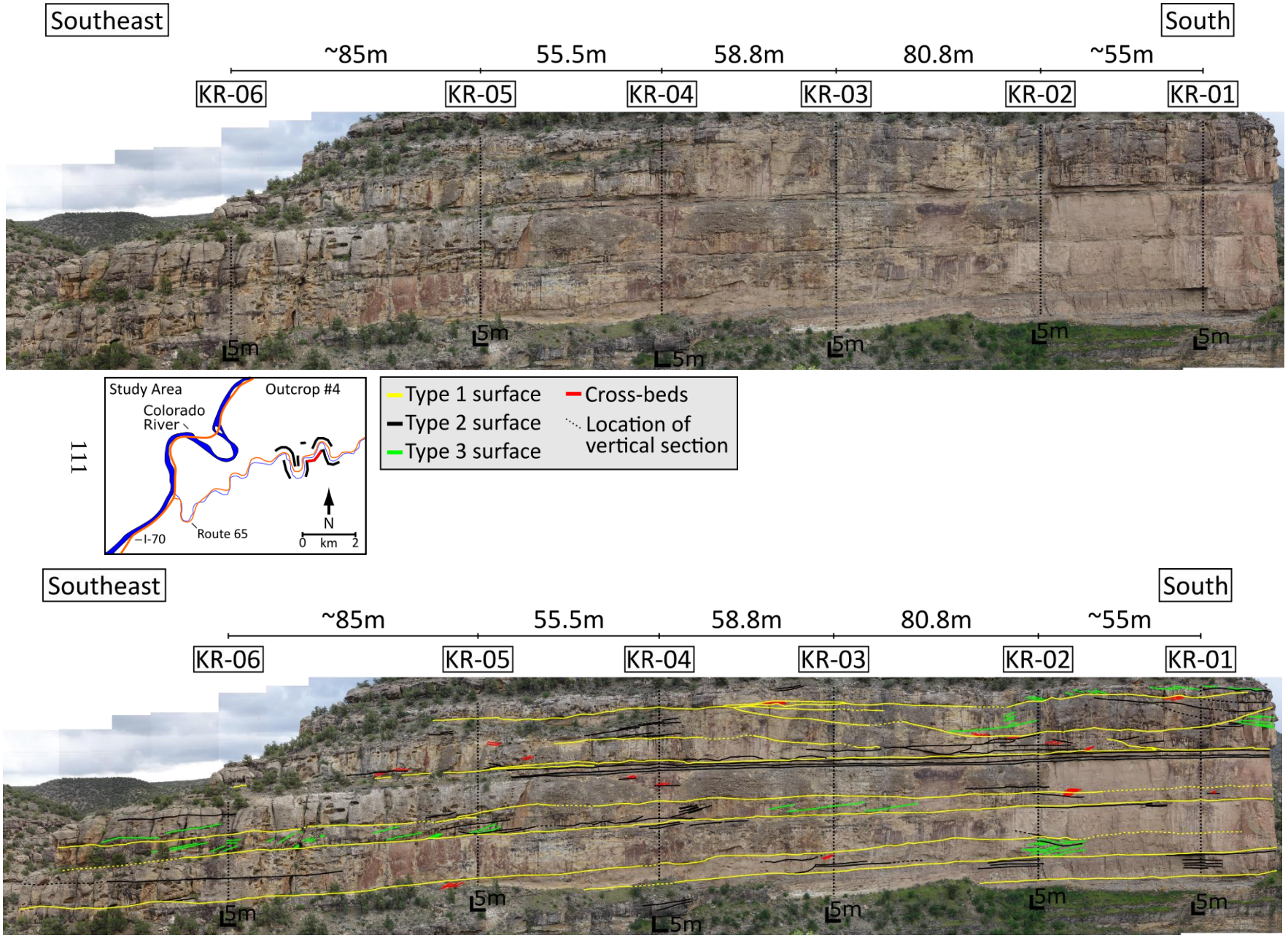
Southeast
South
~85m
55.5m
58.8m
80.8m
~55m
KR-06
KR-05
KR-04
KR-03
KR-02
KR-01
5m
Study Area
Outcrop #4
Colorado River
I-70
Route 65
N
0 km 2
Type 1 surface
Type 2 surface
Type 3 surface
Cross-beds
Location of vertical section
Southeast
South
~85m
55.5m
58.8m
80.8m
~55m
KR-06
KR-05
KR-04
KR-03
KR-02
KR-01
5m

Figure A12 (previous page): Photomosaic of outcrop #4 non-interpreted (upper) and interpreted (lower). Field of view is southeast to the south. Vertical dotted lines are the location of the vertical sections completed with the laser range finder. Key surfaces are labeled in meters that correlate to the measured section. Black bars below each vertical section are 5x5 m scales for those sections of the mosaics. Changes in scale size are due to change in outcrop distance from observer.

Figure A13 (next page): Vertical sections from outcrop #4

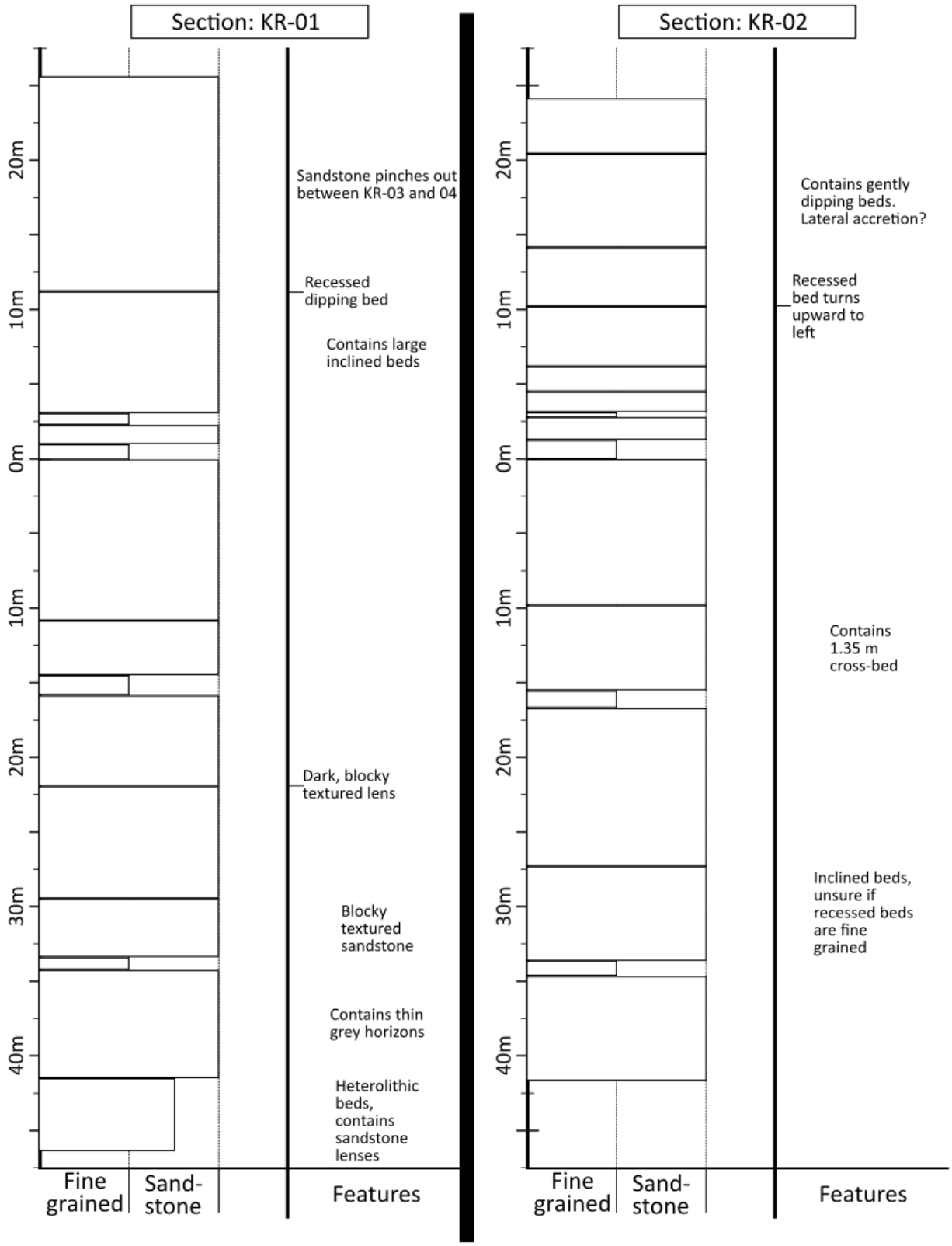
Section: KR-01
20m
10m
0m
10m
20m
30m
40m
Sandstone pinches out between KR-03 and 04
Recessed dipping bed
Contains large inclined beds
Dark, blocky textured lens
Blocky textured sandstone
Contains thin grey horizons
Heterolithic beds, contains sandstone lenses
Fine grained
Sand-stone
Features
Section: KR-02
20m
10m
0m
10m
20m
30m
40m
Contains gently dipping beds. Lateral accretion?
Recessed bed turns upward to left
Contains 1.35 m cross-bed
Inclined beds, unsure if recessed beds are fine grained
Fine grained
Sand-stone
Features

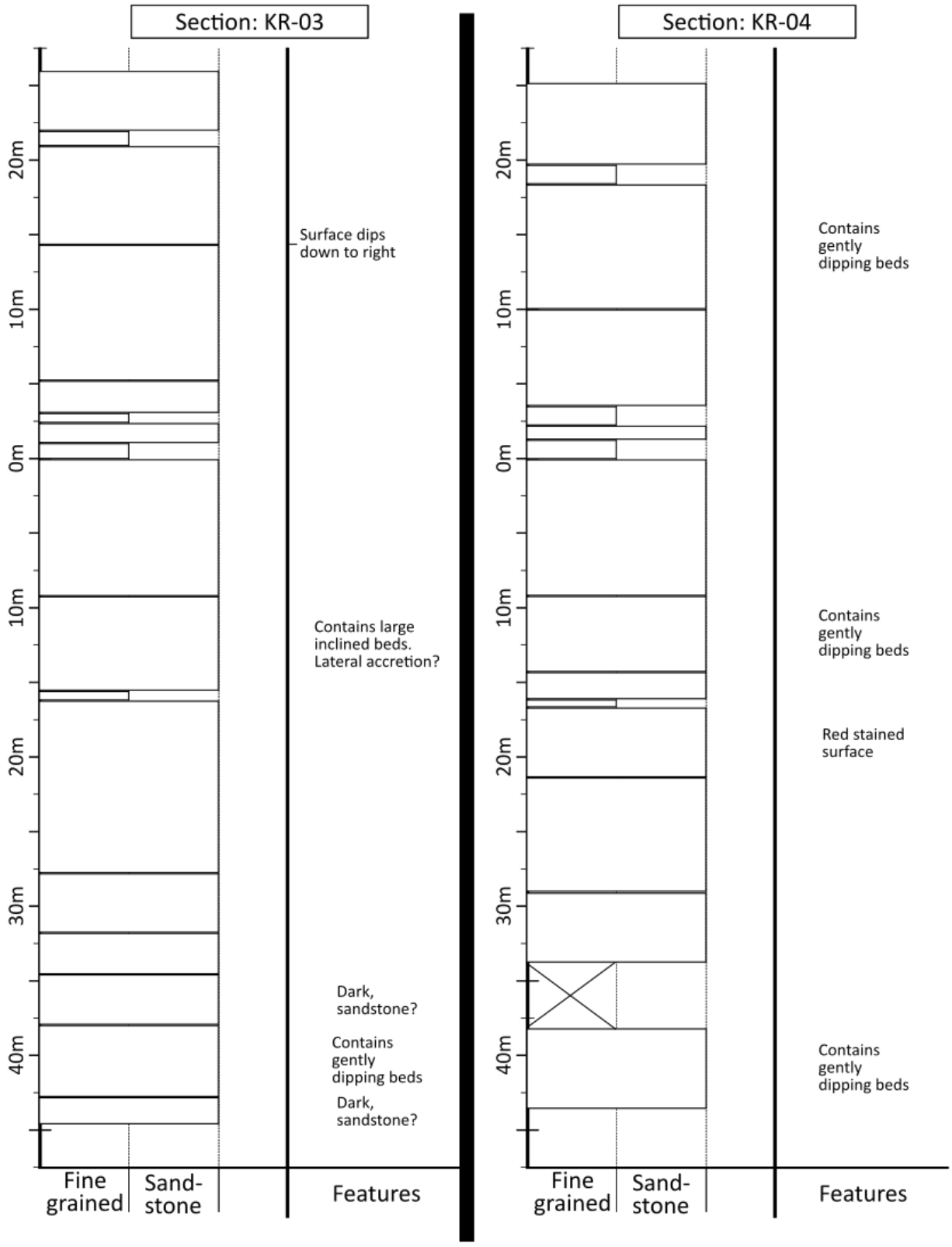
Section: KR-03
20m
10m
0m
10m
20m
30m
40m
Surface dips down to right
Contains large inclined beds. Lateral accretion?
Dark, sandstone?
Contains gently dipping beds
Dark, sandstone?
Fine grained
Sand-stone
Features
Section: KR-04
20m
10m
0m
10m
20m
30m
40m
Contains gently dipping beds
Contains gently dipping beds
Red stained surface
Contains gently dipping beds
Fine grained
Sand-stone
Features

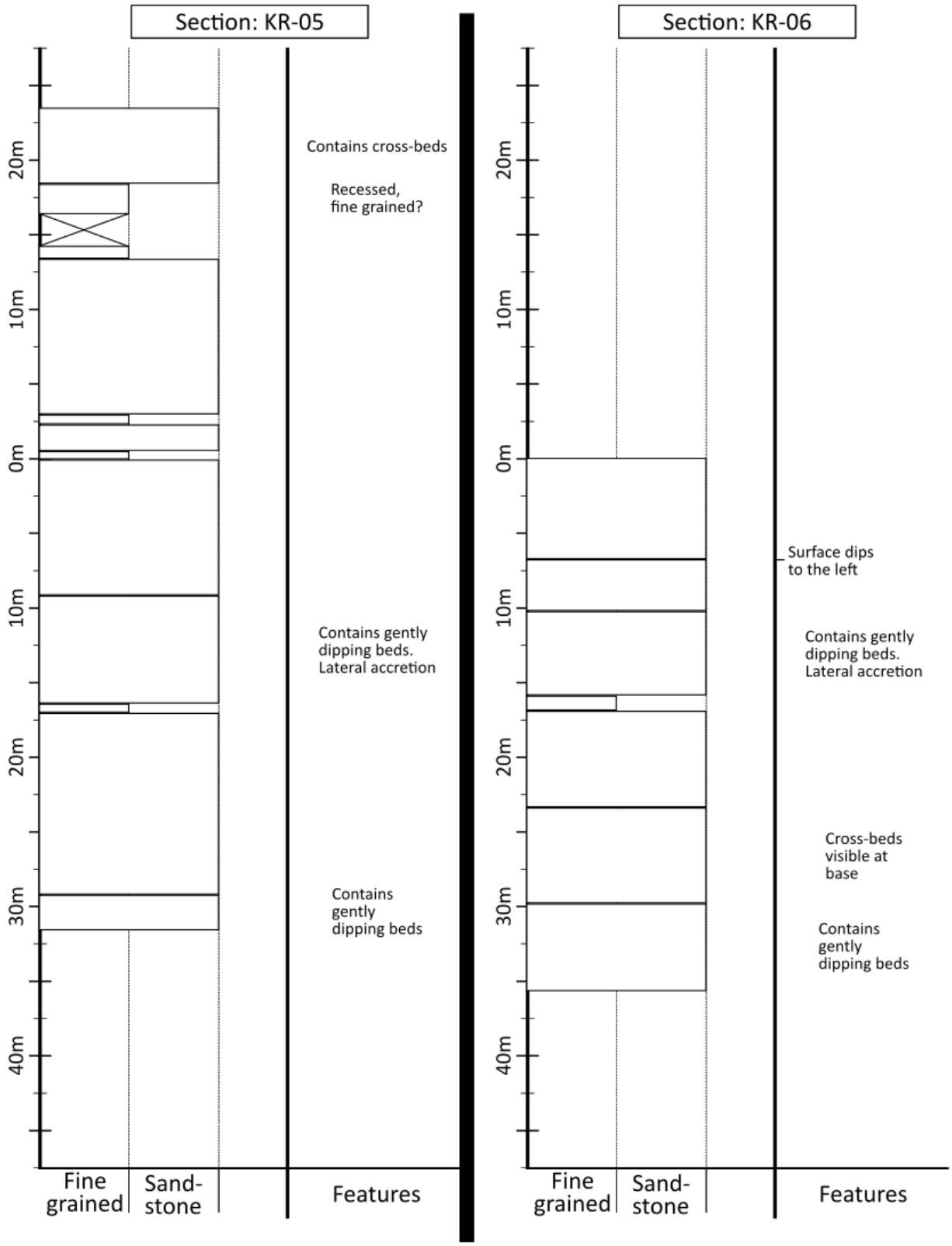
Section: KR-05
20m
10m
0m
10m
20m
30m
40m
Contains cross-beds
Recessed, fine grained?
Contains gently dipping beds. Lateral accretion
Contains gently dipping beds
Fine grained
Sand-stone
Features
Section: KR-06
20m
10m
0m
10m
20m
30m
40m
Surface dips to the left
Contains gently dipping beds. Lateral accretion
Cross-beds visible at base
Contains gently dipping beds
Fine grained
Sand-stone
Features

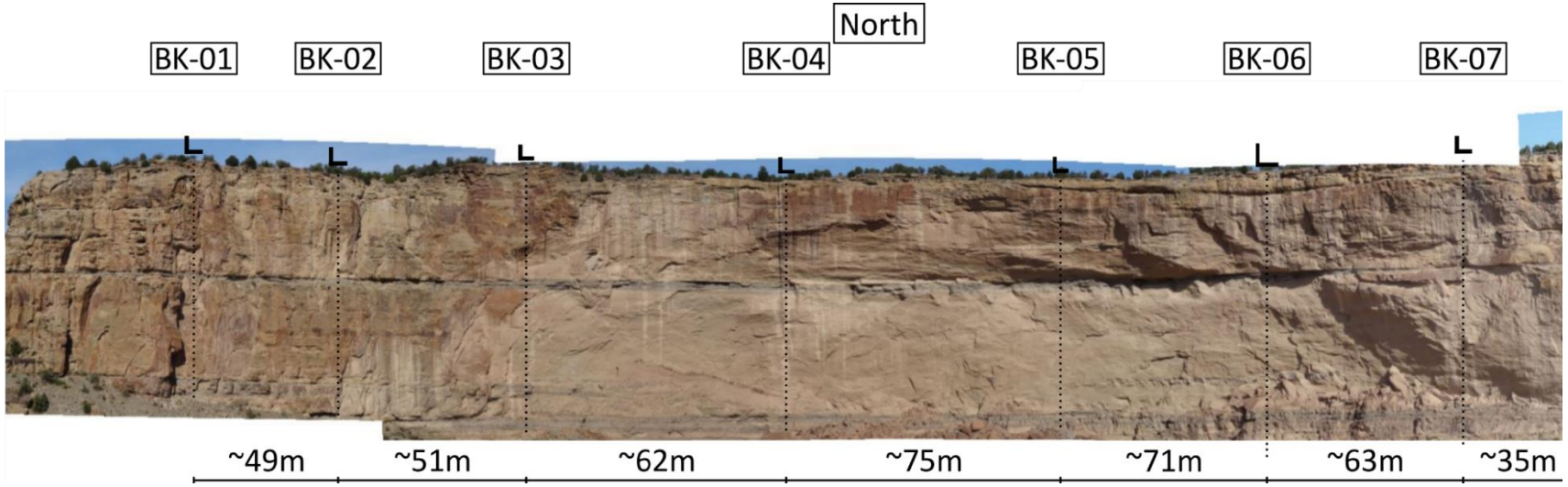
North
BK-01
BK-02
BK-03
BK-04
BK-05
BK-06
BK-07
~49m
~51m
~62m
~75m
~71m
~63m
~35m

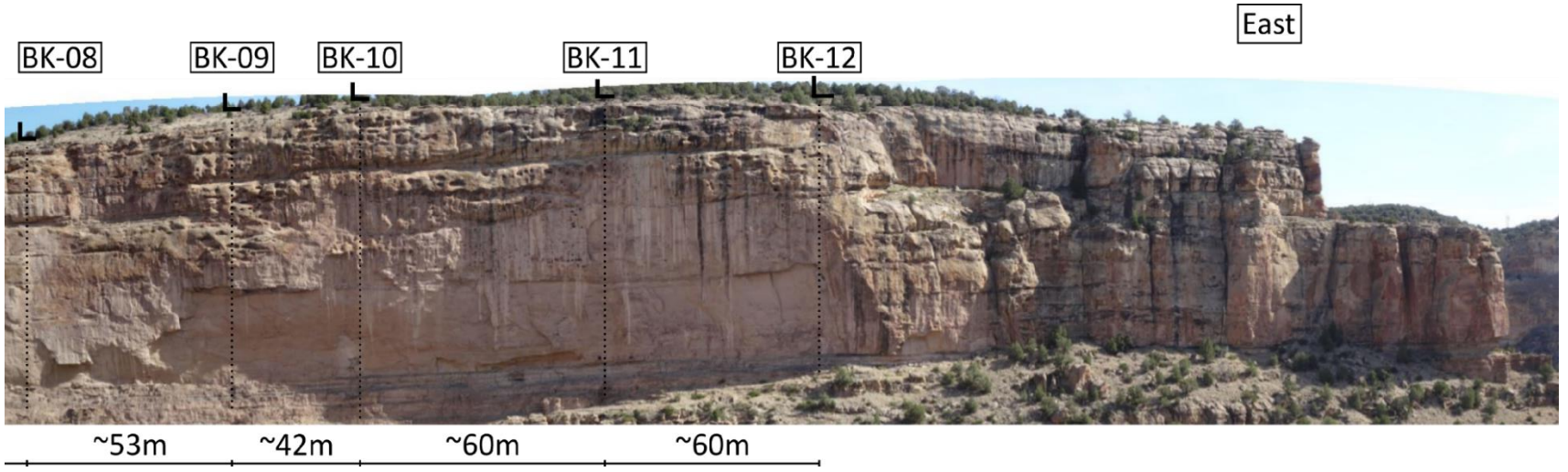
East
BK-08
BK-09
BK-10
BK-11
BK-12
~53m
~42m
~60m
~60m

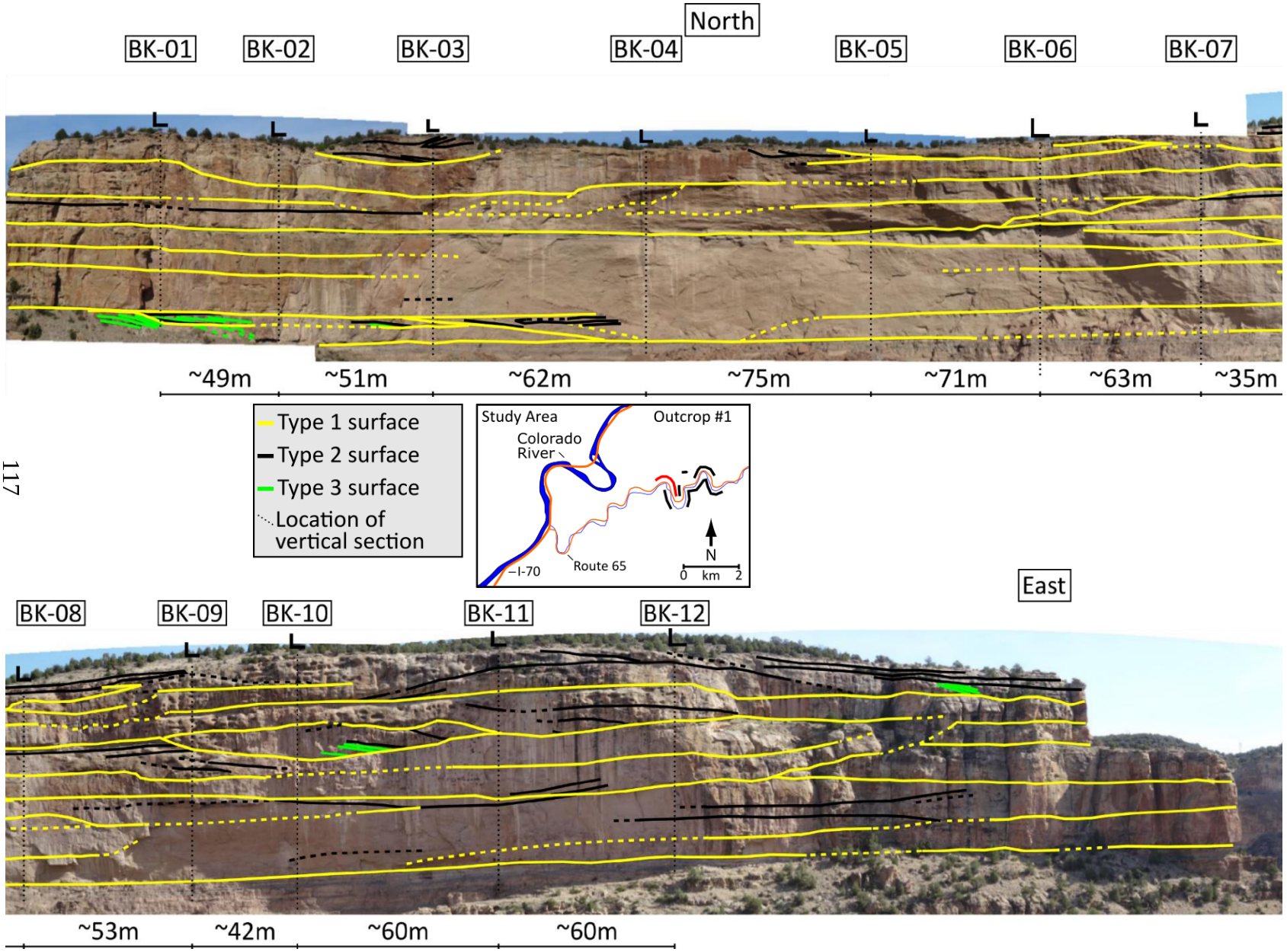
North
BK-01
BK-02
BK-03
BK-04
BK-05
BK-06
BK-07
~49m
~51m
~62m
~75m
~71m
~63m
~35m
Type 1 surface
Type 2 surface
Type 3 surface
Location of vertical section
Study Area
Outcrop #1
Colorado River
I-70
Route 65
N
0 km 2
East
BK-08
BK-09
BK-10
BK-11
BK-12
~53m
~42m
~60m
~60m

Figure A14 (previous page): Photomosaic of outcrop #1 non-interpreted (two pages prior) and interpreted (previous page). Field of view is north to east. Vertical dotted lines are the location of the vertical sections completed with the laser range finder. Key surfaces are labeled in meters that correlate to the measured section. Black bars below each vertical section are 5x5 m scales for those sections of the mosaics. Changes in scale size are due to change in outcrop distance from observer.

Figure A15 (next page): Vertical sections from outcrop #1

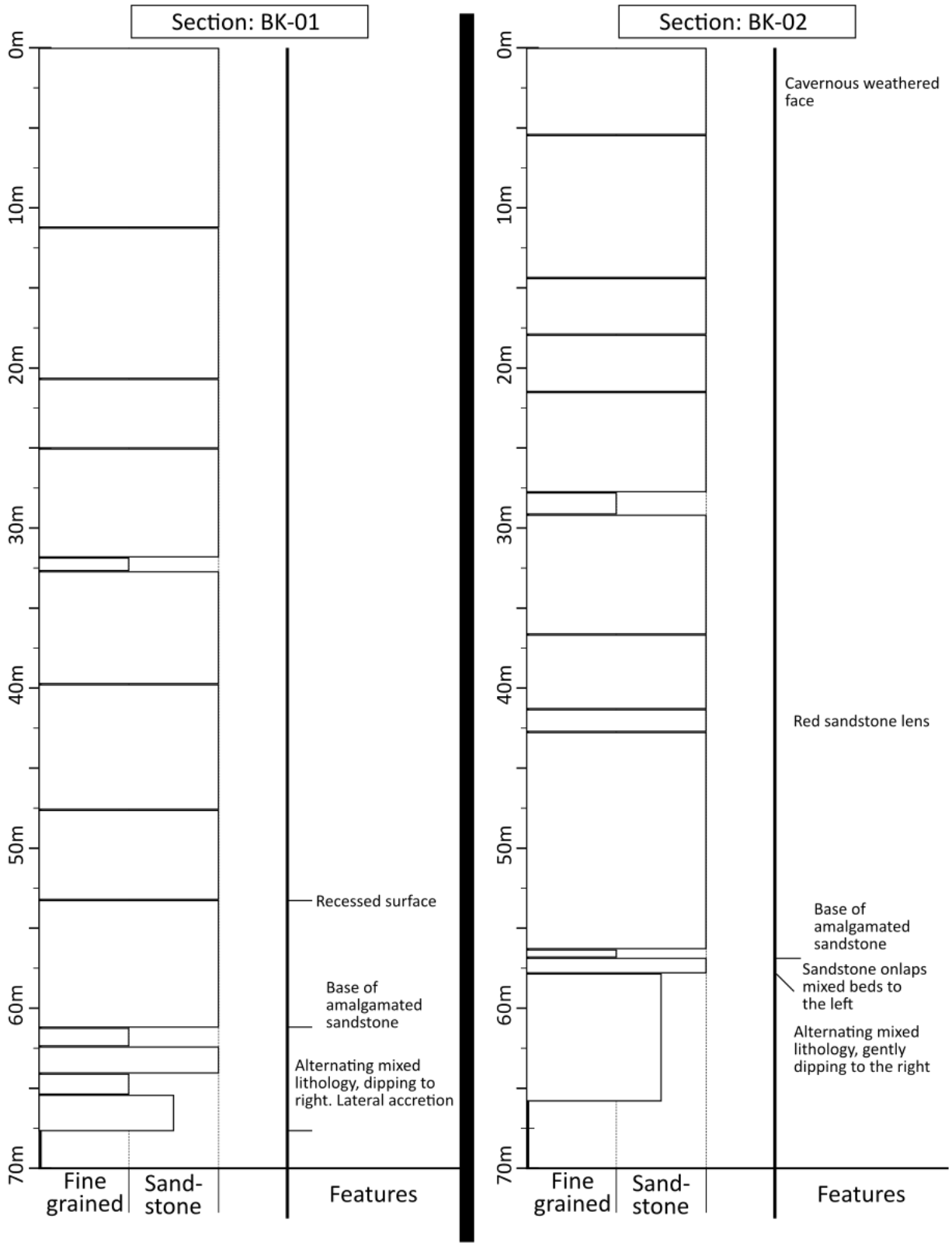
Section: BK-01
0m
10m
20m
30m
40m
50m
60m
70m
Fine grained
Sand-stone
Features
Recessed surface
Base of amalgamated sandstone
Alternating mixed lithology, dipping to right. Lateral accretion
Section: BK-02
Cavernous weathered face
Red sandstone lens
Base of amalgamated sandstone
Sandstone onlaps mixed beds to the left
Alternating mixed lithology, gently dipping to the right

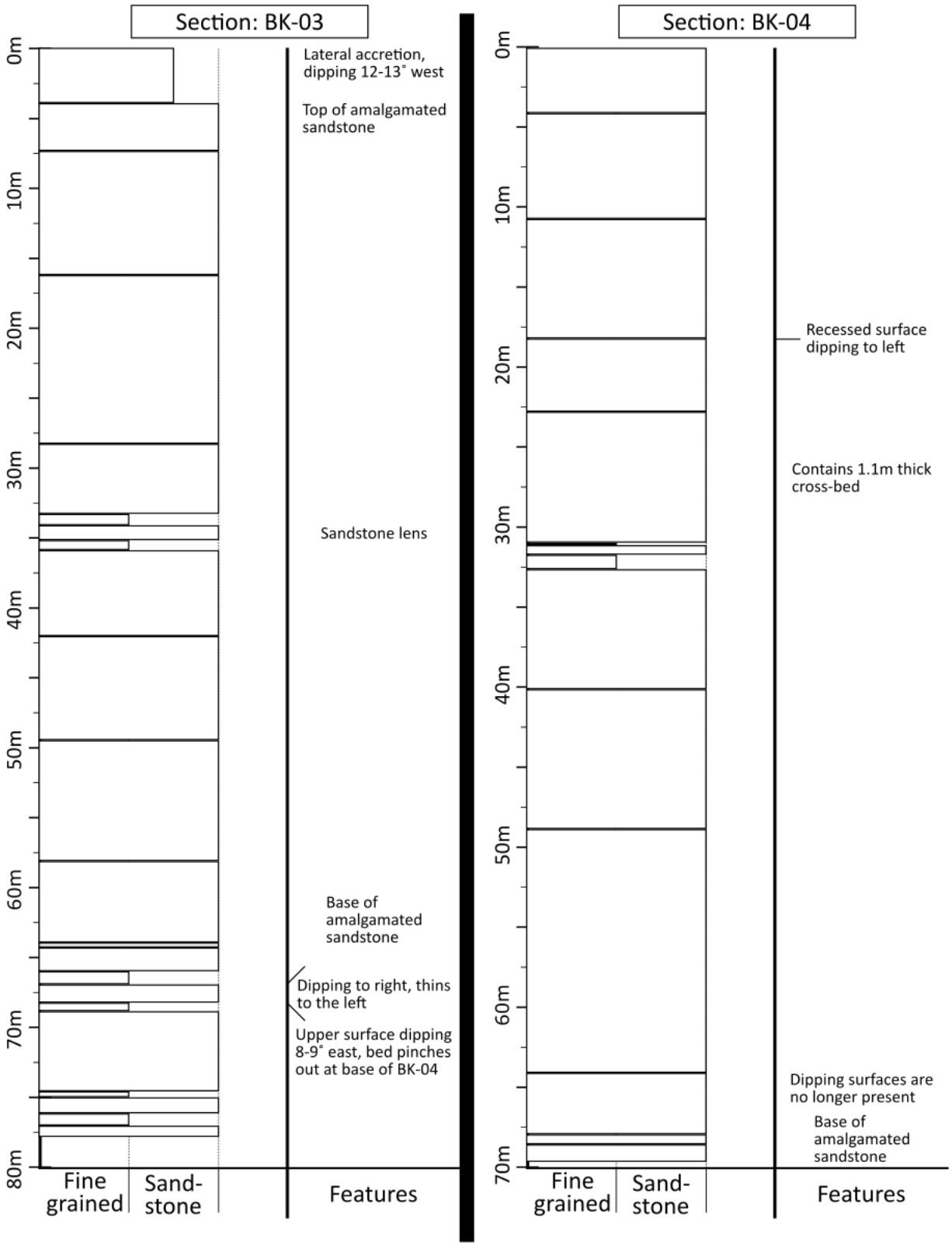
Section: BK-03
0m
10m
20m
30m
40m
50m
60m
70m
80m
Lateral accretion, dipping 12-13˚ west
Top of amalgamated sandstone
Sandstone lens
Base of amalgamated sandstone
Dipping to right, thins to the left
Upper surface dipping 8-9˚ east, bed pinches out at base of BK-04
Fine grained
Sand-stone
Features
Section: BK-04
0m
10m
20m
30m
40m
50m
60m
70m
Recessed surface dipping to left
Contains 1.1m thick cross-bed
Dipping surfaces are no longer present
Base of amalgamated sandstone
Fine grained
Sand-stone
Features

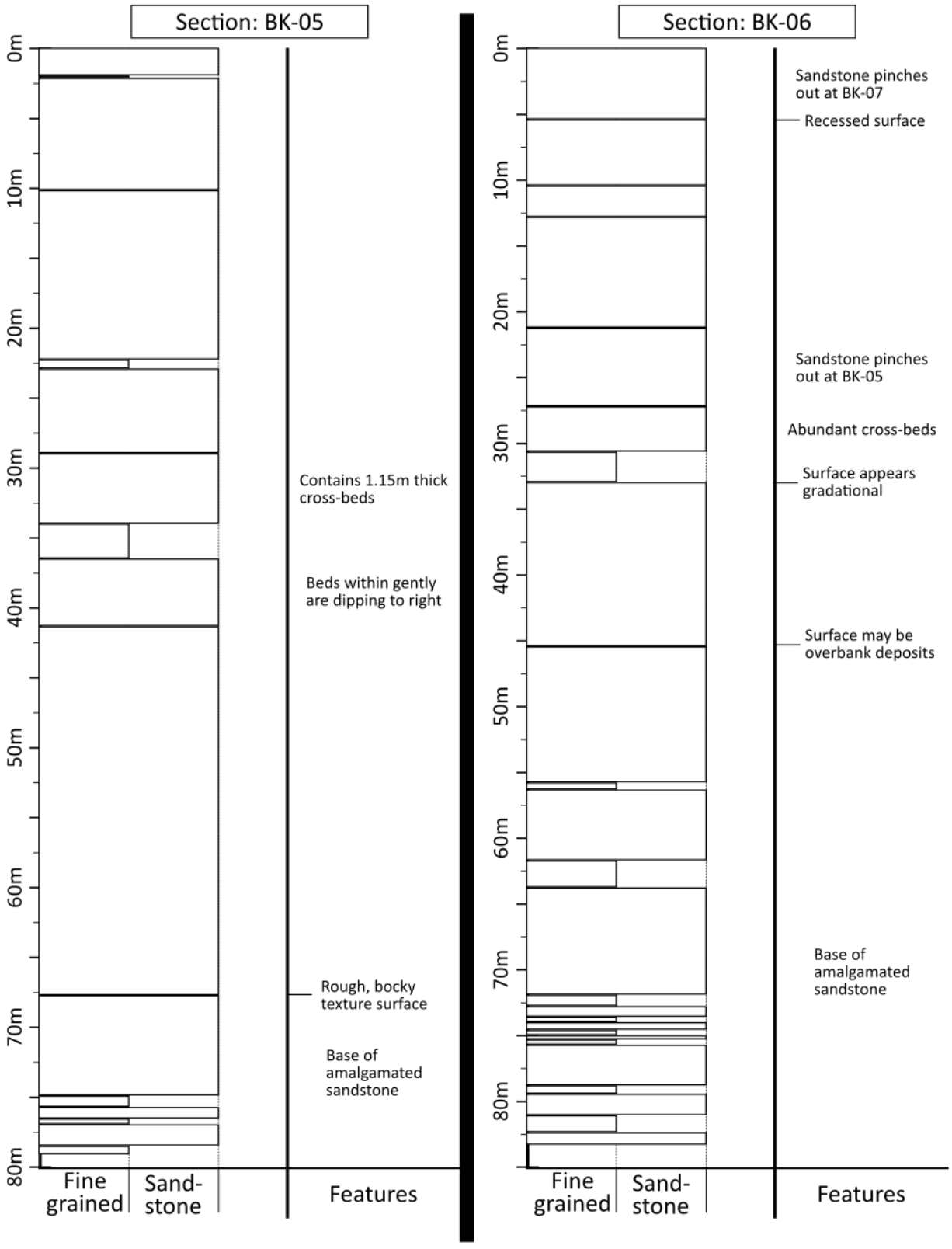
Section: BK-05
0m
10m
20m
30m
40m
50m
60m
70m
80m
Contains 1.15m thick cross-beds
Beds within gently are dipping to right
Rough, bocky texture surface
Base of amalgamated sandstone
Fine grained
Sand-stone
Features
Section: BK-06
Sandstone pinches out at BK-07
Recessed surface
Sandstone pinches out at BK-05
Abundant cross-beds
Surface appears gradational
Surface may be overbank deposits
Base of amalgamated sandstone
Fine grained
Sand-stone
Features

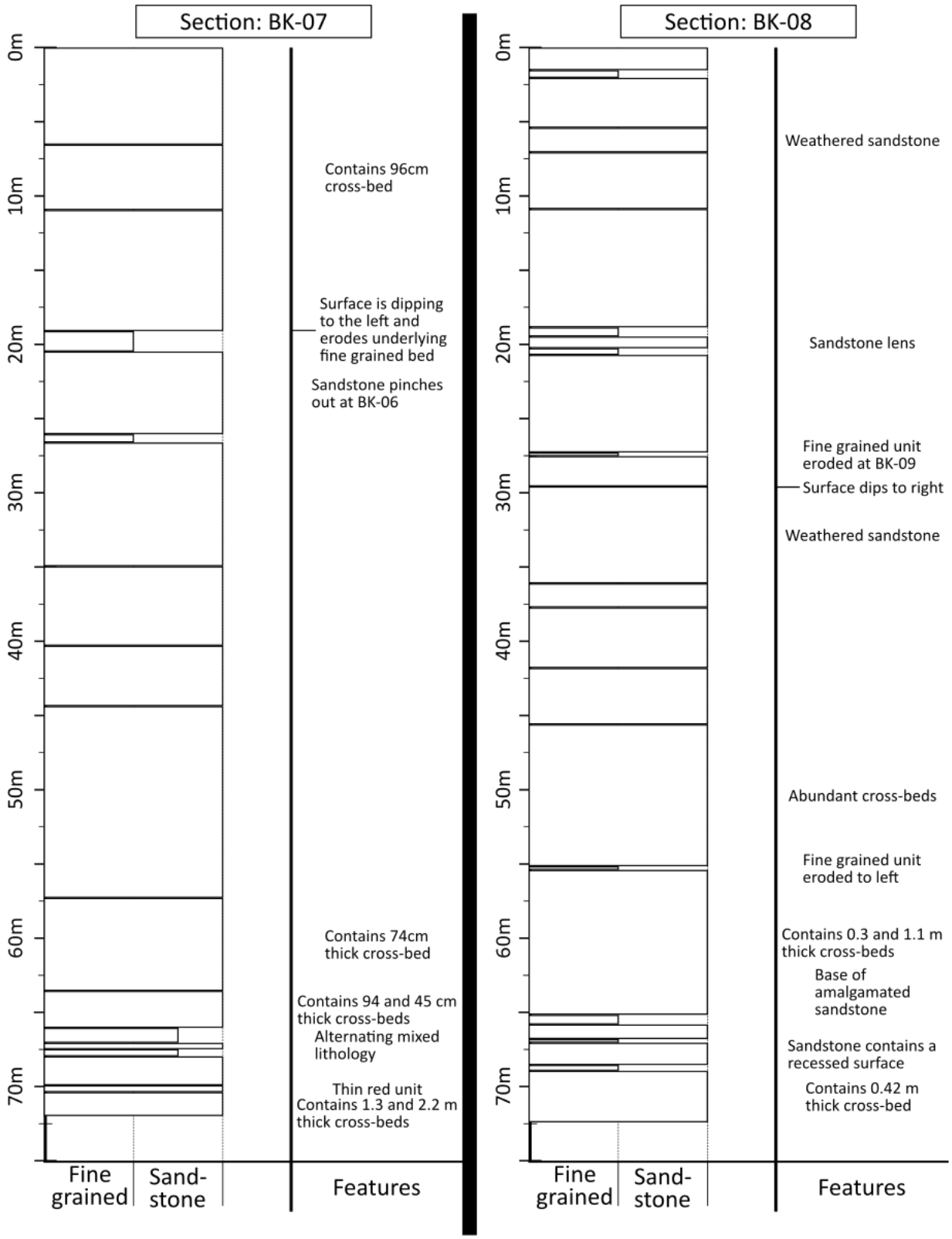
Section: BK-07
0m
10m
20m
30m
40m
50m
60m
70m
Contains 96cm cross-bed
Surface is dipping to the left and erodes underlying fine grained bed
Sandstone pinches out at BK-06
Contains 74cm thick cross-bed
Contains 94 and 45 cm thick cross-beds
Alternating mixed lithology
Thin red unit
Contains 1.3 and 2.2 m thick cross-beds
Fine grained
Sand-stone
Features
Section: BK-08
0m
10m
20m
30m
40m
50m
60m
70m
Weathered sandstone
Sandstone lens
Fine grained unit eroded at BK-09
Surface dips to right
Weathered sandstone
Abundant cross-beds
Fine grained unit eroded to left
Contains 0.3 and 1.1 m thick cross-beds
Base of amalgamated sandstone
Sandstone contains a recessed surface
Contains 0.42 m thick cross-bed
Fine grained
Sand-stone
Features

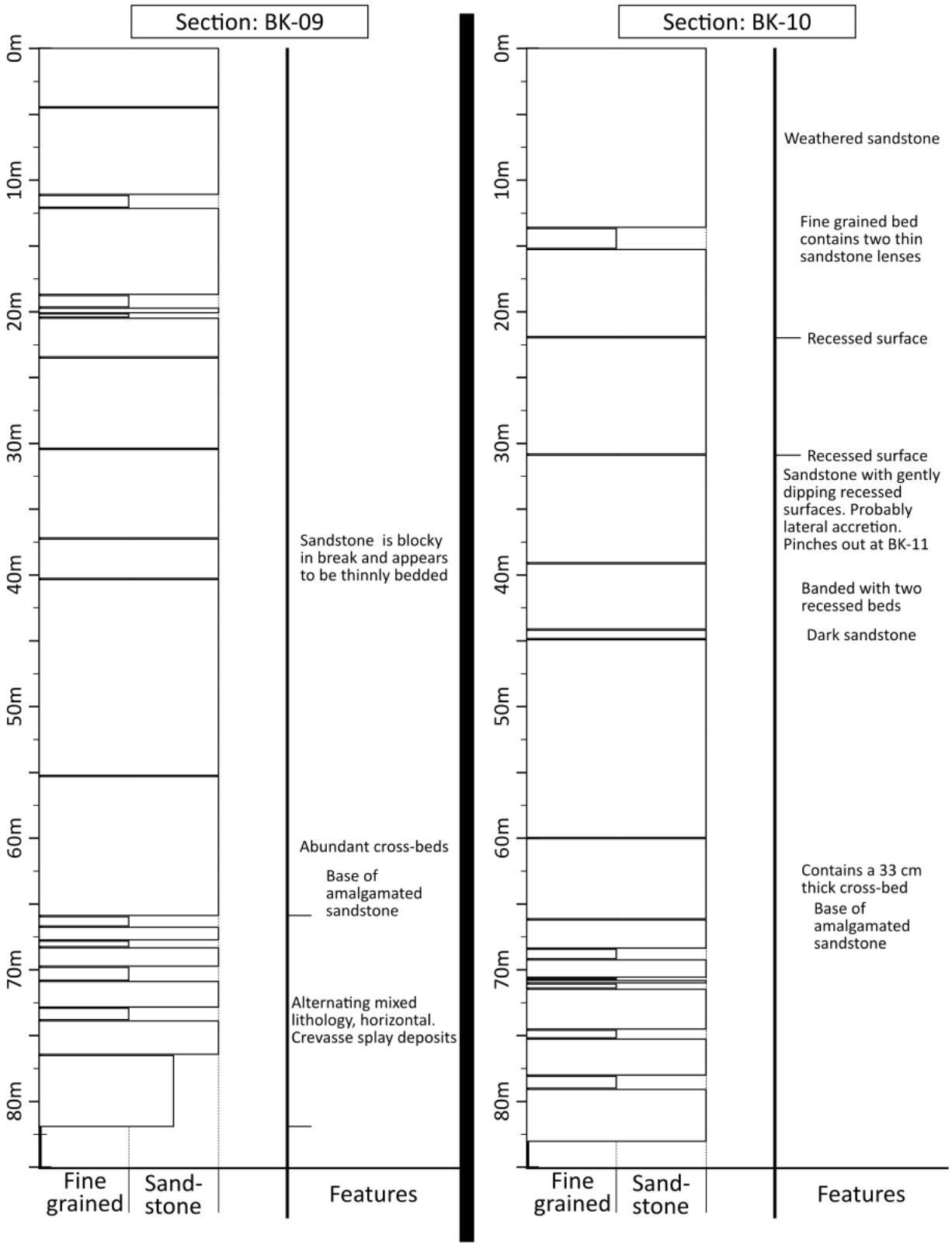
Section: BK-09
0m
10m
20m
30m
40m
50m
60m
70m
80m
Sandstone is blocky in break and appears to be thinnly bedded
Abundant cross-beds
Base of amalgamated sandstone
Alternating mixed lithology, horizontal. Crevasse splay deposits
Fine grained
Sand-stone
Features
Section: BK-10
Weathered sandstone
Fine grained bed contains two thin sandstone lenses
Recessed surface
Recessed surface
Sandstone with gently dipping recessed surfaces. Probably lateral accretion. Pinches out at BK-11
Banded with two recessed beds
Dark sandstone
Contains a 33 cm thick cross-bed
Base of amalgamated sandstone
Fine grained
Sand-stone
Features

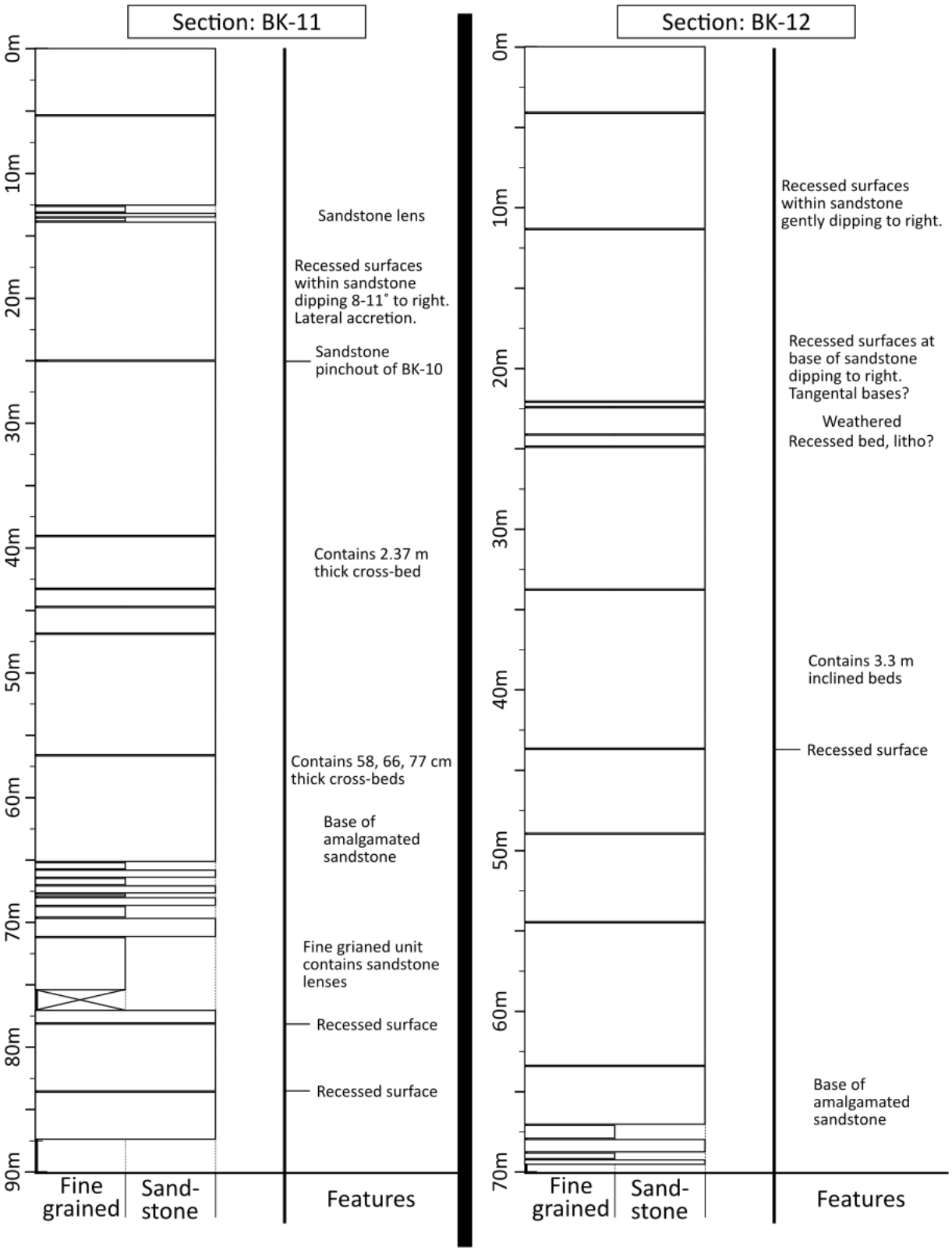
Section: BK-11
0m
10m
20m
30m
40m
50m
60m
70m
80m
90m
Fine grained
Sand-stone
Features
Sandstone lens
Recessed surfaces within sandstone dipping 8-11˚ to right. Lateral accretion.
Sandstone pinchout of BK-10
Contains 2.37 m thick cross-bed
Contains 58, 66, 77 cm thick cross-beds
Base of amalgamated sandstone
Fine grianed unit contains sandstone lenses
Recessed surface
Recessed surface
Section: BK-12
0m
10m
20m
30m
40m
50m
60m
70m
Fine grained
Sand-stone
Features
Recessed surfaces within sandstone gently dipping to right.
Recessed surfaces at base of sandstone dipping to right. Tangental bases?
Weathered Recessed bed, litho?
Contains 3.3 m inclined beds
Recessed surface
Base of amalgamated sandstone

1) Paleo-hydrodynamic calculations

2a) Table 6: Notation

Symbol	Units	Definition
d	L	Flow depth
D_{50b}	L	Particle diameter of average bed load
D*		Dimensionless particle size
g	LT^{-2}	Acceleration due to gravity
h_m	L	Mean bedform height
R		Submerged specific gravity, ($R=(\rho_s/\rho)-1$)
Re_p		Particle Reynolds number
S		Slope
s_m	L	Mean cross-bed thickness
W*		Dimensionless settling velocity
$\frac{u^*_{sf}}{w_s}$		Ratio of skin-friction shear velocity (u^*_{sf}) to paticle settling velocity (w_s)
ρ	ML^{-3}	Fluid density (water)
ρ_s	ML^{-3}	Grain density (Quartz)
ν	L^2T^{-1}	Kinematic fluid viscosity of water at 20˚C

Note: L = length, M = mass and T = time

2b) Paleo-flow depth

2bi) Method of paleo-flow depth calculations

Paleo-flow depth was calculated via methods of Leclair and Bridge (2001). This method was performed because a probability density function (PDF) was not defined for the dataset due to the low count of cross-beds.

Mean bedform height (h_m) was calculated using mean cross-bed thickness (s_m) that was measured in the field.

$$h_m = 2.9\ (\pm 0.7) * s_m$$

Flow depth (d) was then calculated from mean bedform height from the empirical relation provided by Allen (1970).

$$d = 11.6 * h_m^{0.84}$$

2bii) Table 7: Middle Kahuna measured section cross-beds (base of section: 39.191405, -108.245375)

Interval code	Cross-bed thickness [cm]	Average grain size [mm]	Grain size	Flow depth (d) [m]
6	35	0.425	mU	5.6 ± 1.1
6	25	0.3	mL	4.2 ± 0.8
5	40	0.3	mL	6.3 ± 1.3
5	20	0.2135	fU	3.5 ± 0.7
5	35	0.2135	fU	5.6 ± 1.1
5	35	0.3	mL	5.6 ± 1.1
5	20	0.3	mL	3.5 ± 0.7
5	60	0.214	fU	
5	45	0.2135	fU	6.9 ± 1.4
5	30	0.3	mL	4.9 ± 1
5	70	0.425	mU	
5	30	0.3	mL	4.9 ± 1
4	20	0.3	mL	3.5 ± 0.7
4	65	0.300	mL	
4	70	0.300	mL	
4	60	0.214	fU	
4	50	0.3	mL	7.6 ± 1.6

Interval code	Cross-bed thickness [cm]	Average grain size [mm]	Grain size	Flow depth (d) [m]
4	60	0.214	fU	
3	20	0.2135	fU	3.5 ± 0.7
3	25	0.2135	fU	4.2 ± 0.8
3	15	0.2135	fU	2.8 ± 0.6
3	40	0.2135	fU	6.3 ± 1.3
3	30	0.3	mL	4.9 ± 1
3	20	0.3	mL	3.5 ± 0.7
3	100	0.300	mL	
2	75	0.425	mU	
2	65	0.214	fU	
2	40	0.3	mL	6.3 ± 1.3
2	30	0.3	mL	4.9 ± 1
2	90	0.300	mL	
2	20	0.3	mL	3.5 ± 0.7
2	65	0.300	mL	
2	35	0.3	mL	5.6 ± 1.1
2	130	0.300	mL	
2	55	0.2135	fU	8.2 ± 1.7
2	30	0.2135	fU	4.9 ± 1

Interval code	Cross-bed thickness [cm]	Average grain size [mm]	Grain size	Flow depth (d) [m]
2	20	0.2135	fU	3.5 ± 0.7
2	20	0.2135	fU	3.5 ± 0.7
2	60	0.300	mL	
1	40	0.2135	fU	6.3 ± 1.3
1	20	0.2135	fU	3.5 ± 0.7
1	30	0.2135	fU	4.9 ± 1
1	25	0.2135	fU	4.2 ± 0.8
1	15	0.2135	fU	2.8 ± 0.6
1	35	0.2135	fU	5.6 ± 1.1
1	30	0.3	mL	4.9 ± 1
1	20	0.3	mL	3.5 ± 0.7
1	30	0.3	mL	4.9 ± 1
1	10	0.2135	fU	2 ± 0.4
1	25	0.2135	fU	4.2 ± 0.8
1	20	0.2135	fU	3.5 ± 0.7
1	70	0.214	fU	
1	95	0.214	fU	
1	30	0.2135	fU	4.9 ± 1
1	35	0.3	mL	5.6 ± 1.1

Interval code	Cross-bed thickness [cm]	Average grain size [mm]	Grain size	Flow depth (d) [m]
1	50	0.2135	fU	7.6 ± 1.6
1	50	0.2135	fU	7.6 ± 1.6
1	15	0.3	mL	2.8 ± 0.6
1	25	0.3	mL	4.2 ± 0.8
1	25	0.3	mL	4.2 ± 0.8
1	35	0.425	mU	5.6 ± 1.1
1	45	0.425	mU	6.9 ± 1.4
1	10	0.425	mU	2 ± 0.4
1	30	0.425	mU	4.9 ± 1
1	25	0.3	mL	4.2 ± 0.8
1	35	0.3	mL	5.6 ± 1.1
1	34	0.425	mU	5.5 ± 1.1

Note: Flow depth calculations were not included for cross-beds interpreted as unit bars. Table is organized by stratigraphic order.

2biii) Table 8: Inner Canyon measured section cross-beds (base: of section: 39.194697, -108.244818)

Interval code	Cross-bed thickness [cm]	Average grain size [mm]	Grain size	Flow depth (d) [m]
D	25	0.3	mL	4.2 ± 0.8
D	40	0.3	mL	6.3 ± 1.3
D	40	0.3	mL	6.3 ± 1.3
D	50	0.3	mL	7.6 ± 1.6
D	*60*	*0.300*	*mL*	
C	10	0.2135	fU	2 ± 0.4
C	15	0.2135	fU	2.8 ± 0.6
C	10	0.2135	fU	2 ± 0.4
C	10	0.2135	fU	2 ± 0.4
C	10	0.2135	fU	2 ± 0.4
C	15	0.2135	fU	2.8 ± 0.6
C	30	0.2135	fU	4.9 ± 1
C	20	0.3	mL	3.5 ± 0.7
C	25	0.3	mL	4.2 ± 0.8
C	*50*	*0.300*	*mL*	
C	*80*	*0.425*	*mU*	
C	50	0.3	mL	7.6 ± 1.6

Interval code	Cross-bed thickness [cm]	Average grain size [mm]	Grain size	Flow depth (d) [m]
C	50	0.2135	fU	7.6 ± 1.6
C	*140*	*0.300*	*mL*	
C	*125*	*0.300*	*mL*	
C	40	0.3	mL	6.3 ± 1.3
C	45	0.3	mL	6.9 ± 1.4
C	35	0.2135	fU	5.6 ± 1.1
C	25	0.2135	fU	4.2 ± 0.8
C	15	0.3	mL	2.8 ± 0.6
C	45	0.3	mL	6.9 ± 1.4
C	25	0.3	mL	4.2 ± 0.8
C	30	0.3	mL	4.9 ± 1
C	*60*	*0.425*	*mL*	
B	50	0.3	mL	7.6 ± 1.6
B	40	0.3	mL	6.3 ± 1.3
B	25	0.3	mL	4.2 ± 0.8
B	45	0.3	mL	6.9 ± 1.4
B	40	0.3	mL	6.3 ± 1.3
B	40	0.3	mL	6.3 ± 1.3
B	30	0.2135	fU	4.9 ± 1

Interval code	Cross-bed thickness [cm]	Average grain size [mm]	Grain size	Flow depth (d) [m]
B	*60*	0.300	*mL*	
B	15	0.3	mL	2.8 ± 0.6
B	35	0.2135	fU	5.6 ± 1.1
B	30	0.2135	fU	4.9 ± 1
B	20	0.3	mL	3.5 ± 0.7
B	30	0.2135	fU	4.9 ± 1
B	20	0.3	mL	3.5 ± 0.7
A	15	0.2135	fU	2.8 ± 0.6
A	20	0.2135	fU	3.5 ± 0.7
A	25	0.3	mL	4.2 ± 0.8
A	20	0.3	mL	3.5 ± 0.7

Note: Flow depth calculations were not included for cross-beds interpreted as unit bars. Table is organized by stratigraphic order.

2c) Method of paleo-slope calculations

Methods of Lynds et al. (2014)

Method #1

This simplistic approach for estimating a rough depositional slope keeps shields number constant at 1 for very fine to medium sand systems. The submerged specific gravity of quartz is 1.65. This is equation #4 in Lynds et al. (2014).

$$S = \frac{R * D_{50b}}{d}$$

Method #2 with application of the Julien assumption

The approach used in this study allows shields number to change with grain size and incorporates other dimensionless numbers.

The following equations are the presented order of use as in Lynds et al. (2014). The authors of this study encourage the reader to review the methods, explanation, and limitations presented in that article for a complete understanding of its applications.

$$D^* = \frac{(\rho_s - \rho) * g * D^3}{\rho * \nu^2} \quad EQ.7$$

$$logW^* = -3.76715 + 1.92944(logD^*) - 0.09815(logD^*)^2 - 0.00575(logD^*)^3 + 0.00056(logD^*)^4 \quad EQ.6$$

$$Re_p = \frac{D_{50b}\sqrt{(D_{50b} * R * g)}}{\nu} \quad EQ.1$$

The Julien assumption sets the minimum threshold of incipient suspension (u^*_{sf}/w_s) constant. This is justifiable due to experimental studies reaching a constant value (Laursen, 1958; Niño et al., 2003). The minimum threshold for incipient suspension was set to 2 from the Julien assessment. This means that u^*_{sf}/w_s will not change with grain size. More accurate calculations would set the ratio to 3.1 for very fine to fine sand and 1.6 for medium sand systems.

$$S = \left(\frac{R * D_{50b}}{d}\right) * \left(\left(\frac{u^*_{sf}}{w_s}\right) * \left(\frac{W^*}{Re_p}\right)^{\left(\frac{1}{3}\right)}\right)^2 \quad EQ.10$$

3) Modern fluvial database

Table footnote:

ID/gauge with '(#)' at the end of the code is to differentiate from other data points from the same stream gauge. If stream gauge identification codes or cumulative drainage area was not published in the original study it was recorded from the USGS National Water Information System or the Canadian Government Water Office webpage at: https://waterdata.usgs.gov/nwis/inventory and https://wateroffice.ec.gc.ca/.

3a) References

CHURCH, M., AND ROOD, K., 1983, Catalogue of alluvial river channel regime data. Department of Geography, University of British Columbia, Vancouver, Canada, p. 99.

OSTERKAMP, W.R., HEDMAN, E.R., AND WISEMAN, A.G., 1982, Geometry, basin-characteristics, discharge, and particle-size data from gaged stream-channel sites, Western United States, USGS, Open File Report 82-93, p. 56.

SCHUMM, S.A., 1968, River adjustment to altered hydrologic regimen-Murrumbidgee River and paleochannels, Australia, USGS Professional Paper 598.

TRAMPUSH, S.M., HUZURBAZAR, S., AND MCELROY, B., 2014, Empirical assessment of theory for bankfull characteristics of alluvial channels: Water Resources Research, v. 50, p. 9211-9220.

4) Detrital zircon analyses

4a) Methods of mineral separation in detrital zircon samples

Step 1: Crushing

Machines used to bring samples under 1 mm in size include a bottle jack, chipmunk crusher and disk mill. The disk mill was not set to less than ~0.5 mm to avoid breaking individual grains. To prevent contamination between samples all surfaces were blown clean with pressurized air. Crushing surfaces were cleaned with a steel wire brush before crushing, between samples, and after crushing. Acetone was also used to clean the surfaces after all the samples were crushed. Samples that passed through a 1 mm sieve were brought to the next stage of mineral separation.

Step 2: Water table separation

Density separation was completed with a Gemeni Table MK.2, model: GT60 2011. The table was first rinsed and inspected for grains. Water mixed with soap was used on the table as a lubricant for heavy minerals to travel on the table.

Samples were fed onto the table at approximately 1 g/s. The water table was run for about 5 minutes after the last sample fell to allow all grains to be collected. Lighter density sediment was placed into storage. Denser sediment was filtered with isopropyl alcohol to remove any soap attached to the grains and then placed in a drying oven. Between and after processing all samples, everything was washed, rinsed and inspected for grains. After all samples were processed, the table was washed and hand scrubbed with water and vinegar.

Step 3: Removal of magnetite

A hand magnet was placed over the samples to remove magnetite. Care was taken to not sift through the samples to avoid build-up of static electricity. Grains removed by the hand magnet were inspected by binocular microscope to assure that no zircon grains with inclusions of

magnetic minerals were extracted. A Frantz^{TM} isodynamic magnetic separator was not used due to the abundance of zircon grains with magnetite inclusions.

Step 4: Heavy liquids separation

The samples were then placed in a separatory funnel filled with bromoform and methylene iodide (MEI). MEI has a specific gravity of ~3.32 which allows for a second stage of density separation. Sediment was agitated, not stirred, to assure the only separation process was density driven. The denser and lighter sediment were extracted separately with filter papers. Samples were rinsed with acetone and then left to dry under a fume hood for 24 hours.

Step 5: Mounting

The remaining sample was decreased in volume by a microsplitter. This was to assure unbiased and representative splits of the sample. A binocular microscope (Nikon SMZ1000) was used to visually separate zircon grains from other heavy minerals. Zircon grains were identified by tetragonal habit, brittle break, and color. Grains that were rounded from fluvial transport were also included to not bias the sample.

At least 300 zircon grains were collected and orderly placed on tape to hold their position. Epoxy resin was then poured over the grains to create a mount for LA-ICP-MS. The epoxy disk was then polished to expose the surface of as many grains as possible.

4b) Table 5: LA-ICP-MS metadata

Laboratory & Sample Preparation	
Laboratory name	KU Geology Isotope Geochemistry Laboratories
Sample type/mineral	Detrital Zircon

Sample preparation	Epoxy disc
Laser ablation system	
Make, Model & type	Arf excimer 193 nm, Photon Machines Analyte G2, ATLEX 300
Ablation cell & volume	Helex 2, two-volume cell
Laser wavelength (nm)	193
Pulse width (ns)	5
Fluence ($J.cm^{-2}$)	2
Repetition rate (Hz)	10
Spot size (um)	20
Sampling mode / pattern	Single spot
Carrier gas	He, 1.01; Ar, 1.1
Ablation duration (secs)	13 (short method); 23 (long method)
Cell carrier gas flow (l/min)	1.1 l/min
ICP-MS Instrument	
Make, Model & type	Thermo Element2 magnetic sector field ICP-MS
Sample introduction	Ablation aerosol
RF power (W)	1100
Make-up gas flow (l/min)	Ar, 1.1 l/min
sampling depth (µm)	-3.6
Detection system	single detector, counting & analog
Masses measured	^{206}Pb, ^{207}Pb, ^{208}Pb, ^{232}Th, ^{238}U
Integration time per peak (ms)	1-8 (short); 1-5 (long)
Total integration time per analysis (secs)	16 (short method); 23 (long method)
Total method time (secs)	25 (short); 39 (long)
IC Dead time (ns)	4
UO+/U+ (%)	<0.2
$^{238}U+/^{232}Th+$	0.7
Data Processing	
Gas blank (s)	9 (short method, WF-01); 16 (long method, WF-04)
Calibration strategy	GJ-1 used as primary standard, Plešovice, and Fish Canyon Tuff used as secondary standards
Reference Material info	NIST 612 (Jochum et al., 2011) GJ-1 (Jackson et al., 2004) Plešovice (Slama et al., 2008)

	Fish Canyon Tuff (Wotzlaw et al., 2013)
Data processing package used / Correction for LIEF	IGOR PRO, Iolite 2.5
Mass discrimination	IGOR PRO, Iolite 2.5
Common-Pb correction, composition and uncertainty	No common-Pb correction was applied
Uncertainty level & propagation	Age uncertainties are reported as ±2σ absolute
Reproducibility (%)	WF-01: Plešovice= 2.1%, Fish Canyon Tuff= 1.3%; WF-04: Plešovice= 1.4%, Fish Canyon Tuff= 0.9%
Quality control / Validation	Plešovice and Fish Canyon Tuff

4c) U-Pb analyses of detrital zircons and secondary standards

See following table.

Table 6: Detrital Zircon LA-ICP-MS U-Pb Isotopic Data and Ages: WF-01, Top of the Williams Fork Formation, Plateau Creek Canyon (lat. 39.1961, long. -108.1392)[a]

					Corrected Isotopic Ratios								Ages (Ma)[i]							
Grain #[b]	U[c] [ppm]	Th[c] [ppm]	Th/U	eU[d] [ppm]	$^{207}Pb/^{235}U$[e]	±2s[f]	$^{206}Pb/^{238}U$[e]	±2s[f]	Rho[g]	$^{207}Pb/^{206}Pb$[h]	±2s[f]	$^{207}Pb/^{235}U$	±2s	$^{206}Pb/^{238}U$	±2s	$^{207}Pb/^{206}Pb$	±2s	Disc. %[j]	Wtd. Disc.[k]
WF_01_001	475	221	0.47	527	0.085	0.004	0.0128	0.0005	0.33	0.048	0.002	82.6	3.9	82.6	3.2	112	88	0.0	0.0
WF_01_002	198	65	0.33	214	4.420	0.120	0.3031	0.0079	0.70	0.104	0.003	1715	23	1705	39	1695	46	-0.6	0.0
WF_01_003	337	129	0.38	367	0.620	0.021	0.0784	0.0023	0.63	0.057	0.002	490	13	486	14	498	72	0.8	0.3
WF_01_004	267	204	0.76	314	0.185	0.009	0.0269	0.0009	0.27	0.050	0.003	171.6	8.1	171.2	5.5	170	110	0.2	0.0
WF_01_005	644	265	0.41	706	0.244	0.007	0.0346	0.0010	0.37	0.052	0.002	221.5	5.7	219.4	6.4	245	79	0.9	0.4
WF_01_006	92	36	0.39	100	4.300	0.140	0.2960	0.0100	0.77	0.105	0.003	1688	26	1669	52	1709	49	2.3	0.0
WF_01_007	278	90	0.32	299	2.793	0.064	0.2405	0.0061	0.69	0.086	0.002	1352	17	1388	31	1336	48	-3.9	0.0
WF_01_008	361	125	0.35	390	0.504	0.014	0.0682	0.0016	0.47	0.054	0.002	413.7	9.6	425	9.5	369	74	-2.7	-1.2
WF_01_009	635	408	0.64	731	0.170	0.007	0.0246	0.0007	0.40	0.050	0.002	159.5	5.9	156.8	4.2	171	84	1.7	0.5
WF_01_010	*859*	*43*	*0.05*	*869*	*5.040*	*0.260*	*0.3240*	*0.0180*	*0.93*	*0.113*	*0.003*	*1825*	*42*	*1805*	*88*	*1843*	*46*	*2.1*	*0.0*
WF_01_011	612	283	0.46	679	0.099	0.004	0.0144	0.0004	0.22	0.049	0.002	95.5	3.5	91.8	2.5	159	95	3.9	1.1
WF_01_012	101	65	0.64	117	0.081	0.009	0.0122	0.0004	0.18	0.048	0.005	79.3	8	78.3	2.8	90	190	1.3	0.1
WF_01_013	103	89	0.86	124	0.175	0.014	0.0267	0.0011	0.01	0.047	0.004	163	12	169.9	6.9	50	160	-4.2	-0.6
WF_01_014	*22*	*23*	*1.01*	*28*	*0.085*	*0.029*	*0.0117*	*0.0011*	*0.52*	*0.060*	*0.024*	*77*	*28*	*75.1*	*7.3*	*250*	*590*	*2.5*	*0.1*
WF_01_015	149	74	0.49	167	4.880	0.110	0.3180	0.0075	0.51	0.111	0.003	1796	20	1778	36	1820	53	2.3	0.0
WF_01_016	743	330	0.44	821	4.420	0.130	0.2981	0.0100	0.72	0.106	0.003	1714	25	1680	50	1728	50	2.8	0.0
WF_01_017	132	69	0.53	148	5.020	0.130	0.3303	0.0067	0.70	0.110	0.003	1822	21	1839	33	1800	46	-2.2	0.0
WF_01_018	*131*	*49*	*0.38*	*142*	*4.340*	*0.140*	*0.3036*	*0.0098*	*0.76*	*0.102*	*0.003*	*1699*	*25*	*1708*	*49*	*1656*	*48*	*-3.1*	*0.0*
WF_01_019	306	96	0.31	329	4.310	0.089	0.2982	0.0067	0.69	0.105	0.002	1698	16	1686	33	1716	42	1.7	0.0
WF_01_020	920	86	0.09	940	4.880	0.100	0.3265	0.0079	0.80	0.109	0.002	1800	18	1820	38	1777	40	-2.4	0.0
WF_01_021	343	102	0.30	367	2.604	0.042	0.2250	0.0050	0.71	0.084	0.002	1301	12	1308	26	1289	45	-1.5	0.0
WF_01_022	519	185	0.36	563	0.502	0.014	0.0663	0.0014	0.58	0.054	0.002	412.6	9.3	413.9	8.6	393	62	-0.3	-0.1
WF_01_023	130	75	0.57	148	0.087	0.007	0.0126	0.0005	0.01	0.051	0.005	84.2	6.9	80.9	3.3	250	180	3.9	0.5
WF_01_024	142	147	1.04	176	0.790	0.025	0.0948	0.0021	0.45	0.060	0.002	591	14	584	13	635	72	1.2	0.5
WF_01_025	106	89	0.84	127	0.072	0.008	0.0120	0.0005	0.21	0.044	0.005	70.1	7.3	77.1	3.2	-50	190	-10.0	-1.0
WF_01_026	149	37	0.25	157	4.260	0.110	0.3026	0.0059	0.74	0.102	0.002	1683	22	1703	29	1671	45	-1.9	0.0
WF_01_027	360	193	0.54	405	0.198	0.007	0.0295	0.0007	0.32	0.048	0.002	182.8	6.1	187.4	4.2	144	84	-2.5	-0.8
WF_01_028	90	73	0.81	107	2.899	0.079	0.2362	0.0065	0.59	0.089	0.003	1382	22	1366	34	1403	60	2.6	0.0
WF_01_029	376	143	0.38	410	4.340	0.140	0.2980	0.0100	0.86	0.106	0.002	1701	27	1688	50	1731	42	2.5	0.0
WF_01_030	186	64	0.34	201	1.929	0.040	0.1872	0.0041	0.58	0.075	0.002	1092	14	1106	22	1069	54	-3.5	0.0
WF_01_031	139	117	0.84	167	0.081	0.007	0.0126	0.0004	0.52	0.047	0.005	78.5	6.8	80.4	2.4	70	180	-2.4	-0.3
WF_01_032	177	34	0.19	185	2.680	0.068	0.2282	0.0065	0.64	0.086	0.002	1320	19	1329	35	1336	55	0.5	0.0
WF_01_033	*317*	*195*	*0.62*	*362*	*0.858*	*0.025*	*0.0835*	*0.0038*	*0.57*	*0.075*	*0.003*	*628*	*14*	*516*	*22*	*1040*	*82*	*17.8*	*8.0*
WF_01_034	190	415	2.19	287	0.166	0.009	0.0236	0.0006	0.31	0.049	0.003	155.1	7.8	150.6	3.9	200	110	2.9	0.6

Table 6: Detrital Zircon LA-ICP-MS U-Pb Isotopic Data and Ages: WF-01, Top of the Williams Fork Formation, Plateau Creek Canyon (lat. 39.1961, long. -108.1392)[a]

					Corrected Isotopic Ratios								Ages (Ma)[i]							
Grain #[b]	U[c] [ppm]	Th[c] [ppm]	Th/U	eU[d] [ppm]	$^{207}Pb/^{235}U$[e]	±2s[f]	$^{206}Pb/^{238}U$[e]	±2s[f]	Rho[g]	$^{207}Pb/^{206}Pb$[h]	±2s[f]	$^{207}Pb/^{235}U$	±2s	$^{206}Pb/^{238}U$	±2s	$^{207}Pb/^{206}Pb$	±2s	Disc. %[j]	Wtd. Disc.[k]
WF_01_035	145	105	0.73	170	0.076	0.007	0.0119	0.0004	0.14	0.047	0.004	74.1	6.4	76.2	2.6	60	160	-2.8	-0.3
WF_01_036	231	149	0.64	266	0.095	0.007	0.0140	0.0005	0.11	0.051	0.004	92.9	6.9	89.5	2.9	240	160	3.7	0.5
WF_01_037	495	181	0.37	538	0.096	0.004	0.0145	0.0004	0.34	0.049	0.002	93.5	3.5	92.8	2.6	138	92	0.7	0.2
WF_01_038	228	93	0.41	250	4.259	0.081	0.3033	0.0071	0.68	0.103	0.002	1688	16	1706	35	1673	42	-2.0	0.0
WF_01_039	126	99	0.78	149	15.560	0.340	0.5520	0.0130	0.71	0.206	0.005	2851	20	2831	52	2874	35	1.5	0.0
WF_01_040	314	220	0.70	366	0.173	0.008	0.0264	0.0008	0.07	0.049	0.003	161.8	6.7	167.9	4.8	150	110	-3.8	-0.9
WF_01_041	*88*	*42*	*0.48*	*98*	*9.610*	*0.240*	*0.4126*	*0.0099*	*0.73*	*0.172*	*0.004*	*2394*	*23*	*2225*	*45*	*2582*	*39*	*13.8*	*0.0*
WF_01_042	190	164	0.86	229	0.086	0.007	0.0124	0.0004	0.15	0.050	0.004	83.5	6.4	79.1	2.6	250	160	5.3	0.7
WF_01_043	845	386	0.46	936	0.185	0.006	0.0274	0.0007	0.49	0.049	0.002	172.5	4.7	174.1	4.1	169	68	-0.9	-0.3
WF_01_044	283	320	1.13	358	0.172	0.006	0.0255	0.0006	0.26	0.051	0.002	161.2	5.5	162	4	217	87	-0.5	-0.1
WF_01_045	*121*	*76*	*0.63*	*139*	*1.763*	*0.061*	*0.1716*	*0.0051*	*0.52*	*0.076*	*0.003*	*1030*	*23*	*1021*	*28*	*1086*	*74*	*6.0*	*0.0*
WF_01_046	840	189	0.22	884	0.178	0.005	0.0266	0.0007	0.48	0.050	0.002	165.8	4.6	169.2	4.1	165	69	-2.1	-0.7
WF_01_047	261	29	0.11	268	4.459	0.094	0.3073	0.0074	0.76	0.106	0.002	1721	17	1726	36	1729	41	0.2	0.0
WF_01_048	229	102	0.44	253	4.530	0.120	0.3080	0.0082	0.79	0.107	0.002	1736	21	1735	42	1744	42	0.5	0.0
WF_01_049	749	155	0.21	785	2.061	0.059	0.1939	0.0050	0.79	0.079	0.002	1133	20	1141	27	1159	46	1.6	0.0
WF_01_050	*430*	*151*	*0.35*	*465*	*4.420*	*0.220*	*0.3060*	*0.0160*	*0.91*	*0.106*	*0.003*	*1709*	*42*	*1732*	*83*	*1729*	*50*	*-0.2*	*0.0*
WF_01_051	496	52	0.10	508	4.432	0.082	0.3065	0.0060	0.62	0.107	0.002	1719	15	1722	30	1746	41	1.4	0.0
WF_01_052	198	47	0.24	209	1.935	0.050	0.1874	0.0048	0.66	0.077	0.002	1091	17	1106	26	1110	56	0.4	0.0
WF_01_053	287	142	0.49	320	0.189	0.010	0.0282	0.0008	0.25	0.049	0.003	175.4	8.1	179.1	5	150	110	-2.1	-0.5
WF_01_054	347	187	0.54	390	0.180	0.007	0.0268	0.0008	0.40	0.050	0.002	167.6	6.2	170.7	4.7	189	95	-1.8	-0.5
WF_01_055	128	53	0.41	140	4.120	0.110	0.2944	0.0086	0.77	0.103	0.003	1659	23	1661	43	1678	46	1.0	0.0
WF_01_056	672	265	0.39	734	0.193	0.006	0.0282	0.0008	0.59	0.050	0.002	179.1	5	179.1	5.2	180	65	0.0	0.0
WF_01_057	413	17	0.04	417	4.350	0.140	0.2980	0.0100	0.86	0.106	0.003	1706	28	1678	50	1739	45	3.5	0.0
WF_01_058	95	31	0.33	102	0.102	0.011	0.0157	0.0008	0.14	0.048	0.005	97.8	9.7	100.1	4.8	150	190	-2.4	-0.2
WF_01_059	860	254	0.30	920	0.170	0.005	0.0256	0.0007	0.27	0.051	0.002	159.7	4.5	163.1	4.1	193	79	-2.1	-0.8
WF_01_060	191	37	0.20	199	4.397	0.098	0.3103	0.0074	0.72	0.106	0.003	1712	19	1741	37	1733	43	-0.5	0.0
WF_01_061	335	168	0.50	374	4.480	0.110	0.3123	0.0078	0.64	0.105	0.003	1726	21	1756	39	1719	47	-2.2	0.0
WF_01_062	72	52	0.72	84	5.560	0.170	0.3486	0.0091	0.54	0.116	0.004	1908	26	1926	43	1893	53	-1.7	0.0
WF_01_063	220	10	0.05	222	3.691	0.090	0.2797	0.0071	0.71	0.096	0.003	1570	20	1588	36	1548	49	-2.6	0.0
WF_01_064	*16*	*5*	*0.32*	*17*	*1.980*	*0.110*	*0.1959*	*0.0098*	*0.33*	*0.075*	*0.005*	*1121*	*38*	*1166*	*50*	*1080*	*120*	*-8.0*	*0.0*
WF_01_065	748	269	0.36	811	0.547	0.018	0.0717	0.0018	0.68	0.056	0.002	442	12	446	11	460	60	-0.9	-0.3
WF_01_066	381	255	0.67	441	0.185	0.008	0.0283	0.0009	0.48	0.049	0.002	173.1	6.8	179.7	5.4	126	84	-3.8	-1.0
WF_01_067	54	65	1.19	69	1.633	0.060	0.1641	0.0056	0.28	0.072	0.003	982	24	978	31	967	97	-1.1	0.0
WF_01_068	213	103	0.48	237	0.196	0.011	0.0278	0.0010	0.30	0.051	0.003	180.7	9.4	176.9	6	209	100	2.1	0.4

Table 6: Detrital Zircon LA-ICP-MS U-Pb Isotopic Data and Ages: WF-01, Top of the Williams Fork Formation, Plateau Creek Canyon (lat. 39.1961, long. -108.1392)[a]

					Corrected Isotopic Ratios								Ages (Ma)[i]							
Grain #[b]	U[c] [ppm]	Th[c] [ppm]	Th/U	eU[d] [ppm]	$^{207}Pb/^{235}U$[e]	±2s[f]	$^{206}Pb/^{238}U$[e]	±2s[f]	Rho[g]	$^{207}Pb/^{206}Pb$[h]	±2s[f]	$^{207}Pb/^{235}U$	±2s	$^{206}Pb/^{238}U$	±2s	$^{207}Pb/^{206}Pb$	±2s	Disc. %[j]	Wtd. Disc.[k]
WF_01_070	313	271	0.86	377	0.210	0.009	0.0310	0.0009	0.37	0.049	0.002	192.9	7.3	196.8	5.8	161	93	-2.0	-0.5
WF_01_071	273	47	0.17	284	0.781	0.023	0.0969	0.0024	0.42	0.060	0.002	587	14	596	14	600	66	-1.5	-0.6
WF_01_072	249	99	0.40	272	4.730	0.120	0.3166	0.0082	0.73	0.108	0.003	1769	21	1771	40	1763	46	-0.5	0.0
WF_01_073	499	103	0.21	523	0.109	0.004	0.0162	0.0004	0.31	0.049	0.002	105.6	3.8	103.6	2.8	182	93	1.9	0.5
WF_01_074	372	252	0.68	431	0.181	0.008	0.0271	0.0009	0.24	0.049	0.002	168.7	7	172.5	5.6	148	100	-2.3	-0.5
WF_01_075	339	105	0.31	364	4.380	0.120	0.3035	0.0079	0.72	0.106	0.003	1705	22	1707	39	1727	48	1.2	0.0
WF_01_076	76	34	0.45	84	11.930	0.250	0.5050	0.0130	0.75	0.172	0.004	2599	20	2640	56	2579	40	-2.4	0.0
WF_01_077	*411*	*247*	*0.60*	*469*	*0.230*	*0.030*	*0.0258*	*0.0009*	*0.61*	*0.063*	*0.007*	*206*	*23*	*164.2*	*5.9*	*590*	*180*	*20.3*	*1.8*
WF_01_078	77	52	0.68	89	0.083	0.012	0.0123	0.0007	0.00	0.051	0.008	81	11	78.8	4.6	180	270	2.7	0.2
WF_01_079	*54*	*15*	*0.29*	*57*	*0.070*	*0.014*	*0.0118*	*0.0007*	*0.11*	*0.047*	*0.009*	*68*	*13*	*75.5*	*4.4*	*70*	*320*	*-11.0*	*-0.6*
WF_01_080	167	50	0.30	179	4.265	0.099	0.2969	0.0075	0.76	0.104	0.002	1690	18	1674	37	1692	42	1.1	0.0
WF_01_081	233	246	1.05	291	0.178	0.011	0.0263	0.0009	0.29	0.050	0.003	165.8	9.3	167.4	5.3	170	130	-1.0	-0.2
WF_01_082	78	47	0.60	89	4.240	0.130	0.2970	0.0110	0.73	0.105	0.003	1678	25	1689	52	1708	53	1.1	0.0
WF_01_083	1439	438	0.30	1542	0.201	0.006	0.0289	0.0008	0.59	0.051	0.002	185.9	5	183.6	5.2	225	66	1.2	0.5
WF_01_084	*1116*	*61*	*0.05*	*1130*	*1.553*	*0.063*	*0.1192*	*0.0051*	*0.92*	*0.094*	*0.002*	*947*	*25*	*725*	*29*	*1509*	*47*	*23.4*	*8.9*
WF_01_085	*44*	*28*	*0.64*	*51*	*0.086*	*0.015*	*0.0133*	*0.0011*	*0.10*	*0.047*	*0.009*	*85*	*14*	*85*	*7.2*	*60*	*320*	*0.0*	*0.0*
WF_01_086	204	141	0.69	237	0.284	0.015	0.0387	0.0011	0.09	0.053	0.003	253	12	244.9	6.7	350	120	3.2	0.7
WF_01_087	79	31	0.40	86	2.063	0.069	0.1910	0.0056	0.51	0.079	0.003	1133	23	1126	30	1165	63	3.3	0.0
WF_01_088	145	77	0.53	163	5.100	0.130	0.3298	0.0091	0.75	0.114	0.003	1839	21	1835	44	1851	46	0.9	0.0
WF_01_089	146	47	0.32	157	2.815	0.071	0.2312	0.0049	0.60	0.088	0.002	1360	18	1344	25	1402	51	4.1	0.0
WF_01_090	220	86	0.39	240	0.517	0.017	0.0665	0.0019	0.35	0.057	0.002	426	11	415	11	483	77	2.6	1.0
WF_01_091	212	102	0.48	236	4.500	0.110	0.3118	0.0082	0.75	0.105	0.003	1728	20	1753	41	1719	44	-2.0	0.0
WF_01_092	219	75	0.34	237	4.399	0.092	0.3110	0.0065	0.57	0.104	0.003	1714	17	1745	32	1689	46	-3.3	0.0
WF_01_093	21	19	0.91	25	1.286	0.096	0.1316	0.0074	0.37	0.072	0.006	837	44	796	42	970	170	4.9	0.9
WF_01_094	1192	78	0.07	1210	2.659	0.046	0.2172	0.0044	0.76	0.089	0.002	1316	13	1267	23	1410	42	10.1	0.0
WF_01_095	713	249	0.35	772	4.400	0.110	0.3064	0.0094	0.75	0.105	0.003	1710	21	1722	46	1709	47	-0.8	0.0
WF_01_096	179	96	0.54	201	4.231	0.087	0.3003	0.0071	0.73	0.103	0.002	1678	17	1692	35	1673	44	-1.1	0.0
WF_01_097	844	136	0.16	876	4.858	0.100	0.3231	0.0061	0.62	0.110	0.003	1793	18	1804	30	1800	41	-0.2	0.0
WF_01_098	198	103	0.52	222	4.194	0.085	0.2967	0.0060	0.60	0.103	0.003	1673	16	1674	30	1674	47	0.0	0.0
WF_01_099	*58*	*51*	*0.87*	*70*	*0.086*	*0.016*	*0.0119*	*0.0008*	*0.19*	*0.052*	*0.010*	*84*	*15*	*76.2*	*4.8*	*180*	*330*	*9.3*	*0.5*
WF_01_100	37	10	0.27	40	1.735	0.068	0.1763	0.0060	0.39	0.072	0.003	1023	25	1045	33	959	78	-9.0	0.0
WF_01_101	497	307	0.62	569	3.024	0.050	0.2427	0.0052	0.71	0.090	0.002	1413	13	1403	27	1425	42	1.5	0.0
WF_01_102	*683*	*70*	*0.10*	*699*	*6.970*	*0.470*	*0.3810*	*0.0110*	*0.68*	*0.134*	*0.006*	*2112*	*57*	*2078*	*53*	*2139*	*81*	*2.9*	*0.0*
WF_01_103	263	250	0.95	322	0.195	0.008	0.0277	0.0007	0.18	0.051	0.003	180.5	6.5	175.9	4.5	250	110	2.5	0.7

Table 6: Detrital Zircon LA-ICP-MS U-Pb Isotopic Data and Ages: WF-01, Top of the Williams Fork Formation, Plateau Creek Canyon (lat. 39.1961, long. -108.1392)[a]

					Corrected Isotopic Ratios								Ages (Ma)[i]							
Grain #[b]	U[c] [ppm]	Th[c] [ppm]	Th/U	eU[d] [ppm]	$^{207}Pb/^{235}U$[e]	±2s[f]	$^{206}Pb/^{238}U$[e]	±2s[f]	Rho[g]	$^{207}Pb/^{206}Pb$[h]	±2s[f]	$^{207}Pb/^{235}U$	±2s	$^{206}Pb/^{238}U$	±2s	$^{207}Pb/^{206}Pb$	±2s	Disc. %[j]	Wtd. Disc.[k]
WF_01_104	*491*	*461*	*0.94*	*599*	*0.166*	*0.005*	*0.0255*	*0.0006*	*0.03*	*0.048*	*0.002*	*155.9*	*4.3*	*162.4*	*3.7*	*106*	*85*	*-4.2*	*-1.5*
WF_01_105	*554*	*235*	*0.42*	*609*	*4.870*	*0.140*	*0.3382*	*0.0099*	*0.83*	*0.105*	*0.003*	*1794*	*24*	*1876*	*48*	*1714*	*45*	*-9.5*	*0.0*
WF_01_106	80	98	1.23	103	4.330	0.110	0.3040	0.0064	0.50	0.102	0.003	1695	21	1710	32	1666	52	-2.6	0.0
WF_01_107	*52*	*26*	*0.51*	*58*	*0.081*	*0.019*	*0.0119*	*0.0009*	*0.52*	*0.056*	*0.013*	*82*	*18*	*76.1*	*5.8*	*230*	*400*	*7.2*	*0.3*
WF_01_108	549	155	0.28	585	4.195	0.081	0.2824	0.0062	0.70	0.107	0.002	1671	16	1602	31	1747	42	8.3	0.0
WF_01_109	*451*	*83*	*0.18*	*470*	*1.772*	*0.072*	*0.1004*	*0.0040*	*0.73*	*0.129*	*0.004*	*1031*	*26*	*616*	*23*	*2075*	*56*	*40.3*	*16.0*
WF_01_110	194	54	0.28	206	1.802	0.039	0.1779	0.0041	0.57	0.073	0.002	1047	14	1055	22	1021	48	-3.3	0.0
WF_01_111	151	78	0.52	169	0.081	0.009	0.0116	0.0005	0.52	0.051	0.005	81.1	7.8	74.2	2.9	250	190	8.5	0.9
WF_01_112	**75**	**17**	**0.23**	**79**	**0.073**	**0.010**	**0.0110**	**0.0006**	**0.52**	**0.049**	**0.008**	**70.7**	**9.5**	**70.2**	**3.6**	**90**	**270**	**0.7**	**0.1**
WF_01_113	261	75	0.29	279	0.242	0.009	0.0341	0.0009	0.05	0.050	0.002	220.7	7.3	216.3	5.4	213	100	2.0	0.6
WF_01_114	300	79	0.26	318	3.191	0.073	0.2566	0.0064	0.57	0.089	0.003	1453	17	1471	33	1398	53	-5.2	0.0
WF_01_115	220	21	0.10	225	2.866	0.064	0.2398	0.0062	0.72	0.088	0.002	1376	18	1384	32	1380	48	-0.3	0.0
WF_01_116	36	22	0.62	42	1.989	0.089	0.1843	0.0065	0.44	0.078	0.003	1114	29	1089	35	1145	85	4.9	0.0
WF_01_117	307	128	0.42	337	0.200	0.010	0.0300	0.0010	0.38	0.049	0.003	185	8.5	190.5	6.4	131	100	-3.0	-0.6
WF_01_118	976	72	0.07	993	3.113	0.057	0.2512	0.0053	0.69	0.089	0.002	1435	14	1444	27	1411	45	-2.3	0.0
WF_01_119	221	181	0.82	264	0.177	0.010	0.0270	0.0009	0.32	0.049	0.003	164.5	8.8	171.6	5.9	140	120	-4.3	-0.8
WF_01_120	436	68	0.16	452	1.665	0.033	0.1652	0.0038	0.46	0.073	0.002	994	12	985	21	1010	54	2.5	0.0
WF_01_121	244	97	0.40	266	4.205	0.090	0.2942	0.0071	0.65	0.104	0.003	1673	18	1661	35	1709	46	2.8	0.0
WF_01_122	178	42	0.24	188	4.330	0.100	0.2975	0.0081	0.75	0.106	0.003	1702	19	1677	40	1729	44	3.0	0.0
WF_01_123	466	186	0.40	510	3.047	0.066	0.2455	0.0064	0.74	0.091	0.002	1417	17	1414	33	1441	44	1.9	0.0
WF_01_124	409	294	0.72	478	0.171	0.007	0.0258	0.0009	0.28	0.048	0.002	160.3	5.8	164.4	5.6	107	91	-2.6	-0.7
WF_01_125	47	40	0.86	56	0.839	0.050	0.0982	0.0029	0.29	0.061	0.003	621	26	603	17	640	120	2.9	0.7
WF_01_126	45	28	0.62	52	4.270	0.150	0.2956	0.0088	0.54	0.104	0.004	1681	28	1667	44	1710	64	2.5	0.0
WF_01_127	97	42	0.44	106	4.340	0.120	0.2991	0.0082	0.69	0.104	0.003	1700	24	1685	41	1701	49	0.9	0.0
WF_01_128	196	168	0.85	236	0.107	0.007	0.0170	0.0007	0.30	0.046	0.003	102.6	6.7	108.8	4.1	20	130	-6.0	-0.9
WF_01_129	52	75	1.44	70	2.943	0.091	0.2345	0.0068	0.43	0.088	0.003	1392	23	1356	35	1403	70	3.3	0.0
WF_01_130	704	52	0.07	716	1.834	0.039	0.1786	0.0044	0.80	0.074	0.002	1059	15	1059	24	1037	45	-2.1	0.0
WF_01_131	136	45	0.33	147	2.324	0.068	0.2125	0.0062	0.53	0.078	0.003	1216	21	1241	33	1152	63	-7.7	0.0
WF_01_132	2169	780	0.36	2352	0.106	0.004	0.0159	0.0005	0.47	0.048	0.002	102.3	3.2	101.8	2.9	108	75	0.5	0.2
WF_01_133	602	169	0.28	642	4.340	0.110	0.3031	0.0084	0.76	0.103	0.002	1701	22	1705	41	1678	44	-1.6	0.0
WF_01_134	*755*	*170*	*0.22*	*795*	*2.493*	*0.068*	*0.1799*	*0.0063*	*0.85*	*0.100*	*0.003*	*1268*	*20*	*1065*	*34*	*1611*	*47*	*33.9*	*0.0*
WF_01_135	223	144	0.64	257	4.400	0.100	0.3011	0.0076	0.62	0.106	0.003	1712	20	1695	38	1716	49	1.2	0.0
WF_01_136	*143*	*33*	*0.23*	*150*	*0.087*	*0.008*	*0.0120*	*0.0005*	*0.52*	*0.052*	*0.005*	*84.3*	*7.4*	*76.7*	*3*	*300*	*200*	*9.0*	*1.0*
WF_01_137	1387	2430	1.75	1958	0.080	0.003	0.0118	0.0003	0.37	0.049	0.002	78	3	75.6	2	150	81	3.1	0.8

Table 6: Detrital Zircon LA-ICP-MS U-Pb Isotopic Data and Ages: WF-01, Top of the Williams Fork Formation, Plateau Creek Canyon (lat. 39.1961, long. -108.1392)[a]

					Corrected Isotopic Ratios								Ages (Ma)[i]							
Grain #[b]	U[c] [ppm]	Th[c] [ppm]	Th/U	eU[d] [ppm]	$^{207}Pb/^{235}U$[e]	±2s[f]	$^{206}Pb/^{238}U$[e]	±2s[f]	Rho[g]	$^{207}Pb/^{206}Pb$[h]	±2s[f]	$^{207}Pb/^{235}U$	±2s	$^{206}Pb/^{238}U$	±2s	$^{207}Pb/^{206}Pb$	±2s	Disc. %[j]	Wtd. Disc.[k]
WF_01_138	208	136	0.66	240	0.207	0.011	0.0310	0.0011	0.26	0.049	0.003	190.8	9.1	196.5	6.8	140	120	-3.0	-0.6
WF_01_139	1347	472	0.35	1458	0.205	0.005	0.0290	0.0008	0.44	0.051	0.002	189.1	4.3	184.3	4.7	232	68	2.5	1.1
WF_01_140	247	128	0.52	277	0.107	0.007	0.0155	0.0005	0.24	0.050	0.003	102.7	6	98.8	3.1	180	130	3.8	0.7
WF_01_141	151	85	0.56	171	0.182	0.011	0.0269	0.0010	0.03	0.050	0.004	172	10	171	6	190	140	0.6	0.1
WF_01_142	203	185	0.91	246	13.740	0.300	0.5370	0.0120	0.78	0.185	0.004	2734	22	2770	51	2701	39	-2.6	0.0
WF_01_143	93	16	0.18	96	2.493	0.063	0.2168	0.0065	0.65	0.082	0.002	1273	18	1264	34	1240	57	-1.9	0.0
WF_01_144	562	262	0.47	624	0.296	0.010	0.0418	0.0014	0.76	0.050	0.001	262.5	8	263.8	8.9	205	62	-0.5	-0.2
WF_01_145	41	34	0.82	49	2.090	0.075	0.1898	0.0068	0.55	0.077	0.003	1145	25	1119	37	1109	86	-0.9	0.0
WF_01_146	386	147	0.38	421	4.121	0.081	0.2938	0.0065	0.67	0.100	0.002	1662	16	1659	33	1628	45	-1.9	0.0
WF_01_147	53	47	0.89	64	2.029	0.091	0.1859	0.0058	0.51	0.077	0.003	1127	29	1098	32	1115	85	1.5	0.0
WF_01_148	134	55	0.41	147	2.147	0.064	0.1992	0.0049	0.71	0.077	0.002	1172	22	1170	26	1137	53	-2.9	0.0
WF_01_149	218	114	0.52	245	0.804	0.027	0.0973	0.0028	0.51	0.059	0.002	599	15	598	16	566	77	0.2	0.1
WF_01_150	854	90	0.10	875	0.466	0.013	0.0612	0.0016	0.65	0.053	0.002	388	9.1	383	9.5	346	60	1.3	0.5
WF_01_151	203	91	0.45	224	0.194	0.011	0.0294	0.0011	0.30	0.047	0.003	182.2	9.2	187	7	100	120	-2.6	-0.5
WF_01_152	215	91	0.42	236	3.265	0.061	0.2536	0.0067	0.60	0.092	0.003	1476	15	1456	34	1459	52	0.2	0.0
WF_01_153	*668*	*159*	*0.24*	*705*	*1.920*	*0.081*	*0.1401*	*0.0056*	*0.91*	*0.098*	*0.002*	*1087*	*29*	*844*	*32*	*1583*	*43*	*22.4*	*8.4*
WF_01_154	81	152	1.88	116	4.177	0.087	0.3025	0.0084	0.51	0.100	0.003	1672	18	1702	41	1619	53	-5.1	0.0
WF_01_155	*323*	*69*	*0.21*	*339*	*3.350*	*0.190*	*0.2240*	*0.0130*	*0.93*	*0.107*	*0.003*	*1490*	*43*	*1299*	*67*	*1746*	*51*	*25.6*	*0.0*
WF_01_156	*228*	*43*	*0.19*	*238*	*1.526*	*0.051*	*0.1485*	*0.0043*	*0.71*	*0.074*	*0.002*	*944*	*22*	*892*	*24*	*1044*	*61*	*14.6*	*0.0*
WF_01_157	233	18	0.08	237	1.611	0.052	0.1639	0.0041	0.50	0.072	0.002	974	20	978	23	981	67	0.3	0.0
WF_01_158	*368*	*280*	*0.76*	*434*	*0.189*	*0.010*	*0.0256*	*0.0009*	*0.30*	*0.052*	*0.003*	*175.6*	*8.3*	*162.6*	*5.7*	*280*	*110*	*7.4*	*1.6*
WF_01_159	419	109	0.26	445	2.149	0.044	0.2004	0.0044	0.64	0.077	0.002	1165	15	1177	24	1105	46	-6.5	0.0
WF_01_160	105	44	0.41	115	3.046	0.080	0.2476	0.0060	0.50	0.088	0.003	1416	20	1425	31	1379	59	-3.3	0.0
WF_01_161	233	116	0.50	260	0.184	0.010	0.0262	0.0007	0.25	0.050	0.003	170.8	8.3	166.5	4.5	210	110	2.5	0.5
WF_01_162	282	100	0.35	305	4.410	0.120	0.3036	0.0086	0.85	0.104	0.002	1711	22	1707	43	1696	42	-0.6	0.0
WF_01_163	28	17	0.61	31	11.420	0.320	0.4900	0.0130	0.61	0.166	0.005	2563	27	2586	54	2523	48	-2.5	0.0
WF_01_164	141	77	0.54	159	4.274	0.081	0.2958	0.0069	0.59	0.103	0.003	1694	16	1679	34	1683	49	0.2	0.0
WF_01_165	319	95	0.30	341	1.578	0.041	0.1633	0.0042	0.67	0.070	0.002	960	16	975	23	918	54	-6.2	0.0
WF_01_166	113	55	0.48	126	4.180	0.100	0.2987	0.0074	0.72	0.102	0.003	1670	21	1683	37	1655	45	-1.7	0.0
WF_01_167	462	118	0.25	490	4.448	0.092	0.3014	0.0062	0.76	0.105	0.002	1719	17	1697	31	1714	39	1.0	0.0
WF_01_168	239	107	0.45	264	4.345	0.086	0.2996	0.0066	0.55	0.104	0.002	1701	16	1689	33	1708	48	1.1	0.0
WF_01_169	154	36	0.23	163	4.222	0.084	0.3064	0.0054	0.48	0.100	0.002	1677	16	1723	27	1617	46	-6.6	0.0
WF_01_170	371	100	0.27	394	1.204	0.027	0.1306	0.0023	0.45	0.067	0.002	801	12	791	13	827	53	1.2	0.8
WF_01_171	343	219	0.64	394	3.990	0.230	0.2790	0.0170	0.95	0.102	0.003	1619	48	1581	86	1667	45	5.2	0.0

Table 6: Detrital Zircon LA-ICP-MS U-Pb Isotopic Data and Ages: WF-01, Top of the Williams Fork Formation, Plateau Creek Canyon (lat. 39.1961, long. -108.1392)[a]

					Corrected Isotopic Ratios							Ages (Ma)[i]							
Grain #[b]	U[c] [ppm]	Th[c] [ppm]	Th/U	eU[d] [ppm]	$^{207}Pb/^{235}U$[e]	±2s[f]	$^{206}Pb/^{238}U$[e]	±2s[f]	Rho[g]	$^{207}Pb/^{206}Pb$[h]	±2s[f]	$^{207}Pb/^{235}U$	±2s	$^{206}Pb/^{238}U$	±2s	$^{207}Pb/^{206}Pb$	±2s	Disc. %[j]	Wtd. Disc.[k]
WF_01_172	128	77	0.60	146	0.187	0.011	0.0270	0.0008	0.23	0.048	0.003	174.6	10	171.4	5.2	140	130	1.8	0.3
WF_01_173	213	73	0.34	230	13.670	0.220	0.5275	0.0099	0.65	0.186	0.004	2726	15	2729	42	2703	36	-1.0	0.0
WF_01_174	140	134	0.96	171	0.160	0.010	0.0226	0.0007	0.26	0.050	0.003	149.9	8.7	144	4.2	200	140	3.9	0.7
WF_01_175	62	28	0.45	68	1.576	0.051	0.1620	0.0039	0.23	0.070	0.003	958	20	968	22	928	77	-4.3	0.0
WF_01_176	557	195	0.35	603	2.973	0.050	0.2411	0.0053	0.61	0.089	0.002	1401	13	1391	27	1396	44	0.4	0.0
WF_01_177	171	120	0.70	200	3.945	0.097	0.2917	0.0078	0.62	0.098	0.003	1627	19	1649	39	1599	51	-3.1	0.0
WF_01_178	332	97	0.29	355	4.394	0.093	0.3073	0.0067	0.62	0.103	0.003	1711	18	1726	33	1679	45	-2.8	0.0
WF_01_179	1362	44	0.03	1372	4.520	0.110	0.3107	0.0068	0.88	0.105	0.002	1737	21	1743	33	1711	38	-1.9	0.0
WF_01_180	465	136	0.29	497	2.149	0.045	0.1981	0.0049	0.73	0.078	0.002	1163	15	1165	26	1140	46	-2.2	0.0
WF_01_181	281	266	0.95	343	0.530	0.019	0.0701	0.0016	0.34	0.054	0.002	431	13	438.2	9.5	362	81	-1.7	-0.6
WF_01_182	301	64	0.21	316	4.750	0.110	0.3233	0.0080	0.53	0.106	0.003	1776	20	1804	39	1732	48	-4.2	0.0
WF_01_183	275	152	0.55	311	0.191	0.007	0.0280	0.0007	0.20	0.048	0.002	177.4	6.1	178.1	4.6	136	92	-0.4	-0.1
WF_01_184	166	102	0.62	190	0.164	0.011	0.0234	0.0007	0.17	0.049	0.004	153.3	9.3	149.3	4.5	160	140	2.6	0.4
WF_01_185	*907*	*51*	*0.06*	*919*	*2.510*	*0.130*	*0.1728*	*0.0091*	*0.95*	*0.104*	*0.003*	*1268*	*37*	*1026*	*50*	*1705*	*48*	*39.8*	*0.0*
WF_01_186	300	416	1.39	398	0.167	0.006	0.0256	0.0007	0.33	0.047	0.002	156.2	5.5	162.8	4.6	46	81	-4.2	-1.2
WF_01_187	131	58	0.44	145	2.569	0.061	0.2228	0.0051	0.74	0.083	0.002	1295	17	1300	26	1266	45	-2.7	0.0
WF_01_188	466	157	0.34	503	4.382	0.098	0.3037	0.0069	0.80	0.103	0.002	1706	18	1708	34	1682	41	-1.5	0.0
WF_01_189	920	594	0.65	1060	0.187	0.006	0.0267	0.0007	0.21	0.050	0.002	173.8	5.2	169.8	4.4	201	85	2.3	0.8
WF_01_190	*104*	*32*	*0.31*	*111*	*4.090*	*0.130*	*0.2824*	*0.0097*	*0.80*	*0.103*	*0.003*	*1651*	*26*	*1611*	*51*	*1687*	*53*	*4.5*	*0.0*
WF_01_191	220	20	0.09	225	0.225	0.011	0.0327	0.0010	0.40	0.049	0.002	205.2	9.2	207.3	6.3	127	98	-1.0	-0.2
WF_01_192	128	55	0.43	141	0.108	0.010	0.0153	0.0007	0.15	0.052	0.005	103.8	8.8	98.1	4.5	320	190	5.5	0.6
WF_01_193	446	184	0.41	489	0.259	0.010	0.0371	0.0010	0.58	0.050	0.002	234.2	7.9	235	6.3	199	76	-0.3	-0.1
WF_01_194	58	41	0.71	67	0.097	0.015	0.0145	0.0009	0.21	0.047	0.007	92	14	92.8	5.6	20	260	-0.9	-0.1
WF_01_195	912	365	0.40	998	0.249	0.008	0.0349	0.0009	0.57	0.050	0.002	225.1	6.4	221	5.7	214	66	1.8	0.6
WF_01_196	113	41	0.36	123	4.530	0.120	0.3119	0.0071	0.67	0.105	0.003	1733	22	1749	35	1730	45	-1.1	0.0
WF_01_197	87	82	0.95	106	0.174	0.015	0.0241	0.0011	0.52	0.052	0.006	161	13	153.5	6.8	260	190	4.7	0.6
WF_01_198	160	120	0.75	188	0.155	0.011	0.0237	0.0010	0.52	0.047	0.004	145.7	9.3	150.6	6.2	90	150	-3.4	-0.5
WF_01_199	697	314	0.45	771	0.178	0.007	0.0262	0.0009	0.64	0.049	0.002	165.9	5.6	166.5	5.5	153	78	-0.4	-0.1
WF_01_200	145	90	0.62	166	4.040	0.093	0.2928	0.0079	0.46	0.101	0.003	1640	19	1654	39	1639	54	-0.9	0.0
WF_01_201	49	33	0.67	57	0.681	0.036	0.0851	0.0031	0.32	0.059	0.003	527	21	526	19	520	120	0.2	0.0
WF_01_202	144	68	0.47	160	4.330	0.120	0.3000	0.0100	0.68	0.103	0.003	1696	22	1695	52	1687	53	-0.5	0.0
WF_01_203	223	68	0.31	239	4.350	0.120	0.2999	0.0092	0.76	0.105	0.003	1706	22	1694	46	1708	48	0.8	0.0
WF_01_204	*284*	*200*	*0.70*	*331*	*0.078*	*0.011*	*0.0117*	*0.0008*	*0.04*	*0.047*	*0.007*	*76.3*	*9.9*	*74.9*	*5*	*100*	*290*	*1.8*	*0.1*
WF_01_205	132	55	0.41	145	4.490	0.120	0.3028	0.0096	0.71	0.105	0.003	1725	23	1703	47	1716	53	0.8	0.0

Table 6: Detrital Zircon LA-ICP-MS U-Pb Isotopic Data and Ages: WF-01, Top of the Williams Fork Formation, Plateau Creek Canyon (lat. 39.1961, long. -108.1392)[a]

					Corrected Isotopic Ratios								Ages (Ma)[i]							
Grain #[b]	U[c] [ppm]	Th[c] [ppm]	Th/U	eU[d] [ppm]	$^{207}Pb/^{235}U$[e]	±2s[f]	$^{206}Pb/^{238}U$[e]	±2s[f]	Rho[g]	$^{207}Pb/^{206}Pb$[h]	±2s[f]	$^{207}Pb/^{235}U$	±2s	$^{206}Pb/^{238}U$	±2s	$^{207}Pb/^{206}Pb$	±2s	Disc. %[j]	Wtd. Disc.[k]
WF_01_206	1192	1031	0.86	1434	0.196	0.006	0.0285	0.0008	0.56	0.050	0.001	181.3	5	181.2	5.2	190	66	0.1	0.0
WF_01_207	4410	3206	0.73	5163	3.863	0.074	0.2678	0.0072	0.62	0.104	0.002	1604	15	1534	35	1700	42	9.8	0.0
WF_01_208	*44*	*30*	*0.69*	*51*	*3.480*	*0.100*	*0.2469*	*0.0078*	*0.47*	*0.099*	*0.003*	*1524*	*23*	*1421*	*40*	*1629*	*65*	*12.8*	*0.0*
WF_01_209	197	177	0.90	238	0.165	0.010	0.0248	0.0009	0.27	0.048	0.003	154.6	8.4	158	5.7	110	120	-2.2	-0.4
WF_01_210	209	107	0.51	234	4.390	0.110	0.3074	0.0082	0.72	0.104	0.003	1710	21	1726	40	1679	49	-2.8	0.0
WF_01_211	173	125	0.72	202	0.101	0.007	0.0150	0.0006	0.23	0.046	0.004	97.2	6.7	96.1	3.7	80	140	1.1	0.2
WF_01_212	241	182	0.75	283	13.180	0.340	0.5300	0.0150	0.69	0.180	0.005	2691	25	2736	62	2658	44	-2.9	0.0
WF_01_213	108	84	0.78	128	4.130	0.130	0.2890	0.0110	0.53	0.105	0.004	1656	26	1635	53	1703	66	4.0	0.0
WF_01_214	233	63	0.27	248	2.748	0.092	0.2335	0.0064	0.74	0.085	0.002	1337	25	1352	34	1315	53	-2.8	0.0
WF_01_215	*497*	*163*	*0.33*	*535*	*5.650*	*0.150*	*0.3960*	*0.0130*	*0.82*	*0.103*	*0.003*	*1920*	*23*	*2147*	*58*	*1668*	*44*	*-28.7*	*0.0*
WF_01_216	59	32	0.54	66	0.924	0.044	0.1118	0.0044	0.31	0.062	0.003	664	22	682	25	650	120	-2.7	-0.8
WF_01_217	689	142	0.21	722	4.470	0.100	0.3078	0.0073	0.60	0.105	0.003	1725	19	1728	36	1702	44	-1.5	0.0
WF_01_218	606	320	0.53	681	0.164	0.005	0.0240	0.0006	0.34	0.049	0.002	154	4.3	153.1	3.7	165	76	0.6	0.2
WF_01_219	73	53	0.73	85	4.480	0.130	0.3060	0.0089	0.62	0.106	0.003	1724	24	1719	44	1731	50	0.7	0.0
WF_01_220	167	53	0.32	179	4.690	0.120	0.3150	0.0084	0.67	0.107	0.003	1768	20	1769	40	1752	50	-1.0	0.0
WF_01_221	469	58	0.12	483	4.420	0.100	0.3136	0.0092	0.70	0.104	0.003	1722	19	1756	45	1704	49	-3.1	0.0
WF_01_222	137	93	0.68	159	0.082	0.009	0.0121	0.0006	0.52	0.051	0.007	79.8	8.3	77.3	3.6	180	220	3.1	0.3
WF_01_223	344	165	0.48	383	0.187	0.009	0.0284	0.0011	0.55	0.048	0.002	173.7	7.5	180.4	6.7	116	87	-3.9	-0.9
WF_01_225	64	37	0.58	73	2.049	0.059	0.1906	0.0060	0.34	0.079	0.003	1135	20	1123	32	1158	76	3.0	0.0
WF_01_226	1051	53	0.05	1063	4.520	0.110	0.3118	0.0084	0.79	0.106	0.003	1732	21	1748	41	1726	46	-1.3	0.0
WF_01_227	306	138	0.45	338	0.540	0.017	0.0704	0.0024	0.66	0.056	0.002	438	11	438	15	456	74	0.0	0.0
WF_01_228	*676*	*57*	*0.08*	*689*	*3.630*	*0.110*	*0.2433*	*0.0074*	*0.82*	*0.104*	*0.003*	*1555*	*24*	*1402*	*38*	*1682*	*48*	*16.6*	*0.0*
WF_01_229	329	45	0.14	339	4.980	0.100	0.3353	0.0100	0.79	0.107	0.003	1819	19	1868	48	1742	45	-7.2	0.0
WF_01_230	798	317	0.40	872	0.185	0.006	0.0271	0.0009	0.38	0.051	0.002	172.1	4.9	172.2	5.5	226	79	-0.1	0.0
WF_01_231	191	81	0.42	210	2.130	0.060	0.2004	0.0058	0.75	0.080	0.002	1159	19	1177	31	1187	54	0.8	0.0
WF_01_232	28	8	0.29	30	1.658	0.078	0.1610	0.0053	0.54	0.075	0.003	986	30	961	30	1055	88	8.9	0.0
WF_01_233	*90*	*109*	*1.20*	*116*	*0.264*	*0.023*	*0.0268*	*0.0012*	*0.52*	*0.070*	*0.007*	*238*	*18*	*170.2*	*7.2*	*890*	*200*	*28.5*	*3.8*
WF_01_234	470	110	0.23	496	0.258	0.008	0.0371	0.0010	0.34	0.051	0.002	232.7	6.5	234.6	6	225	76	-0.8	-0.3
WF_01_235	430	7	0.02	432	0.531	0.014	0.0690	0.0018	0.55	0.056	0.002	433.4	9.9	430	11	463	67	0.8	0.3
WF_01_236	301	127	0.42	331	0.166	0.007	0.0245	0.0007	0.32	0.050	0.002	155.9	6.2	156.3	4.2	168	97	-0.3	-0.1
WF_01_237	627	296	0.47	697	0.182	0.006	0.0269	0.0008	0.59	0.050	0.002	169.9	4.7	170.7	4.9	188	77	-0.5	-0.2
WF_01_238	*78*	*29*	*0.37*	*85*	*0.117*	*0.014*	*0.0164*	*0.0007*	*0.22*	*0.051*	*0.006*	*111*	*12*	*105.1*	*4.5*	*230*	*210*	*5.3*	*0.5*
WF_01_239	229	98	0.43	252	0.861	0.027	0.1003	0.0026	0.63	0.064	0.002	629	15	616	16	743	60	2.1	0.9
WF_01_240	*146*	*36*	*0.25*	*154*	*0.295*	*0.014*	*0.0443*	*0.0013*	*0.01*	*0.050*	*0.003*	*262*	*11*	*279.6*	*8*	*170*	*120*	*-6.7*	*-1.6*

Table 6: Detrital Zircon LA-ICP-MS U-Pb Isotopic Data and Ages: WF-01, Top of the Williams Fork Formation, Plateau Creek Canyon (lat. 39.1961, long. -108.1392)[a]

					Corrected Isotopic Ratios								Ages (Ma)[i]							
Grain #[b]	U[c] [ppm]	Th[c] [ppm]	Th/U	eU[d] [ppm]	$^{207}Pb/^{235}U$[e]	±2s[f]	$^{206}Pb/^{238}U$[e]	±2s[f]	Rho[g]	$^{207}Pb/^{206}Pb$[h]	±2s[f]	$^{207}Pb/^{235}U$	±2s	$^{206}Pb/^{238}U$	±2s	$^{207}Pb/^{206}Pb$	±2s	Disc. %[j]	Wtd. Disc.[k]
WF_01_241	**94**	**31**	**0.34**	**101**	**0.064**	**0.010**	**0.0109**	**0.0004**	**0.52**	**0.043**	**0.007**	**63.2**	**9.3**	**70**	**2.8**	**-50**	**270**	**-10.8**	**-0.7**
WF_01_242	217	93	0.43	239	0.581	0.019	0.0748	0.0020	0.49	0.056	0.002	464	12	465	12	429	75	-0.2	-0.1
WF_01_243	222	111	0.50	248	0.194	0.010	0.0276	0.0007	0.00	0.052	0.003	180.9	8.7	175.6	4.4	240	130	2.9	0.6
WF_01_244	**128**	**98**	**0.76**	**151**	**0.074**	**0.009**	**0.0107**	**0.0006**	**0.52**	**0.052**	**0.007**	**71.9**	**8.6**	**68.8**	**3.6**	**200**	**240**	**4.3**	**0.4**
WF_01_245	94	101	1.07	118	0.490	0.020	0.0672	0.0023	0.48	0.053	0.002	404	14	419	14	330	94	-3.7	-1.1
WF_01_246	240	39	0.16	249	4.295	0.091	0.3020	0.0056	0.63	0.103	0.002	1692	18	1708	26	1678	42	-1.8	0.0
WF_01_247	223	34	0.15	231	0.501	0.017	0.0660	0.0013	0.42	0.055	0.002	411	12	411.9	8.1	398	76	-0.2	-0.1
WF_01_248	85	26	0.31	91	3.129	0.081	0.2495	0.0051	0.54	0.091	0.003	1440	20	1435	26	1452	55	1.2	0.0
WF_01_249	203	85	0.42	223	0.764	0.023	0.0942	0.0025	0.54	0.060	0.002	577	13	580	15	587	66	-0.5	-0.2
WF_01_250	208	90	0.43	229	0.499	0.014	0.0650	0.0016	0.29	0.055	0.002	410.6	9.6	406	9.6	408	74	1.1	0.5
WF_01_251	384	147	0.38	419	0.102	0.005	0.0159	0.0004	0.18	0.047	0.003	98.5	4.7	101.4	2.7	70	110	-2.9	-0.6
WF_01_252	390	87	0.22	410	4.170	0.094	0.2934	0.0056	0.67	0.103	0.002	1668	19	1658	28	1671	42	0.8	0.0
WF_01_253	157	73	0.46	174	4.251	0.089	0.3025	0.0065	0.71	0.102	0.002	1682	17	1703	32	1659	41	-2.7	0.0
WF_01_254	660	440	0.67	763	0.079	0.003	0.0123	0.0004	0.16	0.047	0.002	77.3	3.3	78.6	2.4	51	99	-1.7	-0.4
WF_01_255	138	69	0.50	155	0.106	0.009	0.0164	0.0006	0.26	0.046	0.004	102.8	7.9	104.6	4	30	150	-1.8	-0.2
WF_01_256	682	326	0.48	759	5.440	0.120	0.3392	0.0088	0.82	0.115	0.003	1892	19	1887	44	1882	42	-0.3	0.0
WF_01_257	166	39	0.23	175	0.178	0.011	0.0270	0.0008	0.26	0.048	0.003	165.4	9.3	171.5	5.1	150	120	-3.7	-0.7
WF_01_258	118	62	0.52	132	4.260	0.110	0.2998	0.0067	0.69	0.103	0.003	1688	23	1689	33	1667	48	-1.3	0.0
WF_01_259	167	53	0.32	179	1.824	0.047	0.1759	0.0039	0.54	0.075	0.002	1052	17	1044	22	1069	54	2.3	0.0
WF_01_260	626	180	0.29	668	4.274	0.083	0.3009	0.0070	0.86	0.103	0.002	1687	16	1699	35	1673	37	-1.6	0.0
WF_01_261	61	24	0.39	67	4.308	0.086	0.3087	0.0073	0.32	0.101	0.003	1693	16	1733	36	1642	54	-5.5	0.0
WF_01_262	146	71	0.49	163	0.078	0.009	0.0117	0.0005	0.52	0.048	0.006	75.7	8.5	74.7	3	110	240	1.3	0.1
WF_01_263	271	51	0.19	283	1.936	0.043	0.1815	0.0044	0.65	0.077	0.002	1092	15	1075	24	1114	49	3.5	0.0
WF_01_264	*83*	*19*	*0.23*	*88*	*12.110*	*0.270*	*0.4421*	*0.0097*	*0.69*	*0.197*	*0.005*	*2610*	*21*	*2358*	*43*	*2798*	*37*	*15.7*	*0.0*
WF_01_265	41	28	0.68	48	1.735	0.064	0.1676	0.0045	0.14	0.076	0.004	1025	26	998	25	1104	99	9.6	0.0
WF_01_266	204	68	0.34	220	2.593	0.084	0.2171	0.0059	0.64	0.088	0.003	1296	24	1266	31	1373	56	7.8	0.0
WF_01_267	136	53	0.39	148	2.561	0.091	0.2195	0.0071	0.60	0.085	0.003	1285	26	1278	37	1299	63	1.6	0.0
WF_01_268	38	24	0.64	44	5.620	0.190	0.3416	0.0097	0.66	0.119	0.003	1923	28	1905	49	1930	50	1.3	0.0
WF_01_269	301	173	0.57	342	0.177	0.006	0.0260	0.0007	0.46	0.049	0.002	165.4	5.4	165.6	4.1	166	75	-0.1	0.0
WF_01_270	4460	114000	25.56	31250	3.874	0.050	0.2719	0.0040	0.70	0.104	0.002	1607.5	10	1550	20	1691	35	8.3	0.0
WF_01_271	213	139	0.65	246	2.609	0.069	0.2217	0.0055	0.76	0.085	0.002	1300	19	1290	29	1301	46	0.8	0.0
WF_01_272	146	41	0.28	156	6.880	0.140	0.3853	0.0093	0.61	0.131	0.003	2099	19	2099	43	2116	46	0.8	0.0
WF_01_273	213	65	0.31	228	1.857	0.044	0.1823	0.0039	0.62	0.075	0.002	1066	16	1079	22	1055	50	-2.3	0.0
WF_01_274	200	53	0.27	212	4.206	0.086	0.2948	0.0058	0.69	0.103	0.002	1673	17	1664	29	1679	43	0.9	0.0

Table 6: Detrital Zircon LA-ICP-MS U-Pb Isotopic Data and Ages: WF-01, Top of the Williams Fork Formation, Plateau Creek Canyon (lat. 39.1961, long. -108.1392)[a]

					Corrected Isotopic Ratios								Ages (Ma)[i]							
Grain #[b]	U[c] [ppm]	Th[c] [ppm]	Th/U	eU[d] [ppm]	$^{207}Pb/^{235}U$[e]	±2s[f]	$^{206}Pb/^{238}U$[e]	±2s[f]	Rho[g]	$^{207}Pb/^{206}Pb$[h]	±2s[f]	$^{207}Pb/^{235}U$	±2s	$^{206}Pb/^{238}U$	±2s	$^{207}Pb/^{206}Pb$	±2s	Disc. %[j]	Wtd. Disc.[k]
WF_01_275	1338	320	0.24	1413	0.250	0.005	0.0362	0.0009	0.45	0.051	0.002	226.7	4.4	228.9	5.4	222	64	-1.0	-0.5
WF_01_276	122	11	0.09	124	0.754	0.034	0.0944	0.0031	0.68	0.058	0.002	570	20	581	18	516	79	-1.9	-0.6
WF_01_277	497	234	0.47	552	1.964	0.042	0.1883	0.0037	0.65	0.076	0.002	1102	14	1112	20	1083	50	-2.7	0.0
WF_01_278	*1221*	*1660*	*1.36*	*1611*	*0.242*	*0.012*	*0.0303*	*0.0007*	*0.39*	*0.057*	*0.003*	*219.8*	*9.8*	*192.6*	*4.6*	*499*	*97*	*12.4*	*2.8*
WF_01_279	*377*	*64*	*0.17*	*392*	*5.130*	*0.140*	*0.3500*	*0.0120*	*0.89*	*0.106*	*0.002*	*1837*	*24*	*1938*	*58*	*1735*	*39*	*-11.7*	*0.0*
WF_01_280	549	900	1.64	761	0.101	0.004	0.0157	0.0004	0.14	0.047	0.002	97.1	3.5	100.4	2.6	78	89	-3.4	-0.9
WF_01_281	173	49	0.29	184	2.128	0.057	0.1927	0.0047	0.57	0.079	0.002	1159	18	1139	25	1178	51	3.3	0.0
WF_01_282	164	56	0.34	177	2.107	0.073	0.1911	0.0060	0.76	0.080	0.002	1150	24	1130	33	1189	50	5.0	0.0
WF_01_283	102	60	0.59	116	2.182	0.067	0.2028	0.0046	0.51	0.078	0.003	1181	21	1190	25	1158	65	-2.8	0.0
WF_01_284	105	83	0.79	124	1.683	0.054	0.1677	0.0050	0.60	0.074	0.002	1002	21	999	28	1028	66	2.8	0.0
WF_01_285	196	72	0.37	212	0.503	0.018	0.0657	0.0018	0.61	0.056	0.002	413	12	410	11	438	75	0.7	0.3
WF_01_286	128	62	0.49	143	4.570	0.100	0.3176	0.0066	0.61	0.105	0.003	1742	19	1777	33	1714	45	-3.7	0.0
WF_01_287	300	136	0.45	332	4.037	0.087	0.2954	0.0068	0.71	0.100	0.002	1639	18	1667	34	1622	40	-2.8	0.0
WF_01_288	638	484	0.76	752	0.086	0.004	0.0131	0.0004	0.23	0.048	0.003	84.2	3.4	84.2	2.5	127	100	0.0	0.0
WF_01_289	117	68	0.58	132	4.407	0.099	0.3079	0.0062	0.38	0.103	0.003	1711	18	1734	29	1671	55	-3.8	0.0
WF_01_290	249	69	0.28	265	4.900	0.110	0.3196	0.0085	0.68	0.113	0.003	1803	18	1786	41	1844	48	3.1	0.0
WF_01_291	*58*	*31*	*0.52*	*66*	*0.093*	*0.016*	*0.0113*	*0.0008*	*0.52*	*0.056*	*0.011*	*89*	*15*	*72.5*	*5.3*	*470*	*350*	*18.5*	*1.1*
WF_01_292	*479*	*448*	*0.94*	*584*	*5.210*	*0.170*	*0.3269*	*0.0087*	*0.67*	*0.116*	*0.004*	*1858*	*29*	*1823*	*43*	*1889*	*54*	*3.5*	*0.0*
WF_01_293	*1480*	*109*	*0.07*	*1506*	*0.380*	*0.016*	*0.0284*	*0.0010*	*0.49*	*0.098*	*0.004*	*326*	*12*	*180.5*	*6.6*	*1571*	*83*	*44.6*	*12.1*
WF_01_294	*43*	*32*	*0.76*	*50*	*1.875*	*0.096*	*0.1806*	*0.0064*	*0.26*	*0.075*	*0.004*	*1063*	*34*	*1069*	*35*	*1050*	*100*	*-1.8*	*0.0*
WF_01_295	314	94	0.30	336	1.774	0.057	0.1781	0.0053	0.73	0.074	0.002	1036	21	1056	29	1025	55	-3.0	0.0
WF_01_296	15	6	0.38	16	3.050	0.150	0.2412	0.0098	0.44	0.094	0.005	1416	37	1399	49	1489	99	6.0	0.0
WF_01_297	170	53	0.31	183	1.580	0.044	0.1630	0.0047	0.64	0.071	0.002	965	17	972	26	934	58	-4.1	0.0
WF_01_298	*65*	*20*	*0.30*	*70*	*0.072*	*0.013*	*0.0117*	*0.0007*	*0.52*	*0.051*	*0.010*	*69*	*13*	*74.7*	*4.4*	*120*	*340*	*-8.3*	*-0.4*
WF_01_299	327	206	0.63	375	0.078	0.006	0.0113	0.0004	0.17	0.049	0.004	76.4	5.9	72.7	2.8	130	160	4.8	0.6
WF_01_300	416	333	0.80	494	4.470	0.130	0.3013	0.0099	0.74	0.107	0.003	1738	23	1696	49	1757	48	3.5	0.0
WF_01_301	142	80	0.56	161	0.085	0.008	0.0142	0.0006	0.31	0.044	0.004	82.4	7.8	90.8	4	-20	170	-10.2	-1.1
WF_01_302	190	102	0.54	214	0.092	0.009	0.0127	0.0006	0.12	0.052	0.005	88.5	7.9	81.3	3.9	270	200	8.1	0.9
WF_01_303	654	650	0.99	807	0.085	0.004	0.0122	0.0003	0.31	0.049	0.002	82.3	4	78	2.2	162	96	5.2	1.1
WF_01_304	*49*	*42*	*0.86*	*59*	*0.081*	*0.015*	*0.0110*	*0.0008*	*0.52*	*0.055*	*0.011*	*78*	*14*	*70.2*	*5*	*330*	*350*	*10.0*	*0.6*
WF_01_305	94	37	0.39	103	2.040	0.078	0.1896	0.0053	0.50	0.079	0.003	1124	26	1119	29	1137	81	1.6	0.0

[a]All locations reported in decimal degrees from a WGS 1984 mercator projection

[b]Emboldened and shaded rows indicate the youngest measured concordant grains. Italicized rows indicate analyses that were not considered for plots and calculations.

[c]U and Th concentrations and Th/U ratios calculated relative to the GJ-1 zircon standard ID-TIMS values using 287 ± 76 ppm for U and 8.4 ± 2.6 ppm for Th (Jackson et al., 2004)

[d]Equivalent U determined by the equation: eU = U ppm + 0.235*Th ppm

[e]Corrected for U-Pb fractionation and background and normalized to the GJ-1 zircon standard ID-TIMS values: $^{207}Pb/^{235}U$ = 0.8093 ± 0.0009 and $^{206}Pb/^{238}U$ = 0.09761 ± 0.00011 (Jackson et al., 2004)

[f]Propagated uncertainty of internal uncertainties (2 SE) and within run reproducibility of GJ-1 (2 SE)

[g]Uncertainty correlation between $^{206}Pb/^{238}U$ and $^{207}Pb/^{235}U$ uncertainties

[h]Corrected for background and Pb isotopic fractionation using the GJ-1 zircon standard ID-TIMS value: $^{207}Pb/^{206}Pb$ = 0.06014 ± 0.00001 (Jackson et al., 2004)

[i]U-Pb ages calculated relative to the GJ-1 zircon standard

[j]Discordance defined as [($^{207}Pb/^{235}U$age – $^{206}Pb/^{238}U$age)/($^{207}Pb/^{235}U$age)]*100

[k]Uncertainty weighted age difference defined as ($^{207}Pb/^{235}U$age - $^{206}Pb/^{238}U$age)/($^{207}Pb/^{235}U$2s age uncertainty) for grains with $^{206}Pb/^{238}U$ ages <850 Ma and ($^{207}Pb/^{206}Pb$age - $^{206}Pb/^{238}U$age)/($^{206}Pb/^{238}U$2s age uncertainty) for grains with $^{206}Pb/^{238}U$ ages ≥850 Ma

Table 7: Standard GJ1 for sample WF-01 LA-ICP-MS U-Pb Isotopic Data and Ages

					Corrected Isotopic Ratios								Ages (Ma)[i]							
Grain #[b]	U[c] [ppm]	Th[c] [ppm]	Th/U	eU[d] [ppm]	$^{207}Pb/^{235}U$[e]	±2s[f]	$^{206}Pb/^{238}U$[e]	±2s[f]	Rho[g]	$^{207}Pb/^{206}Pb$[h]	±2s[f]	$^{207}Pb/^{235}U$	±2s	$^{206}Pb/^{238}U$	±2s	$^{207}Pb/^{206}Pb$	±2s	Disc. %[i]	Wtd. Disc.[k]
Z_GJ1_01	*286*	*8*	*0.03*	*288*	*0.816*	*0.017*	*0.0961*	*0.0021*	*0.60*	*0.061*	*0.002*	*605*	*9.4*	*592*	*12*	*650*	*55*	*2.1*	*1.4*
Z_GJ1_02	288	9	0.03	290	0.820	0.021	0.0988	0.0018	0.58	0.060	0.002	607	11	607	11	611	56	0.0	0.0
Z_GJ1_03	286	8	0.03	288	0.808	0.020	0.0981	0.0018	0.45	0.060	0.002	602	11	603	11	601	60	-0.2	-0.1
Z_GJ1_04	289	8	0.03	291	0.810	0.018	0.0973	0.0020	0.48	0.060	0.002	603	10	598	12	606	60	0.8	0.5
Z_GJ1_05	283	8	0.03	285	0.815	0.019	0.1005	0.0026	0.53	0.059	0.002	606	11	617	15	552	65	-1.8	-1.0
Z_GJ1_06	289	8	0.03	291	0.800	0.021	0.0974	0.0022	0.61	0.059	0.002	596	12	599	13	587	60	-0.5	-0.3
Z_GJ1_07	288	8	0.03	290	0.798	0.021	0.0957	0.0020	0.43	0.060	0.002	595	12	589	12	616	64	1.0	0.5
Z_GJ1_08	283	8	0.03	285	0.810	0.017	0.0986	0.0021	0.31	0.060	0.002	604.9	9.7	606	12	586	62	-0.2	-0.1
Z_GJ1_09	288	8	0.03	290	0.813	0.018	0.0988	0.0017	0.40	0.060	0.002	603	10	607.5	10	594	60	-0.7	-0.5
Z_GJ1_10	289	9	0.03	291	0.821	0.021	0.0973	0.0020	0.45	0.061	0.002	609	12	598	12	635	59	1.8	0.9
Z_GJ1_11	287	8	0.03	289	0.801	0.020	0.0956	0.0020	0.62	0.061	0.002	596	11	589	12	619	55	1.2	0.6
Z_GJ1_12	288	8	0.03	290	0.806	0.019	0.0972	0.0017	0.43	0.060	0.002	601	11	597.9	10	598	60	0.5	0.3
Z_GJ1_13	286	8	0.03	287	0.809	0.020	0.0969	0.0020	0.35	0.061	0.002	601	11	596	12	631	64	0.8	0.5
Z_GJ1_14	287	8	0.03	289	0.815	0.018	0.0973	0.0020	0.38	0.061	0.002	606	10	599	12	643	61	1.2	0.7
Z_GJ1_15	287	8	0.03	289	0.798	0.020	0.0964	0.0022	0.56	0.059	0.002	595	11	593	13	570	58	0.3	0.2
Z_GJ1_16	289	8	0.03	291	0.814	0.020	0.0990	0.0020	0.40	0.060	0.002	605	12	608	12	603	65	-0.5	-0.3
Z_GJ1_17	285	8	0.03	287	0.814	0.020	0.0976	0.0019	0.49	0.061	0.002	604	11	600	11	619	62	0.7	0.4
Z_GJ1_18	289	8	0.03	291	0.797	0.020	0.0977	0.0019	0.48	0.060	0.002	596	11	601	11	601	58	-0.8	-0.5
Z_GJ1_19	286	8	0.03	287	0.801	0.016	0.0975	0.0022	0.45	0.060	0.002	597.9	9	600	13	603	59	-0.4	-0.2
Z_GJ1_20	287	8	0.03	289	0.814	0.021	0.0980	0.0022	0.50	0.060	0.002	604	12	602	13	605	60	0.3	0.2
Z_GJ1_21	289	8	0.03	291	0.791	0.019	0.0977	0.0017	0.42	0.060	0.002	591	11	601	10	582	63	-1.7	-0.9
Z_GJ1_22	286	8	0.03	288	0.810	0.019	0.0992	0.0021	0.26	0.060	0.002	602	11	610	12	577	69	-1.3	-0.7
Z_GJ1_23	285	8	0.03	287	0.824	0.020	0.0973	0.0020	0.53	0.061	0.002	611	11	599	12	684	53	2.0	1.1
Z_GJ1_24	288	8	0.03	290	0.801	0.017	0.0972	0.0020	0.50	0.060	0.002	596.8	9.7	598	12	610	61	-0.2	-0.1
Z_GJ1_25	292	8	0.03	294	0.787	0.021	0.0973	0.0022	0.59	0.058	0.002	590	12	598	13	555	61	-1.4	-0.7
Z_GJ1_26	283	8	0.03	285	0.806	0.020	0.0986	0.0022	0.44	0.061	0.002	599	11	606	13	623	59	-1.2	-0.6
Z_GJ1_27	290	8	0.03	292	0.815	0.023	0.0972	0.0021	0.57	0.061	0.002	606	13	598	12	626	60	1.3	0.6
Z_GJ1_28	287	8	0.03	289	0.809	0.021	0.0971	0.0021	0.60	0.060	0.002	603	12	597	12	607	56	1.0	0.5
Z_GJ1_29	286	8	0.03	288	0.825	0.020	0.0980	0.0020	0.43	0.061	0.002	610	11	602	12	652	59	1.3	0.7
Z_GJ1_30	287	8	0.03	289	0.827	0.017	0.0992	0.0017	0.26	0.060	0.002	611.5	9.6	609.8	10	610	60	0.3	0.2
Z_GJ1_31	288	8	0.03	290	0.809	0.016	0.0980	0.0019	0.46	0.060	0.001	601.5	9.2	602	11	596	51	-0.1	-0.1
Z_GJ1_32	283	8	0.03	285	0.817	0.016	0.0981	0.0016	0.46	0.060	0.001	606	8.7	603.2	9.4	605	53	0.5	0.3

Table 7: Standard GJ1 for sample WF-01 LA-ICP-MS U-Pb Isotopic Data and Ages

					Corrected Isotopic Ratios								Ages (Ma)[i]							
Grain #[b]	U[c] [ppm]	Th[c] [ppm]	Th/U	eU[d] [ppm]	$^{207}Pb/^{235}U$[e]	±2s[f]	$^{206}Pb/^{238}U$[e]	±2s[f]	Rho[g]	$^{207}Pb/^{206}Pb$[h]	±2s[f]	$^{207}Pb/^{235}U$	±2s	$^{206}Pb/^{238}U$	±2s	$^{207}Pb/^{206}Pb$	±2s	Disc. %[j]	Wtd. Disc.[k]
Z_GJ1_33	289	8	0.03	291	0.817	0.022	0.0976	0.0021	0.60	0.060	0.002	605	12	600	13	606	59	0.8	0.4
Z_GJ1_34	289	8	0.03	291	0.812	0.018	0.0969	0.0022	0.41	0.060	0.002	602.8	9.9	596	13	590	64	1.1	0.7
Z_GJ1_35	286	8	0.03	288	0.812	0.018	0.0958	0.0019	0.41	0.061	0.002	603	10	593	10	635	59	1.7	1.0
Z_GJ1_36	*286*	*8*	*0.03*	*288*	*0.814*	*0.020*	*0.0958*	*0.0019*	*0.53*	*0.061*	*0.002*	*604*	*11*	*590*	*11*	*633*	*58*	*2.3*	*1.3*
Z_GJ1_37	290	8	0.03	292	0.792	0.015	0.0966	0.0017	0.40	0.059	0.002	591.8	8.4	594.5	9.7	564	60	-0.5	-0.3
Z_GJ1_38	285	8	0.03	287	0.816	0.015	0.0977	0.0020	0.43	0.060	0.002	605.3	8.3	601	12	611	56	0.7	0.5
Z_GJ1_40	286	8	0.03	288	0.802	0.018	0.0965	0.0023	0.38	0.060	0.002	597	10	596	13	590	67	0.2	0.1
Z_GJ1_41	288	8	0.03	290	0.813	0.020	0.0965	0.0019	0.57	0.061	0.002	603	11	594	11	638	55	1.5	0.8
Z_GJ1_42	289	8	0.03	290	0.807	0.022	0.0980	0.0022	0.49	0.059	0.002	600	12	602	13	559	64	-0.3	-0.2
Z_GJ1_43	286	8	0.03	288	0.807	0.020	0.0991	0.0021	0.47	0.059	0.002	600	11	609	12	583	60	-1.5	-0.8
Z_GJ1_44	285	8	0.03	287	0.825	0.023	0.0978	0.0021	0.55	0.061	0.002	610	13	602	13	631	60	1.3	0.6
Z_GJ1_45	290	8	0.03	292	0.812	0.018	0.0973	0.0022	0.43	0.061	0.002	606	10	599	13	636	65	1.2	0.7
Z_GJ1_46	288	8	0.03	290	0.814	0.020	0.0988	0.0022	0.50	0.060	0.002	607	11	609	13	595	61	-0.3	-0.2
Z_GJ1_47	286	8	0.03	288	0.794	0.018	0.0979	0.0020	0.43	0.059	0.002	592.7	10	602	12	565	59	-1.6	-0.9
Z_GJ1_48	287	8	0.03	289	0.806	0.019	0.0980	0.0021	0.26	0.060	0.002	599	11	602	12	606	71	-0.5	-0.3
Z_GJ1_49	286	8	0.03	288	0.811	0.016	0.0962	0.0018	0.35	0.061	0.002	602.5	9.3	593.5	10	639	58	1.5	1.0
Z_GJ1_50	288	8	0.03	290	0.803	0.018	0.0977	0.0016	0.44	0.059	0.002	599.3	9.9	601	9.6	578	54	-0.3	-0.2
Z_GJ1_51	288	8	0.03	290	0.801	0.020	0.0978	0.0022	0.46	0.060	0.002	596	11	602	13	607	60	-1.0	-0.5
Z_GJ1_52	285	8	0.03	287	0.823	0.018	0.1001	0.0023	0.30	0.060	0.002	609.3	10	615	13	610	63	-0.9	-0.6

Typical 2σ error for GJ1 during this run had an average of 600.7 ± 1.7 Ma and a range of 589-617 Ma (MSWD:0.96, Probability:0.56, n=49). The accepted age of GJ1 is 600.1 Ma ($^{206}Pb/^{238}U$ age, Jackson et al., 2004).

[a]All locations reported in decimal degrees from a WGS 1984 mercator projection

[b]Italicized rows indicate analyses that were not considered for plots and calculations.

[c]U and Th concentrations and Th/U ratios calculated relative to the GJ-1 zircon standard ID-TIMS values using 287 ± 76 ppm for U and 8.4 ± 2.6 ppm for Th (Jackson et al., 2004)

[d]Equivalent U determined by the equation: eU = U ppm + 0.235*Th ppm

[e]Corrected for U-Pb fractionation and background and normalized to the GJ-1 zircon standard ID-TIMS values: $^{207}Pb/^{235}U$ = 0.8093 ± 0.0009 and $^{206}Pb/^{238}U$ = 0.09761 ± 0.00011 (Jackson et al., 2004)

[f]Propagated uncertainty of internal uncertainties (2 SE) and within run reproducibility of GJ-1 (2 SE)

[g]Uncertainty correlation between $^{206}Pb/^{238}U$ and $^{207}Pb/^{235}U$ uncertainties

[h]Corrected for background and Pb isotopic fractionation using the GJ-1 zircon standard ID-TIMS value: $^{207}Pb/^{206}Pb = 0.06014 \pm 0.00001$ (Jackson et al., 2004)

[i]U-Pb ages calculated relative to the GJ-1 zircon standard

[j]Discordance defined as $[(^{207}Pb/^{235}Uage - ^{206}Pb/^{238}Uage)/(^{207}Pb/^{235}Uage)]*100$

[k]Uncertainty weighted age difference defined as $(^{207}Pb/^{235}Uage - ^{206}Pb/^{238}Uage)/(^{207}Pb/^{235}U2s$ age uncertainty) for grains with $^{206}Pb/^{238}U$ ages <850 Ma and $(^{207}Pb/^{206}Pbage - ^{206}Pb/^{238}Uage)/(^{206}Pb/^{238}U2s$ age uncertainty) for grains with $^{206}Pb/^{238}U$ ages ≥850 Ma

Table 8: Standard fish canyon tuff for sample WF-01 LA-ICP-MS U-Pb Isotopic Data and Ages

					Corrected Isotopic Ratios								Ages (Ma)[i]							
Grain #[b]	U[c] [ppm]	Th[c] [ppm]	Th/U	eU[d] [ppm]	$^{207}Pb/^{235}U$[e]	±2s[f]	$^{206}Pb/^{238}U$[e]	±2s[f]	Rho[g]	$^{207}Pb/^{206}Pb$[h]	±2s[f]	$^{207}Pb/^{235}U$	±2s	$^{206}Pb/^{238}U$	±2s	$^{207}Pb/^{206}Pb$	±2s	Disc. %[j]	Wtd. Disc.[k]
FCT_01	330	139	0.42	362	0.029	0.003	0.0047	0.0002	0.13	0.045	0.004	28.9	2.6	30.3	1.2	60	180	-4.8	-0.5
FCT_02	329	129	0.39	359	0.029	0.003	0.0045	0.0002	0.07	0.049	0.006	29.4	2.8	28.7	1.2	150	200	2.4	0.3
FCT_03	*318*	*124*	*0.39*	*347*	*0.028*	*0.003*	*0.0047*	*0.0002*	*0.15*	*0.045*	*0.006*	*27.7*	*2.9*	*29.9*	*1.4*	*-10*	*210*	*-7.9*	*-0.8*
FCT_04	299	112	0.37	325	0.028	0.003	0.0043	0.0002	0.06	0.047	0.006	27.8	3.2	27.6	1.3	60	220	0.7	0.1
FCT_05	397	161	0.41	435	0.029	0.002	0.0044	0.0002	0.24	0.047	0.004	29.2	2.3	28.16	1	80	140	3.6	0.5
FCT_06	604	244	0.40	661	0.030	0.002	0.0045	0.0002	0.09	0.048	0.004	29.8	2.3	28.9	1.1	140	170	3.0	0.4
FCT_07	*679*	*337*	*0.50*	*758*	*0.031*	*0.002*	*0.0046*	*0.0002*	*0.31*	*0.050*	*0.004*	*31.4*	*2.1*	*29.61*	*0.97*	*200*	*140*	*5.7*	*0.9*
FCT_08	1027	568	0.55	1160	0.030	0.002	0.0045	0.0001	0.03	0.047	0.003	29.9	1.5	29.21	0.8	90	120	2.3	0.5
FCT_09	*565*	*232*	*0.41*	*619*	*0.028*	*0.002*	*0.0045*	*0.0002*	*0.32*	*0.046*	*0.003*	*27.8*	*1.7*	*29.2*	*1*	*40*	*120*	*-5.0*	*-0.8*
FCT_10	*540*	*226*	*0.42*	*593*	*0.031*	*0.003*	*0.0045*	*0.0002*	*0.10*	*0.051*	*0.005*	*31*	*2.6*	*28.7*	*1.2*	*220*	*180*	*7.4*	*0.9*
FCT_11	343	332	0.97	421	0.027	0.003	0.0043	0.0002	0.09	0.045	0.006	27	3	27.5	1.3	-40	210	-1.9	-0.2
FCT_12	773	410	0.53	869	0.028	0.002	0.0042	0.0001	0.25	0.047	0.004	27.6	2.1	27.24	0.8	60	150	1.3	0.2
FCT_13	*300*	*189*	*0.63*	*344*	*0.030*	*0.003*	*0.0043*	*0.0002*	*0.10*	*0.051*	*0.006*	*29.5*	*3.1*	*27.5*	*1.4*	*160*	*200*	*6.8*	*0.6*
FCT_14	309	109	0.35	335	0.028	0.004	0.0043	0.0002	0.18	0.048	0.006	27.8	3.6	27.8	1.4	130	230	0.0	0.0
FCT_15	*390*	*163*	*0.42*	*428*	*0.027*	*0.003*	*0.0046*	*0.0003*	*0.03*	*0.043*	*0.005*	*26.9*	*2.8*	*29.2*	*1.6*	*-110*	*210*	*-8.6*	*-0.8*
FCT_16	546	216	0.39	597	0.027	0.002	0.0042	0.0002	0.10	0.047	0.004	27.8	2.3	27.2	1.2	90	160	2.2	0.3
FCT_17	*435*	*213*	*0.49*	*485*	*0.027*	*0.003*	*0.0044*	*0.0002*	*0.05*	*0.044*	*0.004*	*26.9*	*2.5*	*28.4*	*1.3*	*-40*	*170*	*-5.6*	*-0.6*
FCT_18	377	201	0.53	424	0.029	0.003	0.0043	0.0002	0.15	0.049	0.006	28.8	2.8	27.9	1.4	160	230	3.1	0.3
FCT_19	355	128	0.36	385	0.029	0.003	0.0045	0.0002	0.15	0.049	0.006	29	3.1	28.8	1.3	100	220	0.7	0.1
FCT_20	*321*	*128*	*0.40*	*351*	*0.032*	*0.005*	*0.0047*	*0.0002*	*0.37*	*0.051*	*0.007*	*31.9*	*4.4*	*30.3*	*1.6*	*230*	*250*	*5.0*	*0.4*
FCT_21	818	416	0.51	916	0.028	0.002	0.0046	0.0002	0.30	0.046	0.003	28.4	1.8	29.3	1.1	20	130	-3.2	-0.5
FCT_22	619	409	0.66	715	0.027	0.003	0.0043	0.0002	0.24	0.046	0.005	27.1	2.7	27.8	1.2	10	180	-2.6	-0.3
FCT_23	964	512	0.53	1084	0.027	0.002	0.0043	0.0002	0.22	0.047	0.003	27.1	1.5	27.9	1.1	50	120	-3.0	-0.5

Secondary standard Fish Canyon Tuff yielded a weighted mean $^{206}Pb/^{238}U$ date of 28.19 ± 0.3 Ma (2σ) (n=14; MSWD=1.9, Probability: 0.021). The accepted age of Fish Canyon Tuff is 28.642 ± 0.025 Ma to 28.196 ± 0.038 Ma (Wotzlaw et al., 2013).

[a]All locations reported in decimal degrees from a WGS 1984 mercator projection

[b]Italicized rows indicate analyses that were not considered for plots and calculations

[c]U and Th concentrations and Th/U ratios calculated relative to the GJ-1 zircon standard ID-TIMS values using 287 ± 76 ppm for U and 8.4 ± 2.6 ppm for Th (Jackson et al., 2004)

[d]Equivalent U determined by the equation: eU = U ppm + 0.235*Th ppm

[e]Corrected for U-Pb fractionation and background and normalized to the GJ-1 zircon standard ID-TIMS values: $^{207}Pb/^{235}U$ = 0.8093 ± 0.0009 and $^{206}Pb/^{238}U$ = 0.09761 ± 0.00011 (Jackson et al., 2004)

[f]Propagated uncertainty of internal uncertainties (2 SE) and within run reproducibility of GJ-1 (2 SE)

[g]Uncertainty correlation between $^{206}Pb/^{238}U$ and $^{207}Pb/^{235}U$ uncertainties

[h]Corrected for background and Pb isotopic fractionation using the GJ-1 zircon standard ID-TIMS value: $^{207}Pb/^{206}Pb$ = 0.06014 ± 0.00001 (Jackson et al., 2004)

[i]U-Pb ages calculated relative to the GJ-1 zircon standard

[j]Discordance defined as [($^{207}Pb/^{235}U$age – $^{206}Pb/^{238}U$age)/($^{207}Pb/^{235}U$age)]*100

[k]Uncertainty weighted age difference defined as ($^{207}Pb/^{235}U$age - $^{206}Pb/^{238}U$age)/($^{207}Pb/^{235}U$2s age uncertainty) for grains with $^{206}Pb/^{238}U$ ages <850 Ma and ($^{207}Pb/^{206}Pb$age - $^{206}Pb/^{238}U$age)/($^{206}Pb/^{238}U$2s age uncertainty) for grains with $^{206}Pb/^{238}U$ ages ≥850 Ma

Table 9: Standard Plesovice for sample WF-01 LA-ICP-MS U-Pb Isotopic Data and Ages

Grain #[b]	U[c] [ppm]	Th[c] [ppm]	Th/U	eU[d] [ppm]	Corrected Isotopic Ratios							Ages (Ma)[i]						Disc. %[j]	Wtd. Disc.[k]
					$^{207}Pb/^{235}U$[e]	±2s[f]	$^{206}Pb/^{238}U$[e]	±2s[f]	Rho[g]	$^{207}Pb/^{206}Pb$[h]	±2s[f]	$^{207}Pb/^{235}U$	±2s	$^{206}Pb/^{238}U$	±2s	$^{207}Pb/^{206}Pb$	±2s		
PL_1	603	50	0.08	615	0.411	0.014	0.0551	0.0011	0.07	0.054	0.002	349	9.8	345.8	6.9	346	93	0.9	0.3
PL_2	608	47	0.08	619	0.401	0.011	0.0550	0.0015	0.38	0.054	0.002	344	7.6	345.3	9.3	351	65	-0.4	-0.2
PL_3	597	45	0.08	608	0.404	0.012	0.0549	0.0013	0.37	0.053	0.002	343.7	8.7	344.7	7.7	327	72	-0.3	-0.1
PL_4	594	47	0.08	605	0.406	0.010	0.0556	0.0014	0.45	0.053	0.002	345.7	7.1	348.5	8.7	318	71	-0.8	-0.4
PL_5	593	47	0.08	604	0.403	0.010	0.0559	0.0013	0.50	0.053	0.002	343.7	7.2	350.6	8	316	69	-2.0	-1.0
PL_6	547	45	0.08	558	0.408	0.014	0.0542	0.0016	0.37	0.055	0.002	347	10	340.4	10	422	92	1.9	0.7
PL_7	581	45	0.08	592	0.409	0.012	0.0553	0.0011	0.43	0.054	0.002	347.9	8.6	346.9	6.7	370	69	0.3	0.1
PL_8	585	47	0.08	596	0.415	0.014	0.0547	0.0017	0.53	0.055	0.002	352.2	10	343	10	395	85	2.6	0.9
PL_9	594	50	0.08	606	0.407	0.012	0.0556	0.0014	0.53	0.053	0.002	346.5	8.5	348.5	8.5	324	73	-0.6	-0.2
PL_10	578	44	0.08	588	0.405	0.011	0.0554	0.0017	0.48	0.054	0.002	346.1	7.5	347.6	10	335	72	-0.4	-0.2
PL_11	561	43	0.08	571	0.390	0.013	0.0547	0.0014	0.61	0.052	0.002	335.2	9.1	343	8.5	278	72	-2.3	-0.9
PL_12	529	45	0.09	540	0.415	0.013	0.0561	0.0013	0.15	0.054	0.002	352.1	9.3	352.1	7.8	351	87	0.0	0.0
PL_13	550	45	0.08	561	0.404	0.010	0.0541	0.0013	0.47	0.053	0.002	344.1	7.4	339.4	8.2	306	65	1.4	0.6
PL_14	551	43	0.08	561	0.405	0.011	0.0539	0.0014	0.40	0.053	0.002	344.5	8.1	338.2	8.6	319	73	1.8	0.8
PL_15	575	44	0.08	585	0.399	0.012	0.0541	0.0014	0.52	0.053	0.002	341.6	8.4	339.7	8.6	307	69	0.6	0.2
PL_16	566	41	0.07	576	0.393	0.012	0.0543	0.0015	0.74	0.053	0.001	339.7	8.7	340.6	9.1	335	54	-0.3	-0.1
PL_17	604	45	0.07	615	0.402	0.013	0.0545	0.0015	0.50	0.054	0.002	342.3	9.3	342.2	9	362	72	0.0	0.0
PL_18	599	46	0.08	610	0.397	0.010	0.0545	0.0013	0.48	0.053	0.002	339	7.4	341.8	8.2	313	69	-0.8	-0.4

Secondary standard Plešovice yielded a weighted mean $^{206}Pb/^{238}U$ date of 344.6 ± 2.0 Ma (2σ) (n=18; MSWD=0.95, Probability: 0.51). The accepted age of Plešovice is 337.13 ± 0.37 Ma (CA-TIMS age, Slama et al., 2008).

[a]All locations reported in decimal degrees from a WGS 1984 mercator projection

[b]Italicized rows indicate analyses that were not considered for plots and calculations

[c]U and Th concentrations and Th/U ratios calculated relative to the GJ-1 zircon standard ID-TIMS values using 287 ± 76 ppm for U and 8.4 ± 2.6 ppm for Th (Jackson et al., 2004)

[d]Equivalent U determined by the equation: eU = U ppm + 0.235*Th ppm

[e]Corrected for U-Pb fractionation and background and normalized to the GJ-1 zircon standard ID-TIMS values: $^{207}Pb/^{235}U$ = 0.8093 ± 0.0009 and $^{206}Pb/^{238}U$ = 0.09761 ± 0.00011 (Jackson et al., 2004)

[f]Propagated uncertainty of internal uncertainties (2 SE) and within run reproducibility of GJ-1 (2 SE)

[g]Uncertainty correlation between $^{206}Pb/^{238}U$ and $^{207}Pb/^{235}U$ uncertainties

[h]Corrected for background and Pb isotopic fractionation using the GJ-1 zircon standard ID-TIMS value: $^{207}Pb/^{206}Pb = 0.06014 \pm 0.00001$ (Jackson et al., 2004)

[i]U-Pb ages calculated relative to the GJ-1 zircon standard

[j]Discordance defined as $[(^{207}Pb/^{235}Uage - ^{206}Pb/^{238}Uage)/(^{207}Pb/^{235}Uage)]*100$

[k]Uncertainty weighted age difference defined as $(^{207}Pb/^{235}Uage - ^{206}Pb/^{238}Uage)/(^{207}Pb/^{235}U2s$ age uncertainty) for grains with $^{206}Pb/^{238}U$ ages <850 Ma and $(^{207}Pb/^{206}Pbage - ^{206}Pb/^{238}Uage)/(^{206}Pb/^{238}U2s$ age uncertainty) for grains with $^{206}Pb/^{238}U$ ages ≥850 Ma

Table 10: Detrital Zircon LA-ICP-MS U-Pb Isotopic Data and Ages: WF-04, Base of the Williams Fork Formation, Coal Canyon (lat. 39.130840, long. -108.366867)[a]

					Corrected Isotopic Ratios							Ages (Ma)[i]							
Grain #[b]	U[c] [ppm]	Th[c] [ppm]	Th/U	eU[d] [ppm]	$^{207}Pb/^{235}U$[e]	±2s[f]	$^{206}Pb/^{238}U$[e]	±2s[f]	Rho[g]	$^{207}Pb/^{206}Pb$[h]	±2s[f]	$^{207}Pb/^{235}U$	±2s	$^{206}Pb/^{238}U$	±2s	$^{207}Pb/^{206}Pb$	±2s	Disc. %[j]	Wtd. Disc.[k]
WF_04_001	52	35	0.67	61	0.176	0.014	0.0238	0.0006	0.14	0.053	0.004	166	12	151.8	3.9	280	150	8.6	1.2
WF_04_002	*372*	*158*	*0.42*	*409*	*0.191*	*0.007*	*0.0268*	*0.0006*	*0.32*	*0.052*	*0.002*	*177.5*	*5.6*	*170.6*	*3.4*	*276*	*67*	*3.9*	*1.2*
WF_04_003	*590*	*169*	*0.29*	*630*	*2.310*	*0.160*	*0.1690*	*0.0110*	*0.95*	*0.101*	*0.002*	*1212*	*50*	*1006*	*61*	*1643*	*37*	*38.8*	*10.4*
WF_04_004	*1370*	*267*	*0.19*	*1433*	*0.805*	*0.063*	*0.0463*	*0.0024*	*0.81*	*0.125*	*0.005*	*588*	*34*	*292*	*15*	*1995*	*65*	*50.3*	*8.7*
WF_04_005	485	488	1.01	600	0.183	0.007	0.0263	0.0008	0.05	0.051	0.002	170.4	6	167.1	5	227	91	1.9	0.6
WF_04_006	522	235	0.45	577	0.081	0.003	0.0122	0.0003	0.42	0.049	0.002	79.2	3	77.9	1.8	154	74	1.6	0.4
WF_04_007	554	274	0.49	618	0.190	0.006	0.0273	0.0005	0.39	0.051	0.001	177.8	5.1	173.9	3.3	206	60	2.2	0.8
WF_04_008	*1121*	*597*	*0.53*	*1261*	*0.122*	*0.005*	*0.0088*	*0.0003*	*0.63*	*0.102*	*0.003*	*116.4*	*4.6*	*56.5*	*1.6*	*1643*	*60*	*51.5*	*13.0*
WF_04_009	329	120	0.36	357	2.733	0.073	0.2199	0.0047	0.76	0.090	0.002	1338	20	1281	25	1430	31	10.4	6.0
WF_04_010	423	577	1.36	559	0.100	0.004	0.0156	0.0003	0.14	0.047	0.002	96.3	3.3	99.5	1.8	42	66	-3.3	-1.0
WF_04_011	154	26	0.17	160	11.660	0.430	0.4910	0.0140	0.85	0.173	0.003	2570	34	2571	61	2584	26	0.5	0.2
WF_04_012	119	59	0.50	133	6.310	0.140	0.3693	0.0067	0.65	0.123	0.002	2019	20	2025	32	2008	27	-0.8	-0.5
WF_04_013	256	92	0.36	278	1.990	0.076	0.1840	0.0079	0.77	0.079	0.002	1114	25	1087	43	1160	52	6.3	1.7
WF_04_014	238	303	1.27	309	0.171	0.009	0.0260	0.0007	0.11	0.047	0.003	159.7	7.9	165.2	4.3	100	110	-3.4	-0.7
WF_04_015	471	340	0.72	551	2.929	0.059	0.2411	0.0045	0.64	0.088	0.001	1388	15	1392	23	1373	30	-1.4	-0.8
WF_04_016	374	155	0.42	410	0.113	0.005	0.0164	0.0003	0.03	0.050	0.002	109.1	4.4	105.1	2.2	168	89	3.7	0.9
WF_04_017	190	23	0.12	195	0.456	0.014	0.0597	0.0012	0.33	0.056	0.002	380.6	9.5	373.8	7.1	426	59	1.8	0.7
WF_04_018	31	14	0.43	34	1.915	0.058	0.1834	0.0038	0.20	0.075	0.002	1083	21	1085	21	1052	62	-3.1	-1.6
WF_04_019	*182*	*131*	*0.72*	*213*	*0.210*	*0.009*	*0.0286*	*0.0007*	*0.13*	*0.054*	*0.002*	*192.8*	*7.8*	*181.6*	*4.2*	*357*	*95*	*5.8*	*1.4*
WF_04_020	81	23	0.28	86	4.900	0.210	0.3190	0.0100	0.78	0.113	0.003	1794	36	1782	51	1829	46	2.6	0.9
WF_04_021	51	17	0.34	55	1.905	0.058	0.1806	0.0032	0.37	0.076	0.002	1082	21	1070	17	1092	54	2.0	1.3
WF_04_022	123	45	0.37	134	4.260	0.092	0.2972	0.0057	0.52	0.103	0.002	1684	18	1677	28	1683	32	0.4	0.2
WF_04_023	155	106	0.69	180	0.178	0.009	0.0254	0.0005	0.08	0.050	0.003	166.4	8.2	161.9	3	200	110	2.7	0.5
WF_04_024	189	149	0.79	224	0.183	0.011	0.0262	0.0007	0.06	0.049	0.003	169.9	9.1	166.8	4.3	150	130	1.8	0.3
WF_04_025	*273*	*36*	*0.13*	*281*	*3.404*	*0.110*	*0.2261*	*0.0054*	*0.43*	*0.109*	*0.003*	*1504*	*25*	*1314*	*28*	*1781*	*45*	*26.2*	*16.7*
WF_04_026	568	105	0.18	593	0.237	0.006	0.0346	0.0006	0.30	0.050	0.001	215.4	4.7	219.1	4	191	49	-1.7	-0.8
WF_04_027	*177*	*240*	*1.36*	*233*	*2.490*	*0.170*	*0.1038*	*0.0056*	*0.13*	*0.174*	*0.014*	*1261*	*50*	*636*	*33*	*2570*	*140*	*49.6*	*12.5*
WF_04_028	38	23	0.59	43	0.105	0.017	0.0150	0.0005	0.06	0.052	0.009	99	15	95.8	3.2	100	250	3.2	0.2
WF_04_029	264	223	0.84	316	0.192	0.007	0.0274	0.0006	0.15	0.050	0.002	177.7	5.8	174	3.6	187	65	2.1	0.6
WF_04_030	324	212	0.65	374	0.287	0.010	0.0395	0.0009	0.02	0.053	0.002	257	7.7	249.8	5.3	312	81	2.8	0.9
WF_04_031	248	32	0.13	255	11.250	0.200	0.4629	0.0081	0.69	0.175	0.002	2543.5	16	2451	36	2605	20	5.9	4.3
WF_04_032	190	254	1.34	250	0.187	0.012	0.0265	0.0009	0.34	0.051	0.003	174	10	168.8	5.7	230	120	3.0	0.5

Table 10: Detrital Zircon LA-ICP-MS U-Pb Isotopic Data and Ages: WF-04, Base of the Williams Fork Formation, Coal Canyon (lat. 39.130840, long. -108.366867)[a]

					Corrected Isotopic Ratios							Ages (Ma)[i]							
Grain #[b]	U[c] [ppm]	Th[c] [ppm]	Th/U	eU[d] [ppm]	$^{207}Pb/^{235}U$[e]	±2s[f]	$^{206}Pb/^{238}U$[e]	±2s[f]	Rho[g]	$^{207}Pb/^{206}Pb$[h]	±2s[f]	$^{207}Pb/^{235}U$	±2s	$^{206}Pb/^{238}U$	±2s	$^{207}Pb/^{206}Pb$	±2s	Disc. %[j]	Wtd. Disc.[k]
WF_04_033	194	11	0.06	196	2.186	0.063	0.1973	0.0043	0.50	0.081	0.002	1175	20	1160	23	1211	39	4.2	2.2
WF_04_034	201	116	0.58	228	0.189	0.007	0.0282	0.0005	0.18	0.049	0.002	175.2	5.9	179	3.3	131	66	-2.2	-0.6
WF_04_035	71	21	0.30	76	4.010	0.140	0.2762	0.0067	0.40	0.104	0.003	1634	27	1572	34	1697	54	7.4	3.7
WF_04_036	159	66	0.41	175	0.206	0.010	0.0298	0.0006	0.19	0.050	0.002	190.6	8.9	189.5	3.4	193	99	0.6	0.1
WF_04_037	**587**	**300**	**0.51**	**657**	**0.073**	**0.003**	**0.0115**	**0.0002**	**0.11**	**0.046**	**0.002**	**71.8**	**2.5**	**73.8**	**1.4**	**41**	**72**	**-2.8**	**-0.8**
WF_04_038	1	0	0.00	1	3.020	0.700	0.2330	0.0200	0.25	0.098	0.023	1430	180	1370	100	1140	480	-20.2	-2.3
WF_04_039	*1700*	*426*	*0.25*	*1800*	*0.470*	*0.030*	*0.0289*	*0.0012*	*0.32*	*0.117*	*0.007*	*390*	*20*	*183.8*	*7.5*	*1896*	*100*	*52.9*	*10.3*
WF_04_040	181	73	0.40	198	4.481	0.091	0.3090	0.0055	0.62	0.106	0.002	1727	17	1735	27	1736	26	0.1	0.0
WF_04_041	125	102	0.82	149	0.169	0.011	0.0260	0.0007	0.01	0.047	0.003	157.6	9.1	165.3	4.5	60	120	-4.9	-0.8
WF_04_042	**459**	**108**	**0.24**	**484**	**0.078**	**0.003**	**0.0115**	**0.0002**	**0.11**	**0.050**	**0.002**	**75.8**	**3.2**	**73.6**	**1.5**	**180**	**91**	**2.9**	**0.7**
WF_04_043	255	221	0.87	307	0.172	0.010	0.0253	0.0007	0.27	0.049	0.003	160.8	8.2	160.9	4.3	170	110	-0.1	0.0
WF_04_044	455	315	0.69	529	0.087	0.007	0.0139	0.0003	0.37	0.046	0.003	84.7	6.6	88.9	2.2	20	140	-5.0	-0.6
WF_04_045	270	35	0.13	278	4.260	0.150	0.2980	0.0110	0.88	0.106	0.002	1681	29	1677	57	1720	31	2.5	0.8
WF_04_046	320	157	0.49	357	0.166	0.007	0.0244	0.0005	0.08	0.049	0.002	155.4	5.6	155.5	3.1	157	78	-0.1	0.0
WF_04_047	18	14	0.78	22	4.240	0.130	0.3016	0.0061	0.39	0.103	0.003	1679	25	1701	31	1675	49	-1.6	-0.8
WF_04_048	*97*	*41*	*0.43*	*107*	*3.070*	*0.150*	*0.2324*	*0.0060*	*0.45*	*0.098*	*0.005*	*1432*	*34*	*1347*	*31*	*1569*	*86*	*14.1*	*7.2*
WF_04_049	88	35	0.40	96	0.610	0.024	0.0792	0.0018	0.39	0.057	0.002	482	15	491.4	11	477	74	-2.0	-0.6
WF_04_050	70	41	0.58	80	4.080	0.160	0.3000	0.0120	0.44	0.101	0.004	1651	34	1688	59	1629	77	-3.6	-1.0
WF_04_051	426	62	0.14	440	4.940	0.140	0.3267	0.0110	0.57	0.112	0.003	1814	26	1821	52	1823	50	0.1	0.0
WF_04_052	274	75	0.27	292	1.820	0.039	0.1796	0.0035	0.54	0.074	0.001	1053	14	1064	19	1047	33	-1.6	-0.9
WF_04_053	110	30	0.27	117	4.500	0.093	0.3184	0.0061	0.51	0.103	0.002	1733	17	1784	30	1688	32	-5.7	-3.2
WF_04_054	364	122	0.34	393	0.216	0.010	0.0307	0.0009	0.34	0.052	0.002	199.8	8.5	195	5.8	276	98	2.4	0.6
WF_04_055	79	112	1.41	105	0.712	0.037	0.0916	0.0023	0.22	0.056	0.003	544	22	565	14	490	110	-3.9	-1.0
WF_04_056	332	95	0.29	354	0.327	0.009	0.0465	0.0011	0.48	0.051	0.001	287.3	6.8	292.7	6.5	223	54	-1.9	-0.8
WF_04_057	573	241	0.42	630	0.403	0.011	0.0546	0.0014	0.59	0.055	0.001	343.7	7.8	342.7	8.8	388	50	0.3	0.1
WF_04_058	169	24	0.14	175	4.280	0.140	0.2996	0.0094	0.68	0.105	0.003	1686	27	1688	47	1713	45	1.5	0.5
WF_04_059	179	74	0.41	197	2.951	0.062	0.2406	0.0045	0.38	0.089	0.002	1395	16	1389	23	1409	34	1.4	0.9
WF_04_060	*0*	*0*	*0.11*	*0*	-	-	-	-	-	-	-	-	-	-	-	-	-	-	-
WF_04_061	*545*	*101*	*0.18*	*569*	*0.538*	*0.024*	*0.0330*	*0.0009*	*0.72*	*0.118*	*0.004*	*435*	*16*	*209.2*	*5.8*	*1922*	*56*	*51.9*	*14.1*
WF_04_062	84	36	0.42	93	4.285	0.093	0.3000	0.0056	0.48	0.104	0.002	1689	18	1690	28	1695	33	0.3	0.2
WF_04_063	45	12	0.26	47	2.671	0.075	0.2261	0.0041	0.39	0.085	0.002	1321	21	1314	22	1326	47	0.9	0.5
WF_04_064	326	138	0.42	358	0.201	0.007	0.0288	0.0006	0.40	0.051	0.001	185.5	5.6	182.7	3.5	206	61	1.5	0.5
WF_04_065	61	24	0.40	66	2.588	0.069	0.2232	0.0043	0.25	0.084	0.002	1296	20	1298	23	1292	51	-0.5	-0.3
WF_04_066	416	252	0.61	475	0.213	0.006	0.0315	0.0006	0.19	0.049	0.001	196.2	5.3	199.7	3.6	159	57	-1.8	-0.7

Table 10: Detrital Zircon LA-ICP-MS U-Pb Isotopic Data and Ages: WF-04, Base of the Williams Fork Formation, Coal Canyon (lat. 39.130840, long. -108.366867)[a]

					Corrected Isotopic Ratios							Ages (Ma)[i]							
Grain #[b]	U[c] [ppm]	Th[c] [ppm]	Th/U	eU[d] [ppm]	$^{207}Pb/^{235}U$[e]	±2s[f]	$^{206}Pb/^{238}U$[e]	±2s[f]	Rho[g]	$^{207}Pb/^{206}Pb$[h]	±2s[f]	$^{207}Pb/^{235}U$	±2s	$^{206}Pb/^{238}U$	±2s	$^{207}Pb/^{206}Pb$	±2s	Disc. %[j]	Wtd. Disc.[k]
WF_04_067	142	52	0.37	155	5.040	0.130	0.3235	0.0070	0.43	0.113	0.003	1827	23	1806	34	1836	42	1.6	0.9
WF_04_068	*427*	*170*	*0.40*	*467*	*2.455*	*0.068*	*0.1789*	*0.0051*	*0.87*	*0.101*	*0.001*	*1260*	*20*	*1060*	*28*	*1633*	*27*	*35.1*	*20.5*
WF_04_069	123	87	0.71	143	2.619	0.064	0.2191	0.0048	0.26	0.086	0.002	1308	17	1277	26	1322	51	3.4	1.7
WF_04_070	278	94	0.34	300	0.187	0.008	0.0272	0.0006	0.12	0.050	0.002	174.5	6.7	173.1	3.7	193	87	0.8	0.2
WF_04_071	95	34	0.35	102	2.308	0.053	0.2041	0.0035	0.22	0.082	0.002	1215	16	1197	19	1242	43	3.6	2.4
WF_04_072	175	46	0.26	186	4.207	0.079	0.3004	0.0051	0.62	0.102	0.001	1674.5	15	1693	25	1663	25	-1.8	-1.2
WF_04_073	**887**	**484**	**0.55**	**1001**	**0.074**	**0.002**	**0.0114**	**0.0002**	**0.14**	**0.046**	**0.001**	**72.3**	**2.1**	**73.1**	**1.5**	**35**	**57**	**-1.1**	**-0.4**
WF_04_074	82	117	1.44	109	0.081	0.011	0.0111	0.0006	0.34	0.053	0.009	79	11	71.3	4	400	280	9.7	0.7
WF_04_075	68	57	0.84	81	0.076	0.008	0.0120	0.0004	0.27	0.046	0.005	73.8	7.4	77.2	2.7	30	180	-4.6	-0.5
WF_04_076	72	4	0.05	73	13.530	0.260	0.5180	0.0085	0.47	0.188	0.003	2718	18	2690	36	2724	25	1.2	0.9
WF_04_077	64	47	0.73	74	0.113	0.010	0.0165	0.0005	0.34	0.049	0.004	107.5	9.3	105.6	3	170	170	1.8	0.2
WF_04_078	177	127	0.72	207	0.083	0.006	0.0124	0.0003	0.06	0.049	0.004	80.2	5.8	79.4	2	140	140	1.0	0.1
WF_04_079	45	10	0.21	47	5.670	0.140	0.3512	0.0061	0.24	0.117	0.003	1928	22	1940	29	1895	42	-2.4	-1.6
WF_04_080	115	20	0.18	120	4.659	0.099	0.3121	0.0052	0.46	0.108	0.002	1761	17	1751	25	1770	30	1.1	0.8
WF_04_081	498	311	0.62	571	0.390	0.009	0.0536	0.0010	0.45	0.053	0.001	334.4	6.3	336.6	6	314	40	-0.7	-0.3
WF_04_082	**1260**	**1670**	**1.33**	**1652**	**0.076**	**0.003**	**0.0117**	**0.0002**	**0.33**	**0.047**	**0.001**	**74.5**	**2.4**	**74.9**	**1.5**	**74**	**59**	**-0.5**	**-0.2**
WF_04_083	*502*	*16*	*0.03*	*506*	*2.450*	*0.220*	*0.1680*	*0.0150*	*0.97*	*0.105*	*0.002*	*1239*	*64*	*999*	*80*	*1706*	*35*	*41.4*	*8.8*
WF_04_084	186	91	0.49	207	0.180	0.008	0.0268	0.0006	0.02	0.049	0.002	168	6.8	170.1	3.8	158	91	-1.3	-0.3
WF_04_085	90	31	0.35	97	4.276	0.089	0.2986	0.0049	0.46	0.103	0.002	1687	17	1684	25	1680	29	-0.2	-0.2
WF_04_086	15	11	0.75	18	4.190	0.140	0.2930	0.0072	0.30	0.103	0.003	1674	27	1655	36	1679	59	1.4	0.7
WF_04_087	759	355	0.47	842	0.194	0.005	0.0281	0.0005	0.31	0.050	0.001	179.6	4.3	178.8	3.2	175	53	0.4	0.2
WF_04_088	*322*	*106*	*0.33*	*347*	*3.150*	*0.190*	*0.2130*	*0.0130*	*0.92*	*0.106*	*0.002*	*1436*	*48*	*1241*	*69*	*1742*	*39*	*28.8*	*7.3*
WF_04_089	556	165	0.30	595	0.163	0.005	0.0235	0.0005	0.32	0.050	0.001	153	4	149.7	3	209	60	2.2	0.8
WF_04_090	155	232	1.50	210	0.163	0.009	0.0246	0.0006	0.10	0.048	0.003	152.7	7.5	156.4	4.1	134	100	-2.4	-0.5
WF_04_091	66	30	0.45	73	2.990	0.077	0.2422	0.0053	0.49	0.089	0.002	1406	21	1398	27	1406	41	0.6	0.3
WF_04_092	655	440	0.67	758	0.188	0.007	0.0270	0.0006	0.55	0.050	0.001	174.6	5.7	172	3.9	198	59	1.5	0.5
WF_04_093	96	47	0.49	107	4.280	0.089	0.3056	0.0069	0.15	0.102	0.003	1690	17	1718	34	1649	47	-4.2	-2.0
WF_04_094	136	81	0.59	155	0.160	0.008	0.0231	0.0005	0.16	0.051	0.003	152.9	7.2	146.9	3.2	200	100	3.9	0.8
WF_04_095	**512**	**218**	**0.43**	**563**	**0.078**	**0.003**	**0.0117**	**0.0003**	**0.34**	**0.048**	**0.002**	**76.9**	**2.8**	**74.8**	**1.7**	**121**	**73**	**2.7**	**0.8**
WF_04_096	96	32	0.33	104	3.216	0.075	0.2544	0.0048	0.56	0.091	0.002	1464	18	1461	25	1454	36	-0.5	-0.3
WF_04_097	159	99	0.62	182	0.174	0.009	0.0261	0.0006	0.03	0.048	0.003	162.2	7.5	165.8	3.8	130	100	-2.2	-0.5
WF_04_098	996	239	0.24	1052	0.245	0.006	0.0345	0.0007	0.44	0.050	0.001	221.9	5.1	218.6	4.2	213	47	1.5	0.6
WF_04_099	167	77	0.46	185	4.983	0.110	0.3354	0.0064	0.59	0.106	0.002	1815	18	1864	31	1731	28	-7.7	-4.3
WF_04_100	281	49	0.17	292	2.336	0.046	0.2074	0.0034	0.34	0.082	0.001	1225.1	14	1215	18	1236	34	1.7	1.2

Table 10: Detrital Zircon LA-ICP-MS U-Pb Isotopic Data and Ages: WF-04, Base of the Williams Fork Formation, Coal Canyon (lat. 39.130840, long. -108.366867)[a]

					Corrected Isotopic Ratios							Ages (Ma)[i]							
Grain #[b]	U[c] [ppm]	Th[c] [ppm]	Th/U	eU[d] [ppm]	$^{207}Pb/^{235}U$[e]	±2s[f]	$^{206}Pb/^{238}U$[e]	±2s[f]	Rho[g]	$^{207}Pb/^{206}Pb$[h]	±2s[f]	$^{207}Pb/^{235}U$	±2s	$^{206}Pb/^{238}U$	±2s	$^{207}Pb/^{206}Pb$	±2s	Disc. %[j]	Wtd. Disc.[k]
WF_04_101	80	64	0.80	95	0.087	0.009	0.0133	0.0004	0.34	0.047	0.005	84.4	8.3	85	2.4	90	190	-0.7	-0.1
WF_04_102	56	71	1.26	73	0.079	0.011	0.0121	0.0004	0.15	0.048	0.007	76	10	77.7	2.7	130	240	-2.2	-0.2
WF_04_103	46	16	0.36	50	2.834	0.076	0.2300	0.0045	0.34	0.088	0.002	1364	20	1334	23	1368	49	2.5	1.5
WF_04_104	369	23	0.06	374	4.104	0.090	0.2932	0.0059	0.80	0.102	0.001	1655	18	1656	29	1651	24	-0.3	-0.2
WF_04_105	114	57	0.50	127	1.615	0.039	0.1632	0.0030	0.31	0.072	0.002	976	15	974	16	967	46	-0.7	-0.4
WF_04_106	*1090*	*44*	*0.04*	*1100*	*1.419*	*0.085*	*0.0976*	*0.0049*	*0.94*	*0.102*	*0.002*	*889*	*35*	*599*	*29*	*1657*	*33*	*32.6*	*8.3*
WF_04_107	253	256	1.01	313	0.174	0.009	0.0253	0.0005	0.00	0.050	0.002	163.2	7.2	160.8	3.3	184	98	1.5	0.3
WF_04_108	118	48	0.41	129	0.195	0.010	0.0283	0.0006	0.23	0.050	0.002	181.3	8.3	179.8	3.5	169	97	0.8	0.2
WF_04_109	511	4	0.01	512	0.695	0.022	0.0857	0.0020	0.38	0.059	0.002	535	13	531.7	11	565	55	0.6	0.3
WF_04_110	*4*	*14*	*3.42*	*7*	*8.620*	*0.420*	*0.0921*	*0.0044*	*0.32*	*0.675*	*0.038*	*2293*	*42*	*567*	*26*	*4675*	*93*	*75.3*	*41.1*
WF_04_111	160	177	1.11	202	0.160	0.008	0.0233	0.0005	0.14	0.048	0.002	149.9	6.6	148.7	3.2	131	94	0.8	0.2
WF_04_112	231	41	0.18	241	5.160	0.140	0.3323	0.0072	0.54	0.111	0.002	1851	21	1848	35	1820	37	-1.5	-0.8
WF_04_113	271	134	0.49	302	0.082	0.005	0.0128	0.0003	0.11	0.046	0.003	79.5	4.2	82	2	50	100	-3.1	-0.6
WF_04_114	613	271	0.44	677	0.082	0.003	0.0126	0.0003	0.22	0.047	0.002	80.6	3.1	80.6	1.9	76	74	0.0	0.0
WF_04_115	*11*	*19*	*1.64*	*16*	*16.970*	*0.840*	*0.3160*	*0.0140*	*0.51*	*0.391*	*0.015*	*2948*	*53*	*1768*	*66*	*3884*	*63*	*54.5*	*32.1*
WF_04_116	428	157	0.37	465	0.197	0.008	0.0292	0.0007	0.35	0.049	0.002	182	6.7	185.3	4.5	152	71	-1.8	-0.5
WF_04_117	333	108	0.32	358	0.589	0.017	0.0751	0.0018	0.33	0.057	0.002	470.7	11	466.9	11	478	59	0.8	0.3
WF_04_118	106	34	0.32	114	1.823	0.049	0.1799	0.0039	0.51	0.074	0.002	1052	17	1066	21	1024	49	-4.1	-2.0
WF_04_119	249	96	0.39	272	4.590	0.170	0.3120	0.0110	0.93	0.106	0.001	1749	31	1750	55	1726	25	-1.4	-0.4
WF_04_120	342	215	0.63	393	0.192	0.006	0.0285	0.0006	0.21	0.048	0.002	177.9	5.4	181	3.6	122	65	-1.7	-0.6
WF_04_121	222	111	0.50	248	0.161	0.006	0.0247	0.0006	0.16	0.048	0.002	151.1	5.3	157.4	3.7	102	76	-4.2	-1.2
WF_04_122	381	79	0.21	400	0.274	0.008	0.0382	0.0009	0.43	0.052	0.001	245.9	6.6	241.7	5.3	250	55	1.7	0.6
WF_04_123	216	85	0.40	236	4.440	0.190	0.3060	0.0130	0.91	0.107	0.002	1716	36	1716	66	1755	34	2.2	0.6
WF_04_124	43	43	0.99	53	3.830	0.110	0.2772	0.0059	0.47	0.099	0.002	1595	23	1576	30	1633	46	3.5	1.9
WF_04_125	108	52	0.48	120	0.511	0.020	0.0662	0.0015	0.38	0.056	0.002	418	13	412.9	9	435	73	1.2	0.4
WF_04_126	379	108	0.28	404	0.261	0.008	0.0365	0.0008	0.39	0.052	0.002	235.1	6.4	230.7	5.1	267	64	1.9	0.7
WF_04_127	156	99	0.63	179	0.160	0.008	0.0235	0.0006	0.04	0.048	0.002	151.9	7	149.5	3.8	116	100	1.6	0.3
WF_04_128	59	27	0.45	65	1.582	0.050	0.1622	0.0032	0.42	0.071	0.002	964	20	969	18	933	56	-3.9	-2.0
WF_04_129	252	257	1.02	312	0.152	0.007	0.0229	0.0006	0.32	0.047	0.002	143.4	5.9	145.9	3.7	79	82	-1.7	-0.4
WF_04_130	*228*	*85*	*0.37*	*248*	*0.085*	*0.005*	*0.0137*	*0.0003*	*0.22*	*0.045*	*0.003*	*82.1*	*4.5*	*87.8*	*2.2*	*20*	*100*	*-6.9*	*-1.3*
WF_04_131	114	88	0.77	135	0.091	0.008	0.0132	0.0004	0.25	0.050	0.004	88.1	7.5	84.8	2.5	200	160	3.7	0.4
WF_04_132	*88*	*39*	*0.45*	*97*	*4.320*	*0.130*	*0.2807*	*0.0065*	*0.71*	*0.111*	*0.002*	*1702*	*25*	*1594*	*33*	*1808*	*36*	*11.8*	*6.5*
WF_04_133	388	185	0.48	431	0.178	0.006	0.0261	0.0005	0.28	0.049	0.002	166.4	5.2	166.1	3.3	152	64	0.2	0.1
WF_04_134	130	133	1.02	161	0.165	0.009	0.0231	0.0005	0.13	0.051	0.003	154.8	7.8	147.2	3.3	230	110	4.9	1.0

Table 10: Detrital Zircon LA-ICP-MS U-Pb Isotopic Data and Ages: WF-04, Base of the Williams Fork Formation, Coal Canyon (lat. 39.130840, long. -108.366867)[a]

					Corrected Isotopic Ratios							Ages (Ma)[i]							
Grain #[b]	U[c] [ppm]	Th[c] [ppm]	Th/U	eU[d] [ppm]	$^{207}Pb/^{235}U$[e]	±2s[f]	$^{206}Pb/^{238}U$[e]	±2s[f]	Rho[g]	$^{207}Pb/^{206}Pb$[h]	±2s[f]	$^{207}Pb/^{235}U$	±2s	$^{206}Pb/^{238}U$	±2s	$^{207}Pb/^{206}Pb$	±2s	Disc. %[j]	Wtd. Disc.[k]
WF_04_135	114	56	0.49	127	4.219	0.097	0.2947	0.0061	0.67	0.102	0.002	1676	19	1664	30	1664	29	0.0	0.0
WF_04_136	206	31	0.15	213	1.720	0.038	0.1686	0.0031	0.42	0.074	0.001	1015	14	1004	17	1035	35	3.0	1.8
WF_04_137	40	18	0.46	44	4.083	0.110	0.2877	0.0065	0.47	0.103	0.002	1653	22	1629	32	1675	42	2.7	1.4
WF_04_138	372	102	0.27	396	0.257	0.008	0.0356	0.0007	0.27	0.052	0.001	232	6	225.5	4.3	259	58	2.8	1.1
WF_04_139	71	49	0.69	82	0.847	0.027	0.1014	0.0022	0.37	0.059	0.002	622	15	623	13	563	63	-0.2	-0.1
WF_04_140	*384*	*91*	*0.24*	*405*	*1.054*	*0.046*	*0.0722*	*0.0026*	*0.57*	*0.106*	*0.003*	*732*	*21*	*452*	*15*	*1740*	*51*	*38.3*	*13.3*
WF_04_141	163	133	0.81	194	0.190	0.008	0.0276	0.0006	0.37	0.049	0.002	176.7	7.2	175.6	3.9	157	75	0.6	0.2
WF_04_142	*14*	*32*	*2.27*	*22*	*5.480*	*0.230*	*0.0717*	*0.0028*	*0.61*	*0.550*	*0.020*	*1893*	*37*	*446*	*17*	*4365*	*54*	*76.4*	*39.1*
WF_04_143	*708*	*201*	*0.28*	*755*	*0.285*	*0.009*	*0.0351*	*0.0007*	*0.29*	*0.058*	*0.002*	*254.4*	*7*	*222.5*	*4.1*	*530*	*59*	*12.5*	*4.6*
WF_04_144	287	26	0.09	293	6.063	0.130	0.3616	0.0071	0.82	0.120	0.002	1983	19	1993	33	1954	22	-2.0	-1.2
WF_04_145	111	43	0.38	121	3.903	0.091	0.2784	0.0049	0.56	0.100	0.002	1614	19	1583	25	1623	35	2.5	1.6
WF_04_146	319	94	0.29	341	0.083	0.004	0.0129	0.0003	0.07	0.046	0.002	80.8	3.6	82.3	1.8	39	87	-1.9	-0.4
WF_04_147	*214*	*83*	*0.39*	*233*	*2.473*	*0.096*	*0.1771*	*0.0076*	*0.86*	*0.101*	*0.002*	*1270*	*28*	*1049*	*42*	*1628*	*33*	*35.6*	*13.8*
WF_04_148	191	43	0.23	201	2.730	0.140	0.2254	0.0099	0.91	0.087	0.002	1328	38	1307	52	1355	39	3.5	0.9
WF_04_149	112	95	0.84	135	0.155	0.008	0.0226	0.0005	0.07	0.050	0.003	146.4	6.9	144.2	2.9	160	110	1.5	0.3
WF_04_150	111	63	0.57	125	0.180	0.011	0.0253	0.0005	0.34	0.050	0.003	167.3	9.6	160.8	3.2	220	130	3.9	0.7
WF_04_151	*105*	*52*	*0.49*	*117*	*0.213*	*0.021*	*0.0260*	*0.0008*	*0.23*	*0.058*	*0.006*	*195*	*18*	*165.7*	*4.8*	*470*	*190*	*15.0*	*1.6*
WF_04_152	114	46	0.40	125	3.198	0.082	0.2480	0.0045	0.24	0.092	0.002	1455	20	1428	23	1466	39	2.6	1.7
WF_04_153	139	48	0.35	151	4.230	0.090	0.2963	0.0051	0.44	0.103	0.002	1680	17	1672	25	1684	32	0.7	0.5
WF_04_154	*194*	*71*	*0.36*	*211*	*3.725*	*0.075*	*0.2587*	*0.0046*	*0.63*	*0.104*	*0.002*	*1576*	*16*	*1485*	*23*	*1694*	*29*	*12.3*	*9.1*
WF_04_155	302	168	0.56	341	0.087	0.005	0.0132	0.0003	0.07	0.048	0.003	84.2	4.8	84.2	1.6	80	110	0.0	0.0
WF_04_156	85	13	0.16	88	3.860	0.180	0.2770	0.0095	0.63	0.102	0.004	1601	38	1575	48	1659	63	5.1	1.8
WF_04_157	151	70	0.46	167	0.195	0.010	0.0286	0.0007	0.05	0.049	0.002	180.3	8.2	181.9	4.1	169	100	-0.9	-0.2
WF_04_158	69	45	0.66	79	5.545	0.120	0.3399	0.0068	0.60	0.118	0.002	1909	19	1886	33	1926	29	2.1	1.2
WF_04_159	**853**	**693**	**0.81**	**1016**	**0.077**	**0.002**	**0.0117**	**0.0002**	**0.20**	**0.048**	**0.002**	**75**	**2.3**	**74.8**	**1.4**	**98**	**65**	**0.3**	**0.1**
WF_04_160	176	182	1.03	219	0.176	0.009	0.0260	0.0006	0.05	0.049	0.003	164.6	7.6	165.2	3.5	153	100	-0.4	-0.1
WF_04_161	83	69	0.83	99	5.005	0.110	0.3278	0.0070	0.62	0.111	0.002	1822	18	1827	34	1807	30	-1.1	-0.6
WF_04_162	**644**	**240**	**0.37**	**700**	**0.076**	**0.003**	**0.0116**	**0.0002**	**0.20**	**0.047**	**0.002**	**74.5**	**2.6**	**74.1**	**1.4**	**75**	**66**	**0.5**	**0.2**
WF_04_163	230	151	0.66	265	0.081	0.004	0.0122	0.0003	0.30	0.047	0.003	78.9	4.1	78.3	1.9	60	100	0.8	0.1
WF_04_164	35	71	2.02	51	0.170	0.025	0.0231	0.0008	0.15	0.052	0.008	157	22	147.4	5.3	220	260	6.1	0.4
WF_04_165	**108**	**50**	**0.47**	**120**	**0.071**	**0.006**	**0.0115**	**0.0003**	**0.34**	**0.044**	**0.004**	**69.7**	**5.4**	**73.7**	**2**	**-50**	**150**	**-5.7**	**-0.7**
WF_04_166	*90*	*41*	*0.46*	*99*	*1.418*	*0.050*	*0.1445*	*0.0035*	*0.39*	*0.070*	*0.002*	*896*	*20*	*870*	*20*	*943*	*62*	*7.7*	*3.7*
WF_04_167	422	113	0.27	448	0.183	0.006	0.0258	0.0006	0.42	0.051	0.002	170.6	5.4	164.3	3.7	222	65	3.7	1.2
WF_04_168	421	224	0.53	474	0.086	0.004	0.0132	0.0003	0.34	0.046	0.002	83.3	3.7	84.6	2	45	81	-1.6	-0.4

Table 10: Detrital Zircon LA-ICP-MS U-Pb Isotopic Data and Ages: WF-04, Base of the Williams Fork Formation, Coal Canyon (lat. 39.130840, long. -108.366867)[a]

					Corrected Isotopic Ratios							Ages (Ma)[i]							
Grain #[b]	U[c] [ppm]	Th[c] [ppm]	Th/U	eU[d] [ppm]	$^{207}Pb/^{235}U$[e]	±2s[f]	$^{206}Pb/^{238}U$[e]	±2s[f]	Rho[g]	$^{207}Pb/^{206}Pb$[h]	±2s[f]	$^{207}Pb/^{235}U$	±2s	$^{206}Pb/^{238}U$	±2s	$^{207}Pb/^{206}Pb$	±2s	Disc. %[j]	Wtd. Disc.[k]
WF_04_169	172	49	0.29	183	4.783	0.120	0.3204	0.0075	0.69	0.107	0.002	1780	20	1795	38	1752	31	-2.5	-1.1
WF_04_170	*508*	*46*	*0.09*	*519*	*2.255*	*0.081*	*0.1452*	*0.0039*	*0.85*	*0.109*	*0.002*	*1193*	*25*	*874*	*22*	*1788*	*37*	*51.1*	*41.5*
WF_04_171	*69*	*38*	*0.55*	*78*	*0.179*	*0.014*	*0.0237*	*0.0007*	*0.11*	*0.052*	*0.004*	*166*	*12*	*151.3*	*4.1*	*310*	*150*	*8.9*	*1.2*
WF_04_172	1092	324	0.30	1168	0.108	0.004	0.0162	0.0004	0.37	0.048	0.001	103.6	3.5	103.3	2.3	98	61	0.3	0.1
WF_04_173	328	278	0.85	394	0.192	0.006	0.0272	0.0006	0.20	0.051	0.001	178.7	5.3	173.2	3.9	225	63	3.1	1.0
WF_04_174	130	77	0.59	148	0.081	0.007	0.0124	0.0005	0.13	0.049	0.005	79.2	6.3	79.4	2.9	170	170	-0.3	0.0
WF_04_175	101	39	0.38	110	0.831	0.026	0.0991	0.0021	0.15	0.061	0.002	614	14	609.2	12	615	65	0.8	0.3
WF_04_176	458	116	0.25	485	4.881	0.120	0.3316	0.0078	0.71	0.106	0.002	1799	21	1845	38	1746	33	-5.7	-2.6
WF_04_177	128	96	0.75	150	0.112	0.009	0.0155	0.0004	0.17	0.052	0.004	107.5	7.8	98.9	2.7	290	150	8.0	1.1
WF_04_178	133	118	0.89	160	0.158	0.009	0.0233	0.0005	0.16	0.049	0.003	150.3	7.8	148.7	3.2	130	110	1.1	0.2
WF_04_179	81	125	1.54	111	1.577	0.048	0.1608	0.0042	0.39	0.071	0.002	958	19	963	23	955	58	-0.8	-0.3
WF_04_180	486	260	0.53	548	0.183	0.006	0.0271	0.0006	0.29	0.049	0.002	171.2	5.1	172.2	3.8	125	64	-0.6	-0.2
WF_04_181	25	34	1.34	33	3.140	0.110	0.2510	0.0061	0.18	0.091	0.004	1436	28	1442	32	1421	72	-1.5	-0.7
WF_04_182	*392*	*43*	*0.11*	*402*	*1.770*	*0.110*	*0.1276*	*0.0037*	*0.77*	*0.098*	*0.004*	*1014*	*26*	*774*	*21*	*1556*	*73*	*23.7*	*9.2*
WF_04_183	122	35	0.29	130	0.187	0.009	0.0273	0.0006	0.21	0.050	0.002	173.8	7.9	173.4	3.9	182	95	0.2	0.1
WF_04_184	169	32	0.19	176	0.703	0.021	0.0859	0.0019	0.35	0.060	0.002	543	13	531.1	11	589	59	2.2	0.9
WF_04_185	144	29	0.20	151	0.822	0.026	0.0988	0.0020	0.30	0.061	0.002	611	14	607.3	12	617	67	0.6	0.3
WF_04_186	*17*	*39*	*2.26*	*26*	*3.910*	*0.180*	*0.0575*	*0.0027*	*0.45*	*0.493*	*0.022*	*1619*	*37*	*360*	*17*	*4234*	*65*	*77.8*	*34.0*
WF_04_187	139	124	0.89	168	2.949	0.064	0.2410	0.0048	0.48	0.088	0.002	1396	17	1391	25	1394	32	0.2	0.1
WF_04_188	310	135	0.44	342	0.227	0.008	0.0323	0.0006	0.27	0.051	0.002	207.7	6.4	204.6	4	215	75	1.5	0.5
WF_04_189	135	56	0.42	148	4.359	0.091	0.3018	0.0056	0.51	0.105	0.002	1706	17	1700	28	1707	30	0.4	0.3
WF_04_190	219	92	0.42	241	0.192	0.008	0.0281	0.0006	0.18	0.050	0.002	177.7	6.5	178.7	3.8	183	76	-0.6	-0.2
WF_04_191	138	116	0.84	165	0.088	0.007	0.0140	0.0004	0.10	0.046	0.004	85.5	6.6	89.3	2.3	20	140	-4.4	-0.6
WF_04_192	*207*	*99*	*0.48*	*231*	*0.184*	*0.008*	*0.0283*	*0.0006*	*0.22*	*0.048*	*0.002*	*170.7*	*6.8*	*179.6*	*3.6*	*107*	*83*	*-5.2*	*-1.3*
WF_04_193	58	46	0.79	69	0.154	0.013	0.0235	0.0007	0.06	0.049	0.004	144	11	149.8	4.3	130	160	-4.0	-0.5
WF_04_194	285	156	0.55	322	0.177	0.007	0.0258	0.0005	0.14	0.050	0.002	165.2	6.3	164.5	3.1	184	79	0.4	0.1
WF_04_195	270	239	0.89	326	0.083	0.004	0.0122	0.0003	0.05	0.049	0.003	80.3	4	77.9	1.9	150	100	3.0	0.6
WF_04_196	212	24	0.11	218	3.122	0.065	0.2489	0.0043	0.53	0.092	0.001	1437	16	1432	22	1466	29	2.3	1.5
WF_04_197	59	57	0.97	72	0.161	0.015	0.0237	0.0007	0.34	0.051	0.005	151	13	151	4.2	230	180	0.0	0.0
WF_04_198	150	120	0.80	178	0.183	0.010	0.0260	0.0006	0.25	0.051	0.003	169.7	8.5	165.3	3.7	230	100	2.6	0.5
WF_04_199	204	83	0.41	223	0.206	0.008	0.0296	0.0006	0.12	0.051	0.002	189.8	7.1	188.1	3.5	229	86	0.9	0.2
WF_04_200	372	200	0.54	419	0.095	0.005	0.0143	0.0003	0.07	0.048	0.002	91.8	4.2	91.7	1.8	119	91	0.1	0.0
WF_04_201	196	83	0.42	216	0.259	0.011	0.0379	0.0009	0.12	0.050	0.002	234.5	8.6	239.5	5.4	194	88	-2.1	-0.6
WF_04_202	*252*	*117*	*0.46*	*279*	*1.750*	*0.061*	*0.1238*	*0.0039*	*0.78*	*0.103*	*0.002*	*1024*	*22*	*752*	*22*	*1684*	*44*	*26.6*	*12.4*

Table 10: Detrital Zircon LA-ICP-MS U-Pb Isotopic Data and Ages: WF-04, Base of the Williams Fork Formation, Coal Canyon (lat. 39.130840, long. -108.366867)[a]

					Corrected Isotopic Ratios							Ages (Ma)[i]							
Grain #[b]	U[c] [ppm]	Th[c] [ppm]	Th/U	eU[d] [ppm]	$^{207}Pb/^{235}U$[e]	±2s[f]	$^{206}Pb/^{238}U$[e]	±2s[f]	Rho[g]	$^{207}Pb/^{206}Pb$[h]	±2s[f]	$^{207}Pb/^{235}U$	±2s	$^{206}Pb/^{238}U$	±2s	$^{207}Pb/^{206}Pb$	±2s	Disc. %[j]	Wtd. Disc.[k]
WF_04_203	198	73	0.37	215	3.565	0.080	0.2758	0.0054	0.55	0.096	0.002	1542	18	1570	27	1541	32	-1.9	-1.1
WF_04_204	413	213	0.52	463	0.091	0.005	0.0137	0.0003	0.33	0.049	0.002	88.2	4.2	87.4	2.1	142	94	0.9	0.2
WF_04_205	84	22	0.26	89	4.094	0.110	0.2904	0.0075	0.60	0.104	0.002	1653	23	1647	36	1682	37	2.1	1.0
WF_04_206	577	387	0.67	668	0.185	0.006	0.0273	0.0005	0.25	0.050	0.002	172.1	4.8	174.2	3.3	185	66	-1.2	-0.4
WF_04_207	77	16	0.20	81	2.284	0.086	0.2132	0.0061	0.35	0.079	0.003	1205	27	1245	32	1165	68	-6.9	-2.5
WF_04_208	84	38	0.46	93	0.286	0.016	0.0418	0.0010	0.14	0.050	0.003	254	13	264	5.9	180	110	-3.9	-0.8
WF_04_209	66	44	0.67	76	4.410	0.180	0.3184	0.0097	0.42	0.105	0.004	1712	33	1781	47	1699	61	-4.8	-1.7
WF_04_210	58	36	0.61	66	0.183	0.015	0.0276	0.0008	0.01	0.050	0.004	169	13	175.7	4.8	130	150	-4.0	-0.5
WF_04_211	196	182	0.93	239	0.080	0.005	0.0121	0.0003	0.07	0.049	0.003	78	4.2	77.8	2.1	140	120	0.3	0.0
WF_04_212	59	28	0.47	66	0.760	0.030	0.0949	0.0022	0.29	0.059	0.002	574	17	584	13	571	77	-1.7	-0.6
WF_04_213	359	141	0.39	392	0.091	0.004	0.0137	0.0003	0.34	0.049	0.003	88	4.1	87.7	2	160	110	0.3	0.1
WF_04_214	128	51	0.40	140	0.184	0.010	0.0260	0.0007	0.40	0.052	0.003	170.7	8.7	165.2	4.3	250	100	3.2	0.6
WF_04_215	*106*	*108*	*1.02*	*131*	*0.716*	*0.024*	*0.0915*	*0.0020*	*0.37*	*0.058*	*0.002*	*547*	*14*	*564.3*	*12*	*516*	*66*	*-3.2*	*-1.2*
WF_04_216	25	26	1.04	31	0.080	0.024	0.0112	0.0006	0.02	0.059	0.017	76	23	71.9	3.8	60	470	5.4	0.2
WF_04_217	126	66	0.52	142	4.349	0.089	0.3030	0.0060	0.54	0.106	0.002	1703	17	1705	30	1723	33	1.0	0.6
WF_04_218	*600*	*305*	*0.51*	*672*	*1.177*	*0.047*	*0.0728*	*0.0023*	*0.88*	*0.118*	*0.002*	*789*	*22*	*453*	*14*	*1918*	*36*	*42.6*	*15.3*
WF_04_219	615	379	0.62	704	0.188	0.006	0.0277	0.0006	0.44	0.049	0.001	174.6	5	176.1	3.6	148	55	-0.9	-0.3
WF_04_220	250	105	0.42	274	0.181	0.006	0.0276	0.0005	0.13	0.048	0.002	170.4	5.9	175.2	3.4	126	74	-2.8	-0.8
WF_04_221	574	276	0.48	639	0.174	0.005	0.0252	0.0005	0.31	0.050	0.001	162.7	4.4	160.1	3	205	56	1.6	0.6
WF_04_222	*646*	*217*	*0.34*	*697*	*3.070*	*0.170*	*0.2118*	*0.0100*	*0.90*	*0.104*	*0.002*	*1421*	*44*	*1235*	*54*	*1684*	*43*	*26.7*	*8.3*
WF_04_223	405	89	0.22	426	3.005	0.078	0.2475	0.0054	0.62	0.088	0.002	1411	20	1425	28	1388	37	-2.7	-1.3
WF_04_224	170	150	0.89	205	0.203	0.014	0.0277	0.0007	0.10	0.052	0.003	187	12	175.9	4.5	270	130	5.9	0.9
WF_04_225	141	59	0.42	155	5.247	0.120	0.3370	0.0057	0.59	0.114	0.002	1860	19	1872	28	1863	30	-0.5	-0.3
WF_04_226	239	61	0.26	253	4.892	0.100	0.3264	0.0057	0.58	0.110	0.002	1803	18	1820	28	1795	29	-1.4	-0.9
WF_04_227	891	914	1.03	1106	0.158	0.004	0.0236	0.0004	0.35	0.049	0.001	149.2	3.5	150.4	2.5	152	49	-0.8	-0.3
WF_04_228	70	70	1.00	87	0.173	0.013	0.0239	0.0007	0.18	0.051	0.004	161	11	151.9	4.3	250	140	5.7	0.8
WF_04_229	309	131	0.43	340	0.483	0.016	0.0631	0.0011	0.16	0.056	0.002	398.9	11	394.4	6.5	430	65	1.1	0.4
WF_04_230	193	104	0.54	217	0.303	0.010	0.0415	0.0007	0.26	0.053	0.002	269.2	8	262.2	4.4	307	67	2.6	0.9
WF_04_231	*403*	*55*	*0.14*	*416*	*4.470*	*0.300*	*0.2670*	*0.0200*	*0.91*	*0.119*	*0.004*	*1719*	*57*	*1522*	*100*	*1948*	*47*	*21.9*	*4.3*
WF_04_232	21	41	1.94	30	4.120	0.130	0.2915	0.0058	0.18	0.102	0.003	1659	25	1648	29	1654	54	0.4	0.2
WF_04_233	100	62	0.62	115	0.173	0.010	0.0255	0.0007	0.15	0.050	0.003	162.9	8.8	162.3	4.1	200	120	0.4	0.1
WF_04_234	191	217	1.14	242	0.180	0.009	0.0261	0.0005	0.18	0.050	0.002	169.1	7.4	165.9	3.3	199	95	1.9	0.4
WF_04_235	*565*	*198*	*0.35*	*612*	*0.096*	*0.006*	*0.0115*	*0.0002*	*0.45*	*0.061*	*0.003*	*93.1*	*5.1*	*73.6*	*1.6*	*617*	*98*	*20.9*	*3.8*
WF_04_236	499	276	0.55	564	0.193	0.006	0.0286	0.0006	0.26	0.049	0.002	179.6	4.9	181.6	3.5	139	65	-1.1	-0.4

Table 10: Detrital Zircon LA-ICP-MS U-Pb Isotopic Data and Ages: WF-04, Base of the Williams Fork Formation, Coal Canyon (lat. 39.130840, long. -108.366867)[a]

					Corrected Isotopic Ratios							Ages (Ma)[i]							
Grain #[b]	U[c] [ppm]	Th[c] [ppm]	Th/U	eU[d] [ppm]	$^{207}Pb/^{235}U$[e]	±2s[f]	$^{206}Pb/^{238}U$[e]	±2s[f]	Rho[g]	$^{207}Pb/^{206}Pb$[h]	±2s[f]	$^{207}Pb/^{235}U$	±2s	$^{206}Pb/^{238}U$	±2s	$^{207}Pb/^{206}Pb$	±2s	Disc. %[j]	Wtd. Disc.[k]
WF_04_237	152	8	0.05	154	1.872	0.043	0.1781	0.0036	0.46	0.076	0.001	1070	15	1056	20	1085	37	2.7	1.5
WF_04_238	258	101	0.39	282	3.865	0.076	0.2808	0.0047	0.79	0.100	0.001	1607	15	1595	24	1619	22	1.5	1.0
WF_04_239	119	67	0.57	135	4.290	0.120	0.3116	0.0067	0.79	0.102	0.002	1690	23	1748	33	1654	31	-5.7	-2.8
WF_04_240	330	54	0.16	343	0.187	0.008	0.0271	0.0006	0.00	0.050	0.002	173.6	6.7	172.4	4	173	84	0.7	0.2
WF_04_241	301	29	0.10	308	4.090	0.110	0.2903	0.0073	0.72	0.101	0.002	1650	22	1642	37	1651	33	0.5	0.2
WF_04_242	123	72	0.58	140	0.153	0.007	0.0237	0.0006	0.34	0.049	0.003	144.5	6.5	151.4	4.1	140	110	-4.8	-1.1
WF_04_243	*111*	*61*	*0.54*	*125*	*5.220*	*0.190*	*0.3024*	*0.0064*	*0.61*	*0.126*	*0.004*	*1864*	*32*	*1702*	*32*	*2026*	*55*	*16.0*	*10.1*
WF_04_244	751	296	0.39	821	0.096	0.005	0.0145	0.0005	0.27	0.048	0.002	92.7	4.6	93	3	108	100	-0.3	-0.1
WF_04_245	135	71	0.52	152	6.533	0.130	0.3691	0.0070	0.62	0.128	0.002	2052	18	2029	34	2071	27	2.0	1.2
WF_04_246	497	145	0.29	531	3.730	0.140	0.2631	0.0088	0.90	0.103	0.002	1587	29	1511	43	1679	31	10.0	3.9
WF_04_247	74	58	0.79	87	4.169	0.096	0.2928	0.0058	0.53	0.103	0.002	1668	18	1655	29	1681	33	1.5	0.9
WF_04_248	242	121	0.50	270	3.327	0.097	0.2629	0.0073	0.62	0.092	0.002	1489	22	1504	37	1469	45	-2.4	-0.9
WF_04_249	112	19	0.17	117	0.431	0.015	0.0592	0.0012	0.10	0.053	0.002	364.4	11	370.9	7.5	298	73	-1.8	-0.6
WF_04_250	376	234	0.62	431	0.186	0.006	0.0266	0.0005	0.42	0.051	0.001	173.3	5.3	169.5	3.1	217	60	2.2	0.7
WF_04_251	**197**	**78**	**0.40**	**215**	**0.074**	**0.005**	**0.0116**	**0.0003**	**0.05**	**0.047**	**0.003**	**72.6**	**4.9**	**74.2**	**1.9**	**80**	**130**	**-2.2**	**-0.3**
WF_04_252	99	84	0.85	119	0.167	0.010	0.0253	0.0005	0.04	0.048	0.003	156.1	8.7	160.7	3.3	110	110	-2.9	-0.5
WF_04_253	*281*	*129*	*0.46*	*311*	*0.932*	*0.042*	*0.0622*	*0.0014*	*0.40*	*0.108*	*0.004*	*669*	*23*	*388.9*	*8.6*	*1765*	*74*	*41.9*	*12.2*
WF_04_254	191	31	0.16	198	6.170	0.380	0.3600	0.0120	0.53	0.123	0.006	1986	50	1987	60	1978	78	-0.5	-0.2
WF_04_255	74	60	0.81	88	0.171	0.013	0.0239	0.0007	0.34	0.052	0.004	162	11	152.4	4.3	280	150	5.9	0.9
WF_04_256	*368*	*166*	*0.45*	*407*	*3.390*	*0.140*	*0.2197*	*0.0091*	*0.70*	*0.110*	*0.003*	*1498*	*34*	*1277*	*48*	*1793*	*45*	*28.8*	*10.8*
WF_04_257	477	117	0.25	504	3.056	0.084	0.2471	0.0075	0.73	0.091	0.002	1425	23	1423	38	1451	39	1.9	0.7
WF_04_258	*294*	*66*	*0.22*	*310*	*4.180*	*0.310*	*0.2630*	*0.0190*	*0.94*	*0.116*	*0.003*	*1668*	*62*	*1501*	*97*	*1888*	*40*	*20.5*	*4.0*
WF_04_259	*266*	*147*	*0.55*	*301*	*2.553*	*0.071*	*0.1740*	*0.0043*	*0.86*	*0.106*	*0.002*	*1285*	*20*	*1033*	*24*	*1730*	*27*	*40.3*	*29.0*
WF_04_260	63	50	0.80	75	1.966	0.057	0.1883	0.0036	0.46	0.077	0.002	1103	20	1112	20	1108	48	-0.4	-0.2
WF_04_261	*1443*	*40*	*0.03*	*1452*	*2.497*	*0.054*	*0.2002*	*0.0041*	*0.75*	*0.092*	*0.001*	*1275*	*16*	*1176*	*22*	*1461*	*26*	*19.5*	*13.0*
WF_04_262	247	54	0.22	260	4.230	0.140	0.2979	0.0084	0.87	0.104	0.002	1680	27	1679	42	1686	30	0.4	0.2
WF_04_263	140	78	0.56	158	0.528	0.019	0.0682	0.0015	0.13	0.057	0.002	430	13	425.2	9.2	471	79	1.1	0.4
WF_04_264	*1182*	*270*	*0.23*	*1245*	*0.261*	*0.010*	*0.0207*	*0.0006*	*0.66*	*0.088*	*0.002*	*236*	*7.5*	*132.8*	*4.1*	*1397*	*47*	*43.7*	*13.8*
WF_04_265	317	93	0.29	339	1.931	0.043	0.1876	0.0043	0.66	0.075	0.001	1091	15	1108	23	1071	35	-3.5	-1.6
WF_04_266	358	248	0.69	416	0.175	0.006	0.0258	0.0006	0.24	0.049	0.002	163.8	5.4	164.1	3.4	150	72	-0.2	-0.1
WF_04_267	321	38	0.12	330	1.890	0.070	0.1840	0.0073	0.90	0.075	0.001	1075	25	1091	40	1073	32	-1.7	-0.5
WF_04_268	195	32	0.16	202	3.505	0.085	0.2670	0.0053	0.60	0.096	0.002	1528	19	1525	27	1557	32	2.1	1.2
WF_04_269	*508*	*32*	*0.06*	*516*	*1.439*	*0.056*	*0.0928*	*0.0027*	*0.69*	*0.113*	*0.003*	*902*	*23*	*572*	*16*	*1835*	*44*	*36.6*	*14.3*
WF_04_270	*314*	*126*	*0.40*	*344*	*2.215*	*0.095*	*0.1843*	*0.0081*	*0.75*	*0.088*	*0.003*	*1192*	*29*	*1088*	*44*	*1376*	*54*	*20.9*	*6.5*

Table 10: Detrital Zircon LA-ICP-MS U-Pb Isotopic Data and Ages: WF-04, Base of the Williams Fork Formation, Coal Canyon (lat. 39.130840, long. -108.366867)[a]

					Corrected Isotopic Ratios							Ages (Ma)[i]							
Grain #[b]	U[c] [ppm]	Th[c] [ppm]	Th/U	eU[d] [ppm]	$^{207}Pb/^{235}U$[e]	±2s[f]	$^{206}Pb/^{238}U$[e]	±2s[f]	Rho[g]	$^{207}Pb/^{206}Pb$[h]	±2s[f]	$^{207}Pb/^{235}U$	±2s	$^{206}Pb/^{238}U$	±2s	$^{207}Pb/^{206}Pb$	±2s	Disc. %[j]	Wtd. Disc.[k]
WF_04_271	235	171	0.73	275	0.173	0.008	0.0260	0.0005	0.23	0.049	0.002	164.5	6.3	165.4	3.1	138	82	-0.5	-0.1
WF_04_272	*2*	*0*	*0.01*	*2*	*1.760*	*0.380*	*0.0689*	*0.0067*	*0.36*	*0.172*	*0.038*	*910*	*140*	*433*	*41*	*1970*	*470*	*52.4*	*3.4*
WF_04_273	40	62	1.53	55	0.175	0.017	0.0242	0.0008	0.05	0.051	0.005	163	15	154.3	5	250	190	5.3	0.6
WF_04_274	244	120	0.49	272	0.175	0.008	0.0253	0.0007	0.39	0.051	0.002	164.6	6.9	160.8	4.6	242	91	2.3	0.6
WF_04_275	*453*	*148*	*0.33*	*488*	*3.250*	*0.150*	*0.2250*	*0.0110*	*0.88*	*0.105*	*0.002*	*1467*	*35*	*1307*	*56*	*1713*	*42*	*23.7*	*7.3*
WF_04_276	181	59	0.33	195	0.089	0.006	0.0129	0.0004	0.17	0.050	0.003	86.5	5.8	82.6	2.3	210	120	4.5	0.7
WF_04_277	368	72	0.20	385	4.040	0.160	0.2903	0.0100	0.57	0.104	0.004	1640	34	1642	50	1677	79	2.1	0.7
WF_04_278	167	70	0.42	183	4.750	0.150	0.3250	0.0130	0.78	0.106	0.003	1774	26	1822	62	1719	46	-6.0	-1.7
WF_04_279	259	117	0.45	286	4.730	0.180	0.3270	0.0140	0.82	0.106	0.003	1779	31	1830	70	1729	47	-5.8	-1.4
WF_04_280	401	100	0.25	424	0.515	0.012	0.0666	0.0011	0.40	0.056	0.001	421.3	8.3	415.4	6.8	449	45	1.4	0.7
WF_04_281	*248*	*53*	*0.21*	*260*	*2.980*	*0.150*	*0.1111*	*0.0054*	*0.92*	*0.196*	*0.004*	*1398*	*39*	*679*	*31*	*2792*	*32*	*51.4*	*18.4*
WF_04_282	*448*	*230*	*0.51*	*502*	*0.411*	*0.018*	*0.0459*	*0.0021*	*0.46*	*0.064*	*0.002*	*349*	*13*	*289*	*13*	*743*	*65*	*17.2*	*4.6*
WF_04_283	200	22	0.11	205	4.406	0.088	0.3094	0.0058	0.62	0.105	0.002	1714	16	1737	28	1703	29	-2.0	-1.2
WF_04_284	114	220	1.93	166	0.166	0.019	0.0249	0.0009	0.32	0.049	0.005	155	16	158.5	5.9	150	200	-2.3	-0.2
WF_04_285	810	297	0.37	880	0.236	0.007	0.0340	0.0008	0.57	0.050	0.001	214.4	6	215.8	4.9	206	49	-0.7	-0.2
WF_04_286	123	53	0.43	135	4.750	0.130	0.3187	0.0060	0.38	0.108	0.002	1772	22	1785	30	1760	41	-1.4	-0.8
WF_04_287	*0*	*0*	*0.35*	*0*	*615.000*	*45.000*	*5.3200*	*0.7000*	*0.91*	*0.820*	*0.045*	*6516*	*75*	*11780*	*740*	*5010*	*100*	*-135.1*	*-9.1*
WF_04_288	370	203	0.55	418	0.180	0.005	0.0262	0.0005	0.22	0.050	0.002	168.8	4.8	166.4	3.2	179	62	1.4	0.5
WF_04_289	357	180	0.50	399	0.177	0.006	0.0258	0.0005	0.13	0.050	0.002	165.3	5.4	164.4	2.9	178	71	0.5	0.2
WF_04_290	*308*	*79*	*0.26*	*326*	*4.030*	*0.180*	*0.2660*	*0.0120*	*0.65*	*0.108*	*0.004*	*1646*	*34*	*1519*	*60*	*1766*	*69*	*14.0*	*4.1*
WF_04_291	*0*	*0*	*0.00*	*0*	-	-	-	-	-	-	-	-	-	-	-	-	-	-	-
WF_04_292	161	96	0.60	183	0.160	0.008	0.0227	0.0005	0.15	0.051	0.002	150.1	7.4	144.8	3.1	234	100	3.5	0.7
WF_04_293	177	84	0.48	197	0.105	0.005	0.0156	0.0004	0.06	0.049	0.003	100.8	4.6	99.7	2.6	160	100	1.1	0.2
WF_04_294	512	253	0.49	571	0.172	0.009	0.0251	0.0008	0.29	0.050	0.002	160.7	7.3	159.7	4.8	189	94	0.6	0.1
WF_04_295	*213*	*14*	*0.07*	*216*	*2.290*	*0.100*	*0.1578*	*0.0051*	*0.89*	*0.106*	*0.003*	*1217*	*32*	*944*	*29*	*1720*	*43*	*45.1*	*26.8*
WF_04_296	42	14	0.33	45	2.121	0.067	0.1997	0.0046	0.29	0.077	0.002	1154	22	1173	25	1123	62	-4.5	-2.0
WF_04_297	487	97	0.20	510	0.116	0.008	0.0168	0.0006	0.49	0.050	0.003	111.1	6.8	107.1	4	190	110	3.6	0.6
WF_04_298	735	585	0.80	872	0.154	0.007	0.0224	0.0007	0.41	0.049	0.002	145.2	6.5	142.8	4.4	160	90	1.7	0.4
WF_04_299	1148	13	0.01	1151	4.850	0.110	0.3224	0.0073	0.82	0.108	0.002	1793	19	1804	36	1771	25	-1.9	-0.9
WF_04_300	159	172	1.08	200	0.184	0.013	0.0255	0.0006	0.14	0.053	0.004	171	11	162.5	3.9	270	140	5.0	0.8

[a]All locations reported in decimal degrees from a WGS 1984 mercator projection

[b]Emboldened and shaded rows indicate the youngest measured concordant grains. Italicized rows indicate analyses that were not considered for plots and calculations.

[c]U and Th concentrations and Th/U ratios calculated relative to the GJ-1 zircon standard ID-TIMS values using 287 ± 76 ppm for U and 8.4 ± 2.6 ppm for Th (Jackson et al., 2004)

[d]Equivalent U determined by the equation: eU = U ppm + 0.235*Th ppm

[e]Corrected for U-Pb fractionation and background and normalized to the GJ-1 zircon standard ID-TIMS values: $^{207}Pb/^{235}U$ = 0.8093 ± 0.0009 and $^{206}Pb/^{238}U$ = 0.09761 ± 0.00011 (Jackson et al., 2004)

[f]Propagated uncertainty of internal uncertainties (2 SE) and within run reproducibility of GJ-1 (2 SE)

[g]Uncertainty correlation between $^{206}Pb/^{238}U$ and $^{207}Pb/^{235}U$ uncertainties

[h]Corrected for background and Pb isotopic fractionation using the GJ-1 zircon standard ID-TIMS value: $^{207}Pb/^{206}Pb$ = 0.06014 ± 0.00001 (Jackson et al., 2004)

[i]U-Pb ages calculated relative to the GJ-1 zircon standard

[j]Discordance defined as [($^{207}Pb/^{235}U$age – $^{206}Pb/^{238}U$age)/($^{207}Pb/^{235}U$age)]*100

[k]Uncertainty weighted age difference defined as ($^{207}Pb/^{235}U$age - $^{206}Pb/^{238}U$age)/($^{207}Pb/^{235}U$2s age uncertainty) for grains with $^{206}Pb/^{238}U$ ages <850 Ma and ($^{207}Pb/^{206}Pb$age - $^{206}Pb/^{238}U$age)/($^{206}Pb/^{238}U$2s age uncertainty) for grains with $^{206}Pb/^{238}U$ ages ≥850 Ma

Table 11: Standard GJ1 for sample WF-04 LA-ICP-MS U-Pb Isotopic Data and Ages

					Corrected Isotopic Ratios								Ages (Ma)[i]						
Grain #[b]	U[c] [ppm]	Th[c] [ppm]	Th/U	eU[d] [ppm]	$^{207}Pb/^{235}U$[e]	±2s[f]	$^{206}Pb/^{238}U$[e]	±2s[f]	Rho[g]	$^{207}Pb/^{206}Pb$[h]	±2s[f]	$^{207}Pb/^{235}U$	±2s	$^{206}Pb/^{238}U$	±2s	$^{207}Pb/^{206}Pb$	±2s	Disc. %[i]	Wtd. Disc.[k]
Z_GJ1_01	289	8	0.03	291	0.812	0.020	0.0972	0.0019	0.57	0.060	0.001	602.8	11	597.7	11	614	42	0.8	0.5
Z_GJ1_02	293	9	0.03	295	0.823	0.020	0.0975	0.0020	0.40	0.060	0.001	610.8	11	599.4	11	629	45	1.9	1.0
Z_GJ1_03	286	8	0.03	288	0.824	0.022	0.0979	0.0019	0.53	0.061	0.001	610.7	12	603.1	12	631	40	1.2	0.6
Z_GJ1_04	293	9	0.03	295	0.799	0.019	0.0974	0.0018	0.54	0.060	0.001	597.7	10	599.1	11	582	37	-0.2	-0.1
Z_GJ1_05	285	8	0.03	287	0.818	0.017	0.0987	0.0016	0.32	0.060	0.001	607.5	9.7	606.6	9.5	612	40	0.1	0.1
Z_GJ1_06	288	8	0.03	290	0.808	0.018	0.0974	0.0019	0.55	0.060	0.001	601.5	11	600	11	617	38	0.2	0.1
Z_GJ1_07	287	8	0.03	289	0.799	0.018	0.0981	0.0015	0.41	0.059	0.001	595.8	10	603.1	8.8	573	38	-1.2	-0.7
Z_GJ1_08	290	8	0.03	292	0.799	0.016	0.0977	0.0017	0.42	0.059	0.001	595.9	9.2	600.7	10	571	35	-0.8	-0.5
Z_GJ1_09	293	9	0.03	295	0.803	0.017	0.0967	0.0017	0.51	0.061	0.001	598	9.4	595.2	10	640	36	0.5	0.3
Z_GJ1_10	289	8	0.03	291	0.812	0.019	0.0969	0.0016	0.33	0.061	0.001	602.9	10	598	9.5	617	44	0.8	0.5
Z_GJ1_11	291	9	0.03	293	0.811	0.018	0.0973	0.0016	0.37	0.061	0.001	602.5	10	598.5	9.4	633	39	0.7	0.4
Z_GJ1_12	287	8	0.03	289	0.804	0.020	0.0974	0.0017	0.35	0.060	0.001	598.4	11	599.8	10	595	44	-0.2	-0.1
Z_GJ1_13	284	8	0.03	286	0.819	0.018	0.0984	0.0017	0.50	0.060	0.001	608.2	10	604.9	10	600	39	0.5	0.3
Z_GJ1_14	280	8	0.03	282	0.812	0.018	0.0978	0.0019	0.41	0.060	0.001	602.9	9.9	601.5	11	610	36	0.2	0.1
Z_GJ1_15	286	8	0.03	288	0.810	0.018	0.0970	0.0018	0.38	0.061	0.001	603.1	10	596.5	11	642	42	1.1	0.7
Z_GJ1_16	284	8	0.03	286	0.805	0.019	0.0983	0.0017	0.43	0.060	0.001	598.9	11	604.2	10	597	39	-0.9	-0.5
Z_GJ1_17	292	8	0.03	294	0.807	0.018	0.0969	0.0018	0.41	0.061	0.001	600	9.9	596.2	11	622	42	0.6	0.4
Z_GJ1_18	292	9	0.03	294	0.806	0.017	0.0973	0.0018	0.36	0.061	0.001	599.5	9.7	598.2	11	634	40	0.2	0.1
Z_GJ1_19	295	9	0.03	297	0.810	0.019	0.0977	0.0017	0.45	0.060	0.001	602.5	11	601	9.8	606	41	0.2	0.1
Z_GJ1_20	285	8	0.03	287	0.808	0.019	0.0980	0.0018	0.47	0.060	0.001	602.5	11	602.5	10	589	41	0.0	0.0
Z_GJ1_21	289	9	0.03	291	0.795	0.017	0.0978	0.0017	0.37	0.059	0.001	593.6	9.8	601.2	10	575	39	-1.3	-0.8
Z_GJ1_22	284	8	0.03	286	0.819	0.020	0.0974	0.0019	0.51	0.061	0.001	606.7	11	599.1	11	633	40	1.3	0.7
Z_GJ1_23	284	8	0.03	286	0.804	0.019	0.0970	0.0017	0.39	0.060	0.001	598.3	10	596.7	9.7	595	40	0.3	0.2
Z_GJ1_24	278	8	0.03	280	0.808	0.019	0.0983	0.0017	0.38	0.060	0.001	600.6	11	604.1	10	583	42	-0.6	-0.3
Z_GJ1_25	282	8	0.03	284	0.813	0.018	0.0979	0.0016	0.47	0.060	0.001	604.4	9.7	601.8	9.2	615	34	0.4	0.3
Z_GJ1_26	285	9	0.03	287	0.802	0.017	0.0971	0.0016	0.24	0.060	0.001	597.5	9.3	597.4	9.7	603	43	0.0	0.0
Z_GJ1_27	279	8	0.03	281	0.822	0.017	0.0982	0.0017	0.36	0.060	0.001	608.5	9.6	603.9	9.8	618	37	0.8	0.5
Z_GJ1_28	285	8	0.03	287	0.807	0.019	0.0969	0.0017	0.54	0.060	0.001	600.3	11	596.2	10	596	39	0.7	0.4
Z_GJ1_29	287	8	0.03	289	0.808	0.017	0.0973	0.0016	0.13	0.060	0.001	600.8	9.7	598.6	9.4	595	43	0.4	0.2
Z_GJ1_30	278	8	0.03	280	0.823	0.018	0.0984	0.0016	0.37	0.060	0.001	608.9	10	604.8	9.6	586	36	0.7	0.4
Z_GJ1_31	298	9	0.03	300	0.808	0.017	0.0972	0.0017	0.34	0.060	0.001	601.2	9.3	598.8	9.8	607	39	0.4	0.3
Z_GJ1_32	287	8	0.03	289	0.811	0.020	0.0982	0.0017	0.47	0.060	0.001	604.2	11	603.9	9.8	588	41	0.0	0.0

Table 11: Standard GJ1 for sample WF-04 LA-ICP-MS U-Pb Isotopic Data and Ages

					Corrected Isotopic Ratios							Ages (Ma)[i]							
Grain #[b]	U[c] [ppm]	Th[c] [ppm]	Th/U	eU[d] [ppm]	$^{207}Pb/^{235}U$[e]	±2s[f]	$^{206}Pb/^{238}U$[e]	±2s[f]	Rho[g]	$^{207}Pb/^{206}Pb$[h]	±2s[f]	$^{207}Pb/^{235}U$	±2s	$^{206}Pb/^{238}U$	±2s	$^{207}Pb/^{206}Pb$	±2s	Disc. %[i]	Wtd. Disc.[k]
Z_GJ1_33	295	9	0.03	297	0.804	0.018	0.0969	0.0016	0.40	0.060	0.001	599.4	9.9	596.4	9.1	598	37	0.5	0.3
Z_GJ1_34	*249*	*7*	*0.03*	*251*	*0.837*	*0.019*	*0.0982*	*0.0022*	*0.41*	*0.061*	*0.001*	*620.3*	*12*	*604*	*13*	*645*	*46*	*2.6*	*1.4*
Z_GJ1_35	298	9	0.03	300	0.818	0.017	0.0975	0.0019	0.45	0.060	0.001	606.2	9.7	599.5	11	612	40	1.1	0.7
Z_GJ1_36	286	8	0.03	288	0.826	0.019	0.0981	0.0016	0.44	0.061	0.001	612.1	11	602.9	9.6	636	39	1.5	0.8
Z_GJ1_37	287	8	0.03	289	0.801	0.020	0.0977	0.0016	0.33	0.059	0.001	596.3	11	600.6	9.5	573	45	-0.7	-0.4
Z_GJ1_38	287	8	0.03	289	0.811	0.020	0.0976	0.0015	0.29	0.061	0.001	602.1	11	600.1	9	637	42	0.3	0.2
Z_GJ1_39	288	8	0.03	290	0.794	0.017	0.0971	0.0016	0.18	0.060	0.001	593	9.5	597.1	9.1	604	40	-0.7	-0.4
Z_GJ1_40	283	8	0.03	285	0.800	0.019	0.0978	0.0017	0.43	0.060	0.001	596	11	601.3	9.9	601	41	-0.9	-0.5
Z_GJ1_41	283	8	0.03	285	0.817	0.020	0.0981	0.0016	0.30	0.061	0.001	606.9	11	603.2	9.6	645	46	0.6	0.3
Z_GJ1_42	286	8	0.03	288	0.811	0.018	0.0979	0.0017	0.28	0.060	0.001	603.7	10	601.7	10	606	42	0.3	0.2
Z_GJ1_43	293	9	0.03	295	0.809	0.019	0.0966	0.0016	0.37	0.061	0.001	602.5	10	594.3	9.6	619	42	1.4	0.8
Z_GJ1_44	284	8	0.03	286	0.822	0.019	0.0985	0.0017	0.50	0.060	0.001	609.6	11	605.8	9.9	607	39	0.6	0.3
Z_GJ1_45	288	9	0.03	290	0.813	0.019	0.0976	0.0017	0.33	0.061	0.001	603.3	10	600.4	9.8	620	44	0.5	0.3
Z_GJ1_46	290	8	0.03	292	0.802	0.018	0.0971	0.0017	0.31	0.060	0.001	597.2	10	597.1	9.8	604	40	0.0	0.0
Z_GJ1_47	290	8	0.03	292	0.797	0.017	0.0980	0.0018	0.27	0.060	0.001	595.4	9.6	602.4	10	583	39	-1.2	-0.7
Z_GJ1_48	285	9	0.03	287	0.812	0.018	0.0979	0.0017	0.38	0.060	0.001	604.1	9.9	601.9	9.8	601	37	0.4	0.2
Z_GJ1_49	285	8	0.03	287	0.810	0.019	0.0973	0.0016	0.29	0.061	0.001	601.6	11	599.4	9.7	634	42	0.4	0.2
Z_GJ1_50	299	9	0.03	301	0.810	0.017	0.0975	0.0016	0.29	0.060	0.001	602.1	9.6	600	9.1	603	38	0.3	0.2
Z_GJ1_51	292	8	0.03	294	0.805	0.016	0.0978	0.0014	0.23	0.060	0.001	599.5	8.9	601.5	8.4	601	37	-0.3	-0.2
Z_GJ1_52	289	8	0.03	291	0.809	0.020	0.0974	0.0016	0.47	0.060	0.001	601.3	11	600.1	9.4	614	42	0.2	0.1

Typical 2σ error for GJ1 during this run had a weighted average of 600.4 ± 1.4 Ma and a range of 594.3-606.6 Ma (MSWD:0.34, Probability:1, n=51). The accepted age of GJ1 is 600.1 Ma ($^{206}Pb/^{238}U$ age, Jackson et al., 2004).

[a]All locations reported in decimal degrees from a WGS 1984 mercator projection

[b]Italicized rows indicate analyses that were not considered for plots and calculations

[c]U and Th concentrations and Th/U ratios calculated relative to the GJ-1 zircon standard ID-TIMS values using 287 ± 76 ppm for U and 8.4 ± 2.6 ppm for Th (Jackson et al., 2004)

[d]Equivalent U determined by the equation: eU = U ppm + 0.235*Th ppm

[e]Corrected for U-Pb fractionation and background and normalized to the GJ-1 zircon standard ID-TIMS values: $^{207}Pb/^{235}U = 0.8093 \pm 0.0009$ and $^{206}Pb/^{238}U = 0.09761 \pm 0.00011$ (Jackson et al., 2004)

[f]Propagated uncertainty of internal uncertainties (2 SE) and within run reproducibility of GJ-1 (2 SE)

[g]Uncertainty correlation between $^{206}Pb/^{238}U$ and $^{207}Pb/^{235}U$ uncertainties

[h]Corrected for background and Pb isotopic fractionation using the GJ-1 zircon standard ID-TIMS value: $^{207}Pb/^{206}Pb = 0.06014 \pm 0.00001$ (Jackson et al., 2004)

[i]U-Pb ages calculated relative to the GJ-1 zircon standard

[j]Discordance defined as $[(^{207}Pb/^{235}Uage - ^{206}Pb/^{238}Uage)/(^{207}Pb/^{235}Uage)]*100$

[k]Uncertainty weighted age difference defined as $(^{207}Pb/^{235}Uage - ^{206}Pb/^{238}Uage)/(^{207}Pb/^{235}U2s$ age uncertainty) for grains with $^{206}Pb/^{238}U$ ages <850 Ma and $(^{207}Pb/^{206}Pbage - ^{206}Pb/^{238}Uage)/(^{206}Pb/^{238}U2s$ age uncertainty) for grains with $^{206}Pb/^{238}U$ ages ≥850 Ma

Table 12: Standard Fish canyon tuff for sample WF-04 LA-ICP-MS U-Pb Isotopic Data and Ages

					Corrected Isotopic Ratios								Ages (Ma)[i]							
Grain #[b]	U[c] [ppm]	Th[c] [ppm]	Th/U	eU[d] [ppm]	$^{207}Pb/^{235}U$[e]	±2s[f]	$^{206}Pb/^{238}U$[e]	±2s[f]	Rho[g]	$^{207}Pb/^{206}Pb$[h]	±2s[f]	$^{207}Pb/^{235}U$	±2s	$^{206}Pb/^{238}U$	±2s	$^{207}Pb/^{206}Pb$	±2s	Disc. %[j]	Wtd. Disc.[k]
FCT_Tuff_01	89	70	0.79	105	0.029	0.007	0.0045	0.0003	0.13	0.050	0.014	28.4	7.3	29	2.1	100	460	-2.1	-0.1
FCT_Tuff_02	392	167	0.43	431	0.031	0.004	0.0042	0.0002	0.03	0.052	0.006	31.2	3.6	27	1.3	250	230	13.5	1.2
FCT_Tuff_03	358	112	0.31	384	0.030	0.002	0.0043	0.0001	0.05	0.050	0.004	30.2	2.4	27.84	0.9	180	150	7.8	1.0
FCT_Tuff_04	268	102	0.38	292	0.029	0.003	0.0042	0.0002	0.08	0.051	0.005	28.7	3	26.85	0.95	180	200	6.4	0.6
FCT_Tuff_05	443	215	0.48	493	0.026	0.002	0.0043	0.0001	0.13	0.044	0.003	26.4	1.8	27.88	0.9	-50	130	-5.6	-0.8
FCT_Tuff_06	*295*	*94*	*0.32*	*317*	*0.035*	*0.003*	*0.0049*	*0.0002*	*0.29*	*0.051*	*0.005*	*34.5*	*3.1*	*31.55*	*1*	*220*	*170*	*8.6*	*1.0*
FCT_Tuff_07	315	98	0.31	338	0.029	0.003	0.0044	0.0002	0.18	0.047	0.006	28.7	3.3	28.4	1.4	110	220	1.0	0.1
FCT_Tuff_08	618	255	0.41	678	0.029	0.002	0.0044	0.0001	0.24	0.047	0.003	29.1	1.8	28.08	0.9	80	120	3.5	0.6
FCT_Tuff_09	285	89	0.31	306	0.030	0.003	0.0044	0.0002	0.12	0.048	0.004	30.3	2.5	28.4	1.1	160	160	6.3	0.8
FCT_Tuff_10	167	60	0.36	181	0.029	0.004	0.0042	0.0002	0.13	0.048	0.006	29.3	3.6	27.11	1	140	230	7.5	0.6
FCT_Tuff_11	317	97	0.31	340	0.029	0.003	0.0043	0.0002	0.21	0.049	0.005	29.2	2.9	27.7	1.1	140	190	5.1	0.5
FCT_Tuff_12	385	155	0.40	421	0.027	0.002	0.0043	0.0002	0.06	0.045	0.004	27	2.1	27.62	0.97	0	140	-2.3	-0.3
FCT_Tuff_13	*354*	*132*	*0.37*	*385*	*0.032*	*0.003*	*0.0044*	*0.0001*	*0.10*	*0.053*	*0.004*	*31.7*	*2.5*	*28.24*	*0.88*	*300*	*160*	*10.9*	*1.4*
FCT_Tuff_14	453	213	0.47	503	0.028	0.002	0.0044	0.0001	0.15	0.046	0.003	28.2	2.1	28.01	0.89	50	140	0.7	0.1
FCT_Tuff_15	*360*	*181*	*0.50*	*402*	*0.031*	*0.002*	*0.0044*	*0.0002*	*0.18*	*0.050*	*0.004*	*31.2*	*2.5*	*28.15*	*0.94*	*220*	*150*	*9.8*	*1.2*
FCT_Tuff_16	496	285	0.57	563	0.030	0.003	0.0044	0.0002	0.19	0.049	0.004	29.7	2.5	28.53	0.98	160	170	3.9	0.5
FCT_Tuff_17	480	223	0.46	532	0.027	0.002	0.0043	0.0001	0.00	0.045	0.003	27.1	1.7	27.55	0.8	10	110	-1.7	-0.3
FCT_Tuff_18	305	116	0.38	332	0.028	0.003	0.0043	0.0001	0.01	0.050	0.005	28.5	2.7	27.49	0.77	140	180	3.5	0.4
FCT_Tuff_19	270	76	0.28	288	0.030	0.002	0.0043	0.0002	0.11	0.050	0.004	29.5	2.3	27.9	1.2	170	160	5.4	0.7
FCT_Tuff_20	311	113	0.36	338	0.032	0.002	0.0045	0.0002	0.06	0.049	0.004	31.4	2.3	29.27	0.98	140	140	6.8	0.9
FCT_Tuff_21	387	124	0.32	416	0.027	0.002	0.0045	0.0001	0.05	0.045	0.004	27.3	2.3	28.75	0.82	-30	150	-5.3	-0.6
FCT_Tuff_22	269	85	0.31	289	0.030	0.003	0.0044	0.0002	0.29	0.049	0.005	29.8	2.9	28	1.1	130	180	6.0	0.6

Secondary standard Fish Canyon Tuff yielded a weighted mean $^{206}Pb/^{238}U$ date of 27.92 ± 0.23 Ma (2σ) (n=19; MSWD=1.6, Probability: 0.06). The accepted age of Fish Canyon Tuff is 28.642 ± 0.025 Ma to 28.196 ± 0.038 Ma (Wotzlaw et al., 2013).

[a]All locations reported in decimal degrees from a WGS 1984 mercator projection

[b]Italicized rows indicate analyses that were not considered for plots and calculations

[c]U and Th concentrations and Th/U ratios calculated relative to the GJ-1 zircon standard ID-TIMS values using 287 ± 76 ppm for U and 8.4 ± 2.6 ppm for Th (Jackson et al., 2004)

[d]Equivalent U determined by the equation: eU = U ppm + 0.235*Th ppm

[e]Corrected for U-Pb fractionation and background and normalized to the GJ-1 zircon standard ID-TIMS values: $^{207}Pb/^{235}U$ = 0.8093 ± 0.0009 and $^{206}Pb/^{238}U$ = 0.09761 ± 0.00011 (Jackson et al., 2004)

[f]Propagated uncertainty of internal uncertainties (2 SE) and within run reproducibility of GJ-1 (2 SE)

[g]Uncertainty correlation between $^{206}Pb/^{238}U$ and $^{207}Pb/^{235}U$ uncertainties

[h]Corrected for background and Pb isotopic fractionation using the GJ-1 zircon standard ID-TIMS value: $^{207}Pb/^{206}Pb$ = 0.06014 ± 0.00001 (Jackson et al., 2004)

[i]U-Pb ages calculated relative to the GJ-1 zircon standard

[j]Discordance defined as [($^{207}Pb/^{235}U$age – $^{206}Pb/^{238}U$age)/($^{207}Pb/^{235}U$age)]*100

[k]Uncertainty weighted age difference defined as ($^{207}Pb/^{235}U$age - $^{206}Pb/^{238}U$age)/($^{207}Pb/^{235}U$2s age uncertainty) for grains with $^{206}Pb/^{238}U$ ages <850 Ma and ($^{207}Pb/^{206}Pb$age - $^{206}Pb/^{238}U$age)/($^{206}Pb/^{238}U$2s age uncertainty) for grains with $^{206}Pb/^{238}U$ ages ≥850 Ma

Table 13: Standard Plešovice for sample WF-04 LA-ICP-MS U-Pb Isotopic Data and Ages

					Corrected Isotopic Ratios								Ages (Ma)[i]							
Grain #[b]	U[c] [ppm]	Th[c] [ppm]	Th/U	eU[d] [ppm]	$^{207}Pb/^{235}U$[e]	±2s[f]	$^{206}Pb/^{238}U$[e]	±2s[f]	Rho[g]	$^{207}Pb/^{206}Pb$[h]	±2s[f]	$^{207}Pb/^{235}U$	±2s	$^{206}Pb/^{238}U$	±2s	$^{207}Pb/^{206}Pb$	±2s	Disc. %[j]	Wtd. Disc.[k]
Plesovice_01	432	31	0.07	439	0.404	0.010	0.0541	0.0011	0.48	0.053	0.001	344.1	7.2	339.4	6.7	354	45	1.4	0.7
Plesovice_02	424	32	0.07	431	0.400	0.010	0.0553	0.0009	0.32	0.053	0.001	342.2	7.2	346.8	5.7	305	48	-1.3	-0.6
Plesovice_03	423	31	0.07	430	0.397	0.010	0.0542	0.0010	0.36	0.053	0.001	340	7.4	340	6.1	326	55	0.0	0.0
Plesovice_04	433	31	0.07	440	0.399	0.010	0.0540	0.0010	0.31	0.053	0.001	340.5	7.4	339.2	6.2	306	52	0.4	0.2
Plesovice_05	407	29	0.07	414	0.396	0.010	0.0544	0.0010	0.49	0.053	0.001	338.4	7.3	341.3	6.2	318	45	-0.9	-0.4
Plesovice_06	412	30	0.07	419	0.408	0.011	0.0553	0.0011	0.41	0.055	0.001	346.9	7.6	347	6.8	394	49	0.0	0.0
Plesovice_07	425	30	0.07	432	0.403	0.010	0.0542	0.0010	0.37	0.054	0.001	343.6	7.6	340.5	6	359	50	0.9	0.4
Plesovice_08	438	31	0.07	445	0.397	0.010	0.0538	0.0010	0.55	0.054	0.001	339.4	7.1	337.6	6	364	45	0.5	0.3
Plesovice_09	420	30	0.07	427	0.398	0.011	0.0542	0.0010	0.28	0.053	0.001	340	7.7	340.5	6.1	315	49	-0.1	-0.1
Plesovice_10	463	32	0.07	470	0.410	0.011	0.0546	0.0010	0.37	0.054	0.001	348.2	7.8	342.6	6.2	368	51	1.6	0.7
Plesovice_11	432	30	0.07	439	0.395	0.010	0.0541	0.0010	0.41	0.053	0.001	337.6	7.2	339.8	6.1	311	49	-0.7	-0.3
Plesovice_12	424	30	0.07	431	0.400	0.011	0.0540	0.0009	0.28	0.053	0.001	341.1	7.9	338.9	5.4	328	52	0.6	0.3
Plesovice_13	429	30	0.07	436	0.403	0.010	0.0538	0.0011	0.41	0.053	0.001	343.1	7.5	337.9	6.7	341	55	1.5	0.7
Plesovice_14	*423*	*29*	*0.07*	*430*	*0.417*	*0.012*	*0.0546*	*0.0010*	*0.40*	*0.055*	*0.001*	*354*	*8.7*	*342.7*	*6.4*	*427*	*49*	*3.2*	*1.3*
Plesovice_15	434	30	0.07	441	0.403	0.011	0.0539	0.0010	0.20	0.053	0.002	343.7	8.1	338.4	6.2	328	62	1.5	0.7
Plesovice_16	422	29	0.07	429	0.402	0.009	0.0549	0.0009	0.42	0.053	0.001	342.5	6.8	344.2	5.7	328	47	-0.5	-0.2
Plesovice_17	438	31	0.07	445	0.395	0.010	0.0542	0.0010	0.35	0.053	0.001	337.3	7.1	339.9	6	347	53	-0.8	-0.4
Plesovice_18	423	29	0.07	430	0.411	0.011	0.0559	0.0011	0.50	0.053	0.001	349.2	7.6	350.4	7	341	51	-0.3	-0.2
Plesovice_19	434	30	0.07	441	0.404	0.011	0.0557	0.0011	0.32	0.053	0.001	344.9	7.8	349.2	6.4	331	55	-1.2	-0.6
Plesovice_20	443	31	0.07	450	0.400	0.011	0.0555	0.0011	0.38	0.052	0.001	341.3	8.3	348.1	6.5	295	55	-2.0	-0.8
Plesovice_21	437	30	0.07	444	0.401	0.010	0.0545	0.0010	0.40	0.054	0.001	341.7	7.3	341.8	6	349	46	0.0	0.0
Plesovice_22	435	32	0.07	442	0.405	0.011	0.0551	0.0010	0.43	0.054	0.001	345.6	7.8	345.5	6	364	52	0.0	0.0
Plesovice_23	441	30	0.07	448	0.400	0.009	0.0543	0.0009	0.34	0.054	0.001	341.6	6.6	340.5	5.8	345	46	0.3	0.2

Secondary standard Plešovice yielded a weighted mean $^{206}Pb/^{238}U$ date of 342.1 ± 1.3 Ma (2σ) (n=22; MSWD=1.5, Probability: 0.069). The accepted age of Plešovice is 337.13 ± 0.37 Ma (CA-TIMS age, Slama et al., 2008).

[a]All locations reported in decimal degrees from a WGS 1984 mercator projection

[b]Italicized rows indicate analyses that were not considered for plots and calculations

[c]U and Th concentrations and Th/U ratios calculated relative to the GJ-1 zircon standard ID-TIMS values using 287 ± 76 ppm for U and 8.4 ± 2.6 ppm for Th (Jackson et al., 2004)

[d]Equivalent U determined by the equation: eU = U ppm + 0.235*Th ppm

[e]Corrected for U-Pb fractionation and background and normalized to the GJ-1 zircon standard ID-TIMS values: $^{207}Pb/^{235}U$ = 0.8093 ± 0.0009 and $^{206}Pb/^{238}U$ = 0.09761 ± 0.00011 (Jackson et al., 2004)

[f]Propagated uncertainty of internal uncertainties (2 SE) and within run reproducibility of GJ-1 (2 SE)

[g]Uncertainty correlation between $^{206}Pb/^{238}U$ and $^{207}Pb/^{235}U$ uncertainties

[h]Corrected for background and Pb isotopic fractionation using the GJ-1 zircon standard ID-TIMS value: $^{207}Pb/^{206}Pb$ = 0.06014 ± 0.00001 (Jackson et al., 2004)

[i]U-Pb ages calculated relative to the GJ-1 zircon standard

[j]Discordance defined as [($^{207}Pb/^{235}U$age – $^{206}Pb/^{238}U$age)/($^{207}Pb/^{235}U$age)]*100

[k]Uncertainty weighted age difference defined as ($^{207}Pb/^{235}U$age - $^{206}Pb/^{238}U$age)/($^{207}Pb/^{235}U$2s age uncertainty) for grains with $^{206}Pb/^{238}U$ ages <850 Ma and ($^{207}Pb/^{206}Pb$age - $^{206}Pb/^{238}U$age)/($^{206}Pb/^{238}U$2s age uncertainty) for grains with $^{206}Pb/^{238}U$ ages ≥850 Ma